

University of Nottingham
UK | CHINA | MALAYSIA

Faculty of Medicine and Health Sciences

School of Medicine

Investigating the Interactions between Tumour Cells and the Non-tumour Cellular Community in Colorectal Cancer

By

Susanti Susanti

Thesis submitted to the University of Nottingham
for the degree of Doctor of Philosophy

August 2020

ABSTRACT

Colorectal cancer (CRC) is one of the leading causes of cancer-related mortality. It is a heterogeneous disease and several different classifications for CRC have been developed over the years. The most recent classification has identified 4 tumour groups which has been called "Consensus Molecular Subtypes (CMS)". As well as molecular differences in the epithelium, the CMS classification also identifies distinguishing features in the stroma. Thus, tumours belonging to CMS1 have hypermutation in the cancer epithelium and are characterized by a prominent lymphocytic infiltrate. In contrast, tumours belonging to CMS4 have activation of the TGF-b signalling pathway and a dense fibrous stroma. Since CRC arises as a consequence of gene mutation and these mutations only occur in the epithelial cells, it follows that signalling from the epithelial cells may influence the population profile of the cells in the stroma (i.e. the cancer community). This study hypothesized that (i) the cellular community in CRC is non-random and is dictated by signals from the epithelium and (ii) that, in turn, the cellular community can influence tumour kinetics.

To test the relationship between mutations in the cancer cell and the cancer community, it was necessary to build cancer mutation profiles and cancer community profiles of CRC. We aimed initially to classify tumours as either having microsatellite instability (MSI) or being microsatellite stable (MSS). Using PCR (Polymerase Chain Reaction) followed by HRMA (High Resolution Melting Analysis), a new panel of microsatellite markers, consisting of two established markers (BAT25, BAT26) and three novel markers (BCAT25, MYB and EWSR1) was developed and shown to have near perfect concordance with the IHC (immunohistochemistry) for mismatch repair (MMR) proteins and PCR followed by CE (capillary electrophoresis).

The HRMA was also used for mutation detection of other important driver genes including *KRAS*, *BRAF* (exon 11) and *PIK3CA*. The expression pattern of p53 protein was examined using IHC as a surrogate to detect the mutation of *TP53* gene. The DNA content of tumour cells (the "ploidy" status) was assessed by flow cytometry.

A cohort of 99 cases of CRC was retrieved from the archives of the Nottingham University Hospitals NHS trust. This was selected to contain 44 cases which had been shown to be Mismatch Repair deficient (dMMR) and 45 cases which had

been shown to be Mismatch Repair proficient (pMMR). These were confirmed as showing MSI and MSS respectively by the panel of markers described in this project. The frequencies of the mutations in the MSI and MSS (microsatellite stable) CRC were in concordance with published literatures. CRCs with MSI (MSI-CRCs) were enriched for *BRAF* mutation ($p<0.001$) and were all diploid or near-diploid tumours. Conversely, MSS-CRCs were enriched for *TP53* mutation ($p<0.001$) compared to MSI-CRCs and 60% were aneuploid. The presence of diploidy in 40% of MSS-CRCs confirmed that the so-called MACS (microsatellite and chromosomal stable) CRC represented a significant proportion of MSS-CRCs but there was no association between *TP53* mutation and aneuploidy.

Within tumours, there was a negative association between *KRAS* exon 2 and *BRAF* exon 15 mutations ($p<0.05$), Fisher's exact test). Mutations in *KRAS* exon 2 were positively associated with mutations in *PIK3CA* exon 9 ($P=0.046$, Fisher's exact test), whilst, in contrast, there was a significant negative association of mutations in *BRAF* codon 600 with mutation in *PIK3CA* exon 9 ($p=0.026$, Fisher's exact test) when tested in larger cohort of CRC (from Nottingham and Edinburgh). As both *KRAS* and *BRAF* are part of the MAPK (mitogen activated protein kinase) signalling, these findings suggest that co-selection is gene specific but not pathway specific.

In order to profile the cancer community, a novel approach called fm-IHC (faux multiplex immunohistochemistry) was employed. This method allows both the cellular populations to be identified as well as describing the interactions of the members of the community with each other and with the tumour epithelium. This method relies on IHC to identify cell populations and precise registration of multiple images to then allow virtual segmentation and spatial mapping of the cell populations.

In this study, although few significant features were found indicating active stage of TME of MSI tumour such as higher density of proliferating (Ki67+) CD3+ T-lymphocytes and low-apoptotic (BCL-2+) CD20+ B-lymphocytes within the stroma, the *BRAF* mutation are associated with stronger immune features in the TME. *BRAF* mutant tumour had higher density of CD3+ T-lymphocytes and CD20+ B-lymphocytes within the stroma and WTS (whole tissue section) and more proliferating (Ki67+) CD3+ lymphocytes and CD163+ M2-macrophages and BCL2+ (low apoptotic) cellular community, which includes CD3+ and CD8+ T-lymphocytes, CD20+ B-lymphocytes, CD163+ M2-macrophages and CD56+ NK cells in the stroma. *BRAF* mutant also showed

higher correlation between CD8+ cytotoxic T-cell with CD68+ macrophages and CD163+ M2-macrophages in the epithelial.

We also found significance of *TP53* mutation in inducing immune activation within the TME of CRC, indicated by higher intratumoural (epithelial) density of CD3+ T-lymphocytes, CD68+ macrophages, and CD56+ NK cells and higher density of proliferating (Ki67+) NK cells within the stroma of *TP53* mutant tumour. Furthermore, MACS subgroup within the MSS tumour showed higher density of CD56+ NK cells and proliferating (Ki67+) macrophages in the stroma.

To investigate how the cancer community can influence cancer cells, a 3D (three-dimensional) spheroid co-culture model was developed. This model allows multiple cellular populations to be cultured together and, through specific labelling, each population can be tracked during the experiment. We initially sought to investigate the effect on cancer cells induced by the most common cell in the cancer community i.e., the cancer associated fibroblast (CAF). Two different CRC cell lines, HCT116 (classified as CMS4) and DLD1 (classified as CMS1) were co-cultured with CAFs. Proliferation of HCT116 was increased in the presence of CAFs whilst DLD-1 showed no response to the presence of CAFs. Since macrophages were identified as a common population in the cancer community, peripheral blood monocytes (precursors of tissue macrophages) and macrophages were added as a third population to the co-culture. However, any effect of addition of monocytes or macrophages to the growth of either HCT116 or DLD-1 was not observed.

The 3D co-culture model also allowed us to interrogate the specific interactions between genes expressed in the cancer cells and the cancer community. CD24 is a glycosylated cell-surface protein that acts as an oncogene in CRC. HCT116 has no expression of CD24 and thus provides a good model for testing the activity of CD24. Cells which had been transfected with a CD24 expression vector (HCT116CD24) were compared with cells transfected with empty vector (HCT116EV). Co-culture of HCT116CD24 with CAFs resulted in greater cell proliferation of the cancer cells than co-culture of HCT116EVC with CAFs. This apparent effect of CD24-CAF interaction on cell proliferation is a very interesting finding as previous studies in our laboratory showed no effect of CD24 in CRC proliferation using the 2D (two-dimensional) culture system.

Altogether, this study has established models which allow evaluation of gene-

specific effects on the population profile of the cancer community and genotype-specific responses of cancer cells to the cancer community. We have made several interesting observations which need further investigation in order to fully understand the interactions between cancer cell and cancer community.

Thesis-related Publications, Awards and Future Funding

Peer-reviewed Publications

- Nestarenkaite, A., Fadhil, W., Rasmusson, A., **Susanti, S.**, Hadjimichael, E., Laurinaviciene, A., Ilyas, M., Laurinavicius, A., 2020. Immuno-interface score to predict outcome in colorectal cancer independent of microsatellite instability status. *Cancers (Basel)* 12, 2902. *doi:10.3390/cancers12102902.*
- Raposo T.P., **Susanti S**., Ilyas M., 2020, Investigating TNS4 in the Colorectal Tumor Microenvironment Using 3D Spheroid Models of Invasion. Adv. Biosys., 4, 2000031. doi: /abs/10.1002/adbi.202000031
- **Susanti S,** Fadhil W, Murtaza S, …, Ilyas M, 2018, Positive association of *PIK3CA* mutation with *KRAS* mutation but not *BRAF* mutation in colorectal cancer suggests co-selection is gene specific but not pathway specific, Journal of Clinical Pathology, Published Online First: 25 October 2018. doi: 10.1136/jclinpath-2018-205483.
- **Susanti S**, Fadhil W, Ebili HO, …, Ilyas M, 2018, N_LyST: a simple and rapid screening test for Lynch syndrome, Journal of Clinical Pathology, 71(8):713-720. doi: 10.1136/jclinpath-2018-205013

Awards

- 2nd poster prize, Maastricht Pathology 2018, 11th Joint Meeting of the British Division of the International Academy of Pathology and the Pathological Society of Great Britain & Ireland, 19-22 June 2018, Maastricht, Netherland
- Marie Skłodowska -Curie travel and mobility awards for secondment to AstraZeneca, Cambridge, UK as part of the AIDPATH programme for academia and industry collaborations in digital pathology (Marie Curie Action European Union's FP7 Framework Programme), May- June 2017.
- European Association of Cancer Research (EACR) Meeting Bursary to attend 7th EACR-OECI Joint Training Course: Molecular Pathology Approach to Cancer, 8-10 May 2017, Amsterdam, Netherland

Invited Talks

- **Susanti S,** September 2020, Molecular and tumour microenvironment mapping of colorectal cancer, Expert Webinar Series, School of Pharmacy, Management and Science University, Malaysia.
- **Susanti, S,** 2020, Molecular testing for colorectal cancer, in 5th FUSION (Friday University of Riau Scientific Seminar Online) Series: Current update

on treatment and management of colorectal cancer patients, 28 August 2020, Riau, Indonesia.

- **Susanti S,** 2019, Molecular testing for inherited gastrointestinal cancer, in Jogjakarta Pathology Masterclass: Diagnostic Pathology of Gastrointestinal Tract, Liver, and Pancreas: The Essential of Reporting and Recent Updates, Faculty of Medicine Universitas Gadjah Mada, 6-7 December 2019, Jogjakarta, Indonesia
- **Susanti S,** 2019, Towards useful biomarkers in cancer care: what we learn from colorectal cancer, in Workshop on Towards Cancer Precision Medicine in Indonesia, Ministry of Research and Higher Education of Indonesia, 12-14 March 2019, Jogjakarta, Indonesia

Conference Communication

- **Susanti S,** Pitiot A, Ilyas M, Faux multiplex Immunohistochemistry (fm-IHC) to delineate biomarker territories and biomarker co-localisation in colorectal cancer, Leeds Pathology 2019, 12th Joint Meeting of the British Division of the International Academy of Pathology and the Pathological Society of Great Britain & Ireland, 2-4 July 2019, Leeds, UK (poster)
- Raposo TR, **Susanti S,** Ilyas M, Investigating the Role of TNS4 in the Colorectal Tumour Microenvironment Using 3D Spheroid Models of Invasion, Leeds Pathology 2019, 12th Joint Meeting of the British Division of the International Academy of Pathology and the Pathological Society of Great Britain & Ireland, 2-4 July 2019, Leeds, UK (poster)
- **Susanti S,** Raposo TR, Azad A, et al, Three-dimensional co-culture of colorectal cancer spheroid with cancer-associated fibroblast as a model to study immune cell modulation, EACR25, 25th Biennial Congress of the European Association for Cancer Research, 30 June- 3 July 2018, Amsterdam, Netherland (poster)
- **Susanti S,** Grinevičiūtė RB, Hadjimichael E, et al, Intra-tumour Ki67 expression of colorectal cancer does not associate with the tumour genetic features, Maastricht Pathology 2018, 11th Joint Meeting of the British Division of the International Academy of Pathology and the Pathological Society of Great Britain & Ireland, 19-22 June 2018, Maastricht, Netherland (poster)
- **Susanti S,** Fadhil W, Ebili HO, et al, N_LyST: a simple and rapid screening test for Lynch syndrome, Maastricht Pathology 2018, 11th Joint Meeting of the British Division of the International Academy of Pathology and the

Pathological Society of Great Britain & Ireland, 19-22 June 2018, Maastricht, Netherland (poster)

- Raposo TR, **Susanti S,** Nica R, Pitiot A, Ilyas M, Detection of Tumour-Infiltrating Lymphocytes by Content Based Image Retrieval, Maastricht Pathology 2018, 11th Joint Meeting of the British Division of the International Academy of Pathology and the Pathological Society of Great Britain & Ireland, 19-22 June 2018, Maastricht, Netherland (poster)
- **S. Susanti,** H.O. Ebili, W. Fadhil (presenter), et al, Introducing a New Panel of Markers for Microsatellite Instability (MSI) Detection in Colorectal Cancer by High Resolution Melting Analysis, Belfast Pathology 2017, 10th Joint Meeting of the British Division of the International Academy of Pathology and the Pathological Society of Great Britain & Ireland, 19-22 June 2017, Belfast, North Ireland (oral)
- **Susanti, S.,** Ebili, H.O., Fadhil, W., et al, Detection of Microsatellite Instability in Colorectal Cancer FFPE Tissue using High Resolution Melting (HRM) Analysis: The Potential of a New Panel of MSI Markers, Nottingham Molecular Pathology Node Annual General Meeting, 7 October 2017, Nottingham, UK (poster)

Future Funding

- Investigation of the tumour microenvironment in early-onset colorectal cancers, December 2019-November 2022, Bowel Cancer Research UK, £148,570, Named Researcher.
- Improving Clinical Outcome in Indonesia with a Novel diagnostic test for Colorectal Cancer (ICONICC), February 2020- January 2022, Newton Fund Institutional Links, £113,189, Named Researcher
- ColoMelt-DX: robust and affordable molecular diagnostic tool for colorectal cancer, April 2020-March 2022, STI (Science, Technology and Innovation)-Transform Fund, Islamic Development Bank, $100,000, Principal Investigator

Acknowledgements

Foremost, I would like to express my gratitude to my principal supervisor Professor Mohammad Ilyas for all his support, guidance and encouragement throughout my PhD programme and beyond that, to be such an inspiring and supportive mentor for me as an early career researcher. I also sincerely grateful for Dr. Luisa Martinez-Pomares who not only provide me with academic and technical guidance on the research work but also her pastoral support in the completion of my PhD study. Additionally, I would like to thank Dr. Abhik Mukherjee for his support and input in various aspects of this PhD study, including his wise advices on juggling my research and personal life.

I would extend my gratitude to my colleagues, the current and past member of Molecular Pathology Research Group (PRG) who have provided the technical support during the practical work for this study, in particular Dr. Henry Ebili and Dr. Wakkas Fadhil for support in high-resolution melting analysis (HRMA) and Dr. Teresa Raposo for assistance in generating the lentivirus-transduced colorectal cancer cells. I would also acknowledge the support from Prof. Anna Grabowska and her team (Ms. Pamela Collier and Dr. Phil Clarke with regard to the three-dimensional (3D) co- cell culture work, Dr. Alain Pitiot for the histogenic molecular mapping (HMM) registration, Mr. Ridwan Aji Prasetyo for Matlab coding of fm-IHC (faux multiplex immunohistochemistry) data analysis, Dr. Efthymios Hadjimichael for the colorectal cancer cases review and selection and Dr. Sirina Muntaka for providing the human monocytes and macrophages.

Further, I would convey my deepest appreciation to the Islamic Development Bank (IsDB) who has sponsored my PhD study through the High Technology Merit Scholarship Programme (MSP).

Finally, I would not be able to finish this PhD study without support from my family and friends, especially my mother (Mrs. Nurhayati), my sister (Ms. Nurcahaya), husband (Mr. Ciptoaji) and son (Raihan Abiyyuzahy), who always believe in me and provide me with their unconditional love, patience and understanding.

Above all, praise to Allah who always bestowed me with countless blessing including the completion of this PhD study.

Declaration

This work entitled "Investigating the Interactions between Tumour Cells and the Non tumour Cellular Community in Colorectal Cancer" has been composed by Susanti Susanti, and I confirm that the result presented in this thesis is my own work during my period of study at the University of Nottingham, unless otherwise mentioned. No part of this thesis has been submitted for any degree, diploma or any other type of qualification at any other institution.

Susanti Susanti

Nottingham, August 2020

Table of Contents

ABSTRACT i
Thesis-related Publications, Awards and Future Funding v
Acknowledgements viii
Declaration x
Table of Contents xi
List of Figures xvi
List of Tables xix
List of Abbreviations xxii
1. General Introduction 1
1.1. Colorectal Cancer 2
1.1.1. Overview 2
1.1.2. Aetiology, Staging and Treatment 3
1.1.2.1. Aetiology 3
1.1.2.2. Staging 5
1.1.2.3. Treatment 6
1.1.3. Genetic Alteration 9
1.1.3.1. CIN (Chromosomal Instability) 12
1.1.3.1. Wnt signalling 12
1.1.3.1.2.EGFR (Epidermal Growth Factor Receptor) Signalling 13
1.1.3.1.3. *KRAS* 14
1.1.3.1.4. *BRAF* 15
1.1.3.1.5. PI3KCA and PTEN 15
1.1.3.1.6. *TP53* 17
1.1.3.1.7. Loss of 18q 18
1.1.3.2. MSI (Microsatellite Instability) 19
1.1.3.3. CpG island Methylator Phenotype (CIMP) 20
1.1.4. Consensus molecular subtypes (CMS) 21
1.2. Tumour Microenvironment (TME) 22
1.2.1. Overview 22
1.2.2. Cells of Haematopoietic Origins 23
1.2.2.1. Tumour Infiltrating Lymphocytes (TIL) 23
1.2.2.2. Tumour Associated Macrophages (TAM) 25
1.2.2.3. Myeloid-derived Suppressor Cell (MDSC) 32

1.2.3. Cells of Mesenchymal Origins 33
1.2.3.1. Cancer Associated Fibroblast (CAF) 33
1.2.3.2. Mesenchymal Stem Cells (MSC) 34
1.2.3.3. Endothelial Cells (EC) 36
1.2.4. Extracellular Matrix (ECM) Components 37
1.2.5. Spatial Distribution and Interaction of Tumour Microenvironment Components 38
1.3. Aims and Hypothesis 44
2. Materials and Methods 45
2.1. Colorectal Cases Selection 46
2.2. DNA Preparation 47
2.2.1. Extraction 47
2.2.1.1. Formalin-fixed, paraffin-embedded (FFPE) Tissue 47
2.2.1.2. Colorectal cancer (CRC) cell lines 48
2.2.2. Quantification 48
2.3. Polymerase Chain Reaction (PCR) 49
2.3.1. Detection of Microsatellite Instability (MSI) using Novel Panel of Mononucleotide Markers 49
2.3.1.1. Novel MSI markers identification and screening 49
2.3.1.2. Fluorescence-based PCR with high resolution melting analysis (HRMA) 50
2.3.1.3. Capillary electrophoresis (CE) Analysis for MSI 56
2.3.1.4. Limit of Detection (LOD) of MSI Testing 56
2.3.2. Somatic Mutation Detection 56
2.3.2.1. Target gene selection 56
2.3.2.2. Quick Multiplex Consensus -Polymerase Chain Reaction (QMC-PCR) 57
2.3.2.3. *BRAF* V600E Mutation Detection 58
2.4. Flow cytometry for Ploidy Determination 58
2.4.1. Preparation of nuclei suspension from FFPE tissue 58
2.4.2. Flow cytometry 59
2.4.3. Data analysis 60
2.5. Immunohistochemistry (IHC) and Digital Image Analysis (DIA) of Tumour Microenvironment (TME) Markers 60
2.5.1. Automated immunohistochemistry (IHC) 60
2.5.2. Digital image analysis (DIA) 60
2.5.2.1. Faux multiplex immunohistochemistry (fm-IHC) 60

2.6. Three-dimensional (3D) Spheroid Co-culture 62
2.6.1. CRC cell lines 62
2.6.1.1. Cell lines maintenance 62
2.6.1.2. Passaging cells 62
2.6.1.3. Cell Freezing and Thawing 63
2.6.2. Cancer-associated fibroblast (CAF) culture 64
2.6.2.1. Isolation from colon cancer patient tissue 64
2.6.2.2. Fibroblast cell enrichment 65
2.6.2.3. Fibroblast cell maintenance, passaging, freezing and thawing 65
2.6.3. Lentivirus transduction of fluorescence proteins for CRC cell line and CAF 66
2.6.4. Lentivirus transduction of CD24 gene overexpression 67
2.6.5. Human monocytes and macrophages preparation 68
2.6.6. Spheroid co-culture 69
2.7. Statistical Analysis 70
3. Robust Detection of Microsatellite Instability (MSI) using Novel Panel of Mononucleotide Markers 72
3.1. Introduction 73
3.2. Results 75
3.2.1. Validation of IHC as a marker of MMR function 75
3.2.2. Novel MSI biomarker identification, primer design and PCR optimization 76
3.2.3. Limit of detection (LOD) determination of MSI Testing 78
3.2.4. Testing the New Panel of MSI Markers with HRMA 79
3.3. Discussion 83
4. Molecular Profiling of Colorectal Cancer 86
4.1. Introduction 87
4.2. Results 88
4.2.1. Frequency of oncogene somatic mutation on microsatellite stable (MSS) and microsatellite instable (MSI) 88
4.2.2. Association between *KRAS*, *BRAF* and *PIK3CA* mutation 96
4.2.3. Association between *TP53* mutation with the other driver gene mutations 98
4.2.4. DNA content (ploidy) analysis of microsatellite stable (MSS) and microsatellite instable (MSI) 102
4.3. Discussion 110

5. Cellular Community Profiling of Colorectal Cancer Tumour Microenvironment....116
5.1. Introduction....117
5.2. Results....120
5.2.1. Principles of faux multiplex immunohistochemistry (fm-IHC)....120
5.2.1.1. The rationale of sequential sections and choice of biomarkers....120
5.2.1.2. Image scanning and pre-processing....121
5.2.1.3. Precise image registration and data collection....126
5.2.1.4. Data analysis....127
5.2.2. Cellular community mapping of the colorectal cancer tumour microenvironment.....134
5.2.2.1. MSI and MSS....134
5.2.2.2. *BRAF* mutant and wildtype....135
5.2.2.3. *KRAS* mutation....135
5.2.2.4. *PIK3CA* mutation....136
5.2.2.5. *TP53* mutation....136
5.2.2.6. Diploid vs aneuploid....136
5.3. Discussions....137
6. Three-dimensional (3D) Spheroid Co-Culture Model to Study the Interaction of Cancer Cells with Non-Neoplastic Cells in CRC....146
6.1. Introduction....147
6.2. Results....153
6.2.1. Three-dimensional (3D) spheroid culture of CRC cell lines .153
6.2.2. CRC cell lines and CAF 3D spheroid co-culture....155
6.2.3. The role of monocytes and macrophages 3D spheroid co culture of CRC-CAF.... 163
6.2.4. Utilising the CRC- CAF 3D co-culture to study the role of CD24 in tumour growth....179
6.3. Discussion....182
7. Final Discussion....189
7.1. Introduction....190
7.2. Cardinal Findings....190
7.2.1. Simple and rapid molecular test to detect microsatellite instability (MSI)....190

7.2.2. Positive association of *PIK3CA* mutation with *KRAS* mutation but not *BRAF* mutation in colorectal cancer suggests co-selection is gene specific but not pathway specific 192
7.2.3. Genetic features of colorectal cancer associate with distinct spatial tumour microenvironment landscape 193
7.2.4. Three-dimensional (3D) co-culture model reveals differential response of CRC toward stimuli of CAF and the role of CD24 in modulating CRC proliferation 196
7.3. Future perspective 199
References 204
Supplementary Materials 259

List of Figures

Figure 1.1. Staging of colorectal cancer. 8

Figure 1.2. Adenoma to adenocarcinoma transition of CRC tumorigenesis 11

Figure 1.3. Consensus molecular subtypes of colorectal cancer (CMS). 22

Figure 1.4. Biomarker-guided patient stratification for targeted therapy in colorectal cancer. 43

Figure 2.1. The principles of high-resolution melting analysis (HRMA)..... 55

Figure 3.1. Capillary electrophoresis (CE) analysis of microsatellite markers..... 77

Figure 3.2. Limit of detection of MSI screening by high resolution melting analysis (A) and capillary electrophoresis (B)..... 80

Figure 3.3. Detection of microsatellite instability (MSI) and *BRAF* codon V600E mutation using high-resolution melting analysis (HRMA). 81

Figure 3.4. Interobserver variation between two observers on microsatellite (MSI) detection by high resolution melting analysis (HRMA). 82

Figure 4.1. High-resolution melting analysis (HRMA) of driver gene mutations on colorectal cancer. 93

Figure 4.2. Immunohistochemistry (IHC) of p53 on colorectal cancer. (A) Normal/ low expression staining (B) Strong positive staining and (C) Negative staining on the nucleus of the tumour cells..... 94

Figure 4.3. The derivative melting plot of colorectal tumour that showed double mutation in *KRAS* exon 2 and *BRAF* exon 15.....108

Figure 1.1. Flowcytometry analysis of DNA content (ploidy) on microsatellite instable (MSI) and microsatellite stable (MSS) of colorectal cancer.....108

Figure 5.1. Representative images of two adjacent sections of series of sequential sections used for the faux multiplex immunohistochemistry (fm-IHC). 123

Figure 5.2. Representative images of Histogenic Molecular Mapping (HMM) used in the faux multiplex immunohistochemistry (fm-IHC).....124

Figure 5.3. Faux multiplex immunohistochemistry (fm-IHC) using histology molecular mapping (HMM) for pairwise biomarker co-localization.....131

Figure 5.4. Faux multiplex immunohistochemistry (fm-IHC) using histology molecular mapping (HMM) for three biomarkers co-localization on microsatellite instable (MSI) colorectal cancer. 132

Figure 5.5. Faux multiplex immunohistochemistry (fm-IHC) using histology molecular mapping (HMM) for three biomarkers co-localization on microsatellite stable (MSS) colorectal cancer. 133

Figure 6.1. Live cell brightfield imaging of three-dimensional (3D) co-culture spheroid of colorectal cancer (CRC) cell line, SW480, SW620 and LS1034. ..156

Figure 6.2. Three-dimensional (3D) mono-culture spheroid of colorectal cancer (CRC) cell line, HCT116 expressing Td-Tomato.....158

Figure 6.3. Three-dimensional (3D) mono-culture spheroid of colorectal cancer (CRC) cell line, DLD-1 expressing Td-Tomato. 160

Figure 6.4. The growth of three-dimensional (3D) mono-culture spheroid of colorectal cancer (CRC) cell line measured as relative fluorescence unit (RFU). 161

Figure 6.5. Live-cell fluorescence imaging of three-dimensional (3D) mono-culture spheroids of colorectal cancer (CRC) cell line, HCT116 and DLD-1, and cancer-associated fibroblast (CAF). 164

Figure 6.6. Live-cell brightfield imaging of three-dimensional (3D) co-culture spheroid of colorectal cancer (CRC) cell line, HCT116, and cancer-associated fibroblast (CAF). 165

Figure 6.7. Live-cell fluorescence imaging of three-dimensional (3D) co-culture spheroid of colorectal cancer (CRC) cell line, HCT116, and cancer-associated fibroblast (CAF). 166

Figure 6.8. Live-cell brightfield imaging of three-dimensional (3D) co-culture spheroid of colorectal cancer (CRC) cell line, DLD-1, and cancer-associated fibroblast (CAF). 167

Figure 6.9. Live-cell fluorescence imaging of three-dimensional (3D) co-culture spheroid of colorectal cancer (CRC) cell line, DLD-1, and cancer-associated fibroblast (CAF). 168

Figure 6.10. Growth of three-dimensional (3D) co-culture spheroid of colorectal cancer (CRC) cell line, HCT116, and cancer-associated fibroblast (CAF). 169

Figure 6.11. Growth of three-dimensional (3D) co-culture spheroid of colorectal cancer (CRC) cell line, DLD-1, and cancer-associated fibroblast (CAF). 170

Figure 6.12. Growth of three-dimensional (3D) co-culture spheroid of colorectal cancer (CRC) cell line, HCT116, and cancer-associated fibroblast (CAF) in the present of monocytes. 171

Figure 6.13. Growth of three-dimensional (3D) co-culture spheroid of colorectal cancer (CRC) cell line, DLD-1, and cancer-associated fibroblast (CAF) in the present of monocytes. 172

Figure 6.14. Growth of three-dimensional (3D) co-culture spheroid of colorectal cancer (CRC) cell line, HCT116, and cancer-associated fibroblast (CAF) in the present of macrophages. 173

Figure 6.15. Growth of three-dimensional (3D) co-culture spheroid of colorectal cancer (CRC) cell line, DLD-1, and cancer-associated fibroblast (CAF) in the present of macrophages. 174

Figure 6.16.Live cell brightfield imaging of three-dimensional (3D) multicellular co-culture spheroid of colorectal cancer (CRC) cell line with cancer-associated fibroblast (CAF) and monocytic cells. 175

Figure 6.17. Live-cell fluorescence imaging of three-dimensional (3D) multicellular co-culture spheroid of colorectal cancer (CRC) cell line, HCT116, with cancer-associated fibroblast (CAF) and monocytes. 176

Figure 6.18. Live-cell fluorescence imaging of three-dimensional (3D) multicellular co-culture spheroid of colorectal cancer (CRC) cell line, DLD-1, with cancer-associated fibroblast (CAF) and monocytes. 177

Figure 6.19. Expression of CD24 protein following the lentivirus transduction. 180

Figure 6.20. The role of CD24 on the growth of spheroids of CRC cell line, HCT116 with and without cancer-associated fibroblast (CAF). The CRC cells were stably transduced by lentivirus with FUGW plasmid (control) and CD24 gene overexpression. 181

Figure S.1. The Growth of three-dimensional (3D) co-culture spheroid of colorectal cancer (CRC) cell line, HCT116, and cancer-associated fibroblast (CAF). 293

List of Tables

Table 1.1. The 8th edition of the American Joint Committee on Cancer Staging System for colon and rectum cancer (AJCC, 2017). 7

Table 1.2. Genetic biomarkers of colorectal cancer with associated tumour microenvironment characteristic and its clinical significance 27

Table 2.1. Colorectal cancer cell lines characteristics 52

Table 2.2. Mononucleotide repeat microsatellite markers 53

Table 2.3. List of primers for polymerase chain reaction of microsatellite instability and driver genes mutation detection using high-resolution melting analysis..... 54

Table 2.4. Tumour microenvironment markers for immunohistochemistry 61

Table 3.1. Sensitivity and specificity of mononucleotide repeat microsatellite markers 78

Table 4.1. Pattern of p53 immunohistochemistry staining on colorectal cancer 94

Table 4.2. Frequency of driver gene mutations in the Nottingham cohort of colorectal cancer..... 96

Table 4.3. Frequency and association of *KRAS* and *BRAF* mutation in the Nottingham cohort of colorectal cancer..... 99

Table 4.4. Frequency and association of *KRAS* and *PIK3CA* mutation in the Nottingham cohort of colorectal cancer. 100

Table 4.5. Frequency and association of *BRAF* and *PIK3CA* mutation in the Nottingham cohort of colorectal cancer 101

Table 4.6. Frequency and association of *BRAF* exon 15 and *PIK3CA* mutation in the Nottingham and Edinburgh cohort of colorectal cancer 102

Table 4.7. Frequency and association of *TP53* mutation and various hotspots of other driver gene mutations in the Nottingham cohort of colorectal cancer104

Table 4.8. Frequency and association of *TP53* mutation and combined mutations of other driver genes in the Nottingham cohort of colorectal cancer.....105

Table 4.9. Frequency and association of ploidy status, microsatellite instability and various hotspots of driver gene mutations in the Nottingham cohort of colorectal cancer 105

Table 4.10. Frequency and association of ploidy status and combined mutations of the driver genes in the Nottingham cohort of colorectal cancer.....107

Table 5.1. Cellular and functional markers to map tumour microenvironment in the Nottingham cohort of colorectal cancer 125

Table 5.2. Significant spatial density of cellular community and their functional properties of tumour microenvironment in the Nottingham cohort of colorectal cancer 138

Table 5.3. Significant spatial pairwise correlation of cellular community of tumour microenvironment in the Nottingham cohort of colorectal cancer 140

Table S.1. The epithelial density of tumour microenvironment cellular community in the Nottingham cohort of colorectal cancer 260

Table S.2. The non-epithelial/ stromal density of tumour microenvironment cellular community in the Nottingham cohort of colorectal cancer 261

Table S.3. The whole tissue section (WTS) density of tumour microenvironment cellular community in the Nottingham cohort of colorectal cancer 262

Table S.4. Statistical analysis on pairwise biomarker correlations in the Nottingham cohort of colorectal cancer based on microsatellite instability (MSI) status 263

Table S.5. Statistical analysis on pairwise biomarker correlations in the Nottingham cohort of colorectal cancer based on *BRAF* mutation 264

Table S.6. Statistical analysis on pairwise biomarker correlations in the Nottingham cohort of colorectal cancer based on *KRAS* mutation 265

Table S.7. Statistical analysis on pairwise biomarker correlations in the Nottingham cohort of colorectal cancer based on *PIK3CA* mutation 266

Table S.8. Statistical analysis on pairwise biomarker correlations in the Nottingham cohort of colorectal cancer based on *TP53* mutation.....267

Table S.9. Statistical analysis on pairwise biomarker correlations in the Nottingham cohort of colorectal cancer based on ploidy status 268

Table S.10. Statistical analysis on pairwise biomarker correlations in the Nottingham cohort of microsatellite and chromosomal stable colorectal cancer of 269

Table S.11. The whole tissue section (WTS) density of proliferating tumour microenvironment cellular community in the Nottingham cohort of colorectal cancer 270

Table S.12. The epithelial density of proliferating tumour microenvironment cellular community in the Nottingham cohort of colorectal cancer.....271

Table S.13. The non-epithelial/ stromal density of proliferating tumour microenvironment cellular community in the Nottingham cohort of colorectal cancer 272

Table S.14. The whole tissue section (WTS) density of BCL-2 expression within the tumour microenvironment cellular community in the Nottingham cohort of colorectal cancer 273

Table S.15. The epithelial density of proliferating tumour microenvironment cellular community in the Nottingham cohort of colorectal cancer.....274

Table S.16. The non-epithelial/ stromal density of proliferating tumour microenvironment cellular community in the Nottingham cohort of colorectal cancer 275

List of Abbreviations

3-D	Three-dimensional
5-FU	Fluorouracil
α-SMA	α-smooth muscle actin
AJCC	America Joint Committee on Cancer
AKT	Protein kinase B
ANOVA	Analysis of variance
APC	Adenomatous polyposis coli
AREG	Amphiregulin
BAX	BCL2-Associated X Protein
BM	Basement membrane
bp	Base pair
BRAF	v-Raf murine sarcoma viral oncogenes homolog B
BSA	Bovine Serum Albumin
CAF	Cancer-associated fibroblast
Cas9	CRISPR-associated nuclease 9
CBFA1	Core-binding factor alpha 1
CCL2/4	C-C motif ligand 2/5
CDX2	Caudal Type Homeobox 2
CE	Capillary electrophoresis
CEA	carcinoembryonic antigen
CIMP	CpG island methylator phenotype
CIN	Chromosome instability
CNA	Copy number alteration
CMS	Consensus molecular subtype
CRA	Colorectal adenoma
CRC	Colorectal cancer
CRCC	Colorectal Cancer Subtyping Consortium
CRISPR	Clustered regularly interspaced short palindromic repeats
CRUK	Cancer Research United Kingdom
CSF-1	Colony Stimulating Factor-1
CT	Core tumour
CTLA-4	Cytotoxic T-lymphocyte-associated protein 4
CTNNB1	Catenin beta 1

CXCL	CXC-chemokine ligand
DCC	Deleted in colorectal carcinoma
DDRs	Discoidin Domain Receptors
DFS	Disease free survival
DI	DNA index
DIA	Digital image analysis
DSS	Disease specific survival
DMEM	Dulbecco's Modified Eagle's Medium
dMMR	Deficient Mismatch Repair
DNA	Deoxyribonucleic Acid
EC	Endothelial Cell
ECM	Extracellular matrix
EDI	Ecosystem diversity index
EDTA	Ethylene Diamine Tetraacetic Acid
EGF	Epidermal growth factor
EGFR	Epidermal growth factor receptor
EMT	Epithelial to mesenchymal transition
EREG	Epiregulin
ERK	Extracellular-signal-regulated kinase
ESMO	European Society of Medical Oncology
EV	Empty vector
EWSR1	EWS RNA Binding Protein 1
FAK	Focal adhesion kinase
FAP	Familial adenomatous polyposis
FAP	Fibroblast activation protein
FAS-APO1	Fas- apoptosis antigen 1
FBS	Foetal bovine serum
FBXW1	F-box/WD repeat-containing protein 1
FFPE	Formalin-Fixed Paraffin-Embedded
FGF2	Fibroblast growth factor 2
FLA	Fragment length analysis
FLRF	Fetal liver ring finger
FOLFIRI	5-Fluorouracil (5-FU)/folinic acid and irinotecan
FOLFOX	Folinic acid (Leucovorin) Flourouracil (5-FU) and Oxaliplatin (Eloxatin)

FRMD6	FERM domain containing 6
GFP	Green fluorescent protein
GM-CSF	Granulocyte-macrophage colony-stimulating factor
GTP	Guanosine 5’ triphosphate
HB-EGF	heparin-binding EGF-like growth factor
HER2	Human epidermal growth factor
HPNCC	Hereditary nonpolyposis colorectal cancer
HLA	Human Leukocyte Antigen
HMM	Histogenic molecular mapping
HRMA	High resolution melting analysis
HTR2B	5-Hydroxytryptamine Receptor 2B
IBD	Inflammatory bowel disease
IDO	indoleamine 2,3-dioxygenase
IF	Immunofluorescent)
IFN	interferon
IGF1	Insulin-like growth factor 1
IHC	Immunohistochemistry
IL	Interleukin
ILK	Integrin-linked kinase
IM	Invasive margin
iNOS	Nitric oxide synthase
ITGB3	Integrin beta-3
JAK2	Janus kinase 2
KRAS	Kirsten rat sarcoma viral oncogene homolog
KER	Cytokeratin
LAM3	Laminin subunit alpha 2
LNA	Locked nucleic acid
LOD	Limit of Detection
LOH	Loss of heterozygosity
M	Mutant
MACS	Microsatellite and chromosomal stable
MAPK	Mitogen activated protein kinase
M-CSF	Macrophage colony-stimulating factor
MDM2/4	Murine/Human Double Minute 2/4
MDSC	Myeloid-derived Suppressor Cell
MGMT	O-6-Methylguanine-DNA Methyltransferase

MSC	Mesenchymal Stem Cells
Min	Minute
miRNA	MicroRNA
MLH1/2	MutL Homolog 1/2
MMP	Matrix metalloproteases
MMR	Mismatch Repair
MOI	Multiplicity of infection)
MSH2/3/6	MutS homolog 2/3/6
MSI	Microsatellite instability
MSI-H	MSI-High
MSS	Microsatellite stable
NCI	National Cancer Institute
NICE	National Institute of Clinical and Healthcare Excellence
NGF	Nerve growth factor
NGS	Next Generation Sequencing
NO	Nitric oxide
NRAS	Neuroblastoma RAS viral oncogene homolog.
OS	Overall survival
P53	Tumour protein 53
PBS	Phosphate buffered saline
PCR	Polymerase chain reaction
PD-1	Programmed cell death protein 1
PDGFR	Platelet-derived growth factor receptor
PD-L1	Programmed death-ligand 1
PDM	Pre-diagnostic Multiplex
PFS	Progression free survival
PI3K	Phosphatidylinositol 3-Kinase
PIK3CA	Phosphatidylinositol-3-kinase Catalytic Alpha
PIP2/3	phosphatidylinositol 4,5 biphosphate-3
pMMR	Proficient Mismatch Repair
PMS2	PMS1 Homolog 2
POLE	Polymerase epsilon.
PTEN	Phosphatase and tensin homolog
QMC	Quick-multiplex consensus
RAF	Rapid Accelerated Fibrosarcoma
RAS	Rat Sarcoma

RFU	Relative fluorescence unit
RNA	Ribonucleic Acid
ROS	Reactive oxygen species
RTK	Receptor tyrosine kinase
SNA	single nucleotide alteration
SMAD2/4	Mother Against Decapentaplegic homolog 2/4
SSD	Specific single diagnostic
STAT3	Signal transducer and activator of transcription factor 3
STR	Short tandem repeat
TAM	Tumour-associated macrophages
Ta	Annealing temperature
TCF/LEF	T-cell Factor/ lymphoid enhancer factor
TCGA	The Cancer Genome Atlas
TGF-α/β	Transforming growth factor alpha/beta
TGFBR2	Transforming growth factor beta receptor 2
TME	Tumour microenvironment
TMN	Tumour metastasis node
TNC	Tenascin-C
TNF	Tumour necrosis factor
TP53	Tumour protein p53
Treg	Regulatory T cell
UICC	Union of International Cancer Control
UK	United Kingdom
USA	United States of America
VEGFA/B	Vascular endothelial growth factor A/B
WHO	World Health Organization
WT	Wild type
WTS	Whole tissue section
XELOX	Capecitabine (Xeloda) and oxaliplatin
ZEB1	Zinc-finger E-box binding homeobox

1. General Introduction

1.1. Colorectal Cancer

1.1.1. Overview

Colorectal cancer (CRC) is one of the leading causes of cancer-related mortality. The estimated incidence of CRC worldwide in 2018 was about 1.8 million cases, comprising 11% of all cancer diagnosis, with approximately 881,000 deaths making it the 2nd deadliest cancer worldwide (Bray, et al., 2018). There were 41,112 new cases of CRC in the UK (United Kingdom) in 2013 with 56 % of the cases being men and 44 % being women, according to CRUK (Cancer Research UK). To date, in the UK, CRC is the fourth most common cancer and accounts for approximately 12 % of all new cases (www.cancerresearchuk.org/health-professional/cancer-statistics/statistics-by-cancer-type/bowel-cancer, May 2020).

Globally, there is a trend of increased incidence and mortality of CRC in less developed countries whereas in more developed countries such as Canada, USA (United States of America), UK, Singapore, and Japan, there has been a drop-in mortality due to improved treatment options and early detection efforts (such as colonoscopy, flexible sigmoidoscopy, computed tomography colonography, faecal immunochemistry, and faecal occult blood testing) which allow the removal of pre-cancerous or early stage malignant polyps (Arnold, et al, 2017; Rawla, et al, 2019). In the USA, relative survival at 5 years were 90% for localized disease, 70% for regional disease, and 12% for distant metastatic disease (Edwards, et al, 2010). Similarly, in the UK, 92% people with CRC will survive their disease for 5 years or more if the disease was diagnosed at its early stage, compared with only 10% people when the disease is diagnosed at the latest stage (CRUK, 2016).

1.1.2. Aetiology, Staging and Treatment

1.1.2.1. Aetiology

It is well established that CRC develops slowly over the years and arises from the epithelial linings of colon/rectum wall. Normal epithelial cells initially develop into benign or pre-malignant polyps (called adenomas) before becoming malignant (adenocarcinoma) in 10-20 years (Steward, et al, 2006). Like other type of cancers, the pathogenesis of CRC is characterised by the accumulation of mutations in tumour suppressor genes/ oncogenes.

Several risk factors have been associated with colorectal cancer, categorised into modifiable and non-modifiable (Johnson, et al, 2013; Taunk and Calderwood, 2015). Modifiable risk factor includes lifestyle-related risks that can be avoided such as smoking, alcohol consumption, ionising radiation, obesity and dietary (red and processed meat), whereas non-modifiable risk factors are uncontrollable factors including increasing age, personal history of inflammatory bowel disease and genetic inheritance (Haggar and Boushey, 2009; Edwards *et al.*, 2010; Tarraga-Lopez, et al, 2014). Known predisposition including hereditary genetic disorders such as LS (Lynch syndrome) and familial FAP (adenomatous polyposis) and chronic intestinal inflammation such as Inflammatory Bowel Disease (IBD) in total account for about 20 % of CRC cases (Bardhan and Liu, 2013).

More than 90% of colorectal cancer cases occur in people aged 50 or older and the incidence rate is more than 50 times higher in persons aged 60 to 79 years than in those younger than 40 years (Haggar and Boushey, 2009). Interestingly, there is global increase of the proportion of young people (<50 years old) being diagnosed with CRC (You, et al, 2012; Murphy, et al, 2017). CRC in young patients has been reported to be associate with left-sided, more

advance and metastatic disease (Chang, et al, 2012; Fu, et al, 2014; Wang, et al, 2015). However, conflicting results were reported on survival outcome of the young patients as compared to the older patients. While some research showed worse survival, a reasonable portion of studies described similar or even better survival of young and older patients of CRC (Wang, et al, 2015; Khan, et al, 2016; Rho, et al, 2017).

Although predisposed to numerous types of cancers (such as ovaries, endometrial, stomach, small intestine), LS, also known as HPNCC (hereditary nonpolyposis colorectal cancer), is the most common genetic syndrome that causes CRC, accounting for 4-6% of total cases (Jasperson, et al, 2010). In LS, the lifetime risk of developing CRC is 66% in men and 43% in women with median age at diagnosis of 42 years and 47 years, respectively (Stoffel, et al, 2009). Inactivating germline mutation of the DNA MMR (mismatch repair) gene including *MLH1*, *MLH2*, *MSH2*, *MSH3*, *MSH6* or *PMS2* are reported to be responsible for the LS (Lynch & de la Chapelle, 1999). Accelerated carcinogenesis commonly occurs in the case of LS, in which a tiny colonic adenoma may emerge as a carcinoma within 2 to 3 years, as opposed to more than 10 years this process may take in the general population, thus putting it as a risk factor for CRC to develop in young people (Jass & Stewart, 1992; Lynch & de la Chapelle, 1999). In contrast to general feature of CRC in young patients, CRC arising from LS (although usually occurs in younger age) were located on the right side of the colon and develop from adenomas that tend to be larger with high-grade dysplasia and/or villous histology in comparison to sporadic adenomas (Lynch & de la Chapelle, 1999; Kwak & Chung, 2007).

Adenomatous polyposis (FAP) is the second most common predisposing genetic syndrome, accounting for about 1% of CRC, in which, for these individuals, the lifetime risk of CRC approaches 100% without intervention such as colectomy (Jasperson, et al, 2010). Inherited mutation of the *APC* (adenomatous polyposis

coli) tumour suppressor gene has been reported as the main genetic event that is responsible for the FAP, characterised by multiple colonic adenomas occurring at an early age, occasionally during the preteen years, and proliferating throughout the colon, with malignant change in most patients by the age of 40 to 50 years (Lynch & de la Chapelle, 1999).

Inflammatory Bowel Disease (IBD) represents a group of intestinal disorders that cause prolonged inflammation of the digestive tract. it is well-recognised that patients with IBD, such as UC (ulcerative colitis) and Crohn's disease, are at increased risk of developing colitis-associated CRC that correlates with the extent and duration of the inflammation (Freeman, et al, 2008; Kim, et al, 2014; Adami, et al., 2016). It was estimated that 18% of patients with a 30-year history of ulcerative colitis will develop CRC (Aedan, et al, 2001).

1.1.2.2. Staging

The histopathology based TNM (Tumour-Node-Metastasis) approach described by the UICC (Union of International Cancer Control) has been applied as a consensus to classify CRC into 4 main stages (with several substages), which determine the disease prognosis and patient treatment (IUCC, 2009). The TNM staging system is described in figure 1.1 and table 1.1. This system has been largely used to replace the earlier system, Dukes' stages, which was introduced by Cuthbert Dukes in 1932 and its modifications including Astler-Coller's classification (Dukes, 1932; Astler & Coller, 1954). The initial Dukes' staging described rectal cancer, yet it was widely applied for the entire colon, into 3 categories; Dukes A indicates a tumour confined in the mucosa, whilst Dukes B describes the invasion through the bowel wall and penetration of the muscularis propria and Dukes C describes the involvement of the lymph node (Dukes, 1932). Subsequently, several staging methods were introduced to modify the initial Dukes system, such as addition of Dukes D to describe the presence of

distant metastasis (Astler & Coller, 1954; Fitzgerald, 1982; Haq, et al, 2009; Akkoca, et al, 2014). Nonetheless, the most recent guidelines from the Royal College of Pathologists follow the TNM system and does not include the Dukes' staging anymore (https://www.rcpath.org/uploads/assets/c8b61ba0-ae3f-43f1-85ffd3ab9f17cfe6/G049-Dataset-for-histopathological-reporting-of-colorectal-cancer.pdf, August, 2020).

1.1.2.3. Treatment

Based on a guideline published by ESMO (European Society of Medical Oncology), the main treatment for CRC patients with primary CRC at all stages (stage 1-3) are resection and anastomosis which can be followed by adjuvant therapy with chemotherapeutic agents such as the combination of oxaliplatin and 5-FU (5-Fluorouracil)/folinic acid (FOLFOX) or Capecitabine and oxaliplatin (XELOX) for the high-risk patients (stage 2-3) (Labianca, et al., 2010). The ESMO recommendation for unresectable metastatic CRC patients (stage 4) included the use of standard chemotherapy combinations, FOLFOX or XELOX, or combination of 5-FU)/folinic acid and irinotecan (FOLFIRI) as well as the addition of biological targeted agents such as bevacizumab, a monoclonal antibody against VEGF-A (vascular endothelial growth factor-A) and aflibercept (anti VEGF-A, B and placenta growth factor) (Van Cutsem, et al., 2014). Moreover, the ESMO guideline also suggested the use of anti EGFR (epidermal growth factor receptor) such as cetuximab and panitumumab for metastatic CRC patients with wildtype *KRAS*, either as a single agent or in combination with any chemotherapy regimen, except bevacizumab (Van Cutsem, et al., 2014). Despite being used in most of the regimen, it is been reported that the MSI (microsatellite instability) tumour has poor response to 5-FU therapy (Ribic, et al., 2003; Guetz, et al, 2009; Schmoll,et al, 2012; Webber, et al, 2015).

Table 1.1. The 8th edition of the American Joint Committee on Cancer Staging System for colon and rectum cancer (AJCC, 2017)

Stage	T	N	M	Dukes	Modified Astler-Coller
0	Tis	N0	M0	-	-
I	T1	N0	M0	A	A
	T2	N0	M0	A	B1
IIA	T3	N0	M0	B	B2
IIB	T4a	N0	M0	B	B2
IIC	T4b	N0	M0	B	B2
IIIA	T1-T2	N1//N1c	M0	C	C1
	T1	N2a	M0	C	C1
IIIB	T3-T4a	N1//N1c	M0	C	C2
	T2-T3	N2a	M0	C	C1/C2
	T1-T2	N2b	M0	C	C1
IIIC	T4a	N2a	M0	C	C2
	T3-T4a	N2b	M0	C	C2
	T4b	N1-N2	M0	C	C3
IVA	Any T	Any N	M1a	-	-
IVB	Any T	Any N	M1b	-	-
IVC	Any T	Any N	M1c	-	-

Primary Tumour (T)

Tx	Primary tumour cannot be assessed
T0	No evidence of primary tumour
Tis	Carcinoma in situ: intraepithelial or invasion of lamina propria
T1	Tumour invades submucosa
T2	Tumour invades muscularis propria
T3	Tumour invades through the muscularis propria into peri colorectal tissues
T4a	Tumour penetrates to the surface of the visceral peritoneum
T4b	Tumour directly invades or is adherent to other organs or structures

Regional Lymph Nodes (N)

Nx	Regional lymph nodes cannot be assessed
N0	No regional lymph node metastasis
N1	Metastasis in 1–3 regional lymph nodes
N1a	Metastasis in one regional lymph node
N1b	Metastasis in 2–3 regional lymph nodes
N1c	Tumour deposit(s) in the subserosa, mesentery, or nonperitonealized pericolic or perirectal tissues without regional nodal metastasis
N2	Metastasis in 4 or more regional lymph nodes
N2a	Metastasis in 4–6 regional lymph nodes
N2b	Metastasis in 7 or more regional lymph node

Distant Metastasis (M)

M0	No distant metastasis
M1	Distant metastasis
M1a	Metastasis confined to one organ or site (for example, liver, lung, ovary, nonregional node
M1b	Metastases in more than one organ/site
M1c	Peritoneal metastases with or without metastasis of other organs

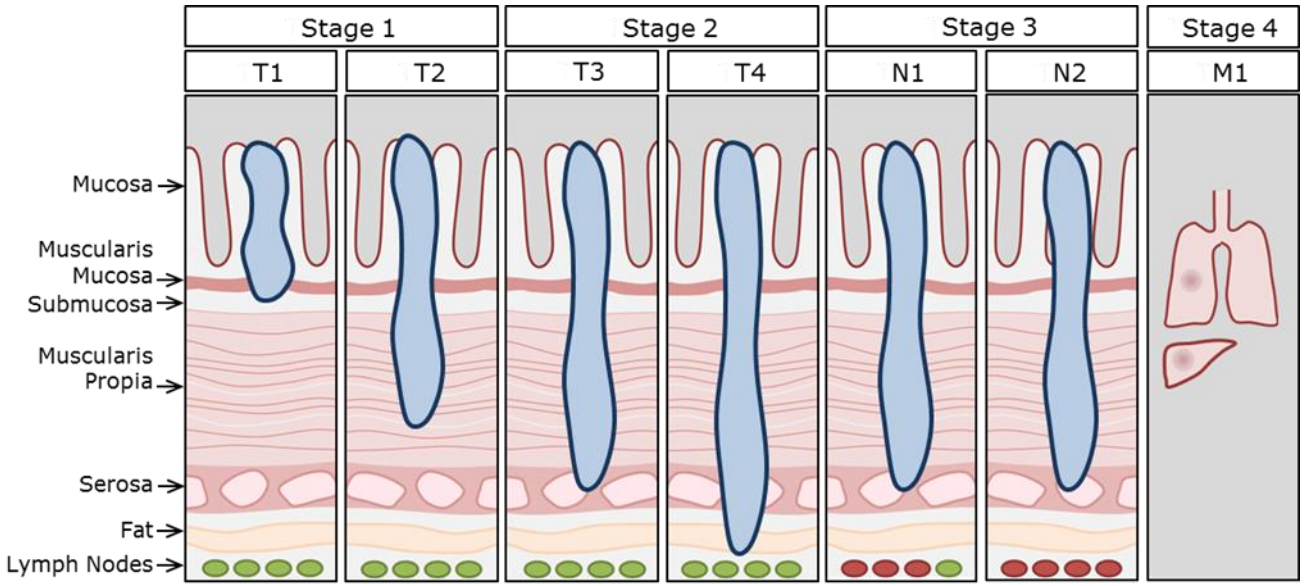


Figure 1.1. Staging of colorectal cancer. Adopted from Dipiro, et al, 2014, Colorectal Cancer, Pharmacotherapy: *A Pathophysiologic Approach 9th ed*.

1.1.3. Genetic Alteration

Colorectal tumour develops along a variety of different genetic pathways, which may be closely linked to the clinical features of the disease such as prognosis and response to the treatment (Brenner et al., 2014). In 1990, Fearon and Vogelstein were first to propose a genetic model for CRC tumorigenesis, describing it as a series of genetic alteration as depicted in Figure 1.2. It has been reported that mutation in the *APC* gene occurs in the very earliest stage of tumorigenesis resulting in hyperproliferation of gut epithelium, which subsequently develops into adenoma. This process involves the" two-hit" loss of tumour suppressor function (through somatic mutation of one APC allele and loss of the wild type allele) in combination with mutational activation of oncogenes, such as the RAS family (Fearon & Vogelstein, 1990; Pino & Chung, 2010). Further mutation and allelic deletion of genes on chromosomes 17p (*TP53)* and 18q (*SMAD2, SMAD4)*, have been suggested to contribute to the transformation of late-stage adenoma to carcinoma. Conversion of a normal cell to a carcinoma requires the accumulation of mutation on at least four to five genes which are the key genes controlling the cell cycle, intracellular signalling, and apoptosis (Fearon & Vogelstein, 1990). The transformation of the epithelial cells has been proposed to modulate the functions of stromal cells into favouring cancer cell growth, survival, invasion, and metastasis (Peddareddigari, et al, 2010). In fact, the new theory of Evo-Eco Index suggests that a tumour should be classified based on the "evolutionary" attributes of the cancer cell, which includes the change of cancer heterogeneity over the time, and the "ecology" attributes of the surrounding microenvironment (Maley, et al, 2017).

It is well postulated that the transition of adenoma to carcinoma is determined by the acquisition of the essential sequence of driver mutations which implies

that adenoma and carcinoma should differ by the presence of specific driver mutation. However, emerging research show some possibilities other than the classical model of Vogelstein. Recently, a study by Cross and colleagues (2018) suggests that CRC progression from adenoma to carcinoma does not necessarily led by the rigorous/ sequential driver mutations and may involves punctuated evolution. In this study, the evolutionary landscape of CRA (colorectal adenoma) were compared to carcinoma and the findings reveal that CRA can also harbour mutations in some of the essential driver genes and it occurs not particularly in conventional order (Cross, et al, 2018). This study showed that with the limitation of sample size, CRA showed a similar somatic burden on SNA (single nucleotide alteration) including indel (insertion and deletion) that cover tier 1 mutations (the pathogenic CRC driver genes such as APC, *KRAS*, *BRAF*, *TP53*, SMAD3, SMAD4) and tier 2 mutations (uncertain pathogenic changes in CRC or pan-cancer driver genes), although higher somatic CNA (copy number alteration) due to chromosomal gain or loss was higher in the carcinoma. CRA, in which distinct genotype-phenotype combination of could co-exist, were found to be more heterogeneous genetically compared to CRC. Yet, as speculated by the authors, colon carcinoma apparently does not need to arise from the sub-clone with the greatest number of driver mutation and adenoma evolution is undulating in a punctuated fashion. Moreover, this study shows that CRC topologies were often characterised by long trunks (variants ubiquitous across biopsies) with comparatively short branches and leaves (relatively few sub-clonal variants), thus appearing 'palm tree-shaped'. In more established carcinoma, positive selection of almost all driver mutations appeared on the phylogenetic trunk, suggesting the weak sub-clonal selection and indicative to the stabilising selection. This report refines the Vogelstein model and support the theory of "big-bang" model of CRC proposed earlier (Sottoriva, et al, 2015).

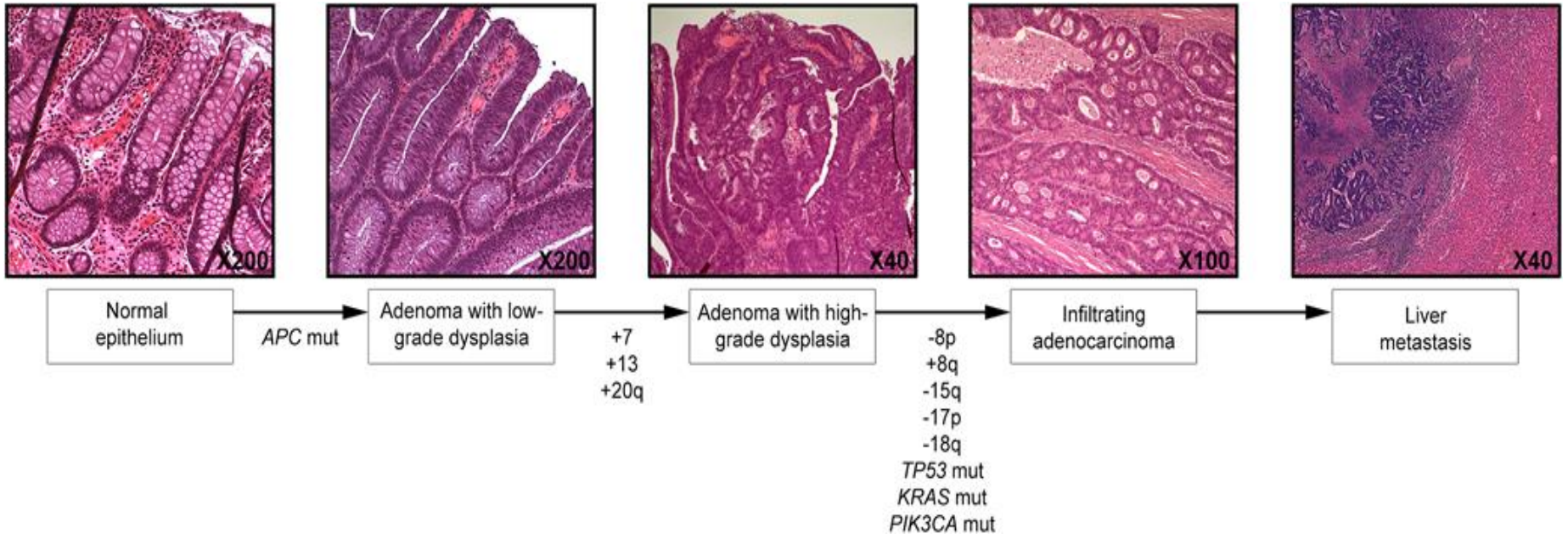


Figure 1.2. Adenoma to adenocarcinoma transition of CRC tumorigenesis. Initiating APC mutation is present in most low-grade adenomas. Chromosomal instability affecting chromosome 7,13 and 20q with additional genomic imbalance of many important oncogenes, such as *TP53*, *KRAS*, *PIK3CA* and loss of tumour suppressor genes such as SMAD3/4 encodes within the chromosome 18q, result in transition of adenoma to adenocarcinoma with invasive phenotype. Histological sections are representative images stained with haematoxylin and eosin (H&E). Adopted from Reid, et al, 2019, The landscape of genomic copy number alteration in colorectal cancer and their consequences on gene expression levels and disease outcome*, Molecular Aspects of Medicine 69*, pp. 48-61.

While CRC carcinogenesis is very complex, some of genetic features of CRC have been reported to show significant clinical values as prognostic and predictive factor, as summarized in table 1.2. The section below highlights some of the genetic variations that represent the main molecular pathways of CRC and could contribute to patient stratification, which are CIN (chromosomal instability), MSI and CIMP (CpG Island Methylator Phenotype)

1.1.3.1. CIN (Chromosomal Instability)

Chromosomal instability (CIN) is the traditional adenoma-carcinoma trail and still considered the major pathway for the development of sporadic CRC. It is also known as the canonical pathway in CRC carcinogenesis.

1.1.3.1.1. Wnt signalling

As has been known for many years, about 85% of sporadic CRC cases were categorized as CIN as they showed frequent structural changes of the chromosomes as well as aneuploidy (Lengauer, et al, 1997; Grady, 2004). The CIN subtype follows the classical Fearon and Vogelstein model of CRC tumorigenesis. It primarily starts with protein truncating mutations in the *APC* suppressor gene located in chromosome 5q, which leads to aberrant Wnt activation, the major proliferation pathway regulating renewal of colorectal epithelium (Rowan, et al, 2000). APC is a component protein complex that targets cytoplasmic β-Catenin for degradation. In most sporadic cases, frameshift and nonsense mutations of *APC* gene lead to premature protein degradation which subsequently inhibits the APC- β-Catenin complex, result in free β-Catenin to translocate to the nucleus. There is forms a transcriptional activating complex with TCF/LEF transcription factors and activates transcription of many genes. β-Catenin is central to activation of Wnt signalling pathway (Polakis, 2007).

Multiple cellular functions are affected by the Wnt target genes such as regulators of cell cycle progression (c-myc and cyclin D1), cell proliferation, angiogenesis, and apoptosis (Behrens, 2005). As well as *APC*, mutation in some other genes, such as *AXIN1/2* and β-catenin, have been reported as Wnt activating mutations although in a smaller frequency (5-6%) of CRC (Kitaeva, et al, 1997; Samowitz, et al, 1999; Schatoff, et al, 2007; Mazzoni & Fearon, 2014). In majority of cases, following the APC mutation, multiple independent somatic mutation of key driver genes occur that are critical for tumour progression and/or maintenance (Table 1.2).

Recently, it has also been discovered that RSPO (R-spondin) / RNF43 / ZNRF3 is an alternative method of activating Wnt signalling. Membrane E3 ligase ZNRF3 and RNF43 are critical negative feedback regulators of the Wnt pathway, which function through promoting ubiquitination and degradation of Wnt receptors. R-spondin proteins (RSPO1-4) serve as natural antagonists of ZNRF3/RNF43. To maintain strong and sustained Wnt/β-catenin signalling, cancers need to overcome ZNRF3/RNF43-mediated feedback inhibition. Indeed, mutations of RNF43/ZNRF3 and recurrent translocations of RSPO2/RSPO3 have recently been identified in various cancers. Significantly, genetic alterations in RNF43/ZNRF3/RSPO2/RSPO3 have shown promise as predictive biomarkers in pre-clinical models for the efficacy of upstream Wnt inhibitors (Hao, et al, 2016)

1.1.3.1.2. EGFR (Epidermal Growth Factor Receptor) Signalling

In addition to the Wnt pathway, EGFR pathway is also recognised as an important player in CRC pathogenesis. The EGFR is a transmembrane glycoprotein that belongs to the ErbB family member RTK (receptor tyrosine kinase). It has an extracellular ligand binding domain and an intracellular tyrosine-kinase domain (Scaltriti and Baselga, 2006; Krasinskas, 2011). The binding of EGFR to its ligand which include EGF (epidermal growth factor), TGF

(transforming growth factor) -α, EREG (epiregulin), betacellulin, HB-EGF (heparin-binding EGF-like growth factor), AREG (amphiregulin), epigen, heregulin, and neuregulins 1-4, induces the phosphorylation of various intracellular tyrosine kinase components which activate two main downstream signalling pathways; MAPK (mitogen activated protein kinase) pathway and the PI3K (phosphatidylinositol-3-kinase)/ AKT (phosphatidylinositol-3-kinase) pathway, that are important in tumour promoting growth, progression and survival (Yarden & Sliwkowski, 2001; Hynes & Kane, 2005; Khan, et al, 2019). The upregulation of EGFR is found in significant proportion of CRC (30-70%) and been associated with poorer prognosis, particularly in metastatic disease (Mayer, et al, 1993; Messa, et al, 1998; Goldstein & Armin, 2001; Resnick, et al, 2004). These findings have served as the basis of the development of targeted anti-EGFR mAB (monoclonal antibody) such as cetuximab and panitumumab that has shown efficacy in metastatic CRC both as monotherapy and in combination with chemotherapy (Jonker, et al, 2007; van Cutsem, et al, 2007; Price, et al, 2014). Nevertheless, activating mutation on the downstream effector of the EGFR signalling both in MAPK and PI3K/AKT pathways such as *KRAS*, *BRAF* and *PIK3CA* are strong predictors for anti-EGFR resistance (Tian, et al, 2012; Therkildsen, et al, 2014; Khan, et al, 2019).

1.1.3.1.3. *KRAS*

In the clinical setting, one of the molecular markers that has been routinely used as a predictive tool is *KRAS* (Kristen Rat Sarcoma Viral Oncogene) mutation, particularly in metastatic colorectal cancer. Around 40% cases of CRC exhibited *KRAS* point mutation in hot spot regions in exon 2 (codon 12, 13) while smaller percentage of mutations occur in other regions of the gene such as exon 3 (codon 61) and 4 (codon 146) (Vaughn *et al*., 2011). Mutation in *KRAS* exon 2 has been associated with poorer survival of CRC patients (Foltran *et al*., 2015; Phipps *et al*., 2013). Moreover, as *KRAS* is a proto-oncogene

molecule in MAPK (Ras-Raf-MEK) pathway which is downstream of signalling triggered by EGFR ligand binding. Mutations in *KRAS* codon 12 and 13 result in low response to anti-EGFR therapy in metastatic CRC patients (De Roock *et al*., 2008; van Cutsem *et al*., 2011). Nonetheless, as reviewed by Biswas, *et al.* (2016), many studies showed conflicting results about the association between *KRAS* mutations and response to standard chemotherapy in rectal cancer.

1.1.3.1.4. *BRAF*

The *BRAF* (v-Raf murine sarcoma viral oncogene homolog B) gene encodes a member of Raf kinase family which is part of the MAPK (Ras-Raf-MEK) pathway of EGFR signalling, downstream to *KRAS*. Mutation, mainly in codon 600, has been found in about 20% of CRC cases (Vaughn *et al*., 2011). *BRAF* mutation was found to be more likely to occur simultaneously with high microsatellite instability and DNA methylation status, showing typical clinical features such as poor grade, mucinous and high infiltration of lymphocytes (Qi Li *et al*., 2006). Lower overall survival was observed in advance and recurrent CRC patients with *BRAF* mutation (Yokota *et al*., 2011). Meta-analysis studies revealed that *BRAF* mutation was a predictive factor for poor prognosis in stage II/III CRC receiving resection surgery and adjuvant chemotherapy and in metastatic CRC patient treated with anti-EFGR mAB therapy (Pietrantonio *et al*., 2015; Yuan *et al*., 2013; Zhu *et al.,* 2016). It is common consensus that mutation of *BRAF* and *KRAS* are mutually exclusive, yet few reports have suggested highly aggressive concomitant mutation of both oncogenes, presumably due to intratumorally heterogeneity (Larki, et al, 2017; Vittal, et al, 2017; Midthun, et al, 2019).

1.1.3.1.5. PI3KCA and PTEN

Another gene that is also found to be altered in CRC is *PIK3CA* (Phosphatidylinositol-4,5-Bisphosphate 3-Kinase Catalytic Subunit Alpha), a catalytic unit of PI3K that involve in the downstream of EGFR signalling through

PI3K/AKT pathway, which consequently regulates cellular processes such as proliferation, survival, apoptosis, and migration (Vivanco and Sawyers, 2002). The prevalence of *PIK3CA* mutations in both exon 9 (codon 542 and 545) and 20 (codon 1047) combined were reported to be around 15% compare to 3.5% in exon 20 only; the mutation was associated with *KRAS* mutation and high CIMP status and not significantly correlated with main clinicopathology features of the disease, except for showing the mucinous characteristic (Nosho *et al*., 2008; Zhang *et al*., 2015). In stage II and III colon cancer, *PIK3CA* mutation showed prognostic value in predicting tumour recurrence and poor overall survival (Shen *et al*., 2016). However, conflicting results reported by other studies showed that there was no statistically significant correlation found between *PIK3CA* mutation status and CRC prognosis (Foltran *et al*., 2015; Ogino *et al*., 2013). Interestingly, *PIK3CA* mutation has been suggested to be a favourable condition for post-diagnosis aspirin treatment for CRC patients (Paleari *et al*., 2015).

The *PTEN (phosphotase and tensin homolog)* gene encodes a protein tyrosine phosphatase enzyme that dephosphorylates PIP3 (phosphatidylinositol-3,4,5 triphosphate) and thereby inhibits PI3K function. Loss of *PTEN* results in constitutive activation of the PI3K-AKT pathway and supports tumour development (Krasinskas, 2011; Kotelevets, et al, 2018). In CRC, genetic alteration of *PTEN* is found in about 20-30% through several mechanisms including mutation at the (A)6 repeat in exon 7 and 8 (suggesting an aetiological role of MMR deficiency), LOH (loss of heterozygosity) at locus 10q23 and or promoter methylation (Mollinari & Frattini, 2014). *PTEN* mutation was reported to associate with mucinous histology, MSI, CIMP and *BRAF* mutations, indicating the involvement on the sporadic MSI carcinogenesis (Day, et al, 2013). The loss of *PTEN* function has been correlated with more advance disease, poorer prognosis, and resistance of anti-EGFR therapy (Nassif, et al,

2004; Frattini, et al, 2007; Sawai, et al, 2008; Therkildsen, et al, 2014).

1.1.3.1.6. *TP53*

The genetic change of *TP53* gene is very well studied in many types of cancer. The gene, located in chromosome 17, encodes the p53, a tumour suppressor protein that regulates cellular response to stress, including aberrant proliferative signals, oxidative stress, and DNA damage. It has been known as "the guardian of the genome" that maintains genomic stability by regulating diverse transcription factors involved in cell cycle, apoptosis, senescence, DNA metabolism, cell differentiation, motility, migration, angiogenesis, immune response, and so on through vast array of targets. Among these are cell cycle inhibitor p21, apoptosis regulator BAX and FAS-APO1, and caspase regulator DR5 (Pino & Chung, 2010). Under normal condition, p53 is negatively regulated by E3-ubiquitin ligase, and the related protein MDM4 (also known as MDMX), which bind to the transactivation domain of p53 and target it for degradation by ubiquitination. This mechanism will maintain low level of the protein in normal condition (Li & Lazano, 2013).

Inactivation of p53 plays an important role in the development of CRC (Russo, et al, 2005). Mutation of *TP53* has been reported in 4%–26% of adenomas, 50% of adenomas with invasive foci, and in 50%–75% of CRC, defining its role in the transition from an adenoma to carcinoma (Leslie, et al, 2002). Most mutations are missense mutation in exon 5-8, covering hotspot codons such as 175, 245,248, 273 and 282 (Beraoud & Soussi, 2003; Lopez, et al, 2012). In CRC, mutation of *TP53* has been associated with poorer prognosis and lower response to chemo and anti-EGFR therapy (Russo, et al, 2005; Lacopetta, et al, 2006; Bortolomeo, et al, 2014; Domingo, et al, 2018).

1.1.3.1.7. Loss of 18q

In addition to the *TP53* mutation that is located in chromosome 17p, the LOH at chromosome 18q is also a major step involved in the transition of adenoma to carcinoma in CRC. This genetic alteration has been reported in about 70% of CRC primary tumour, especially in advance stage (Fearon & Vogelstein, 1990). The chromosome 18q encodes some important tumour suppressor genes such as *SMAD2* and *SMAD4* gene (Jass, et al, 1999; Goel, et al, 2003; Matsuzaki, et al, 2005; Agino, et al, 2007). SMAD proteins are involved in TGF-β signalling pathway and act as the intracellular transcription factor for various genes such as *c-myc, CBFA1, FLRF*, and furin that are responsible for regulation of cell growth, differentiation, and apoptosis (Hahn, et al, 1996; Pino & Chung, 2010) Nonetheless, the alteration in some other regions of the chromosome 18, including the p-arm, have also been reported to occur in CRC and have both prognostic and predictive value (Reid, et al, 2019).

In general, allelic imbalance of chromosome 18q has been described as poor prognostic marker for CRC and mutation in this locus is inversely associated with MSI (Wanatabe, et al, 2001; Popat, et al, 2005; Agino, et al, 2007; Roth, et al, 2012; Ma, et al, 2014; Sefrioui, et al, 2016). In addition, the allelic loss of 18q was reported to associate with poorer response to 5-FU yet has shown to have better response to capecitabine adjuvant monotherapy (Boulay, et al, 2002; Matevska-Geshkovska, 2018). Moreover, the LOH on specific region of 18q11.2-q12.1, was reported to be predictive factor in bevacizumab therapy for metastatic CRC. This region encodes about 20 type of proteins, nevertheless the only one that has been found to be significantly expressed in CRC which is the is epiligrin, encoded by the LAM3 gene (van Dijk, et al, 2018).

1.1.3.2. MSI (Microsatellite Instability)

About 15% of CRC are categorised as MSI which develops through a defect of the DNA repair mechanism, in particular MMR. Inherited mutation of MMR genes is observed in LS or hypermethylation of the promoter region of the genes in the case of the sporadic counterpart.

Microsatellite instability (MSI) subtype of CRC showed a deficiency and loss of function in the DNA MMR genes such as of *MLH1, MLH2, MSH2, MSH3, MSH6* or *PMS2.* Loss of MMR results in changes in the length of microsatellites (normal segments of DNA consisting of multiple repeats of sequences 1-6 nucleotide in length (Peltomaki, 2003; Boland & Goel, 2010; Marzouk & Schofield, 2011). While germline mutations of one of the MMR gene are responsible for LS, hypermethylation silencing of *MLH1* is the most common mechanism for MMR inactivation and it is responsible for the sporadic CRC tumours (Veigl, et al, 1998; Herman, et al, 1998; Cunningham, et al, 1998).

Screening of MSI group among CRC patients has significant importance in patients' management, since this subtype of CRC has been shown to be closely related to LS, a hereditary form of the disease. Numerous studies have shown that, due to the high risk of multiple cancers and its relatively high prevalence, there is a clinical and economic benefit to be gained by screening CRC for LS (Grosse, et al, 2015; Leenen, et al, 2016; Snowsill, et al, 2017). While definitive diagnosis of LS can only be made by demonstration of a germline mutation in an MMR gene, the possibility of LS can be inferred if a tumour is shown to be dMMR (deficient mismatch repair) or shown to have MSI.

However, approximately 10%–15% of sporadic CRC will also show dMMR/MSI due to somatic loss of MMR function (Chiaravalli, et al, 2001). Epigenetic silencing of the MLH1 gene is the most common cause of dMMR in sporadic tumours and very rarely occurs in LS (Poynter, et al, 2008; Bouzourene, et al,

2010). Thus, sporadic tumours with dMMR/MSI can be distinguished from tumours arising in LS by demonstrating methylation of the MLH1 promoter. Similarly, somatic mutation of *BRAF* is common in sporadic tumours with MSI but very rarely occurs in tumours arising in LS (Dheng, et al, 2004; Bouzourene, et al, 2010; Thiel, et al, 2013).

Generally, the MSI subtype, which includes LS, has been reported to have better prognosis and survival rate with distinct clinicopathological features including located in the proximal colon, poorly differentiated with mucinous histology and high lymphocytic infiltration in peri and intratumoral areas (Lawes et al., 2003; Popat et al., 2005; Raut et al., 2014). Unlike CRC with CIN, the tumours with MSI are generally diploid or near-diploid. More recently, our group and others have identified a subgroup within the non MSI CRC. These tumours (which are MSS) can be then classified into two subgroups i.e., those which are characterised by aneuploidy (termed here chromosomal instability in colorectal cancers, CIN-CRC) and those characterised by diploidy (termed here microsatellite and chromosomal stable colorectal cancers, MACS-CRC).

Tumours with a high mutation rate, such as the MSI CRC appear to evoke a stronger immune response including high lymphocytes infiltration through generation of neo-antigens (Xio, et al, 2015; Germano, et al, 2017). MSI tumours were also shown to be enriched with checkpoint proteins as PD-1, PD-L1, and CTLA-4, that determine objective and durable response to immunotherapies in metastatic CRC (Llosa, et al, 2015; Rosenbaum, et al, 2016; Overman, et al, 2018; Narayanan, et al, 2019).

1.1.3.3. CpG island Methylator Phenotype (CIMP)

Another classification, the CIMP, is becoming a significant consideration in CRC taxonomy. It has been reported that patients' survival was associated with the increased methylation of CpG islands - genomic regions with high content of

cytosine and guanine nucleotides located around the promoter region of most tumour suppressor and DNA repair genes, consequently silencing the genes (Juo et al., 2014; Simons et al., 2013; Toyota et al., 1999). CIMP-high has been reported to be associated with worse prognosis and poor response to 5-FU treatment (Murcia, et al, 2018; Phipps, et al, 2014; Juo, et al, 2014; Simons et al., 2013; Cha, et al, 2016). Although a considerable proportion (5-10%) of MSS tumours have CIMP-high, most tumours with CIMP-high are MSI, therefore, it may serve as a confounder for CIMP status to be used as a biomarker (Ogino & Goel, 2008).

1.1.4. Consensus molecular subtypes (CMS)

The most recent classification has come from the CRCC (Colorectal Cancer Subtyping Consortium) which has proposed four CMS (consensus molecular subtypes) of colorectal cancer (Guinney et al., 2015). As described in Figure 1.3, in general, CMS1 represents the majority of MSI tumours with high hypermethylation status, frequent *BRAF* mutation and low level of somatic copy number alteration (SCNA) while the other 3 groups (CMS2-4) show the characteristic of CIN. Interestingly, as compared to the other CIN subtypes, CMS3 exhibits less degree of SCNA with CIMP low characteristic, frequent *KRAS* mutation and mixed MSI status. Nonetheless, the paper highlighted that none of the subtypes is defined by a unique individual event or in other words, none of the genetic alteration is specific to a particular subtype, suggesting a poor genotype-phenotype relationship. Despite its limitations, the CMS classification has been able to further refine the non MSI group using gene expression data, revealing that (i) CMS2 shows more of epithelial differentiation with upregulation of Wnt and Myc pathways, (ii) CMS3 displays a prominent metabolic signature and (iii) CMS4 exhibits more complex carcinogenesis with activation of TGF-β, EMT, angiogenesis, inflammation and stromal infiltration.

Yet it is important to note that multiple studies have shown that the CMS4 transcriptomic signature is mostly driven by stroma rather than epithelial cancer cells (Isella et al., 2015; Dunne, et al, 2016; Isella et al, 2017)

CMS1 MSI immune	CMS2 Canonical	CMS3 Metabolic	CMS4 Mesenchymal
14%	37%	13%	23%
MSI, CIMP high, hypermutation	SCNA high	Mixed MSI status, SCNA low, CIMP low	SCNA high
BRAF mutations		*KRAS* mutations	
Immune infiltration and activation	WNT and MYC activation	Metabolic deregulation	Stromal infiltration, TGF-β activation, angiogenesis
Worse survival after relapse			Worse relapse-free and overall survival

Figure 1.3. Consensus molecular subtypes of colorectal cancer (CMS). The proposed molecular classification of CRC based on gene expression studies. MSI, microsatellite instability; CIMP, CpG island methylator phenotype; SCNA, somatic copy number alteration, TGF- β (Transforming Growth Factor-β). Adopted from Guinney, et al., 2015, The consensus molecular subtypes of colorectal cancer, *Nat Med* 21, pp.1350–1356.

1.2. Tumour Microenvironment (TME)

1.2.1. Overview

Over the last decade, TME has emerged as an important hallmark in cancer playing significant roles during multistep tumorigenesis including tumour growth, invasion, and metastasis. A tumour is no longer seen as a group of homogenous cancer cells but rather is depicted as a collection of several cell types that function both individually and jointly in the tumour biology. The TME consists of EC (endothelial cells) that formed the tumour-associated vasculature, pericytes which are mesenchymal-type cells that line around the endothelial tubes of blood vessels, CAF (cancer-associated fibroblasts) that

secrete various extracellular matrix components and a series of immune inflammatory cells (Hanahan and Weinberg, 2011). It is important to note that, in addition to the epithelial component, the TME also contributes to tumoural phenotypic features such as cell adhesion molecules, metabolites, ligands and numerous soluble factors (Gallon et al., 2014). Furthermore, interaction of tumour cells with the microenvironment also determines its lymphovascular and neurological networks (Deschoolmeester et al., 2011). Nevertheless, despite the importance of stromal components and inflammatory infiltrates, they have not generally been considered so far in constructing the molecular classification of CRC.

Colorectal cancer is immunogenic (Galluzi, et al, 2017). The extent of immune cell infiltration has been proposed to be correlated with tumour molecular make up and consequently may determine prognostic and predictive factors of the diseases. High rates of T lymphocytes infiltration, particularly CD8+ cytotoxic T-cells, were strongly associated with better PFS (progression free survival) and OS (overall survival) (Galon et al., 2006; Mlecnik et al., 2014; Mlecnik et al., 2016). Yet, other immune cells such as B cells, NK cells, MDSC (myeloid derived suppressor cells), macrophages and several subsets of T-helper cells have been shown to exhibit prognostic significance. Table 1.2 summarise the association of TME characteristic with the known genetic biomarkers of CRC with and its potential clinical significance.

1.2.2. Cells of Haematopoietic Origins

1.2.2.1. Tumour Infiltrating Lymphocytes (TIL)

In a landmark study, Galon et al. (2006) were the first to suggest that immunological data (comprised of type, density and location of the immune community within the tumour area) were better patient survival predictors than

the histopathology data described in the UICC-TNM staging system. High rates of T lymphocytes infiltration, particularly CD8+ cytotoxic T-cells, were strongly associated with better progression PFS and OS; the findings that gave rise to the Immunoscore approach which uses a panel of only 2 types of tumour infiltrating lymphocytes (TIL) which are CD3/CD45RO, CD3/CD8 or CD8/CD45RO positive cells as a prognostic tool in CRC (Galon et al., 2006; Mlecnik et al., 2014; Mlecnik et al., 2016). In addition, increased numbers of CD3+ cells and the cell ratio of CD8+/FOXP3+ have also been reported to correlate with improved disease-free survival (Flaherty et al., 2016). As a matter of fact, a predictive algorithm-based model for overall and disease-free survival of CRC, consisting of 6 immune markers which were CD3, CD45RO, IL17, CD15, tryptase, and FOXP3, has been proposed to be use as a complimentary prognostic factor to the TNM staging system (Chen et al., 2016).

The MSI group of tumours has been strongly associated with higher rate of intraepithelial lymphocytes and better prognosis possibly due to better anti-tumour immunity compared to other subtypes of CRC (Deschoolmeester et al., 2011). It was proposed that the intraepithelial lymphocytes may arise due to loss of MMR. This may increase the frequency of frame shift mutations in MSI tumour which might in turn (i) increase the number and activity of tumour-specific effector memory T cells and (ii) induce the synthesis of more targetable neo- antigens (Mlecnik et al., 2016).

Despite it being extensively reported that the MSI group of CRC has shown to have a better prognosis due to high amount of lymphocytic infiltration, a recent study by Mlecnik et al. (2016) concluded that measuring the immune infiltration using the immunoscore approach would serve as a better predictive tool for the disease prognosis and recurrence, regardless of its microsatellite instability status. This study revealed a subclass of MSS group that has a high expression of immune related genes, particularly T cytotoxic and Th1 cells, which showed

a significantly lower risk of relapse, similar to the MSI group. In addition, although a significant dissimilarity in mutational pattern between MSS and MSI groups was observed, these genetic differences did not correlate with the patients' survival (Mlecnik et al, 2016). Yet, it is worth noting that TCGA (The Cancer Genome Atlas) data reveals a group of MSS tumours which show high mutational load (CGAN, 2012), which, in theory, should be more immunogenic. There is high probability that this subset of MSS overlaps with the hypermutated type, which includes tumours with MSI as well as *POLD1* and *POLE* mutations (Palles, et al, 2013).

Thus far, adaptive immune cells, in particular various types of T cells, have been the focal points being investigated in order to comprehend the role of the microenvironment in cancer progression. Less knowledge has been gathered about the nature and clinical significance of innate immune system effector cells, particularly myeloid cells that are present near tumour areas. Macrophages are usually the most abundant infiltrating myeloid cell found within the TME. Conventionally, macrophages are considered anti-tumoural agents due to their cytotoxic properties. However, there is a growing body of evidence showing that as a key player during inflammation, macrophages demonstrate a plasticity which can support cancer development. As reviewed by Braster et al. (2015), a high rate of CD68+ macrophages has been reported to negatively correlate with prognosis of patients with different types of malignancies including breast, bladder, renal and oesophagus carcinoma, endometrial tumour, cholangiocarcinoma, and non-Hodgkin lymphoma.

1.2.2.2. Tumour Associated Macrophages (TAM)

Tumour-associated macrophages (TAM) are macrophages that exist in close proximity to or within tumour networks. Some review articles have been published recently summarizing the emerging studies that been carried out to

reveal the biological function of TAM in cancer development. TAM, derived from circulating monocytes in blood and recruited to tumour sites by chemo attractants such as CCL2 & CCL5 (Chemokine (C-C motif ligand 2 and 5) and growth factor, including VEGF, TGF-β and CSF-1 (Colony Stimulating Factor-1), have the capability to express distinct phenotypes and functions in response to the signals received from the TME (Erreni et al., 2011; Komohara et al., 2016).

The complexity of macrophage activation may contribute to the conflicting results found so far about the role of the infiltrating macrophages in the TME. It is well accepted that CD68 is a pan-macrophagic marker that ubiquitously expressed both in M1 and in M2 groups. Although it may not be considered as conclusive markers, CD86 is highly expressed in M1 cells, whereas CD163 is commonly associated to M2 polarization (Vogel, et al, 2014; Bertani, et al, 2017). As seen in many other types of cancer, the expression of CD68+ macrophages has been significantly linked to a more pro-angiogenic environment in locally advance CRC by increasing VEFG-A level, microvascular density and endothelial area, thus, favouring cancer metastasis (Marech et al., 2016). Furthermore, a higher frequency of CD163+ macrophages was found to be related to advanced tumour stage and shorter survival, even though the prognostic relevance was independent of the tumour stage (Shabo et al., 2014; Herrera, et al, 2013). In addition, another subset of M2-like macrophages, CD14+ CD169+ cells have been linked to IL-10 and CEA (carcinoembryonic antigen) plasma level of CRC patients (Li et al., 2015). On the contrary, low levels of CD68+ macrophages have been linked to the activation of TGF-β signalling and unfavourable survival of CRC patients (Gulubova et al., 2013). Similarly, infiltration of CD68+ macrophages in colorectal tumours, both CT (core tumour) and IM (invasive margin) areas, was found significantly higher in the MSI patients that generally have better prognosis (Mlecnik et al., 2016).

Table 1.2. Genetic biomarkers of colorectal cancer with associated tumour microenvironment characteristic and its clinical significance

Genetic features (mutation)	Location	Prevalence	Principal alteration	Gene function	Tumour microenvironment characteristic	(Potential) Clinical utility
MSI	Genome wide	~ 15%	Deficiency in MMR protein (*MLH1*, *MLH2*, *MSH2*, *MSH3*, *MSH6* or *PMS2*), highly overlap with CIMP (Ogino, et al, 2006; Ogino, et al, 2007)	-	High check-point molecules, including PD-L1, PD-L1, CTLA4, LAG3 and TIM3 expression (Rosenbaum, et al, 2016; Narayanan, et al, 2019), High lymphocytic, CD68 and M1 macrophage infiltration (Schwitalle, et al, 2008; LIosa, et al, 2015; Angelove, et al, 2015; Becht, et al, 2016; Lal, et al, 2018, Korehisa, et al, 2018)	Good prognosis for stage II and III (Popat, et al, 2005; Lockhead, et al, 2013; Goldstein, et al, 2014). Poor response to 5-FU therapy (Ribic, et al., 2003; Guetz, et al, 2009; Schmoll,et al, 2012; Webber, et al, 2015). Good response to immune check point inhibitors (Le, et al, 2015; Overman, et al, 2017)
KRAS	12p1	~ 30–50%	Hotspot regions in exon 2 (codon 12, 13), exon 3 (codon 61) and exon 4 (codon 146), associated with *PIK3CA* mutation (Susanti, et al, 2018; De-Roock et al, 2008)	Cell proliferation, survival and transformation	Low PD-L1 expression (Rosenbaum, et al, 2016), low CD4+ T cell signature (Lal, et al, 2018), high density of CD163+ cell within invasive margin (Kwak, et al, 2016), higher infiltration of CD20+ B-lymphocytes on wildtype (Berntsson,et al, 2016),	Poor prognosis (Taieb, et al, 2016; Schmoll, et al, 2012; Foltran et al, 2015; Phipps et al, 2013; Dallol, et al, 2016; Renaud, et al, 2015; Domingo, et al, 2018). Low response to anti-EGFR therapy in metastatic disease (Amado, et al, 2008; Loupakis, et al, 2009; De-Roock et al., 2008; van Custem et al 2011, Therkildsen, et al, 2014; Bartolomeo, et al, 2014; Peeters, et al, 2015)
BRAF	3q26	~ 20%	Mainly in codon 600, likely to occur with MSI and CIMP-high (Weisenberger, et al, 2006; Ogino, et al, 2006)	Cell proliferation and survival	High PD-L1 expression (Rosenbaum, et al, 2016), High lymphocytic infiltration (Kwak, et al, 2016; Hamada, et al, 2017; Lal, et al, 2018), probably due to overlap with MSI status	Poor prognosis in advance and metastatic disease, in particular among MSS (Taieb, et al, 2016; Lockhead, et al, 2013; Pietrantonio et al, 2015; Yuan, et al, 2013; Balker, et al, 2018; Yang, et al, 2018; Renaud, et al, 2015; Schmoll,et al, 2012; Yokota, et al, 2011; Domingo, et al, 2018).

Genetic features (mutation)	Location	Prevalence	Principal alteration	Gene function	Tumour microenvironment characteristic	(Potential) Clinical utility
						Low response to anti-EGFR therapy in metastatic disease (Zhu, et al, 2016; Therkildsen, et al, 2014; De Roock, et al, 2010; Nicolantonio, et al, 2008; Bartolomeo, et al, 2014; Alonso, et al, 2016)
PIK3CA	3q26	~ 17%	Hotspot regions in exon 9 (codon 542 and 545) and exon 20 (codon 1047), overlap with *KRAS* mutation and CIMP-high (Nosho, et al, 2008; Zhang et al, 2015), negatively associated with *BRAF* mutation (Susanti, et al, 2018)	Cell proliferation, migration, survival, production of new proteins and transport of materials within cells	No evidence	Poor prognosis (Dallol, et al, 2016; Shen, et al, 2016) Good predictive for aspirin treatment (Paleari, et al, 2015). Low response to anti-EGFR therapy in advance disease (Sartore-biachi, et al, 2009; de Roock, et al, 2010; Schmoll,et al, 2012; Therkildsen, et al, 2014; Huang, et al, 2014)
NRAS (*KRAS* isoform)	1p13	~ 6%	Hotspot regions in exon 2 (codon 12, 13), exon 3 (codon 61) and exon 4 (codon 146)	Cell proliferation, survival and transformation	low CD4+ T cell signature (Lal, et al, 2018)	Low response to anti-EGFR therapy in advance disease (De rock, et al, 2010; Schmoll,et al, 2012; Therkildsen, et al, 2014; Ciardielo, et al, 2014; Bokemeyer,et al, 2014; Sorich, et al, 2014; Bartolomeo, et al, 2014; Peeters, et al, 2015)
PTEN	10q23	~ 20%	Mutation at the (A)6 repeat in exon 7 and 8, allelic loss at the 10q23 locus, promoter methylation	Negative regulator of the PI3K/AKT signaling pathway	No evidence	Poor prognosis (Laurent-Puig, 2009, Pentheroudakis, et al, 2014; Sarizaki, et al, 2011). Low response to anti-EGFR therapy in advance disease (Frattini, et al, 2007; Loupkis, et al, 2009; Wang, et al, 2012; Schmoll,et al, 2012; Shen, et al, 2012; Therkildsen, et al, 2014)
TP53	17p13	~ 40–50%	Mutation in exon 5-8, covering hotspot codons such as 175, 245,248, 273 and 282	Cell cycle arrest and apoptosis induction	No evidence	Poor prognosis (Munro, et al, 2005; Russo, et al, 2005; Lacopetta, et al, 2006; Schmoll,et al, 2012; Sarasqueta, et al, 2013; Domingo, et al, 2018).

Genetic features (mutation)	Location	Prevalence	Principal alteration	Gene function	Tumour microenvironment characteristic	(Potential) Clinical utility
						Low response to anti-EGFR therapy in advance CRC (Bortolomeo, et al, 2014)
APC	5q21	~ 30–70%	Mutation cluster region in codons 1282–1581, affecting *β*-catenin binding site	Inhibition of Wingless/Wnt signalling and cytoskeletal regulation	No evidence	Poor prognosis (Loviq, et al, 2002; Chen, et al, 2009; Chen, et al, 2013; Yamashita, et al, 2017; Schell, et al, 2016), yet better prognosis in proximal MSS subtype (Jorissen, et al, 2015)
CTNNB1	3p22	~4–15% (~ 50% in tumours without APC mutations)	N-terminal exon-3 hotspot mutations (T41A, S45F, S45P) or mutations in the APC/Axin binding domain (K335I, W383R)	Regulation of Wnt pathway target genes that promote tumour growth and invasion	High lymphocytic infiltration (Hamada, et al, 2017)	Better prognosis in obese patients (Morikawa, et al, 2011). Poor prognosis in older patients (Nadine,et al, 2016)
TGFBR2	3p24	~ 13%	Mutation of coding mononucleotide repeats; associated with MSI	Receptor for TGF-β that controls cell cytostasis, apoptosis, migration and EMT	Induced T-cell response (Mlenick, et al, 2016)	Good prognosis (Lacopetta, et al, 1998; Wanatabe, et al, 2001; Fernandez-perlarta,et al, 2005), highly overlap with MSI prognosis (Shima, et al, 2011)
Loss of 18q	18q	~ 60%	Allelic loss of *DCC, SMAD2* and *SMAD4*, inversely associated with MSI (Ogino, et al, 2007)	Tumour suppressor, SMAD2 and SMAD4 are related to downstream of TGF-β signalling	Loss of SMAD4 promotes the accumulation of myeloid-derived suppressor cell (MDSC) (Inamoto, et al, 2016)	Poor prognosis (Wanatabe, et al, 2001; Font, et al, 2001; Diep, et al, 2003; Popat, et al, 2005; Sheffer, et al, 2009) and good response to capecitabine (Matevska-Geshkovska, 2018) *DCC* associated with poor prognosis in MSS (Sefrioui, et al, 2016). *SMAD4* and *SMAD2* associated with poor prognosis (Roth, et al, 2012; Schmoll,et al, 2012; Ma, et al, 2014, Jia, et al, 2017, Mei, et al, 2018) and poor response to 5-FU (Boulay, et al, 2002; Zhang, et al, 2014)
FBXW7	4q31	~ 10%	Missense and nonsense point mutations scattered	Ubiquitin ligase tagging multiple oncogenic proteins	No evidence	Poor prognosis

Genetic features (mutation)	Location	Prevalence	Principal alteration	Gene function	Tumour microenvironment characteristic	(Potential) Clinical utility
			in exon 7-10, with 3 hotspots that alter the core of arginine residues (Arg465, Arg479 and Arg505)			
POLE	12q24	~ 1%	Mutation of proofreading (exonuclease) domain, associated with MSS	catalytic subunit of DNA polymerase ε (Pol ε), involves in leading DNA strand replication before cell division	High lymphocytic infiltration (Domingo, et al, 2016)	Poor prognosis, Good response of check point inhibitor

5-FU, 5- fluorouracil. *APC*, adenomatous polyposis coli. *BRAF*, v-Raf murine sarcoma viral oncogene homolog B. CIMP, CpG island methylator phenotype. CTLA4, cytotoxic T-lymphocyte-associated protein 4. *CTNNB1*, catenin beta 1. *DCC*, deleted in colorectal carcinoma. *EGFR*, epidermal growth factor receptor. *KRAS*, kristen rat sarcoma viral oncogene. EMT, epithelial mesenchymal transition. *FBXW7*, F-box/WD repeat-containing protein 7. LAG3, lymphocyte-activation gene 3. MMR, mismatch repair. MSI, microsatellite instability. MSS, microsatellite stable. *NRAS*, neuroblastoma RAS viral oncogene homolog. PD-L1, programmed death-ligand 1. *PIK3CA*, phosphatidylinositol-4,5-bisphosphate 3-kinase catalytic subunit alpha. PI3K/AKT, phosphatidylinositol-4,5-bisphosphate 3-kinase/ Protein Kinase B. *PTEN*, phosphatase and tensin homolog. *SMAD2*, mothers against decapentaplegic homolog 2. *SMAD4*, mothers against decapentaplegic homolog 4. *POLE*, polymerase epsilon. TGF- β, transforming growth factor- β. TGFBR2, transforming growth factor beta receptor 2. TIM3, T cell immunoglobulin and mucin domain- containing protein 3.

The recent study on the association of CRC molecular subtypes and immune/ stromal classification revealed that both MSI-like (CMS1) and the mesenchymal-like (CMS4) subgroups which showed good and poor prognosis, respectively, had higher densities of CD68 macrophages than the canonical and metabolic subtypes (CMS2 and CMS3). This may explain the contradicting findings so far with regard to the prognostic value of the macrophages in the TME. It is likely that different subsets of macrophages affect cancer growth in a distinctive manner.

A recent finding supports the idea of macrophage plasticity, showing that the phenotypes of macrophages found in colorectal tumour were different with those found in the corresponding non-tumour bowel tissue; the former expressed higher level of CD11b and CD34 and lower degree of CD33 as compare to the macrophages located in the normal gut tissues (Norton et al., 2016). Correspondingly, a highly specific genetic fingerprint (23 genes panel) of monocytes isolated from peripheral blood of CRC patients was observed on early onset and over disease progression, in which the gene expression profile was found to be reversible depending on the release of soluble factors by cancer cells; therefore, this can be promisingly applied for diagnosis and follow up of the disease (Hamm et al., 2016).

Better understanding of the mechanism involved in plasticity regulation of macrophages in TME may also be important to support the better use of anticancer strategies, as different anticancer agents can uniquely polarize macrophages into different phenotypes with distinct functions. Ionising radiation and several cytotoxic drugs such as 5-FU, cisplatin, paclitaxel, taxane and docetaxel were suggested to increase the number of M1 macrophages while the *KIT* oncogene inhibitor Imatinib and EGFR inhibitor cetuximab might drive macrophages polarization toward the M2 phenotype (Jinushi, et al, 2015).

1.2.2.3. Myeloid-derived Suppressor Cell (MDSC)

The link between chronic inflammation and tumorigenesis is well-established. One mechanism being proposed with regard to the role of chronic inflammation in promoting tumour onset and development is through the production of MDSC, an immature heterogenous population of myeloid cells that are present in most cancer patients and which accumulate in the blood, lymph nodes, bone marrow, and tumour sites (Ostrand-Rosenberg & Sinha, 2009; Gabrilovich, et al, 2012).The signal from chemokines, CCL2 and/or CCL5 within the TME attracts MDSC to tumour lesions and subsequently secretion of S100A8 and S100A9 by the myeloid cells activate the MAPK and NFκB signalling that help promoting tumour growth (Foell, et al, 2007).

The MDSC inhibits both innate and adaptive immunity through vast array of mechanisms, including (i) inhibition of T lymphocytes proliferation and inducing its apoptosis, (ii) activation of Treg (regulatory T cell), (iii) inducing inflammatory milieu by modifying production of cytokines such as IL-10, TGF-β1, NO (nitric oxide) and ROS (reactive oxygen species) and (iv) promoting angiogenesis. These collectively will subvert the immune surveillance and then prevent the elimination of newly transformed cancerous cells (Pan, et al, 2010; Umansky, et al, 2016). Further, once a cancer is established, the MDSC is likely to inhibit the efficacy of immunotherapy (Marx, 2008).

In humans, the MDSC does not have a universal marker and is loosely classified as predominantly granulocytic (expressing markers such as CD15, CD66b, CD33) or monocytic (expressing CD14) and lack of mature myeloid cell markers, such as HLA (Human Leukocyte Antigen)-DR (Gabrilovich, et al, 2007). Recent studies have suggested a better description of the MDSC into two major subsets based on their phenotypic and morphological features, which are PMN-(polymorphonuclear) and M-(monocytic) MDSC. PMN-MDSC are

defined as $CD11b^{+}CD14^{-}CD15^{+}$ or $CD11b^{+}CD14^{-}CD66b^{+}$ and M-MDSC as $CD11b^{+}CD14^{+}HLA\text{-}DR^{-/lo}CD15^{-}$. CD33 myeloid marker can be used instead of CD11b since very few $CD15^{+}$ cells are $CD11b^{-}$ (Bronte, et al, 2016).

In CRC, the presence of circulating and tumour-resident $Lin^{-/low}HLA\text{-}DR^{-}CD11b^{+}CD33^{+}$ MDSC in patient samples has been correlated with more advance disease stage and metastasis (Sun, et al, 2012; Zhang, et al, 2013; Katerman, et al, 2014; OuYang, et al, 2015). Accumulation of granulocytic MDSC in patients with metastatic CRC could predict the efficacy of 5-FU, oxaliplatin, and bevacizumab (FOLFOX–bevacizumab) drug treatment (Limagne, et al, 2016). Interestingly, the loss of tumour suppressor protein SMAD4, has been correlated to the accumulation of the monocytic MDSC phenotype, $CD11b^{+}$, $CD33^{+}$, and $HLA\text{-}DR^{-}$ and promotes CRC progression (Inamoto, et al, 2016).

1.2.3. Cells of Mesenchymal Origins

1.2.3.1. Cancer Associated Fibroblast (CAF)

The Cancer associated fibroblast (CAF) is the major mesenchymal component of tumour stroma and has been linked to poor prognosis and indicative for chemoresistance in CRC, which may relate to the poor prognosis of the mesenchymal subtype/ CMS-4 CRC (Tsujino, et al, 2007; Wikberk, et al, 2013; Berdiel-acer, et al, 2015; Calon, et al, 2015; Guinney et al., 2015; Dunne, et al, 2015; Hu, et al, 2015). The most common markers of CAF are α-SMA (α-smooth muscle actin) and FAP (fibroblast activation protein) (Shiga, et al, 2015). The recruitment of CAF to the tumour is governed by the growth factors, predominantly TGF-β, released by the cancer cells and infiltrating immune cells which in-turn support tumour progression (Calon, et al, 2015). Also,

cancer cells induce CAF production of IL-6 which stimulates the expression VEGF and STAT3 signalling, resulting in increased angiogenesis (Nagasaki, et al, 2013). Interaction of the cancer cell and CAF stimulates the release of various chemokines that leads to the recruitment of MDSC (Herrera, et al, 2013; Kumar,et al, 2017). Altogether, this to some extent, supports the finding of enriched infiltrating immune cell, fibroblasts and angiogenesis signatures in mesenchymal subtype (CSM4) of CRC with poor prognosis (Becht, et al, 2016). Nonetheless, some research has unveiled the possibility of anti-tumoral property of CAF, in which CAF depletion resulted in reduce vasculature thus increasing hypoxia leading to more undifferentiated and invasive cancer phenotype (Tommelein, et al, 2015).

Given the emerging knowledge about the significance of CAF in inducing tumour growth and immunosuppressive milieu within the microenvironment, intervention with anti-CAF therapies has shown a potential value in pre-clinical model yet less successful in the clinical trial (Scott, et al, 2003; Narra, et al, 2007; Kraman, et al, 2010). The possible strategy is to use these agents in combination with immune check point inhibitors, aiming to reduce the immunosuppressive microenvironment and enhance the immune cell activation, in particular within the non-inflamed phenotypes (Harper, et al, 2013).

1.2.3.2. Mesenchymal Stem Cells (MSC)

Together with CAF and EC (endothelial cells), the MSC (mesenchymal stem cells, which are sometimes referred to as mesenchymal stromal cells, are one of the components of the stromal cell niche in the intestine that is characterised as $CD45^-$, $Epcam^-$ cells. MSC are non-haemopoietic multipotent adult and highly plastic cells with robust tri-lineage differentiation capacity into osteoblasts, adipocytes or chondrocytes. MSC have fibroblast-like morphology. In fact, it

has been proposed that the MSC are the precursors of CAF, in which once exposed to the tumour, MSC show similar surface markers as CAF ie. α-SMA, FAP, PDGFR (platelet-derived growth factor receptor)-β and vimentin. (O'Malley, et al, 2016). This has limited the understanding of individual function of MSC and CAF within the TME. Nevertheless, some in-vitro and in-vivo studies suggested that bone-marrow derived MSC promote CRC through several inflammation-induced mechanisms including suppression of apoptosis, induction of invasion, metastasis and angiogenesis (Huang, et al, 2013; Li, et al, 2015; Liu, et al., 2011; Quante, et al, 2011; Shinagawa, et al., 2010).

Recruitment of MSC to the TME is facilitated by gradients of chemokines, such as CXCL (CXC-chemokine ligand)- 12 and 16, produced mainly by CAF (Stagg, 2008; Jung, et al, 2013). The presence of MSC in the TME and its direct interaction with other TME components including tumour, endothelial, and immune cells contributes to the immunosuppressive milieu. Through secretion of cytokines, for instance CSF-1 (colony stimulating factor-1), tumour-associated MSC induced the infiltration of several types of innate immune cells including neutrophils, MDSC, monocytes and macrophages (Cho, et al, 2013; Shi, et al, 2013; Ren, eta la, 2012; Yu, et al, 2016). MSC can induce neutrophils and the switch of macrophages to pro-tumour M2 phenotypes (Hof-Nahor, et al, 2012; Abumaree, et al, 2013). MSC also have been reported to inhibit the function of adaptive immune effector cells including CD4+ and CD8+ T cells through the production of high level of iNOS (nitric oxide synthase), IDO (indoleamine 2,3-dioxygenase) and chemokines such as CXCL9 and CXCL10 in response to the inflammatory cytokines ie. IFN-γ and TNF (tumour necrosis factor) produced by the immune effector cells (Meisel, et al, 2004; Krampera, et al., 2006; Ren, et al, 2008; Wang, et al, 2014; Su, et al, 2014, Chinnadurai, et al, 2014). In addition, the downregulation of the adaptive immune effector cells and NK (natural killer) cells by MSC is also facilitated through induction of

Treg due to increase production of TGFβ and other soluble factors mentioned earlier in this section (Patel, et al, 2010; Spaggiari, et al, 2008).

Although a majority of literature supports the role of MSC as pro-tumourigenic some studies have shown that MSC have anti-tumoral activity in dextran sulfate sodium (DSS)-induced colitis mouse model (Fan, et al, 2012; Chen, et al, 2014; Nasuno, et al, 2014). This has opened a paradigm of MSC as a therapeutic target for colitis. In addition, modified MSC have been proposed to be used as vehicle to deliver anti-cancer agents due to their migration/ tumour homing property (Harati, et al, 2015; Kikuchi, et al, 2014; Knoop, et al, 2015; Kucerova, et al, 2007; Kalimuthu, et al, 2018).

1.2.3.3. Endothelial Cells (EC)

Endothelial cells (EC) are the key players in the development of blood and lymphatic vessels. Compare to in the normal tissues, EC in the TME showed more irregularity in size and shape with ruffled margins and some branching in the vessel lumen creating intracellular gap resulting in the formation of "blood lakes" (Dudley, 2012). High vascular density in the invasive front of CRC is associated with tumour recurrence, metastasis and mortality (Raza, et al, 2010). Combination of low number of proliferating-VEGF expressing EC and high number of infiltrating leukocytes has been correlated with improved prognosis of CRC compare with either parameter alone (Baeten, et al, 2006).

Through the release of the Notch ligand, DLL1, and activation of Notch downstream signalling, EC promote stem cell phenotypes in the perivascular region of CRC (Lu, et al, 2013). A recent study showed that TNC (Tenascin-C) was upregulated in tumour vascular EC of CRC and correlated with CRC multistage carcinogenesis and metastasis; the reduction of tumour-derived TNC could attenuate HUVEC (human umbilical vein endothelial cell) proliferation, migration and tube formation through the ITGB3 (Integrin beta-3)/ FAK (focal

adhesion kinase)/ Akt signalling pathway (Wang et al, 2019). Another molecule, SPARCL1 was reported to be involved in the vessel stabilisation dictated by the Th1-rich TME, contributing to the more favourable prognosis (Nashchberger, et al, 2016).

Often, tumour-derived EC, expressing both epithelial and mesenchymal markers, were observed in the blood of CRC patients, and this can be used to identify the early stage (<IIA) of CRC (Cima, et al, 2016). Moreover, the presence of circulating EC was reported as independent poor prognostic factor for metastatic CRC (Rahbari, et al, 2017).

1.2.4. Extracellular Matrix (ECM) Components

In the last decade, there is an increased interest regarding the role of ECM (extracellular matrix) components in cancer tumorigenesis. The ECM, with distinct biochemical and biomechanical properties, undergoes remodelling during cancer development and progression to provide the niche of microenvironment that promotes abnormal cell behaviour and tumour associated inflammation and angiogenesis (Tlsty and Hein, 2001; Crotti, et al, 2016). It is also worth noting that the interaction of ECM components with its receptors such as integrins and the DDRs (Discoidin Domain Receptors) that are present in various cellular components of TME including CAF and immune cells, has been reported to contribute to cancer development too (Multhaupt, et al, 2015).

The BM (basement membrane) is a specialised form of ECM that separates colon epithelium from the stroma in the lamina propria. Under physiological condition, the BM proteins are secreted by both epithelial and mesenchymal cells and rearranged into sheet-like structure with 100-300 nm thickness (Simon-Assmann, et al, 1995). The colon BM constituents include Collagen IV with other proteins such as the proteoglycan perlecan and the glycoproteins laminin,

fibronectin, and nidogen. The stromal ECM is composed of similar components already present in the BM, but predominantly with collagen type I which allows the construction of three-dimensional fibrillar structure (Worthley et al., 2010). Beside the normally occurring structural proteins, other constitutive elements of ECM of tumours are those proteins and molecules secreted by tumour epithelium and stroma cells, which is collectively called the secretome (Naba, et al, 2012).

In CRC, loss of BM integrity is one of common ECM marker associated with metastatic disease and poor survival (Lazaris, et al, 2003; Delektorskaya & Kushlinskii, 2011). Some other work has shown that changes in Collagen density and alignment occurs in gastrointestinal high-grade dysplasia polyps and malignant tissue (Adur, et al, 2014; Birk, et al, 2014). Interestingly, Collagen degradation during stroma remodeling releases several fragmented peptides which can be easily detected in plasma and urines (Broker et al., 2013). Beside collagens, other ECM proteins are deregulated in CRC. A primary vs metastatic comparative study of the secretome has suggested that proteases, including ADAM 9 & 10, TSL1 and MMP1, 2, 9, 11 and 12, were peculiar to primary colon tumour and found solely in the primary tumour and not in the metastasis site, suggesting their role in the migration process (Naba et al., 2014). Another study comparing the ECM components of normal colon and colon tumour with liver metastatic revealed the enrichment of aerobic glycolysis signatures and increased vasculature within the TME (Romero-Lopez, et al, 2016).

1.2.5. Spatial Distribution and Interaction of Tumour Microenvironment Components

Immunoscore is the leading translational "biomarker" that utilizes the features of the TME. This approach relies on the quantification of two anti-tumour

lymphocytes population which were CD3/CD45RO, CD3/CD8 or CD8/CD45RO positive cells within the core CT and IM of tumours (Galon et al., 2014; Mlecnik et al., 2016). The score ranges from 0 to 4, with 0 as the lowest score when low numbers of immune cells were found in both CT and IM sections (Galon, et al., 2014). The test appears to be a solid prognostic factor for DFS (disease free survival), DSS (disease specific survival) and OS in CRC and also gives rise to new strategies in immunotherapy either as a new drug target or a predictive tool for the existing drugs such as anti-CTL4, anti PD-1 and anti-PDL1 (Galon, et al., 2014). Subsequently, other studies have suggested the utility of spatial lymphocytes count, primarily CD3+, CD8+ and granzyme B+ cells, to predict patient survival and chemotherapy response in hepatic metastatic CRC (Berthel, et al, 2017; Blazer et al, 2008; Halama, et al, 2011; Tanis, et al, 2015). The emerging findings have strongly shown that the conventional TNM staging no longer provides complete prognostic information as it relies only on tumour cells and neglects the existing of tumours microenvironment, which plays a significant role in immunoediting responses, balancing tumours invasiveness and the host defence system.

Collectively, the findings described above put forward the potential of spatial mapping of TME as prognostic and predictive tools of various types of cancer, including colorectal, that warrant further investigations. For example, it was suggested that direct contact between TAM and cancer cells is necessary for their cell-cell interaction which is concomitant with survival and tumorigenic properties of cancer stem cells, and which consequently contribute to cancer progression and therapy response (Komohara et al., 2016). It is therefore of interest to determine whether the geographical investigation of macrophages in the TME is correlated to some clinical features such as tumour staging. There is also the potential of combining two or more cellular features of TME such as their colocalization, for instance using multiplex IHC (immunohistochemistry)

to improve the power of the biomarkers (Remark, et al, 2016).

The translation of the spatial marker analysis into routine clinical practice will require whole tissue-section evaluation, considering both the CT, IM and stromal areas. For instance, considering the large number of immune infiltrates and heterogeneity of each section of the tumour and its surrounding microenvironment, a computer-assisted analysis of the stained histopathology slides is critical der to providing more precise and reproducible data with minimal inter-observer variability (Galon, et al., 2014). Thus, this will give rise to a new field in digital pathology as histology data provide important morphological and spatial characteristics of both cancer and stroma cells that may not be obtained from molecular profiling or proteomic studies alone. The spatial image analysis on cancer histology can be directed to define the tumour areas, measure the distances between cancer cells and the microenvironment components as well as to cluster each type of cells in the tumour network (co-localisation) to determine the geographical correlations that may have powerful clinical implications (Heindl et al., 2015).

The introduction of the molecular pathways and genetic markers to CRC classification, in addition to the morphological features, has opened a plethora of new potential biomarkers. However, the implementation of detail genomic analysis such as CMS classification into clinical practice is less likely to occur soon. Also, despite the enormous information obtained from the high-throughput analysis such as sequencing, several limitations should be considered such the lack of direct correlation with the histological/ cytometric features as well as the caveat of spatial heterogeneity of the tissue sample (Kather, et al, 2018). Furthermore, as the tumours are usually surrounded by non-neoplastic cells from the microenvironment, it is apparent that the isolated tumour DNA or RNA may be contaminated by genomic materials from adjacent

non-cancerous cells, which by some means may contribute to the observed biological characteristics. Thus, the new platform that enables the spatial landscape of TME to be capture in parallel with transcriptomic or genomic data should be envisaged to be incorporated into the search of useful biomarkers with the feasibility of translation to the clinical practice as proposed in Figure 1.4. Emerging technologies such as mass spectrometry imaging and Digital Spatial Profiling (Nanostring Technologies) may be beneficial in this regard.

Although on other cancer entities, tumour EDI (ecosystem diversity index), a new term which was derived from well-established ecology concept, has been introduced to describe TME heterogeneity based on cell compositions on histology sections and shown to correlate with poor prognosis in high grade (grade 3) but not in low grade (grade 1 and 2) breast cancer patients. Interestingly, there was enhanced prognostic value of EDI when it was linked to the mutation status of *TP53* and several genes on chromosome 4p14 and 5q13 (Natrajan et al., 2016). Similarly, mutation in Wnt–β-catenin pathway such as *APC* and *CTNNB1*, that is enriched in CMS2 and CMS3 of CRC, has been linked to reduced T-cell recruitment via inhibition of antigen-presenting cell (Luke, et al, 2016; Pai, et al, 2017; Spranger, et al, 2018). Studies in other cancer entities and mouse model have also suggested that *PTEN* loss and *TP53* mutation may contribute to the less effective priming of T-cell and some innate immune cells including dendritic and NK cells, resulting in non-inflamed tumour phenotype (Spanger, et al, 2018; Tumeh, et al, 2014; Dientsmans, et al, 2017).

In CRC, CMS works well as for prognosis; however, data acquisition and analysis is relatively complex (Wang, et al, 2018). A recent study reporting an IHC-based classifier based on five markers (CDX2, FRMD6, HTR2B, ZEB1, and KER), complemented by the MSI status, has successfully identify molecular colorectal cancer subtypes and uncover subtype-specific therapeutic benefit.

The alternative approach of utilising surrogate indicators for the CMS classifications by combining several key biomarkers from both epithelial and microenvironment of the tumour is encouraging (Figure 1.4). This will improve the potential of translation to clinical practise. Most importantly, as prognostic markers are less actionable as far as clinical intervention is concerned, this also can be used for biomarker-guided clinical trial design.

Despite the growing number of potential biomarkers being reported, there are only few clinically relevant biomarkers in CRC (Sepulveda, et al, 2017). Among them are RAS and *BRAF* mutation screening for anti-EGFR therapy and MSI status for anti-PD1 treatment (van Cutsem, et al, 2014). Considering the complexity of cancer (both the intrinsic properties of the cancer cells and the interaction with its TME) the translation of detailed biomarker evaluation to a clinical setting remains a great challenge. Nonetheless, refined description of the environment may have value in predicting disease progression as well as patient responses toward currently available treatment options including chemo-, radio- and immuno- therapies.

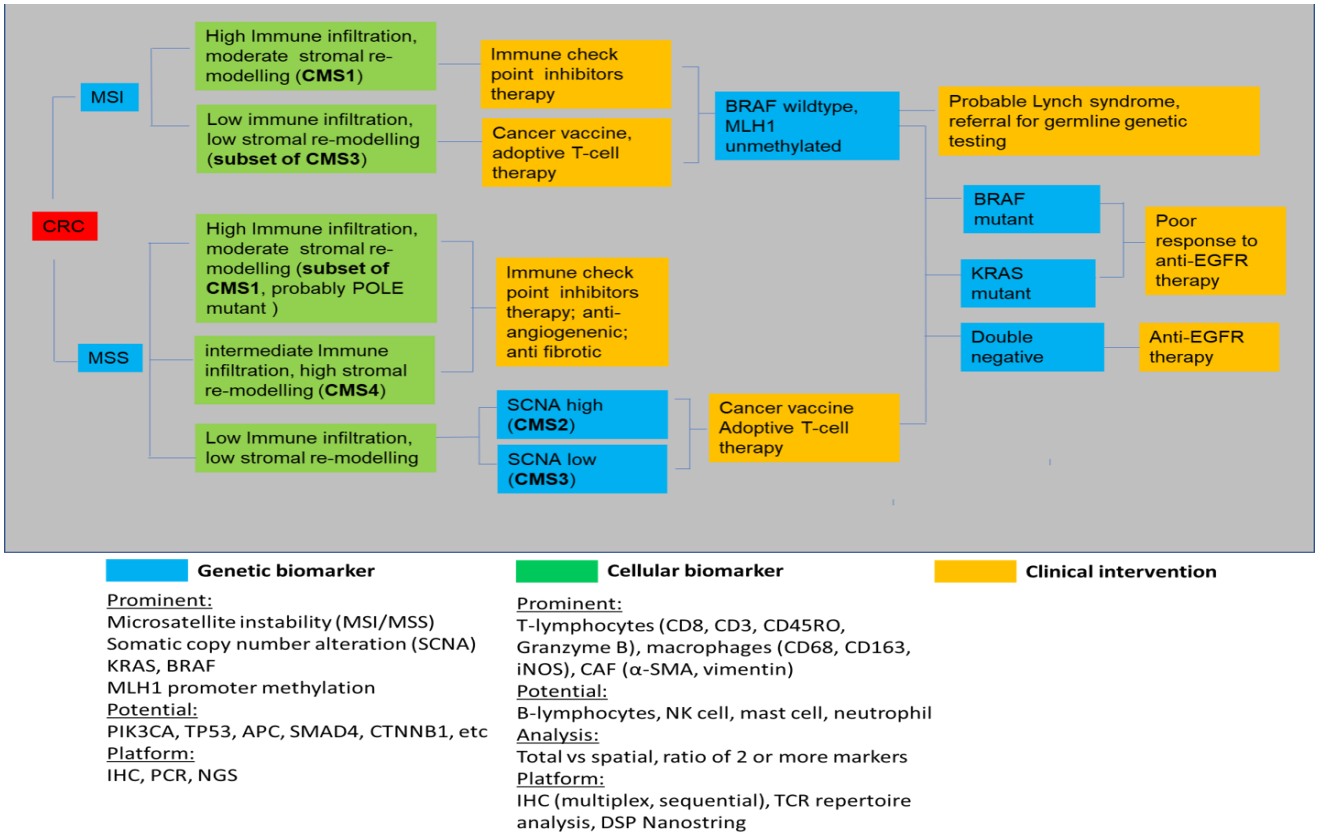


Figure 1.4. Biomarker-guided patient stratification for targeted therapy in colorectal cancer. The diagram proposes the use of several key biomarkers, both genetic and cellular, that are key features of CMS (Consensus Molecular Sub-type) classification to stratify patients and guide the personalised therapy. Some prominent biomarkers such MSI, T-lymphocytes and stromal infiltrates, *MLH1* methylation, somatic copy number alteration, *BRAF* and *KRAS* mutations are utilised subsequently. Nonetheless, although CIMP is one of the focal points of CMS classification, it is greatly overlap with MSI and *BRAF* mutation, therefore, being excluded in this propose model. Emerging biomarkers, both genetic, cellular and proteomic, particularly with detail spatial analysis can be included to refine the prognostic and predictive power of the current biomarkers.

1.3. Aims and Hypothesis

It is well established that CRC is genetically heterogenous and shows a resilient connection with inflammation. Hence, it serves as an appropriate paradigm to unveil the clinical importance of TME especially the infiltrating immune and inflammatory cells in the pathology of the disease. The overarching aim of this study was to investigate the interaction between the cancer cells and non-cancerous cellular community in CRC, based on the underlaying hypothesis that the hypothesis that (i) the cellular community in CRC is non-random and is dictated by signals from the epithelium secondary to genetic changes and (ii) that reciprocally, the cellular community within the TME can influence tumour growth. The objectives of this study included:

1. Select and collect the archived primary tumour tissue to build the Nottingham discovery cohort of CRC.
2. Develop a simple PCR-based assay to determine the microsatellite instability status of CRC cases
3. Perform the genotyping of the CRC cases for important driver gene mutations
4. Map the TME components of CRC and study its correlation with the genetic characteristics
5. Develop a three-dimensional (3D) co-culture model to study the interaction between cancer cells and other cellular components of tumour.

2. Materials and Methods

2.1. Colorectal Cases Selection

Nottingham cohort of resected primary CRC were selected and retrieved from the archives of the NUH (Nottingham University Hospital), Histopathology Department. CRC cases to be used in the project was searched through WinPath system by entering the keywords "MSI" and "MSS". The pathology reports of the search results were reviewed and 101 CRC cases, consisted of 46 cases for MSI (microsatellite instability) and 55 cases for MSS (microsatellite stable) that have complete immunostaining data were selected. Histopathology review of tissue section slides for each case was carried out with the assistance of a pathologist, Dr. Efthimios Hadjimichael, to determine which corresponding block that will be used for spatial immune cells mapping and genetic profiling. Tissue blocks with high tumour content will be used for the genomic testing and sections with wide coverage of TME (tumour microenvironment) will be ideally used for the immune mapping study. Access to tissues and ethics approval were granted by Nottingham Health Sciences Biobank, which has approval as an IRB from North West—Greater Manchester Central Research Ethics Committee (REC reference: 15/NW/0685).

For validation of MSI markers, 88 cases of CRC were retrieved from the archives of the Royal Infirmary of Edinburgh, Pathology Department, which had previously been tested for expression of MMR (mismatch repair) proteins or MSI. Of these, which called as the Edinburgh cohort, 45 cases were MSI and 43 cases were MSS. Access to anonymised use of tissues was granted by Tissue Governance NHS Lothian under ethics approval number SR783.

2.2. DNA Preparation

2.2.1. Extraction

2.2.1.1. Formalin-fixed, paraffin-embedded (FFPE) Tissue

DNA was extracted from FFPE tumour samples. One or two 20µm thick sections (depending on tissue surface area) were cut from each block and immediately placed into a 1.5 mL collection tube. Deparaffinization of the tumour sections was carried out using 2 rounds of xylene (Sigma Aldrich, Cat: 214763) incubation, each for 10 minutes, followed incubation with ethanol (Sigma Aldrich, Cat: 34852) at gradient concentration of 100%, 90% and 70%, each for 10 minutes. Following the removal of the final supernatant of the deparaffinization step, DNA extraction was carried out using the QIAamp DNA FFPE tissue kit (Qiagen, UK) following the manufacturer's protocol. The tissue pellets were re-suspended in 180 µL Buffer ATL and 20 µL Proteinase K were added to the clear lower clear phase, then the samples were mixed by vortexing. The samples were then incubated at 56°C overnight on the rocking/rolling surface (350 rpm), to ensure the samples were completely lysed. The next day, samples were incubated further at 56°C for 1 hour. Then, 200 µL AL buffer with 200 µL ethanol (100%) were then added to the lysate and mixed thoroughly by vortexing. The entire lysate was transferred to a QIAamp MinElute column with 2 mL collection tube followed with a subsequent centrifugation step at 10,000 rpm for 1 minute to ensure the lysate has completely pass through. The column was then placed in a clean 2 mL collection tube. Subsequently, 500 µL AW1 buffer (diluted with ethanol) was added to the column and centrifuged at 8000 rpm for 1 minute). A new collection tube was added to the column and the same procedure was repeated for buffer AW2. The column was then centrifugation at 14,000 rpm for 3 minutes afterward to dry the membrane in the column. Elution of bound DNA was achieved through the

addition of 20-50 µL of ATE buffer to the membrane followed by 5 minutes incubation at the room temperature. The DNA-contained flow through was collected from the column following the centrifugation at 14,000 rpm for 1 minute.

2.2.1.2. Colorectal cancer (CRC) cell lines

For PCR optimization and LOD (limit of detection) determination, high quality DNA template of CRC cell lines (see table 2.1) were used. Cell lines DNA were isolated using GenElute Mammalian Genomic DNA Mini Prep Kit (Sigma-Aldrich, USA) according to the manufacture's protocol. Briefly, $5x10^6$ cells were pelleted and resuspended in 200 µL of Resuspension solution followed by RNase treatment with 20 µl of RNase A Solution for 2 minutes at room temperature. Following this, 20 µL of Proteinase K was added and 200 µl of Lysis solution to lyse the cells. Five hundred µL of Column Preparation Solution was added to a GenElute column and centrifuged at 10,000 rpm for 1 minute and the flow through discarded. Two hundred µL of ethanol was added to the cell lysate and vortexed before loading onto the column. The sample was centrifuged at 10,000 rpm for 1 minute and placed in a new collection tube. The sample was washed by adding 500 µL of Wash Solution and centrifuged at 10,000 rpm for 1 minute and then was placed in a new collection tube. This was followed by a second wash with centrifugation for 3 minutes. The column was then centrifuged at 10,000 rpm for 1 minute and placed in a new collection tube. Two hundred µL of Elution Solution was added to the membrane and incubated for 5 minutes and then centrifuged for 1 minute at 10,000 rpm.

2.2.2. Quantification

Following the extraction, DNA concentration was estimated using Nanodrop 2000 UV spectrophotometry (Thermo Scientific, Wilmington, DE). A 260/280 ratio of 1.8 - 2 is generally accepted as good quality DNA for PCR (polymerase

chain reaction). All DNA samples were adjusted to a concentration of 20 ng/μL using Nuclease Free Water (Qiagen, Cat: 129114) before performing PCR.

2.3. Polymerase Chain Reaction (PCR)

2.3.1. Detection of Microsatellite Instability (MSI) using Novel Panel of Mononucleotide Markers

2.3.1.1. Novel MSI markers identification and screening

The initial work on screening of potential MSI markers was carried out by another group member (Dr. Henry Ebili). A total of 11 different mononucleotide repeat microsatellite loci with potential use as sensitive markers of MSI were tested. Of these, two markers (BAT 25 and BAT 26) are established MSI markers although the primers for these loci were redesigned. Two markers (BCAT-25 and TYMS 26) were identified via bioinformatics analyses by our group. We have previously described BCAT-25 as a useful marker (Fadhil, et al, 2012; Fadhil, et al, 2014). Two markers (EWSR1 and MONO-27) were identified from published research articles (Zhang, et al, 2008; Kishore, et al, 2014; Kondelin, et al, 2015) and five markers (MYB, ANGEL2, *TP53* (BAT34CA), FBXO46 and TCF4) were identified in the SelTar database (www. seltarbase. org). Table 2.2 lists all the mononucleotide repeat microsatellite markers, their genomic locations, amplicon sizes, the lengths of the mononucleotide repeat and the ranges of optimum annealing temperature.

Primers were designed using a combination of online design tools: MFEprimers (http:// mfeprimer. igenetech. com), UCSC in silico PCR (http:// rohsdb. cmb. usc. edu/ GBshape/ cgi- bin/ hgPcr) and Reverse Complement (http://www. bioinformatics. org). Gradient PCR using CRC cell lines DNA as template, followed by high resolution melting analysis (HRMA), was used and determined the optimum annealing temperature (Ta) of the primers. A range of metrics

were used in order to define the best primers for the new MSI panel including reproducibility, PCR efficiency and range of functioning annealing temperature.

2.3.1.2. Fluorescence-based PCR with high resolution melting analysis (HRMA)

In order to test for MSI using HRMA, PCR was carried out for each sample on the ABI 7500 FAST Real-Time PCR System (Applied Biosystems). Each reaction was carried out in a final volume of 10 µL and contained 5 µL of 2× Hot Shot Diamond PCR master mix (Client Life Science, Cat: HS002) and 0.5 µL of 20× (25 µM) EvaGreen dye (Biotium, Cat: 31000); each primer final concentration was at 0.25 µM and 20 ng DNA template. Primer sequences are listed in table 2.3.

The PCR was performed using a three-step procedure: 1 cycle of 95°C/5 min; 45 cycles of 95°C/10 s×1, 55°C/30 s×1, 72°C/30 s×1; and 1 cycle of 72°C/2 min. Subsequently, HRMA was performed in-tube immediately after PCR and consisted of heating to 95°C for 15 s, rapid cooling to 60°C and maintenance at 60°C for 1 min. This was followed by slow ramping up at 0.03°C/s to 95°C during which fluorescent data were captured. The melting data were analysed following normalisation but without temperature shifting using the ABI HRM software V.2.0 (Applied Biosystems). Samples were regarded as MSI if ≥2 markers (40%) showed instability; otherwise, they were regarded as MSS tumours.

In HRMA analysis, changes in the nucleotide sequences give rise to the formation of heteroduplexes that are less stable than homoduplexes of either wild type or mutant sequence, therefore, they melt at a lower temperature. Typically, the difference plot is generated after normalising in order to differentiate mutant from normal samples. The greater the proportion of

heteroduplexes, the more pronounced the difference of the melting curves compared to pure homoduplexes.

As shown in figure 2.1, pre- and post-melt regions are defined by pairs of vertical bars placed before and after the active melt region. The area of data between the pair of bars to the left of the active melt region is used by the software to designate 100% fluorescence—where every amplicon is double-stranded. This level is shown at the far left of the aligned melt curve. The change in fluorescence for each sample, seen to the right of the 100% fluorescence point, is scored as the true fluorescence change and is used to plot the aligned melt curve (Figure 2.1a).

The post-melt region is delineated by the pair of parallel lines to the right of the active melt region and is used by the software to determine the 0% fluorescence point—where every amplicon is single-stranded. The aligned plot provides a scaled view of the data, enabling easy discrimination of sequence variants that display true differences in their melt curve behaviours. This is in contrast to the raw data that is affected by the variable intensity of fluorescence between each sample. Often, differences between melt curves are small. Small differences are best visualized using a difference plot (Figure 2.1b). In this plot, sample curves are subtracted from a single reference (typically a wild-type control), run in the same experiment.

Table 2.1. Mononucleotide repeat microsatellite markers

Marker	Genome Location	Gene/ Position	Source of Marker	Published Mutation Rate	Repeat Size	PCR Product Size	Primer Ta Range
BCAT 25	3p22.1	CTNNB1/3'UTR	Bioinformatic analysis; previously reported by our group (Fadhil, et al, 2012; Fadhil, et al, 2014)	Unknown	T25	100 bp	50-60°C
BAT 25	4q12	CKIT/intron 13	Literature (Parsons, et al, 1995; Dietmaier, et al, 1997; Zhou, et al, 1997; Boland, et al, 1998)	96-100%	T25	85 bp	46-64°C
BAT 26	2p21-p16.3	*MSH2*/intron 5	Literature (Liu, et al, 1994; Dietmaier, et al, 1997; Zhou, et al, 1997; Boland, et al, 1998)	92.5-100%	A26	77 bp	45-65°C
ANGEL2	1q32.3	ANGEL2/transcribed pseudogene	www.seltarbase.org	97.8%	T17	65 bp	45-65°C
ESWR1	22q12.2	EWSR1/3'UTR	Literature (Kishore, et al, 2014)	99.5%	T16	70 bp	45-60°C
FBXO46	19q13.32	FBXO46/3'UTR	www.seltarbase.org	95-100%	T13	57 bp	45-60°C
TP53 (BAT34CA)	17p13.1	*TP53*/3'UTR	www.seltarbase.org	87.5%	18A	69 bp	47-65°C
TCF4	18q21.2	TCF4/intronic	www.seltarbase.org	83.5%	T13	54 bp	47-65°C
MONO27	2p22.1	MAP4K3/intron 13	Literature (Bacher, et al, 2004)	98.3%	A27	78 bp	55-65°C
MYB	6q23.3	MYB/intronic	www.seltarbase.org	100%	T23	75 bp	47-65°C
TYMS26	18p11.32	TYMS/5'UTR	Bioinformatic analysis	Unknown	A26	78 bp	45-65°C

Ta, annealing temperature.

Table 2.2. List of primers for polymerase chain reaction of microsatellite instability and driver genes mutation detection using high-resolution melting analysis

Target Gene		Forward	Reverse
BAT25 (85 bp)		5′-GTGATTCTCTAAAGAGTTTTGTGTTTTGT-3′	5′-TGGCTCTAAAATGCTCTGTTCTCAA-3′
BAT26 (77 bp)		5′-GCCCTTAACCTTTTTCAGGTAA-3′	5′-CATTTTTTAACCATTCAACATTTTTAA-3′
BCAT25 (100 bp)		5′-TCTGTAATGGTACTGACTTTGCT-3′	5′-AACTTAACACTACGAGAGACTTAAAA-3′
MYB (75 bp)		5′-CTTACACCTCTGGGCTTTATAGCTT-3′	5′-CAAAAATGTAAAACACGATATGATAAAGCA-3′
EWSR1 (70 bp)		5′-AACAATGTTCATGGTTGTGATGT-3′	5′-TGACTCTTTATAAACATTTGGAATTTTA-3′
BRAF exon 15 (70 bp)		5′-TTCATGAAGACCTCACAGTAAA-3′	5′-GACCCACTCCATCGAGAT-3′
BRAF exon 11	Outer (189 bp)	5′-TGTTTGGCTTGACTTGACTTT-3′	5′-CTTGTCACAATGTCACCACATTACATA-3′
	Inner (135 bp)	5′-GACGGGACTCGAGTGATGAT-3′	5′-TGTCACAATGTCACCACATTACA-3′
KRAS exon 2	Outer (92 bp)	5′-TTATAAGGCCTGCTGAAAATGACTGAA -3′	5′-TGAATTAGCTGTATCGTCAAGGCACT -3′
	Inner (62 bp)	5′-TGAATATAAACTTGTGGTAGTTGG- 3′	5′-GCTGTATCGTCAAGGCACTCT -3′
KRAS exon 3	Outer (152 bp)	5′-CCAGACTGTGTTTCTCCCTTC-3′	5′-AAAGAAAGCCCTCCCCAGT-3′
	Inner (145 bp)	5′-TGTGTTTCTCCCTTCTGAGGA-3′	5′-AAGAAAGCCCTCCCCAGT-3′
KRAS exon 4	Outer (160 bp)	5′-AGACACAAAACAGGCTCAGGA-3′	5′-TTGAGAGAAAAACTGATATATTAAATGAC-3′
	Inner (105 bp)	5′-GACACAAAACAGGCTCAGGACT-3′	5′-CAGATCTGTATTTATTTCAGTGTTA-3′
PIK3CA exon 1	Outer (168 bp)	5′-CACGACCATCATCAGGTGAA-3′	5′-GGAGGGGGTATTTTCTTGCT-3′
	Inner (129 bp)	5′-ATGCCCCCAAGAATCCTAGT-3′	5′-GAGGGGGTATTTTCTTGCTTC-3′
PIK3CA exon 9	Outer (197 bp)	5′-CTGTGAATCCAGAGGGGAAA-3′	5′-GCACTTACCTGTGACTCCATAGAA-3′
	Inner (103 bp)	5′-AAGGGAAAATGACAAAGAACAG-3′	5′-CACTTACCTGTGACTCCATAGAAA-3′
PIK3CA exon 20	Outer (201 bp)	5′-TGAGCAAGAGGCTTTGGAGT-3′	5′-CCTATGCAATCGGTCTTTGC-3′
	Inner (115 bp)	5′-GCAAGAGGCTTTGGAGTATTTC-3′	5′-TTTTCAGTTCAATGCATGCTG-3′

bp: base pair (amplicon size)

A

B

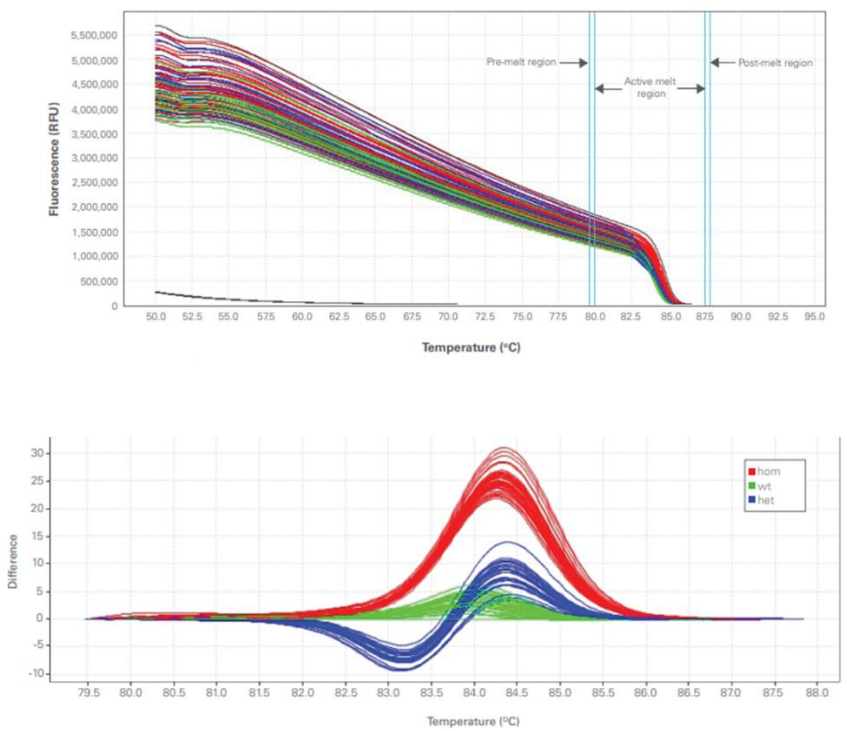


Figure 2.1. The principles of high-resolution melting analysis (HRMA). A. Raw data melt curve (Curve colors represent different samples). Data collected during a high- resolution melt curve experiment exhibits a range of initial fluorescence readings. The active melt region is designated by pre- and post-melt regions (double bars) that are used to align the data, producing a clearer view of the melt curve results. B. Difference plot. Sample curves are subtracted from a reference curve (usually a wild-type control). This view accentuates differences between similar melt curves. Green = wild type, Red = homozygous, Blue = heterozygous. Adopted from "A Guide to High Resolution Melting (HRM) Analysis", Applied Biosystem, USA (https://www.gene-quantification.de/ab-hrm-guide.pdf).

2.3.1.3. Capillary electrophoresis (CE) Analysis for MSI

The status of MSI was also determined using MSI Analysis System version 1.2 manufacturer's instructions (Promega) in collaboration with Dr. Joanne Fields from East Midlands Regional Molecular Genetics Service, Nottingham University Hospitals, NHS Trust, Nottingham, UK. Five mononucleotide markers (BAT-25, BAT-26, NR-21, NR-24, MONO-27), and two pentanucleotide markers (Penta-D, Penta-E), for sample identity checking, were amplified using fluorescently labelled primers in a multiplex PCR. For most samples, normal DNA (FFPE normal tissue or venous blood) was also tested. Products were analysed by capillary electrophoresis on an Applied Biosystems 3130xl Genetic Analyzer (Life Technologies) using the kit internal lane standard, and data analysed using GeneMapper® software. The sample that showed microsatellite instability at ≥2 mononucleotide loci was interpreted as MSI-high, instability at a single mononucleotide locus as MSI-low, and no instability at any of the loci tested as microsatellite stable (MSS).

2.3.1.4. Limit of Detection (LOD) of MSI Testing

The LOD for MSI by both HRMA and CE was tested using spiked DNA samples using methods as described above. DNA of HCT116, a confirmed MSI cell line, was spiked into DNA of known MSS cell line, SW837, to produce mixtures of DNA that contain various proportion of mutant allele, 50%; 25%; 12.5%; 6.25%; 3.125% and 1.625%.

2.3.2. Somatic Mutation Detection

2.3.2.1. Target gene selection

The selection of targets genes was based on the known driver mutations occur in CRC. Selected genes and hotspots have been routinely investigated, including

KRAS (exon 2, 3, and 4), *PIK3CA* (exon 9 and 20) and *BRAF* (exon 11 and 15). Primers, listed in table 2.3, were previously designed and optimised in our lab (Fadhil et al., 2010).

2.3.2.2. Quick Multiplex Consensus -Polymerase Chain Reaction (QMC-PCR)

The PCR protocol consists of two steps which are PDM (pre-diagnostic multiplex) reaction using a set of outer primers of targeted genes followed by SSD (specific single diagnostic) reaction using an inner pair of corresponding primer for each gene. PCR reaction of the PDM stage was carried out in a final volume of 20 µL, contained 5 µL of 1x Hot Shot Diamond PCR master mix, up to 8 pairs of outer primer of CRC oncogenes with each primer final concentration at 0.187 µM and 20 ng of genomic DNA. The DNA enrichment was then carried out by a 2-steps PCR: 1 cycle of 95°C/5 min; 45 cycles of 95°C/10 s×1, 55°C/30 s×1, 72°C/20 s×1. For the SSD stage 10 µL of PCR reaction was used, contained 5 µL of 1x Hot Shot Diamond PCR master mix, 1 µL of 20x (25 µM) EvaGreen dye, inner primer pair for the single target hotspot with each primer final concentration at 0.25 µM and 1 µL of 1: 100 dilution of PCR product from the PDM reaction. A 3-steps PCR was then conducted as follow: 1 cycle of 95°C/5 min; 45 cycles of 95°C/10 s×1, 55°C/30 s×1, 72°C/20 s×1; and 1 cycle of 72°C/2 min.

A 10 µL aliquot of PCR products were transfer into a well in 96-well black shell PCR plate (BioRad, Cat: HSP9666) and then 10 µL of mineral oil (SigmaAldrich, Cat: M8662) was added into the well. The plate then centrifuged at 2000 rpm for 5 minutes prior to being loaded into the LightScanner HR96 machine (IdahoTech, USA).

2.3.2.3. *BRAF* V600E Mutation Detection

Routinely, our laboratory employed a two stage PCR for detection of somatic mutation on CRC cases, called the QMC-PCR (Quick Multiplex Consensus-Polymerase Chain Reaction) as described on previous section of this chapter. Nonetheless, for the purposes of developing a robust protocol to screen for Lnych Syndome (Susanti, et al, 2018), a single-stage PCR test with novel primers, as listed in table 2.3 were designed specifically for detection of mutation at *BRAF* codon 600. The PCR protocol was optimised for similar setup as described for the novel MSI panel, which was 1 cycle of 95°C/5 min; 45 cycles of 95°C/10 s×1, 55°C/30 s×1, 72°C/30 s×1; and 1 cycle of 72°C/2 min. Similar to the MSI panel, HRMA was performed in-tube following the PCR, consisted of heating to 95°C for 15 s, rapid cooling to 60°C and maintenance at 60°C for 1 min. This was followed by slow ramping up at 0.03°C/s to 95°C during which fluorescent data were captured. The melting data were analysed following normalisation but without temperature shifting using the ABI HRM software V.2.0 (Applied Biosystems).

2.4. Flow cytometry for Ploidy Determination

2.4.1. Preparation of nuclei suspension from FFPE tissue

Whole nuclei were extracted from FFPE tissues using a modification of the method of Hedley *et al*. (1983). A single 30-µm-thick section was cut. Sections were de-waxed in 2 rounds of 10 minutes incubation of xylene and rehydrated in graded alcohols at concentration of 100% for 10 minutes, 90%; 70%; and 50 % for each 3 minutes. The sections were washed in distilled water twice and then digested at 37°C in 1 mL of 1.5% pepsin (Sigma Aldrich, Cat: p-7000) in 0.9% NaCl (Sigma Aldrich, Cat: S9888) pH 1.5 for 2 hours with intermittent vortex mixing. Following digestion, the sections were vigorously vortexed for

60 seconds to release the nuclei. The suspended nuclei and remaining tissues were then passed through a 70-µm nylon filter (BD Falcon, Cat: 352350) and centrifuged at 1,500 rpm for 5 minutes. The supernatant was removed, and the pellet was re-suspended and washed twice in PBA; made of 0.1% BSA (bovine serum albumin) (Sigma Aldrich, Cat: B6917) in PBS (phosphate buffer saline) (Sigma Aldrich, Cat: D8537) to remove residual pepsin. The cell pellet then was re-suspended in the staining solution in the flow cytometer tubes. The staining solution for each sample (per tube) consisted of 5 µL of 10 mg/ mL RNase (Sigma Aldrich, Cat: R4642) and 25 µL of 1 mg/ mL propidium iodide (Sigma Aldrich, Cat: P864) in 0.5 mL PBA. The samples were covered with aluminium foil and then incubated at 37°C for at least 20 minutes.

2.4.2. Flow cytometry

Flow cytometry was performed on a Beckman Coulter FC500 flow cytometer using doublet discrimination on a DNA fluorescence area *vs*. peak plot (Ormerod et al*.,* 1998). Fluorescence from a minimum of 30,000 events per sample was captured over 1024 channels. Each tumour sample consists of tumour cells together with stromal cells and lymphocytes. The non-tumour cells are diploid and were used to set internal parameters and as internal controls. The PMT (photomultiplier tube) voltage of the flow cytometer was adjusted so that the G0/G1 peak of the non-tumour cells was captured at a channel number >200. The G0/G1(2c) and G2/M (4c) peaks of the internal controls were assigned to the channel with the maximum fluorescence for each, and a sample was acceptable if there was linearity between the G0/G1 and G2/M peaks (i.e. the ratio was between 1.95 and 2.05), the G2/M peak did not exceed 10% of the total events, the proportion of events at >6c (i.e. clumps) was not >1% and the co-efficient of variation of the G0/G1peak for the internal controls was <6%.

2.4.3. Data analysis

Data analysis was performed using the WEASEL v2.7 software (Walter and Eliza Hall Institute, Parkille, Australia; http://www.wehi.edu.au). The DI (DNA index) for additional peaks was calculated as the ratio of the channel position of the tumour G0/G1 peak to the control G0/G1 peak. Tumour samples were considered diploid/near diploid when the DI was between 0.9 and 1.1 and aneuploid when the DI was outside these ranges. If the G2/M (4c) peak of the controls comprised more than 10% of the total and there was a corresponding 8c peak, the tumour was deemed as tetraploid.

2.5. Immunohistochemistry (IHC) and Digital Image Analysis (DIA) of Tumour Microenvironment (TME) Markers

2.5.1. Automated immunohistochemistry (IHC)

One selected FFPE block of each cases of the Nottingham cohort CRC were selected for IHC. Sequential sections were cut at 4 µM thickness from the FFPE blocks. Immunohistochemistry (IHC) for protein markers of TME cellular population were performed on the sequential tissue sections using automated slide staining system (Benchmark ULTRA, Ventana Medical System, Tucson, AZ) following the diagnostic protocol that been established by the Histopathology Department, NUH as detailed in table 2.4 and digital slides were produced using the Aperio AT2 slide scanner (Leica Biosystems).

2.5.2. Digital image analysis (DIA)

2.5.2.1. Faux multiplex immunohistochemistry (fm-IHC)

Image analysis on sequential digital images was carried out in collaboration with Dr. Alain Pitiot (Ilixa Ltd, London, UK). For each block, all consecutive IHC

images were registered to the middle one in the block, thereby establishing accurate correspondence across all markers of the TME cellular community (i.e. a particular landmark in one registered IHC image can be found at the same position in all the other registered IHC image). Each registered image was then down sampled by a factor of 10 to account for small differences across consecutive images and small registration inaccuracies. Finally, the down sampled, registered images were automatically colour separated and threshold in order to obtain expression maps, which were used to establish correlations across combination of markers.

Table 2.3. Tumour microenvironment markers for immunohistochemistry

Marker	Antibody
CD3	CD3/2GV6; 790-4341 (Roche, USA)
BCL-2	bcl-2/124; 790-4464 (Roche, USA)
CD163	PA0090 (Leica, USA)
CD20	CD20/L26; 760-2531 (Roche, USA)
CD56	CD56/MRQ-42; 760-4596 (Roche, USA)
CD68	MO814 (Agilent, USA)
CD8	CD8/SP57; 790-4460 (Roche, USA)
Ki67	Ki-67/30-9; 790-4286 (Roche, USA)
BerEP4	MO804 (Agilent, USA)

Each image was divided into "frames", called as "super-pixels" measuring 10X10 pixels (yielding more than 200,000 frames per image) and each frame was allocated a co-ordinate. Histogenic Molecular Mapping (HMM) was used for precise registration of sequential tissue sections (using one image as the index image) and the images were shifted so that each matched co-ordinate in the sequential images represented the same landmark in the index image. This allowed the expression of several markers to be measured in each frame thereby allowing point-by point correlation of all the markers with each other and pairwise correlation. In addition, density of each markers was calculated

based on the ratio of number of positive super-pixels to the total number of super-pixels. The BerEP4 staining was used to "virtually segmented" tumour epithelium (only BerEP4+ super-pixels) and the stroma (BerEP4- super-pixels).

2.6. Three-dimensional (3D) Spheroid Co-culture

2.6.1. CRC cell lines

Some well-described CRC cell lines including HCT116, SW480, SW620, DLD-1 were used in this project as described in Table 2.1 and were obtained from the group of Prof. Ian Tomlinson at the Molecular and Population Genetics Laboratory, London Research Institute, Cancer Research UK, London. The identity of these cell lines was authenticated by STR (short tandem repeat) profiling using PCR-single locus technology, performed by Eurofins (certificate attached in the appendix).

2.6.1.1. Cell lines maintenance

Cells were grown in DMEM (Dulbecco's Modified Eagle's Medium) (Gibco, Cat: 11965092) supplemented with 10% heat-inactivated FBS (foetal bovine serum) (Sigma Aldrich, Cat: F7524), 1% of 200 mM L-glutamine (Sigma Aldrich, Cat: G8540) and no addition of antibiotics. The cells were maintained usually in T75 flask (Corning, Cat: CLS3275) at 37ºC in incubator under a humidified 5% CO2 atmosphere. The growing cells were monthly tested for mycoplasma and frequently (every 1-2 days) checked under the microscope for cells viability and for any unusual growth such as contamination. Cell were fed twice weekly by changing the media to a fresh DMEM media, containing FBS and L-glutamine.

2.6.1.2. Passaging cells

The cultured cells were passaged when 70-80% confluency was reached. Media was removed and cells washed twice with PBS. Cells were detached by

incubation with 1 mL of trypsin-EDTA (Sigma Aldrich, Cat: T4049) for up to 5 minutes until they were completely detached from the flask surface. The trypsin was neutralised by the addition of 4 mL of DMEM media containing FBS and L-glutamine. Cells in suspension were pelleted by centrifugation at 1,500 rpm for 5 minutes, the media were discarded, and the cells were resuspended in a volume of media dependent upon the split ratio (i.e. 10 ml for a 1:10 split ratio). One mL cell suspension was transferred to a new flask containing 9 ml of DMEM containing 10% FBS. Experimental works were undertaken on cell lines with a passage number of less than 10 from the first defrosting.

2.6.1.3. Cell Freezing and Thawing

For cells thawing, vials containing cells were heated up in water bath at 37°C, then transferred into universal tubes containing 9 mL of growth media, containing PBS and L-glutamine and centrifuged at 1,500 rpm for 10 minutes. Supernatant was then aspirated, and cell pellets were resuspended into 10 ml of culture media as describe earlier and transferred to a clean T75 flask. Cells were then incubated and observed under microscope frequently (1-2 days) to check confluency and contamination.

When cells reached approximately 70-80% of confluency, cells were washed twice with PBS and detached by incubating them with 2 mL of trypsin/EDTA for 5 minutes at 37°C. The cells were then suspended in 8 mL of DMEM media containing FBS and L-glutamine to neutralise the trypsin and pelleted by centrifugation at 1,500 rpm for 5 mins. Cell pellet was then resuspended in 5 mL of freezing mixture, consists of 90% FBS and 10% DMSO (Sigma Aldrich, Cat: D2650) and transferred into Cryo-Vial (Corning, Cat: CLS430659) and stored in liquid nitrogen storage container.

2.6.2. Cancer-associated fibroblast (CAF) culture

2.6.2.1. Isolation from colon cancer patient tissue

Cancer-associated fibroblasts (CAF) were isolated from human colon carcinoma resection specimen. Access to tissues and ethics approval were granted by Nottingham Health Sciences Biobank, under HRA REC approved project 08-H0403-37, titled "The derivation of new cancer biomarkers and their use in pre-clinical efficacy testing" led by Prof. Anna Grabowska of Division of Cancer and Stem Cell, School of Medicine, University of Nottingham.

The tissue sample was washed with HBSS/AA (Sigma Aldrich, Cat: H6648). Tissue was allowed to settle then medium aspirated (if the medium appears to contain cells, these can be harvested and put into culture as a pre-digest sample). Tissue disaggregation and digestion were performed using 2.4U/mL Dispase (Invitrogen, Cat: 17105041) and 100U/mL collagenase type II (Invitrogen, Cat: 17101-015) for 2 hours at 37^0C with rotation. As much as 10ml Dispase/Collagenase solution in HBSS/AA was used for per mL of tissue. Undigested material was allowed to settle out and subsequently the cell suspension was carefully removed and pipetted into a sterile universal, then top up with RPMI-1640 medium (Sigma Aldrich, Cat: R0883). Cell suspension was centrifuged at 1,500 rpm for 5 minutes. The media then aspirated out. If the cell pellet appears 'contaminated' with red blood cells, 1 mL RBC lysis buffer was added and mixed with a pipette a few times then incubated at room temperature for 1 minute. The sterile-filtered RBC lysis buffer was made of 4.4 g ammonium chloride (Sigma Aldrich, cat: 213330); 0.5 g potassium bicarbonate (Sigma Aldrich, cat: 237205); and 0.018 g EDTA (Sigma Aldrich, cat: E9884) dissolved in distilled water and adjusted to pH 7.35 with 0.1 M sodium hydroxide (Sigma Aldrich, cat: S5881) . The cell pellet was washed one more time with 10 mL of RPMI-1640 medium and cell suspension was

centrifuged again at 1,500 rpm for 5 minutes. After centrifugation, the supernatant was aspirated, and cell pellet was resuspended in PCA media, consisted of DMEM media supplemented with 20% heat-inactivated FBS, 2mM L-glutamine, 0.1% hydrocortisone (w/v), and 0.75% bovine insulin (w/v). For the medium to large pellet, 3-4 mL PCA medium was added, and cell suspension was transferred to one well of a collagen-coated 6-well plate. Within 1-2 days, depending on the cell growth, the cells were then detached from the well using TrypLE Express Enzyme (Gibco, Cat: 12605-028) and transferred into T25 flask (Corning, Cat: CLS430639).

2.6.2.2. Fibroblast cell enrichment

Gradual enzymatic detachment was used to enrich the fibroblast cells from the previously isolated primary cells. Sub-confluent flask was examined microscopically, and fibroblast growth area was marked. The growth medium was then aspirated, and the flask was washed gently with 10 mL HBSS/AA. Subsequently, 5-10 mL of dispase solution was added and the flask was incubated at 37^0C. The flask was examined at regular intervals. Fibroblasts come off more easily than epithelial cells thus, the fibroblasts population should round up and lift off before the other. When the majority of the fibroblasts have lifted off and before the other population begin to detach, the cell suspension was removed from the flasks into a sterile universal tube and centrifuged at 1,500 rpm for 5 minutes. Cell pellet was resuspended in PCA growth media and culture in a new T75 flask.

2.6.2.3. Fibroblast cell maintenance, passaging, freezing and thawing

The enriched primary fibroblast was cultured in PCA media in T75 flask at 37ºC in incubator under a humidified 5% CO2 atmosphere. The growing cells were monthly tested for mycoplasma and frequently (every 1-2 days) checked under

the microscope for cells viability and for any unusual growth such as contamination. Cell were fed twice weekly by changing the media to a fresh culture media.

The cultured cells were passaged or frozen when 70-80% confluency was reached according to similar protocol used for the CRC cell lines. Yet, the detachment of the fibroblasts from the culture flask was achieved using TrypLE Express Enzyme instead of trysin-EDTA. Experimental works were undertaken on these primary cells within a passage number of less than 10 from the first isolation. Similar thawing protocol as CRC cell lines was applied to the fibroblasts.

2.6.3. Lentivirus transduction of fluorescence proteins for CRC cell line and CAF

The lentiviral plasmid components were acquired from Addgene: Transfer plasmids: Rix-PGK-Tom-W (Cat: 25813) and FUGW (Cat: 14883), Packaging plasmid: psPAX2 (Cat: 12260) and Envelope plasmid: pMD2.G (Cat: 12259).

Viral particles were packaged in 50-80% confluent HEK293T cells seeded at a density of $1.5x10^6$/10 cm petri dishes. The vector mixture was made by adding 2 µg transfer plasmid (Rix-PGK-Tom-W or FUGW); 1500ng psPAX2 packaging plasmid and 500ng pMD2.G envelope plasmid up to 40µL serum-reduced OPTI-MEM (Gibco, Cat: 31985062). The vector mixture then added into a proportion of 24 µL Fugene 6 (Promega, Cat: E2691) in 136 µL serum-reduced OPTI-MEM. After 72 hours of transfection, lentiviruses were concentrated by ultracentrifugation at 3,000 rpm (10,000 x g) at 4°C for 4 hours in a 10% sucrose buffer (Jiang et al, 2015). Lentivirus titers were examined by Lenti-go stix quick test (Takara Bio, 631280).

Colorectal cancer cell lines were firstly transduced with TdTomato lentivirus at

excessive MOI (multiplicity of infection) to ensure complete transduction efficiency. Cancer-associated fibroblasts were transduced with FUGW lentivirus to induce EGFP expression also at excessive MOI. Maintenance of complete transduction efficiency was routinely inspected by observation of TdTomato and EGFP expression across several passages, using a wide-field fluorescence microscope (Nikon TiE).

2.6.4. Lentivirus transduction of CD24 gene overexpression

To establish the stable CD24 overexpressed CRC cell line, similar protocol of lentivirus transduction for fluorescence proteins as described in the previous section was used to introduce the CD24 clone using FUGW insert into the HCT116 cells. The complete CDS of CD24 except for the termination codon (TAA) was inserted into FUGW to create a fusion protein with EGFP in the plasmid.

Viral particles were packaged in 50-80% confluent HEK293T cells seeded at a density of 1.5x106/10 cm petri dishes. The vector mixture was made by adding 2 µg transfer plasmid FUGW inserted with CD24 clone; 1500ng psPAX2 packaging plasmid and 500ng pMD2.G envelope plasmid up to 40µL serum-reduced OPTI-MEM (Gibco, Cat: 31985062). The vector mixture then added into a proportion of 24 µL Fugene 6 (Promega, Cat: E2691) in 136 µL serum-reduced OPTI-MEM. After 72 hours of transfection, lentiviruses were concentrated by ultracentrifugation at 3,000 rpm (10,000 x g) at 4°C for 4 hours in a 10% sucrose buffer (Jiang et al, 2015). Lentivirus titers were examined by Lenti-go stix quick test (Takara Bio, 631280). The HCT116 were firstly transduced with FUGW lentivirus at excessive MOI to ensure complete transduction efficiency. Maintenance of complete transduction efficiency was routinely inspected by western blot across several passages to determine the level of CD24 protein expression using SWA11 antibody, a kind gift from Prof.

P. Altevogt from German cancer Research Center.

2.6.5. Human monocytes and macrophages preparation

Human monocytes and macrophages were kindly prepared by Dr. Sirina Muntaka from the research group of Dr. Luisa Martinez-Pamores from the School of Life Sciences, University of Nottingham, UK. Ethics approval were granted Fauclty of Medicine and Health Science, University of Nottingham under REC approved project 195-1801, titled "The Immunology of Infammatory and Infectious Disease".

Buffy coat from Blood Bank (Sheffield, UK) was diluted in PBS to a total volume of 140 mL and distributed among four 50 mL Falcon tubes (Greiner Bio-One, Cat: 227270) containing 15 mL Histopaque-1077 (Sigma-Aldrich, Cat: 10771) in each tube. The tubes were centrifuged at 2,000 rpm (800 x g) for 30 minutes in a low acceleration/deceleration speed (clean tissue culture centrifuge: acceleration 1). The white layer (peripheral blood mononuclear cells - PBMCs) was collected with a Pasteur pipette and transferred to a new 50 mL tube (2 Falcon 50 ml tubes for the four white layers) and then filled with PBS and centrifuged at 1,500 rpm (350 x g) for 10 minutes. Supernatant was discarded carefully in order not to lose the pellet. Wash was repeated 2 more times. Two pellets were joined in one 50 mL Falcon tube, filled with PBS to 50 mL. Cells were counted using trypan blue (Gibco, Cat: 15250061) in 1:2 dilution.

The remaining cells were centrifuged at 1,500 rpm for 5 minutes. The supernatant was discarded. The pellet was resuspended in MACs buffer consists of 2 mM EDTA (Sigma-Aldrich, Cat: E7889) and 0.5 % FBS in PBS in a volume of 80 µL buffer per 10^7 cells and incubated with human CD14 magnetic microbeads (Miltenyi Biotec, Cat: 130-050-201) in 10 µl of CD14 beads per 10^7 cells on ice (Singh, 2012) in the dark for 15 minutes. CD14+ cells were

washed with 20 mL of MACS buffer and centrifuged at 1,500 rpm (350 x g) for 5 minutes. Supernatant was discarded and the pellet was resuspended in 3 mL MACS® buffer and applied through a pre-cooled LS MACS® magnetic separation column (Miltenyi Biotec, Cat: 130-042-401) attached to the Quadro MACS separation unit (Miltenyi Biotec, Cat: 130-090-976), as recommended by manufacturer. The column was washed two times using 3 mL of MACS® buffer. The LS column was then removed from the magnet and 5 mL of MACS® buffer was added into the column. The cells quickly flushed in a clean 20 mL tube and centrifuged at 1,500 rpm (350 x g) for 5 minutes. The supernatant then discarded, and the pellet finally resuspend in RPMI media containing 15% AB serum (Sigma-Aldrich, Cat: H4522), 2mM Glutamax (Gibco, Cat: 35050-038) and 10 mM HEPES (Sigma-Aldrich, Cat: H0887). The cells were plated at 10^6 cells/500 µL for each well in a 24-well low attachment plate (Corning, Cat: CC22) (Singh, 2012). The cells were incubated in the presence of rh GM-CSF (Granulocyte-macrophage colony-stimulating factor) (Miltenyi Biotec, Cat: 130-093-864) at 50 ng/mL or M-CSF (macrophage colony-stimulating factor) at 50 ng/mL and IL-4 (Miltenyi Biotec, Cat: 130-093-920) at 25 ng/mL at 37 °C for 7 days. Fresh media (500 µL) and cytokines supplements were added at day 3. For M1 macrophages, cells are incubated in the presence of M-CSF at 50 ng/mL with addition of rhINF-γ (R&D Systems, Cat: 285 -IF -100) at 20 ng/mL on the 6^{th} day.

2.6.6. Spheroid co-culture

Cells suspensions of the TdTomato expressing CRC cell lines were seeded in 6-replicates in Ultra-low attachment 96-well plates with black opaque walls and clear, round well-bottom (Corning, Cat: CLS4515) at $2.0x10^4$ cells/mL in a final volume of 100 µL alone or in a mix with CAF expressing the GFP ($2.0x10^3$ cell/well total), in Fluorobrite DMEM (Gibco, Cat: A1896701) supplemented with

10% FBS and 6 mM L-glutamine (Sigma Aldrich, Cat: G8540). The plates were then centrifuged at 1,500 x g for 10 minutes at acceleration and deceleration 6 in a Heraeus™ Megafuge™ 16 centrifuge (ThermoScientific). Spheroids or aggregate formation was confirmed in 24-48 hours. Daily measurement of TdTomato fluorescence was taken in a FluoStar Omega plate reader (BMG Labtech) that been set to perform bottom reading at 544 nm excitation and 590nm emission wavelength at gain 2500. Fluorescence of GFP was measured at 488 nm excitation and 520 nm emission wavelength at gain 1500. Fluorescence readings were normalised to day 0 (1 hour after seeding) to account for initial differences in seeded cell numbers between the experimental groups. Brightfield and fluorescence images of spheroids were taken daily for volumetric quantification using a widefield inverted microscope (Nikon TiE). Volumetric analysis was performed using ImageJ wand tracing tool in 8-connected mode to determine the area of each spheroid. Mean spheroid radius was determined by assuming an approximation to the area of the circle ($A = \pi r^2$) and from there inferred the volume of the spheroid ($V=\frac{4}{3}\pi r^3$). Volumetric growth was normalised to day 1 or day 2 after seeding (following the formation of sphere-like structure) to account for initial differences in seeded cell numbers between the experimental groups.

2.7. Statistical Analysis

Prior to statistical analysis, datasets were checked for normality using Shapiro-Wilk test. SPSS Statistics software v.24 (IBM) was used for the analysis of genetic marker and TME population. Association analysis of different genetic markers were done using Fisher Exact test. For cellular markers density analysis, comparisons between two groups of non-parametric values were performed by Mann-Whitney test. For colocalization analysis of cellular markers, Pearson's product moment correlation analysis was performed to

study the co-existence of TME population within different compartment of the tissues. The unpaired T-test was used to compare the means of Z-transformed Pearson's correlation value between groups. Multiple regression analysis was performed to determine the significant predictors for markers colocalization. Proliferation and volumetric assays of the spheroid were analysed on GraphPad Prism v.7 (GraphPad) by 2-way ANOVA with multiple comparisons by Tukey test. Statistical significance was considered for values of $P<0.05$

3. Robust Detection of Microsatellite Instability (MSI) using Novel Panel of Mononucleotide Markers

3.1. Introduction

Although there are many different molecular classifications, a grouping identified in almost everyone is that which describes two distinct pathways of genomic instability i.e., MSI (microsatellite instability) and MSS (microsatellite stable). The MSS pathways is also referred to as the CIN (chromosomal instability) pathway. Cancers which are MSS develop along the canonical pathway of CRC (colorectal cancer) carcinogenesis through the accumulation of sequential mutations on various oncogenes and tumour suppressor genes, including APC, *KRAS*, *BRAF* and *TP53* (Fearon & Vogelstein, 1990; Pino & Chung, 2010). Meanwhile, cancers which have MSI develop have a defect in the DNA MMR (mismatch repair) protein, through either the inherited mutation observed in the LS (Lynch Syndrome) or hypermethylation of the promoter region of the genes in the case of the sporadic counterpart. The loss of function of DNA mismatch MMR genes such as *MLH1, MLH2, MSH2, MSH3, MSH6* or *PMS2*, results in a high mutation rate which is most easily detected by changes in length of microsatellite regions due to uncorrected strand slippage events during DNA replication (Peltomaki, 2003; Boland & Goel, 2010; Marzouk & Schofield, 2011).

Loss of MMR function therefore leads to a state of genome wide hyper-mutation and is seen in the CMS1 group (also called the mutator phenotype). Immunohistochemistry (IHC) can be used test for expression of the MMR proteins and MSI can be inferred if there is loss of any one of the proteins. Although IHC is a robust methodology with reported sensitivity and specificity of around 95% (Lindor, et al, 2002; Yuan, et al, 2015), the association of loss of protein expressions with MSI phenotype is not absolute. In some cases, mainly in the MSI-Low subtype or where a missense mutation results in loss of function, positive staining for all MMR proteins has been observed (Umar, et al,

2004). Confirmation of the mutator phenotype can only be obtained by actually demonstrating an increased mutation rate through testing for MSI.

In 1997, a workshop held by NCI (National Cancer Institute) have recommended the use of 5 markers as a reference panel for defining the MSI status, which are mononucleotide repeats BAT25 and BAT 26 and dinucleotide repeats D5S246, D2S123, and D17S250; samples with mutations found in more than 2 markers are interpreted as MSI-High while samples showing mutation only in one marker are classified as MSI-Low (Boland, et al, 1998). The revised version of NCI recommendation suggested that since mononucleotide markers were found to be more sensitive, additional mononucleotide markers (BAT40 and or MYCL) should be applied if only dinucleotide markers that are positive (Umar, et al, 2004). Since then, a panel of 5 quasi monomorphic mononucleotide repeats (BAT25, BAT26, NR21, NR 22 and NR 24) as MSI markers has been reported to show an increase sensitivity (100%) as compared to the NCI panel (Suraweera, et al, 2002).

Currently, this panel is now adopted in most diagnostic genetic labs and MSI screening protocols mostly involve the use of PCR with fluorescently tagged primers followed by CE (capillary electrophoresis) of the amplicon fragments. Alternatively, non-tagged primers can be used followed by DHPLC (denaturing high performance liquid chromatography) to measure the melting-temperature–dependent migration of reannealed amplicons through a solid-phase column. Nonetheless, the complexity of this approaches makes it relatively less suitable for robust use, in addition to the presence of stutter peaks that can complicate the data analysis (Janavicius, et al, 2010).

The application of HRMA (high-resolution melting analysis) following fluorescence-based PCR in detecting polymorphism within microsatellite regions

has been proposed, mainly in the area of plant science (Arthofer, et al, 2011; Distefano, et al, 2012; Ganopoulos, et al, 2011; Mackay, et al, 2008; Mader, et al, 2008; Pasqualone, et al, 2015; Xanthopoulou, et al, 2014). Despite being less studied, determination of microsatellite instability in CRC clinical samples showed that HRMA exhibits more than 90 % sensitivity and specificity in separating the MSI from MSS group, which also been confirmed by capillary electrophoresis (Janavicius, 2010). As previously published, our group also has been utilizing HRMA platform to screen for MSI on DNA derived from CRC patient tumour tissues. A panel of six mononucleotide repeats, consisting of 5 former mentioned markers, BAT25, BAT26, NR21, NR22 and NR24, with addition of BCAT25 marker, has been used to evaluate the MSI status in which showing instability at two or more markers (Fadhil, et al, 2012; Fadhil, et al, 2014).

In this chapter, the potential of new microsatellite markers was explored to further refine the use of HRMA as a low cost and robust method in detecting MSI in CRC using FFPE (formalin-fixed paraffin-embedded) clinical samples.

3.2. Results

3.2.1. Validation of IHC as a marker of MMR function

The Nottingham CRC case cohort was selected using IHC expression of MMR proteins as a marker of MMR function. A total of 99 cases were retrieved of which 46 had been deemed as being dMMR (deficient in MMR function) and 53 had been deemed to be proficient in pMMR (proficient in MMR function). Since there is a possibility of interpretation error of the IHC, it was necessary to confirm that the interpretation of the IHC was a correct reflection of the MMR function. A sub-group of 33 cases (15 MSI/18 MSS) was therefore tested by PCR followed by CE. Testing was undertaken by molecular genetic lab of NUH

(Nottingham University Hospital). There was 100% concordance between the IHC analysis and MSI test results, confirming that dMMR assessed by IHC and MSI are synonymous. Conversely, pMMR is considered identical with the MSS phenotype. This meant that the IHC could be used as a "gold standard" for validation of the MSI panel. The example of electropherogram for MSI and MSS cases are depicted at Figure 3.1.

3.2.2. Novel MSI biomarker identification, primer design and PCR optimization

As described in chapter 2 in this thesis, 11 different potential microsatellite markers were identified through literature search and bioinformatic analysis on various database including the Selective Targets in Human MSI-H Tumorigenesis Database (www.SelTar*base*.org). Selection criteria were (i) the mononucleotide repeat size is more than 10 bases and (ii) the published rate of mutation of the marker in MSI tumours of CRC and gastric cancer is >80%. Primers for PCR targeting the microsatellite regions were designed to give short amplicons (< 150 bp) to increase the sensitivity of the HRMA. The PCR protocol using the designed primers were optimised using cell lines DNA. A range of metrics were used in order to define the best primers including reproducibility, PCR efficiency and range of functioning annealing temperature. This part of the project was mainly carried out by the former member of our group, Dr. Henry Ebili.

Optimised protocols for each MSI markers were then tested using a small number of cases from the Nottingham cohort with known MSI/ MSS status. While BCAT25, BAT25 and BAT26 were tested with 27 samples (23 MSI and 4 MSS), all the other markers were tested with the 45 samples (23 MSI and 22 MSS).

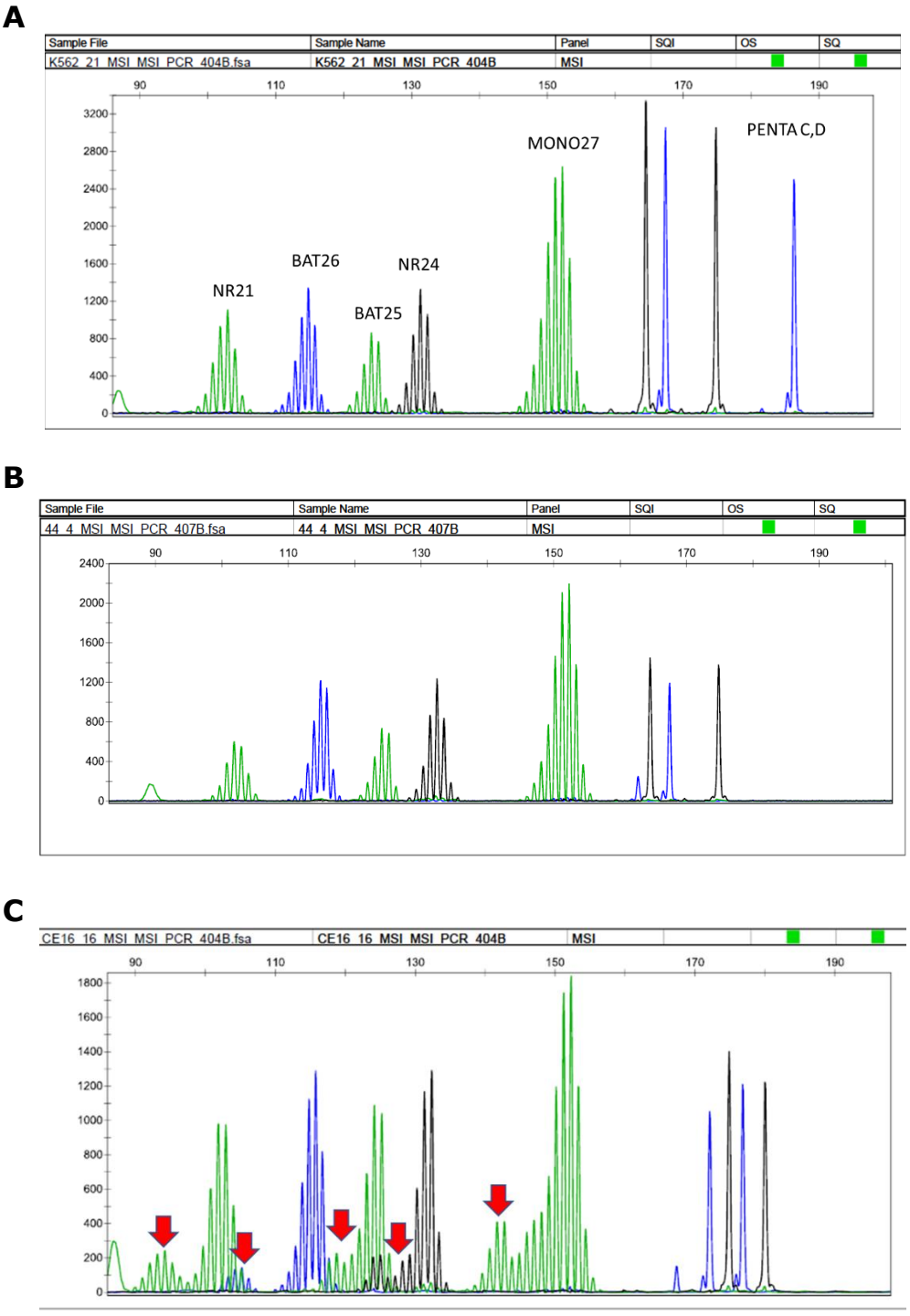


Figure 3.1. Capillary electrophoresis (CE) analysis of microsatellite markers. The CE was completed using Promega MSI System version 1.2 using 5 mononucleotide and 2 pentanucleotide markers as indicated. Electrogram are representative of samples from (A) Normal tissue (B) MSS tumour and (C) MSI tumour. Instability was observed when fragments analysis shown shifted allelic sizes of the mononucleotide markers (indicated with red arrows) compare to the normal sample.

From 11 different potential microsatellite loci, a panel of five markers comprising BAT25, BAT26, BCAT25, *MYB* and *EWSR1* was chosen as the one showing the best performance for the specificity and sensitivity as detailed in Table 3.1.

Table 3.1. Sensitivity and specificity of mononucleotide repeat microsatellite markers

MSI marker	True-positive	True-negative	False - positive	False-negative	Sensitivity (%)	Specificity (%)
BCAT25	23	4	0	0	100	100
BAT25	22	3	0	1	95.7	100
BAT26	21	3	0	1	95.5	100
ANGEL2	21	22	0	2	91.3	100
EWSR1	22	22	0	1	95.6	100
FBXO46	23	20	2	0	100	90.9
TCF4	21	22	2	0	91.3	100
TP53	23	22	0	0	75	100
MYB	22	22	0	1	95.7	100
MONO27	21	20	2	2	91.3	90.9
TYMS26	21	22	0	2	91.3	100

3.2.3. Limit of detection (LOD) determination of MSI Testing

In order to test the LOD of the new MSI biomarkers using the HRMA and to compare it to the standard screening platform, which is CE, two diploid cell lines were chosen for spiking experiments. DNA of HCT116, a confirmed MSI cell line, was spiked into DNA of known MSS cell line, SW837, to produce mixtures of DNA that contain various proportion of mutant allele, 50%; 25%; 12.5%; 6.25%; 3.125% and 1.625%. Each of these samples were then subjected to MSI fluorescence-based PCR prior to HRMA and CE analysis.

The HRMA relies on the formation of heteroduplexes that are less stable than homoduplexes of either wild type or mutant sequence, therefore, they melt at a lower temperature. To differentiate mutant from normal samples, difference plot of melting curve is generated. In this plot, sample curves are subtracted from a single reference (typically a wild-type control), run in the same

experiment. Overall, for the MSI markers, sufficient difference of melting pattern could be observed with confidence, using manual mutant calling, when MAF (mutant allele frequency) was as low as 6.25% in the sample, although for most markers, the HRMA analysis could still discriminate the spiked samples with the MAF of 1.56%. This detection level was found to be similar to limit of detection of the current standard method, the fluorescence multiplex PCR-based capillary electrophoresis that is being used clinically for MSI screening as depicted in Figure 3.2.

3.2.4. Testing the New Panel of MSI Markers with HRMA

A panel of five markers comprising BAT25, BAT26, BCAT25, MYB and EWSR1 was optimised for PCR followed by HRMA in order to detect MSI. This panel was used to test the 99 cases of the Nottingham cohort (46 dMMR and 53 pMMR). The cases were tested blind and the data were reviewed by two observers. Both observers correctly called every case. The panel was validated using the Edinburgh cohort of 88 (45 dMMR/MSI and 43 pMMR/MSS) which had been tested by PCR/CE. These were tested separately and in a blinded fashion. The HRM data were analysed by the same two observers and one observer correctly called all cases while the other observer miscalled two cases of MSI as MSS. Although the generally used threshold of instability at ≥2 markers (40%) for a call of MSI was applied, most cases usually showed instability at four to five markers and only one case, out of the total of 91 cases designated dMMR/MSI, was found to have instability at only two markers. Of the cases designated as MSS, 7% (7/96) had instability at one marker only while the remainder did not show any alteration in the microsatellite markers. Representative HRMA of MSI markers on CRC samples included in the Nottingham cohort are shown on Figure 3.3. The derivatives melting plot of the equivocal samples that cause the interobserver variability were depicted in Figure 3.4.

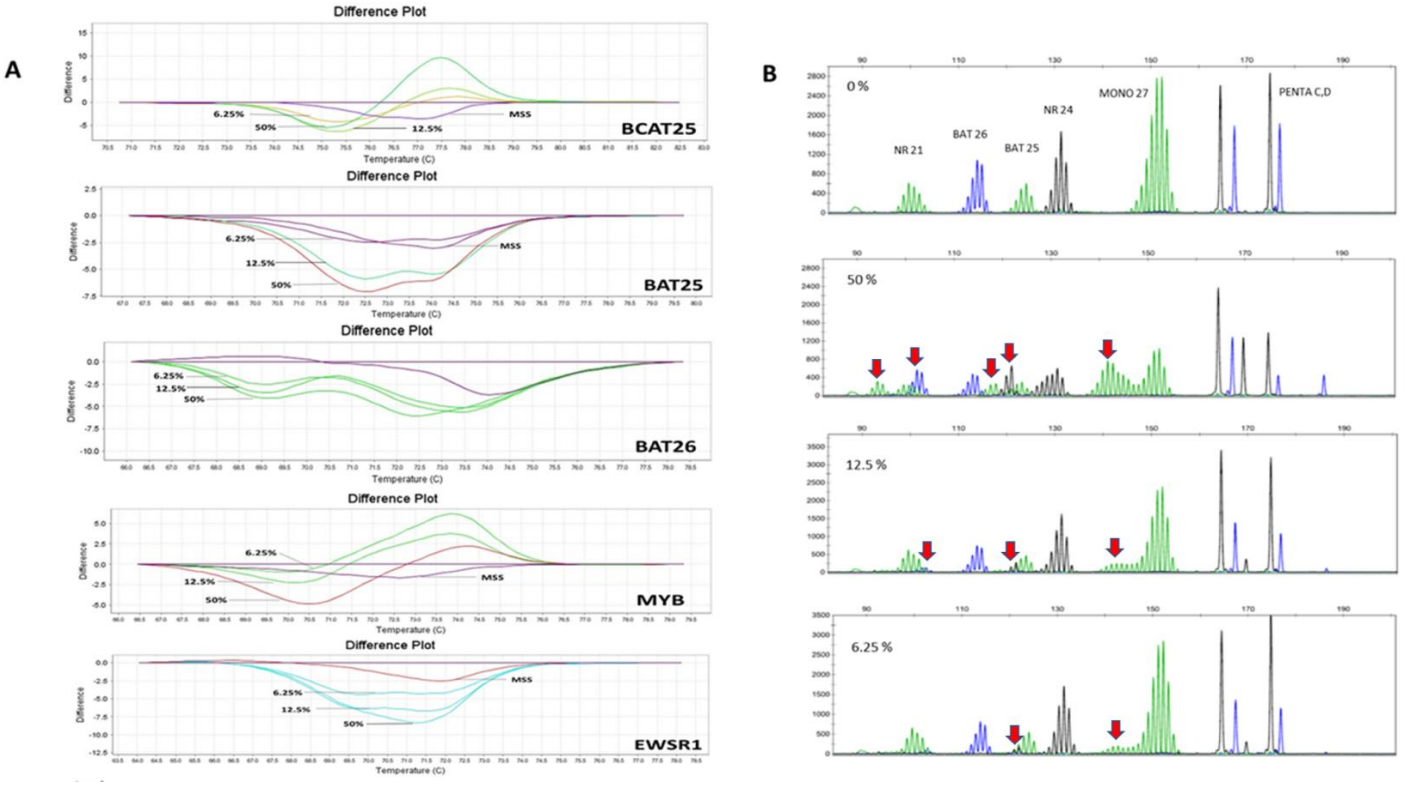


Figure 3.2. Limit of detection of MSI screening by high resolution melting analysis (A) and capillary electrophoresis (B). Cell line GT from HCT116 (MSI) was admixed to DNA from SW837 (MSS) to produce different proportion of mutant alleles with calculated percentage as indicated. HRMA was performed following one-stage fluorescence-labelled PCR run on ABI FAST 7500 machine on the panel of 5 mononucleotide microsatellite markers as indicated using ABI HRM v.2 software. The difference plots were subtracted from normalized fluorescence data using the one of the MSS sample an internal standard. Samples containing different amount of mutant DNA clearly show different melting pattern as compare to the MSS standard. Despite only single replicate of each samples were shown, the samples were run and analysed in triplicate with similar results. The capillary electrophoresis was completed using Promega MSI System version 1.2 using 5 mononucleotide and 2 pentanucleotide markers as indicated. Instability was observed when fragments analysis shown shifted allelic sizes of the mononucleotide markers compare to the normal sample.

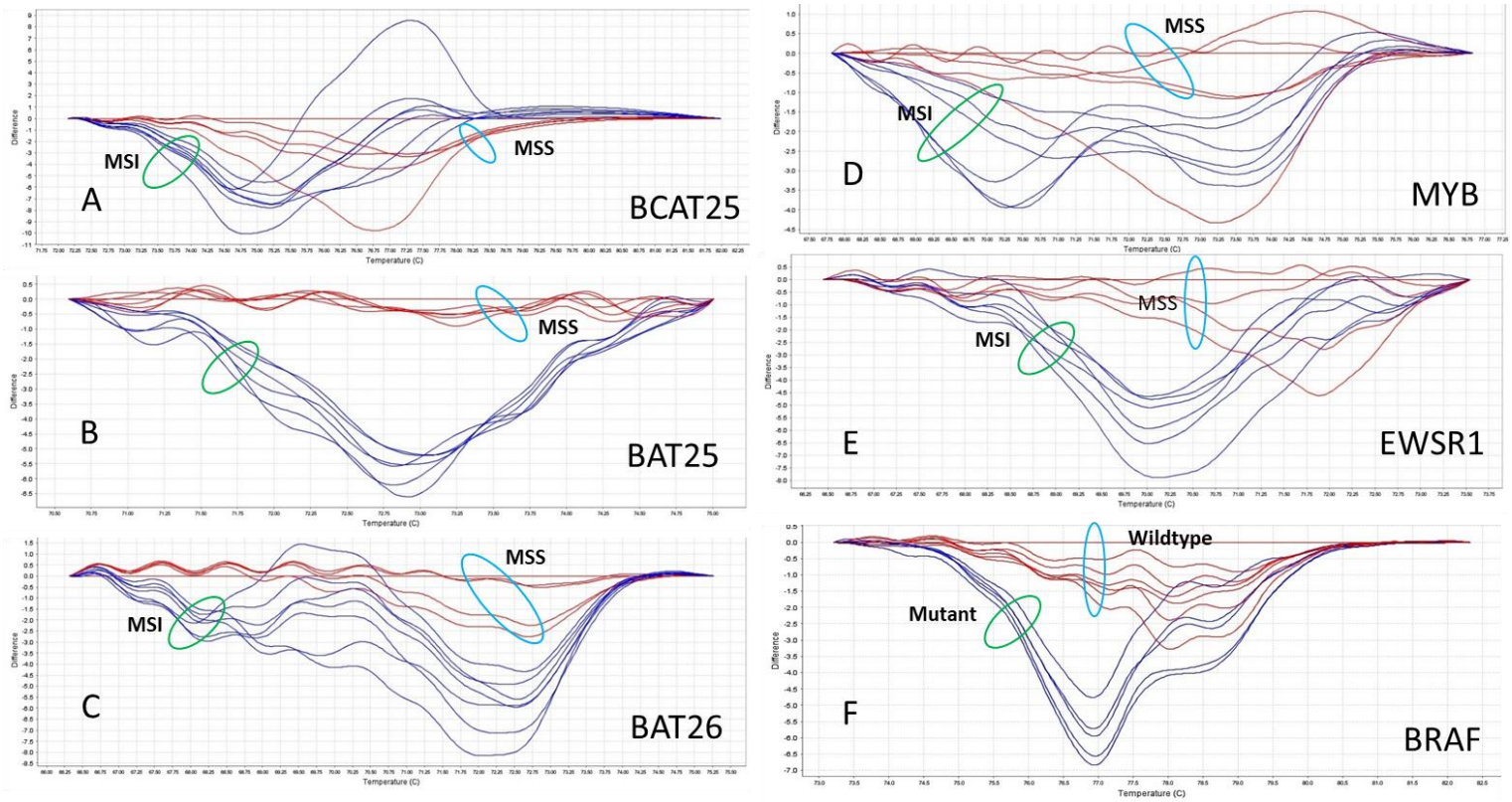


Figure 3.3. Detection of microsatellite instability (MSI) and *BRAF* codon V600E mutation using high-resolution melting analysis (HRMA). Representative randomized cases of colorectal cancer(n=12) were tested using panel of five MSI mononucleotide markers and *BRAF* codon V600E on single PCR run. It can be clearly seen that the derivative melt curves of the tumours with microsatellite instability (MSI) are different from those that are microsatellite stable (MSS). If any marker in a tumour with MSI is stable, it will usually melt in the same way as the markers in the MSS tumours. Similarly, the mutant cases of *BRAF* can be easily discriminated from the wildtype by observing the derivative melting plot.

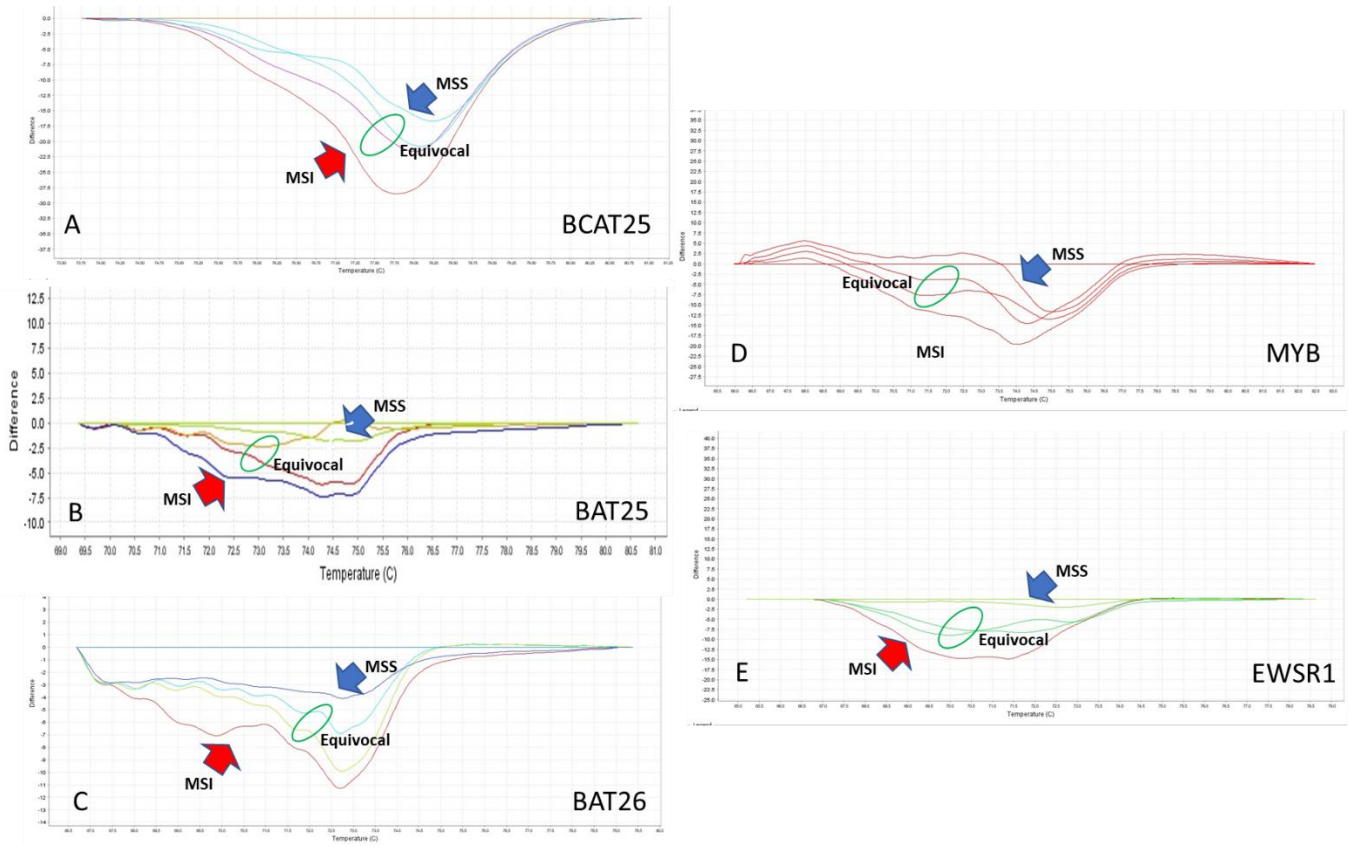


Figure 3.4. Interobserver variation between two observers on microsatellite (MSI) detection by high resolution melting analysis (HRMA). The derivative melting plot of five MSI markers for the two equivocal samples, indicated by the green circle were shown together with the sample that clearly showing as MSI, indicated by the red arrow and microsatellite stability (MSS), indicated by the blue arrow. Each sample were examined in duplicate, however, only representative of one difference melting plot were shown for each sample. The equivocal samples were likely to have low number of heteroduplexes thus the less prominent differences in derivative melting curve were observed.

3.3. Discussion

In this chapter a panel of five markers was developed, which includes two established markers (BAT25, BAT26) and three novel markers (BCAT25, *MYB* and *EWSR1*) for the detection of MSI using HRMA. Using DNA from an MSS cell line spiked with different amounts of a cell line which has MSI, the HRMA method has a similar LOD as CE analysis (≈6.25% mutant DNA), but CE analysis can be complicated by stutter bands that can cause difficulty in allele sizing (Javanicius, et al, 2010; Stewart, et al, 2011).

The panel was validated in two different cohorts which had been tested for MMR protein expression or MSI as part of routine diagnostic testing. Each cohort was tested separately and, when combined, the panel showed near perfect concordance in a total of 187 CRC. Analysis of the HRM data was undertaken by two observers, demonstrating that the data analysis is easy and reproducible. One observer correctly called all cases while the other observer miscalled two cases of MSI as MSS. This perhaps due to the low number of heteroduplexes for those particular sample (maybe caused by less effective PCR or low tumour content) which led to the less prominent difference in derivative melting curve between these MSI cases and the MSS and or control samples running at the same experiment.

The MSI markers developed in this project involves a panel of five PCRs that are performed in a single run using a single cycling programme. It could hugely improve workflow in the laboratory since HRMA is performed in-tube on completion of the PCR and, in contrast to CE or dHPLC, transfer of PCR products to another platform for further analysis is not required. Most modern real-time PCR machines will have HRMA capabilities and expensive specialist equipment is not required. This reduces the cost of the testing both in terms of equipment

and time. Furthermore, since it is a closed-tube test, the risk of laboratory contamination with PCR products is eliminated.

Although the test was designed for research purposes, it would potentially have use in the diagnostic setting once fully validated. As well as the cost savings and the reduced risk of contamination, the ease of the methodology and data interpretation means this test could probably be performed in non-specialist diagnostic pathology laboratories. This becomes pertinent when considering that testing for MSI is likely to increase in diagnostic practice as it provides information which can be used to stratify patients into groups eligible for treatment with 5-fluorouracil-based therapy (Des Guetz, et al, 2009; Klingbiel, et al, 2015; Weber, et al, 2015) or immunotherapy (Llosa, et al, 2015; Xiao, et al, 2015; Le, et al, 2015; Overman, et al, 2017).

Recent guidelines from NICE have recommended that all CRCs are screened for the possibility of LS. Discriminating LS-associated MSI from sporadic MSI requires further testing for *BRAF* mutation and *MLH1* promoter methylation. As shown in the next chapter, *BRAF* mutation can be detected by HRMA. Although not directly relevant to this work, an HRMA-based test for *MLH1* promoter methylation was also developed later (by former member of the group, Dr. Wakkas Fadhil to the panel; data now shown in this thesis) and established a closed-tube panel test for LS screening called N_LyST (Nottingham Syndrome Test) (Susanti, et al, 2018). Thus, in a single PCR-run and using a single thermocycling protocol, it is possible to test for MSI, *BRAF* mutation and MLH1 promoter methylation in order to screen for LS. Compared to the standard methodology being used in diagnostic labs, this would be a huge improvement in efficiency and cost.

An important question is whether the HRMA-based test—since it is a screening

test—is relevant in the era of NGS (next-generation sequencing). The sheer sequencing power of NGS platforms would allow the MMR genes and multiple microsatellites to be sequenced in a single test (Nowak, et al, 2017; Redford, et al, 2018) However, microsatellite regions can be problematic from some NGS platforms and, where there is low tumour epithelium content, great sequencing depth maybe required. The economic analyses performed as part of the NICE guidelines concluded that it was more cost-effective to screen the tumour samples prior to germline sequencing (NICE, 2017). Since this test can be performed in less time than that required for library preparation and sequencing with NGS, a case for including the test in the testing pathway can be made. Furthermore, this test can be easily employed in resource-limited countries where the use of NGS is still less feasible. We are very confident of its utility (where sample quality is low) and its portability (it does not require expensive machines and has minimal infrastructure requirement). Moreover, HRMA protocols and data analysis are simple and can be performed by trained laboratory technicians. Thus, this test can be applied widely as point of care (POC) services.

In summary, a panel for the detection of MSI has been developed and validated in CRC cohort from both Nottingham and Edinburgh. We accept that there is a slight degree of circularity in as much as part of the validation was done on the Nottingham cohort of 99 cases which had previously been tested by IHC for expression of MMR proteins. These cases were next tested for mutation in key driver genes.

4. Molecular Profiling of Colorectal Cancer

4.1. Introduction

Colorectal cancer (CRC) is a heterogeneous disease and tumours develop along a variety of different genetic pathways, which may be closely linked to the clinical features of the disease such as prognosis and response to the treatment (Brenner *et al*., 2014). In 1990, Fearon and Vogelstein were the first to propose a genetic model for CRC tumorigenesis, describing it as a series of genetic alteration. It has been reported that mutation on 5q chromosome, which is the somatic mutation of the *APC* (adenomatous polyposis coli) gene together with the loss of the wild-type allele, occurs in early stage of tumorigenesis results in hyperproliferation of gut epithelium, which subsequently develops into adenoma in combination with mutational activation of oncogenes, in particular the *Ras* family (Fearon & Vogelstein, 1990; Pino & Chung, 2010). Further, allelic deletion of chromosomes 17p and 18q, in particular the mutation of p53 gene followed by allelic loss, have been suggested to contribute to the transformation of late-stage adenoma to carcinoma especially after the accumulation of mutation on at least four to five genes (Fearon & Vogelstein, 1990).

The most established molecular classification of CRC was based on two major distinct pathways of genomic instability in CRC carcinogenesis, which are CIN (chromosomal instability) or interchangeably considered as MSS (microsatellite stable) and MSI (microsatellite instability). About 85% of sporadic CRC cases were categorized as CIN as they showed frequent structural changes of the chromosomes as well as aneuploidy. The remainder (about 15%) were MSI, that showed a deficiency in the DNA mismatch repair (MMR) genes such as of MLH1, MLH2, MSH2, MSH3, MSH6 or PMS2. Loss of MMR function resulted in changes in the length of microsatellites (normal segments of DNA consisting of multiple repeats of sequences 1-6 nucleotide in length (Peltomaki, 2003; Boland & Goel, 2010; Marzouk & Schofield, 2011).

Defective MMR (mismatch repair) proteins that give rise to MSI can be caused either by germline mutations of the MMR genes in LS (Lynch syndrome) or by somatic hypermethylation of the MLH1 gene and rarely, somatic mutations of the MMR genes in sporadic CRC (Eshleman & Markowitz, 1995; Haraldsdottir, et al, 2014). Defective MMR leads to hypermutation of the genome, possibly generating tumour neoantigens (Eshleman, et al, 1995; Heemskerk, et al, 2013; Llosa, et al, 2015). Arguably, this may explain the observation of the profound lymphocyte infiltration and better outcomes in CRC with MSI (Popat, et al, 2005; Lockhead, et al, 2013; Goldstein, et al, 2014; LIosa, et al, 2015; Angelove, et al, 2015; Becht, et al, 2016; Lal, et al, 2018). Currently, the screening for the DNA dMMR (deficient mismatch repair) and/or MSI status is widely implemented in the clinical diagnosis of CRC, mainly due to (i) the significant association with the LS (Giardiello, et al, 2014; NICE, 2017), (ii) lack of benefit of 5-fluoruracil adjuvants in patients with MSI tumours was reported (Jover, et al, 2009; Schmoll, et al, 2012; Webber, et al, 2015), and (iii) good response to immune check point inhibitors (Le, et al, 2015; Overman, et al, 2017).

This chapter of the thesis describes the molecular profile of two main subtypes of CRC, the MSI and MSS using the FFPE (formalin-fixed paraffin-embedded) clinical samples. The association between the genetic features was also explored.

4.2. Results

4.2.1. Frequency of oncogene somatic mutation on microsatellite stable (MSS) and microsatellite instable (MSI)

Of the 101 CRC case of the Nottingham cohort, 99 cases were screened for the

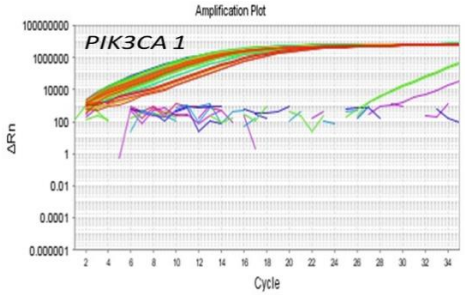
somatic genetic mutation on several hotspots of well-reported oncogenes, including *KRAS*, *BRAF* and *PIK3CA*. The mutation detection was carried out using fluorescence-based PCR followed by the HRMA (high-resolution melting analysis), similar to the MSI detection discussed in the previous chapter of this thesis. Our research group has developed the QMC (Quick Multiple Consensus)-PCR (polymerase chain reaction) and used it extensively for somatic mutation detection (Fadhil, *et al.*, 2010; Ibrahem, *et al.,* 2010; Ebili, et al, 2017). This technique was designed mainly for FFPE-derived DNA which usually considered as low-quality templates for PCR. It is a two-step nested procedure, consisting of two stages which are the PDM (pre-diagnostic multiplex) reaction using a mix of up to 10 pairs of the outer primers and the SSD (specific single diagnostic) reaction in which each hotspot is amplified individually.

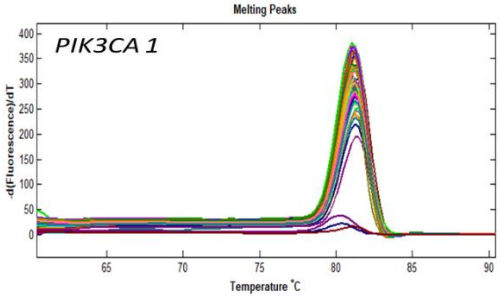
In this project, the QMC-PCR was employed to investigate the mutation covering the hotspots on *KRAS* exon 2, 3, and 4; *PIK3CA* exon 9 and 20 and *BRAF* exon 11. The outer primer pairs for these targets were combined on one multiplex PCR reaction. The inner primer pair for each target was then used to amplify each target. The inner primers were designed and used in previous studies in our group (Ibrahem, et al, 2010, Fadhil, et al, 2010, Fadhil, et al, 2014) to provide the final amplicon size about 150bp to ensure the sensitivity of the HRMA. Positive and negative controls for mutation screening included in this study have been previously confirmed by NGS (Next generation sequencing) for specific targets and used as reference controls for data normalisation. The differences in DNA melting between wild-type and mutant allele can be observed simply in the melting plots generated by the software. The amplification plot, the melting curve and the normalised derivative melting curve for all targets included in the QMC-PCR were shown on Figure 4.1.

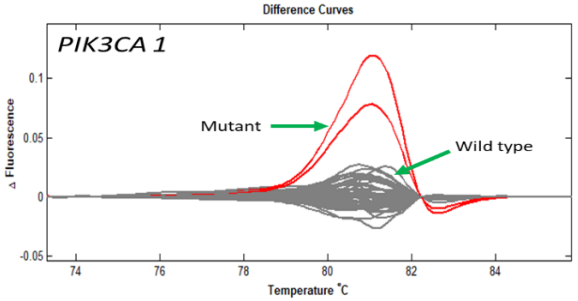
New primers to screen for *BRAF* codon 600 mutation were designed and optimised to work as a single-stage test using the cycling conditions for MSI

testing described in the chapter 3 of this thesis with the purpose to develop a panel to screen for LS. Primers were optimised and tested on cell lines with known *BRAF* mutation status (data not shown). Representative HRMA of *BRAF* codon 600 on CRC samples included in the Nottingham cohort is depicted on Figure 3.3 along with the MSI marker

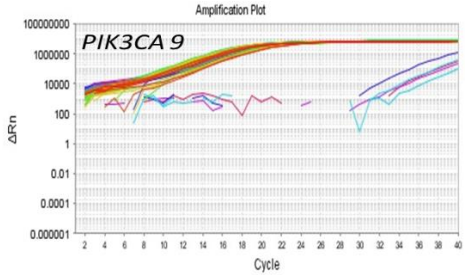
A

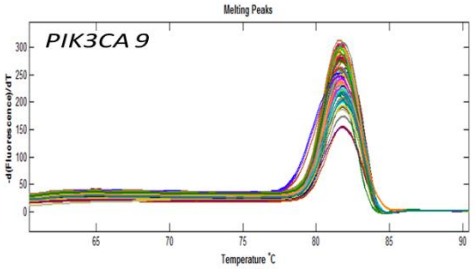

Amplification Plot
PIK3CA 1
ΔRn
Cycle

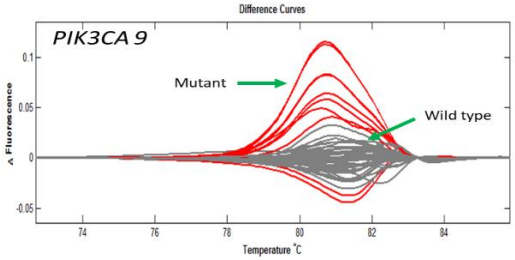

Melting Peaks
PIK3CA 1
-d(Fluorescence)/dT
Temperature °C


Difference Curves
PIK3CA 1
Mutant
Wild type
Δ Fluorescence
Temperature °C

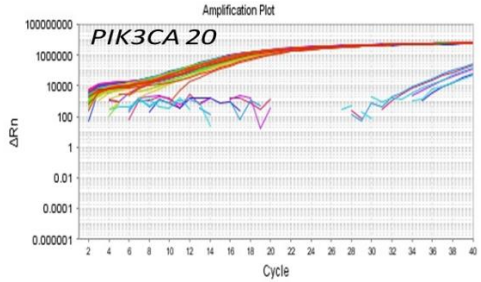
B

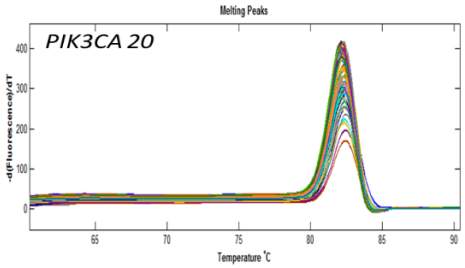

Amplification Plot
PIK3CA 9
ΔRn
Cycle

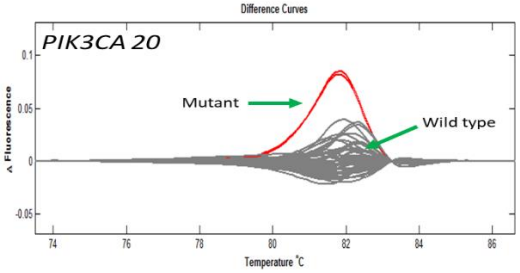

Melting Peaks
PIK3CA 9
-d(Fluorescence)/dT
Temperature °C


Difference Curves
PIK3CA 9
Mutant
Wild type
Δ Fluorescence
Temperature °C

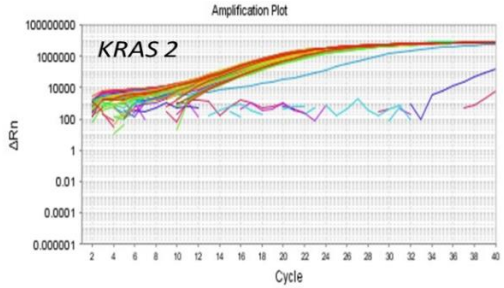
C

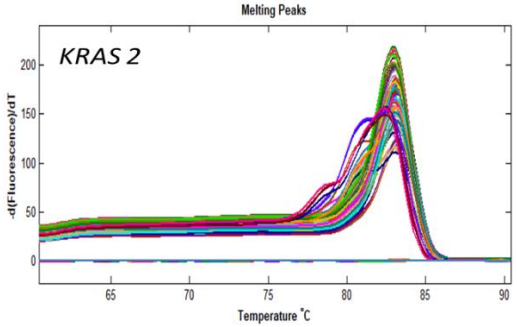

Amplification Plot
PIK3CA 20
ΔRn
Cycle

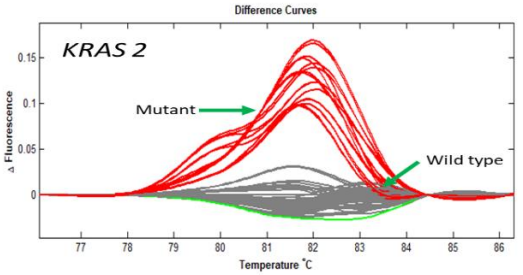

Melting Peaks
PIK3CA 20
-d(Fluorescence)/dT
Temperature °C


Difference Curves
PIK3CA 20
Mutant
Wild type
Δ Fluorescence
Temperature °C

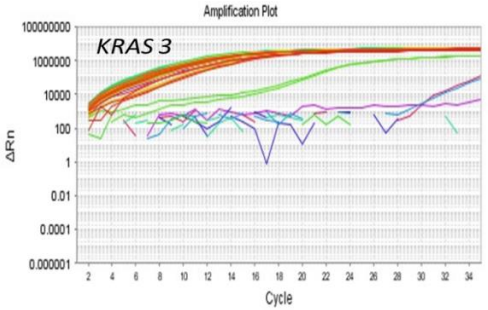
D

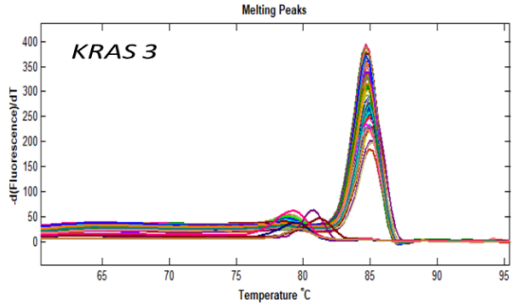

Amplification Plot
KRAS 2
ΔRn
Cycle

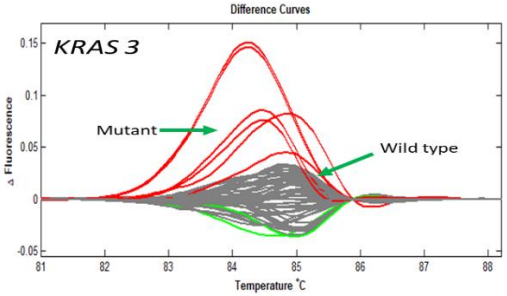

Melting Peaks
KRAS 2
-d(Fluorescence)/dT
Temperature °C


Difference Curves
KRAS 2
Mutant
Wild type
Δ Fluorescence
Temperature °C

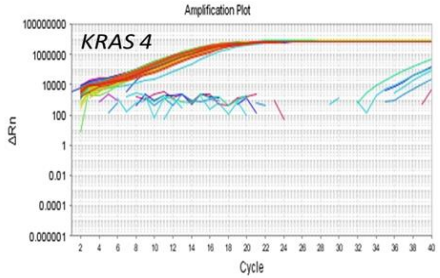
E

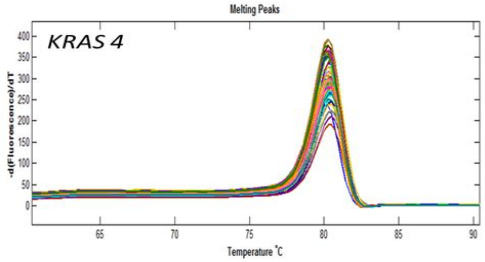

Amplification Plot
KRAS 3
ΔRn
Cycle

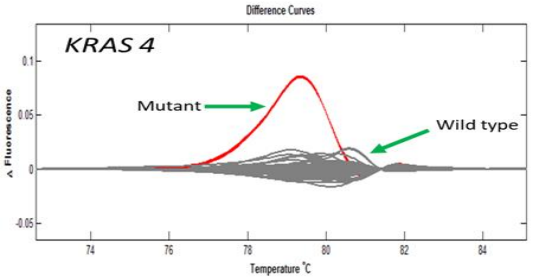

Melting Peaks
KRAS 3
-d(Fluorescence)/dT
Temperature °C


Difference Curves
KRAS 3
Mutant
Wild type
Δ Fluorescence
Temperature °C

F


Amplification Plot
KRAS 4
ΔRn
Cycle


Melting Peaks
KRAS 4
-d(Fluorescence)/dT
Temperature °C


Difference Curves
KRAS 4
Mutant
Wild type
Δ Fluorescence
Temperature °C

G

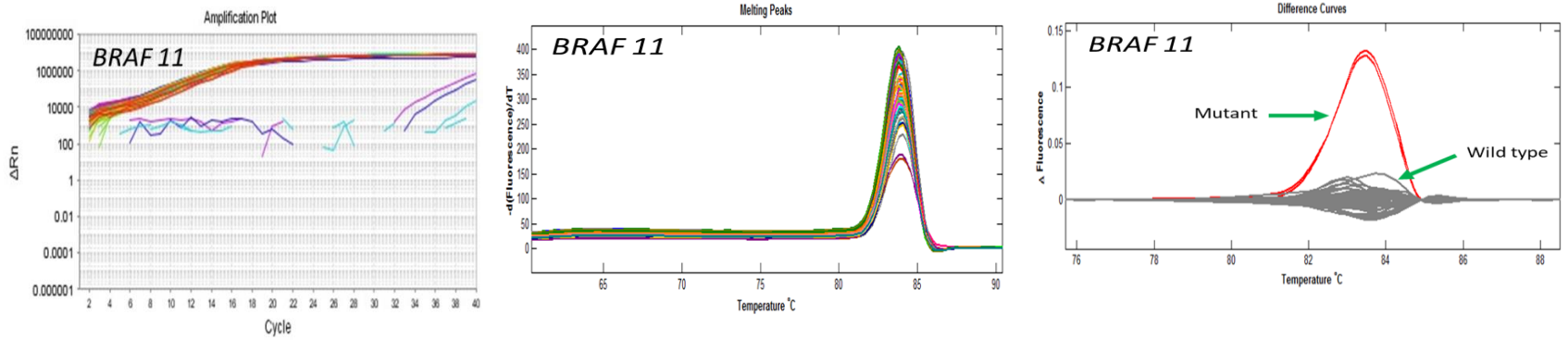


Figure 4.1. High-resolution melting analysis (HRMA) of driver gene mutations on colorectal cancer. The PCR amplification plot (left panel), the derivative melting curve (middle panel) and the difference plot and variant calling (right panel) of (A) *PIK3CA* exon 1; (B) *PIK3CA* exon 9; (C) *PIK3CA* exon 20; (D) *KRAS* exon 2; (E) *KRAS* exon 3; (F) *KRAS* exon 4 and (G) *BRAF* exon 11. The PCR was carried out and the amplification plot was derived from the FAST 7500 Real-Time PCR (Applied Biosystem, USA). The HRMA was carried out using the LightScanner HRM system (Idaho Technology, USA). The temperature shift was performed following the normalization of the fluorescence (Y) axis onto a 0 to 100% scale followed by auto scanning analysis with the "common vs variant" grouping to determine mutant and wildtype samples. The internal instrument-sensitivity setting was set as normal with the threshold of 4%. Each sample was run in duplicate and the inconclusive results were subjected to another run of PCR followed by HRMA.

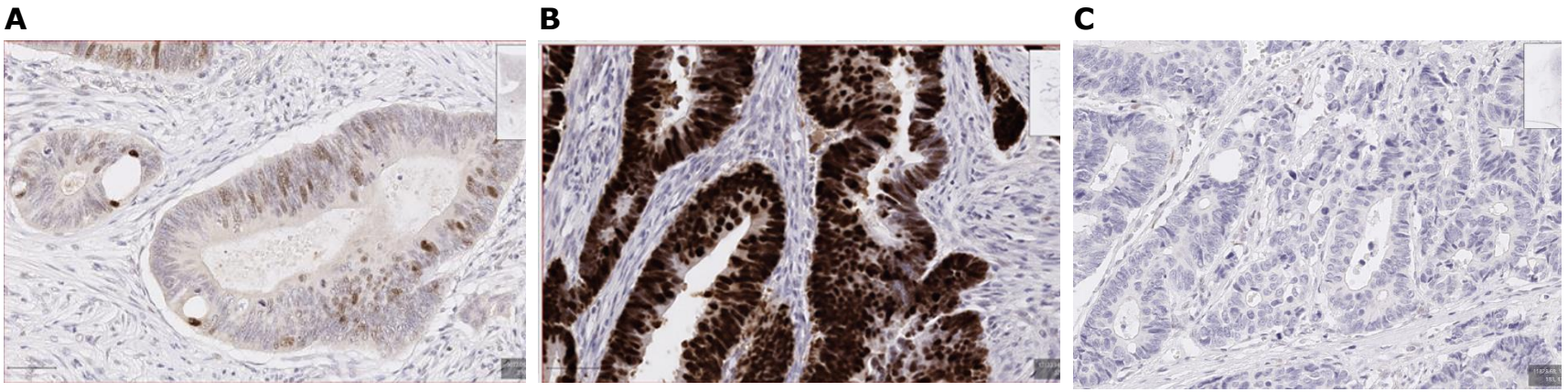


Figure 4.2. Immunohistochemistry (IHC) of p53 on colorectal cancer. (A) Normal/ low expression staining (B) Strong positive staining and (C) Negative staining on the nucleus of the tumour cells. Digital images were captured on Aperio AT2 slide scanner (Leica, USA) at 20x magnification. The strong positivity and negativity of the IHC staining indicate *TP53* mutation.

Table 4.1. Pattern of p53 immunohistochemistry staining on colorectal cancer

	p53 staining (number of cases)		
	Negative	Positive	Normal
MSI	4	5	35
MSS	15	25	15

The expression pattern of p53 protein was examined using IHC as a surrogate to detect the mutation of *TP53* gene. This approach was selected due to the fact that mutation of *TP53* in CRC occurs on wide range of positions within the DNA binding domain, (exon 5-8), covering hotspot codons such as 175, 245,248, 273 and 282 (Lacoppeta, et al, 2003). This makes the low-throughput PCR with HRMA less effective for screening for *TP53* mutation. The IHC of p53 protein has been reported as a fast and reliable method to detect the somatic mutation for *TP53*. As depicted in Figure 4.2, the tumour tissue with normal/ wildtype expression of *TP53* showed a low level of nuclear expression of the p53 protein whereas the mutant showed either the strong overexpression (>10% of tumour cells) or completely loss of expression of the protein. Table 4.1 described the frequency of three staining pattern among the MSI and MSS cases.

The frequency of the somatic mutation at various hotspot of the oncogenes found on the Nottingham Cohort of CRC is listed on Table 4.2. The comparison was made based on the microsatellite instability status. The results showed the high concordance with the published literature. The *KRAS* mutation was found on 10 out of 44 (22.7%) of MSI-CRC and 25 out of 55 (45.5%) of MSS-CRC. Majority (31.3%) of *KRAS* mutation was in exon 2 (covering codon 12 & 13) with only 5% of total cases showing mutation in exon 3 (covering codon 59-61). One case had mutations on both exon 2 and 3. No mutation was found on *KRAS* exon 4 (covering codon 146). The *PIK3CA* mutation was found on 9 (20.5%) of MSI with one case showed mutations on exon 1 and 20, and 8 (14.5%) of MSS cases. Mutation of the *BRAF* gene was found on 24/44 (45.5%) of MSI cases with one case showing mutation on both exon 11 and 15, and 6/55 (10.9%) of MSS cases. This frequency of mutation is consistent with published data and confirms the significant association of MSI with *BRAF* exon 15 mutation ($P<0.0001$, Fisher's exact test). As seen in table 4.2, the IHC

results showed that 9/44 (20.5.%) of MSI cases and 40/55 (72.7%) of MSS cases harboured *TP53* mutation. Based on the IHC staining pattern, 19 out of 49 mutant cases (38%) showed negative staining, while the remaining of 30 cases (62%) showed strong positive staining. The fisher-exact test showed that *BRAF* exon 15 (V600E) mutation was significantly higher among the MSI cases meanwhile *TP53* mutation was significantly greater on the MSS cases (p<0001 for both, Fisher's exact test).

Table 4.2. Frequency of driver gene mutations in the Nottingham cohort of colorectal cancer

		Microsatellite instability		**Fisher's exact test Exact significance (2-sided)**
		MSI (n=44)	MSS (n=55)	
KRAS exon 2	Mutant	10 (22.7%)	21 (38%)	0.128
	Wild type	34 (77.3%)	34 (62%)	
KRAS exon 3	Mutant	0 (0%)	5 (9%)	0.064
	Wild type	44 (100%)	50 (91%)	
KRAS exon 4	Mutant	0 (0%)	0 (0%)	NA
	Wild type	44 (100%)	55 (100%)	
PIK3CA exon 1	Mutant	1 (2.3%)	0 (0%)	0.444
	Wild type	43 (97.7%)	55 (100%)	
PIK3CA exon 9	Mutant	5 (11.4%)	7 (12.7%)	1.000
	Wild type	39 (88.6%)	48 (87.3%)	
PIK3CA exon 20	Mutant	4 (9.1%)	1 (1.8%)	0.168
	Wild type	40 (90.9%)	54 (98.2%)	
BRAF exon 11	Mutant	1 (2.3%)	1 (1.8%)	1.000
	Wild type	43 (97.7%)	54 (98.2%)	
BRAF exon 15	Mutant	24 (45.5%)	5 (9%)	<0.0001*
	Wild type	20 (54.5%)	50 (91%)	
TP53	Mutant	9 (20.5%)	40 (72.7%)	<0.0001*
	Wild type	36 (79.5%)	15 (27.2%)	

4.2.2. Association between *KRAS*, *BRAF* and *PIK3CA* mutation

Mutation in *KRAS*, *BRAF* and *PIK3CA* are commonly present in colorectal cancer (CRC). *KRAS* and *BRAF* form part of the MAPK signalling pathway and *KRAS* lies immediately upstream of *BRAF*. Consequently, *KRAS* and *BRAF* mutations are

mutually exclusive with mutation in either one causing activation of MAPK signalling (De Roock, et al, 2010). Our result validates this negative association between *KRAS* exon 2 and *BRAF* exon 15 mutations as described in Table 4.3 (p=0.018), Fisher's exact test). The association remained significant when combined *KRAS* and *BRAF* mutations at different hotspots were tested (P=0.012, Fisher's exact test. The association is not exclusive to either MSI or MSS subgroup. Interestingly, although considered as very rare phenomena, there were 4 MSI cases that showed mutations on both *BRAF* exon 15 and *KRAS* exon 2. The difference plot of the HRMA of the 4 double mutants were depicted in Figure 4.3.

We first then tested the Nottingham cohort for association of mutation in different hotspots of *KRAS* and *PIK3CA*. Mutations in *KRAS* exon 2 were significantly associated with mutations in *PIK3CA* exon 9 (P=0.046, Fisher's exact test) and the association was not exclusive to either MSI or MSS subgroup. There was however neither an association between *KRAS* exon 2/*PIK3CA* exon 1 nor between *KRAS* exon 2/ *PIK3CA* 20 as detailed on table 4.4. We then explored the association between mutation of *BRAF* and *PIK3CA*. As shown in table 4.5, no significant association between *BRAF* and *PIK3CA* mutations in the Nottingham cohort of CRC was found.

Our analysis showed an association between mutation of *KRAS* and *PIK3CA.* This is in line with reports in the literature and prompted us to wonder whether there was a similar association between mutation of *BRAF* and *PIK3CA.* This would be intuitive as both *KRAS* and *BRAF* form part of the MAPK signalling pathway and somatic mutations in these genes are mutually exclusive. We did not find an association within the Nottingham cohort but, given that *BRAF* mutations are much less common than *KRAS* mutation, it was decided to test the previously described Edinburgh cohort of CRC in order to expand the data set. This cohort was tested for mutation in *PIK3CA* exon 9 and exon 20 and

BRAF exon 15 mutations and the data from the two cohorts were combined in order to test the association with *BRAF* exon 15 (codon 600) mutation. Mutations in *BRAF* codon 600, *PIK3CA* exon 9 and exon 20 were detected in 54/187 (28.9%), 23/187 (12.3%) and 8/187 (4.3%) samples, respectively. Unexpectedly, as detailed on table 4.6, a significant negative association of mutations in *BRAF* codon 600 with mutation in *PIK3CA* exon 9 (p=0.034, Fisher's exact test) was found, regardless to the MSI status. Furthermore, there was neither an association between *BRAF* codon 600/*PIK3CA* exon 20 nor between *BRAF* codon 600/ combined *PIK3CA* exon 9 and exon 20.

4.2.3. Association between *TP53* mutation with the other driver gene mutations

We also tested the Nottingham cohort for association of *TP53* mutation and mutation in different hotspots of *KRAS, BRAF* and *PIK3CA*. As detailed in table 4.7, there was a significant association between *TP53* mutation with *KRAS* exon 2 mutation among the MSS (P=0.012, Fisher's exact test). As shown in table 4.8, when the analysis was carried out on the combined mutation from different hotspot, a significant association between *TP53* and *PIK3CA* mutation in the MSS subgroup (P=0.028) was also found.

Table 4.3. Frequency and association of *KRAS* and *BRAF* mutation in the Nottingham cohort of colorectal cancer

			KRAS		
			Exon 2		**Fisher's exact test Exact significance (2-sided)**
			Mutant (n=31)	**Wildtype (n=68)**	
	MSI	Mutant	0	1	1.000
		Wildtype	10	33	
***BRAF* exon 11**	MSS	Mutant	1	0	0.382
		Wildtype	20	34	
	All	Mutant	1	1	1.000
		Wildtype	30	67	
	MSI	Mutant	4	20	0.472
		Wildtype	6	14	
***BRAF* exon 15**	MSS	Mutant	0	5	0.144
		Wildtype	21	29	
	All	Mutant	4	25	0.018*
		Wildtype	27	43	
All *BRAF*	MSI	Mutant	4	20	0.472
		Wildtype	6	14	
	MSS	Mutant	1	5	0.390
		Wildtype	20	29	
	All	Mutant	5	25	0.058
		Wildtype	26	43	
			Exon 3		
			Mutant (n=5)	**Wildtype (n=94)**	
	MSI	Mutant	0	1	NA
		Wildtype	0	43	
***BRAF* exon 11**	MSS	Mutant	0	1	1.000
		Wildtype	5	49	
	All	Mutant	0	2	1.000
		Wildtype	5	92	
	MSI	Mutant	0	24	NA
		Wildtype	0	20	
***BRAF* exon 15**	MSS	Mutant	0	5	1.000
		Wildtype	5	45	
	All	Mutant	0	29	0.318
		Wildtype	5	65	
***BRAF* combined**	MSI	Mutant	0	24	NA
		Wildtype	0	20	
	MSS	Mutant	0	6	1.000
		Wildtype	5	44	
	All	Mutant	0	30	0.319
		Wildtype	5	64	
			Combined		
			Mutant (n=35)	**Wildtype (n=64)**	
***BRAF* combined**	MSI	Mutant	4	20	0.472
		Wildtype	6	14	
	MSS	Mutant	1	5	0.204
		Wildtype	24	25	
	All	Mutant	5	25	0.012*
		Wildtype	30	39	

Table 4.4. Frequency and association of *KRAS* and *PIK3CA* mutation in the Nottingham cohort of colorectal cancer.

			KRAS		**Fisher's exact test Exact significance (2-sided)**
			Exon 2		
			Mutant (n=31)	**Wildtype (n=68)**	
***PIK3CA* exon 1**	MSI	Mutant	1	0	0.227
		Wildtype	9	34	
	MSS	Mutant	21	34	NA
		Wildtype	0	0	
	All	Mutant	1	0	0.313
		Wildtype	30	68	
***PIK3CA* exon 9**	MSI	Mutant	2	3	0.317
		Wildtype	8	31	
	MSS	Mutant	5	2	0.092
		Wildtype	16	32	
	All	Mutant	7	5	0.046*
		Wildtype	24	63	
***PIK3CA* exon 9**	MSI	Mutant	1	3	1.000
		Wildtype	9	31	
	MSS	Mutant	0	1	1.000
		Wildtype	21	33	
	All	Mutant	1	4	1.000
		Wildtype	30	64	
***PIK3CA* combined**	MSI	Mutant	3	6	0.402
		Wildtype	7	28	
	MSS	Mutant	5	3	0.236
		Wildtype	16	31	
	All	Mutant	8	9	0.154
		Wildtype	23	59	
			Exon 3		
			Mutant (n=5)	**Wildtype (n=94)**	
***PIK3CA* exon 1**	MSI	Mutant	0	1	NA
		Wildtype	0	43	
	MSS	Mutant	0	0	NA
		Wildtype	5	50	
	All	Mutant	0	1	1.000
		Wildtype	5	93	
***PIK3CA* exon 9**	MSI	Mutant	0	5	NA
		Wildtype	0	39	
	MSS	Mutant	0	7	1.000
		Wildtype	5	43	
	All	Mutant	0	12	1.000
		Wildtype	5	82	
***PIK3CA* exon 9**	MSI	Mutant	0	4	NA
		Wildtype	0	40	
	MSS	Mutant	1	0	0.091
		Wildtype	4	50	
	All	Mutant	1	4	0.233
		Wildtype	4	90	
***PIK3CA* combined**	MSI	Mutant	0	9	NA
		Wildtype	0	35	
	MSS	Mutant	1	7	0.559
		Wildtype	4	43	
	All	Mutant	1	16	1.000
		Wildtype	4	78	
			Combined		
			Mutant (n=35)	**Wildtype (n=64)**	
***PIK3CA* combined**	MSI	Mutant	3	6	0.402
		Wildtype	7	28	
	MSS	Mutant	6	2	0.123
		Wildtype	19	28	
	All	Mutant	9	8	0.105
		Wildtype	26	56	

Table 4.5. Frequency and association of *BRAF* and *PIK3CA* mutation in the Nottingham cohort of colorectal cancer

			BRAF **Exon 11**		**Fisher's exact test Exact significance (2-sided)**
			Mutant (n=2)	**Wildtype (n=97)**	
***PIK3CA* exon 1**	MSI	Mutant	0	1	1.000
		Wildtype	1	42	
	MSS	Mutant	0	0	NA
		Wildtype	1	54	
	All	Mutant	0	1	1.000
		Wildtype	2	96	
***PIK3CA* exon 9**	MSI	Mutant	0	5	1.000
		Wildtype	1	38	
	MSS	Mutant	0	7	1.000
		Wildtype	1	47	
	All	Mutant	0	12	1.000
		Wildtype	2	85	
***PIK3CA* exon 9**	MSI	Mutant	0	4	1.000
		Wildtype	1	39	
	MSS	Mutant	0	1	1.000
		Wildtype	1	53	
	All	Mutant	0	5	1.000
		Wildtype	2	92	
***PIK3CA* combined**	MSI	Mutant	0	9	1.000
		Wildtype	1	34	
	MSS	Mutant	0	8	1.000
		Wildtype	1	46	
	All	Mutant	0	17	1.000
		Wildtype	2	80	
			***BRAF* 15**		
			Mutant (n=29)	**Wildtype (n=70)**	
***PIK3CA* exon 1**	MSI	Mutant	1	0	1.000
		Wildtype	23	20	
	MSS	Mutant	0	0	NA
		Wildtype	5	50	
	All	Mutant	1	0	0.293
		Wildtype	28	70	
***PIK3CA* exon 9**	MSI	Mutant	1	4	0.160
		Wildtype	23	16	
	MSS	Mutant	0	7	1.000
		Wildtype	5	43	
	All	Mutant	1	11	0.172
		Wildtype	28	59	
***PIK3CA* exon 9**	MSI	Mutant	3	1	0.614
		Wildtype	21	19	
	MSS	Mutant	0	1	1.000
		Wildtype	5	49	
	All	Mutant	3	2	0.148
		Wildtype	26	68	
***PIK3CA* combined**	MSI	Mutant	4	5	0.710
		Wildtype	20	15	
	MSS	Mutant	0	8	1.000
		Wildtype	5	42	
	All	Mutant	4	13	0.771
		Wildtype	25	57	
			Combined		
			Mutant (n=30)	**Wildtype (n=69)**	
***PIK3CA* combined**	MSI	Mutant	4	5	0.710
		Wildtype	20	15	
	MSS	Mutant	0	8	0.577
		Wildtype	6	41	
	All	Mutant	4	13	0.576
		Wildtype	26	56	

Table 4.6. Frequency and association of *BRAF* exon 15 and *PIK3CA* mutation in the Nottingham and Edinburgh cohort of colorectal cancer

			***BRAF* exon 15**		**Fisher's exact test Exact significance (2-sided)**
			Mutant (n=61)	**Wildtype (n=126)**	
***PIK3CA* exon 9**	MSI	Mutant	3	7	0.083
		Wildtype	50	29	
	MSS	Mutant	0	30	0.375
		Wildtype	8	77	
	All	Mutant	3	20	0.034*
		Wildtype	58	106	
***PIK3CA* exon 20**	MSI	Mutant	5	1	0.395
		Wildtype	48	35	
	MSS	Mutant	0	2	1.000
		Wildtype	8	88	
	All	Mutant	5	3	0.116
		Wildtype	56	123	
***PIK3CA* Combined**	MSI	Mutant	8	7	0.774
		Wildtype	45	29	
	MSS	Mutant	0	15	0.352
		Wildtype	8	75	
	All	Mutant	8	22	0.528
		Wildtype	53	104	

4.2.4. DNA content (ploidy) analysis of microsatellite stable (MSS) and microsatellite instable (MSI)

We performed ploidy analysis on half of the cases of Nottingham cohort. This comprised a total of 43 cases including of 23 MSI and 20 MSS cases. FFPE tissue of normal colon was used for flow cytometry set-up and to guide the gating strategy as describe in Figure 4.3. A primary gate was applied to the forward- and side-scatter (FS Lin and SS Lin, respectively) plot to exclude the debris, apoptotic and transected nuclei with incomplete, partial DNA content which are prominent in FFPE tissue. In principle, cell population with the population with low granularity (SS Lin) was selected. The population with higher size (FS Lin) was excluded to avoid the analysis of nuclei aggregate. Further, the population was then gated for singlets (doublets discrimination) based on DNA fluorescence area (FL3Lin) vs. peak plot (AUX).

All of MSI tumour were diploid while among the MSS, 12/20 (60%) cases were

aneuploid and the remaining 8/20 (40%) cases were diploid. As shown in Figure 4.4, the diploid tumour was determined by single G0/G1 peak. The presence of single peak indicates that all cells have the same DNA content and, since the samples contain cells from the cancer community, this indicates that both cancer cells and stromal cells have the same DNA content. The DNA index (DI) was calculated based on the DNA fluorescence modal ratio of the G0/G1 of the tumour tissue to the normal tissue (diploid). Samples with DI between 0.9 to 1.1 were consider diploid (gated as W0). The aneuploid samples showed double G0/G1 peaks, the diploid peak (W0) that represented the stromal population and the aneuploid peak from the tumour nuclei with DI > 1.1

Detailed in the table 4.9, as expected, there was a significant association of ploidy with the MSI status with all the MSI appearing to be diploid (P<0.0001, Fisher's exact test). We also found the positive association between *BRAF* exon 15 mutation and diploid tumour (P= 0.003, Fisher's exact test). As seen in table 4.10, the association remained significant when different hotspot mutations of *BRAF* was combined (P=0.004, Fisher's exact test). This finding may relate to the strong association between *BRAF* mutation and MSI status. Nonetheless, the association was not significant when the MSI and MSS (CIN vs MACS) subgroup were analysed separately.

Table 4.7. Frequency and association of *TP53* mutation and various hotspots of other driver gene mutations in the Nottingham cohort of colorectal cancer

			TP53		**Fisher's exact test Exact significance (2-sided)**
			Mutant (n=49)	**Wildtype (n=50)**	
***KRAS* exon 2**	MSI	Mutant	2	8	1.000
		Wildtype	7	27	
	MSS	Mutant	11	10	0.012*
		Wildtype	29	5	
	All	Mutant	13	18	0.387
		Wildtype	36	32	
***KRAS* exon 3**	MSI	Mutant	0	0	NA
		Wildtype	9	35	
	MSS	Mutant	4	1	1.000
		Wildtype	36	14	
	All	Mutant	4	1	0.204
		Wildtype	45	49	
***KRAS* exon 4**	MSI	Mutant	0	0	NA
		Wildtype	9	35	
	MSS	Mutant	0	0	NA
		Wildtype	40	15	
	All	Mutant	0	0	NA
		Wildtype	49	50	
***PIK3CA* exon 1**	MSI	Mutant	1	0	0.205
		Wildtype	8	35	
	MSS	Mutant	0	0	NA
		Wildtype	40	15	
	All	Mutant	1	0	0.495
		Wildtype	48	50	
***PIK3CA* exon 9**	MSI	Mutant	2	3	0.566
		Wildtype	7	32	
	MSS	Mutant	3	4	0.079
		Wildtype	37	11	
	All	Mutant	5	7	0.760
		Wildtype	44	43	
***PIK3CA* exon 20**	MSI	Mutant	1	3	1.000
		Wildtype	8	32	
	MSS	Mutant	0	1	0.273
		Wildtype	40	14	
	All	Mutant	1	4	0.362
		Wildtype	48	46	
***BRAF* exon 11**	MSI	Mutant	1	0	0.205
		Wildtype	8	35	
	MSS	Mutant	1	0	1.000
		Wildtype	39	15	
	All	Mutant	2	0	0.242
		Wildtype	47	50	
***BRAF* exon 15**	MSI	Mutant	5	19	1.000
		Wildtype	4	16	
	MSS	Mutant	5	0	0.308
		Wildtype	35	12	
	All	Mutant	10	19	0.077
		Wildtype	39	31	

Table 4.8. Frequency and association of *TP53* mutation and combined mutations of other driver genes in the Nottingham cohort of colorectal cancer

			TP53		**Fisher's exact test Exact significance (2-sided)**
			Mutant (n=49)	**Wildtype (n=50)**	
***KRAS* Combined**	MSI	Mutant	2	8	1.000
		Wildtype	7	27	
	MSS	Mutant	14	11	0.016
		Wildtype	26	4	
	All	Mutant	16	19	0.673
		Wildtype	33	31	
***BRAF* Combined**	MSI	Mutant	5	19	1.000
		Wildtype	4	16	
	MSS	Mutant	6	0	0.173
		Wildtype	34	15	
	All	Mutant	11	19	0.126
		Wildtype	38	31	
***PIK3CA* Combined**	MSI	Mutant	3	6	0.360
		Wildtype	6	29	
	MSS	Mutant	3	5	0.028*
		Wildtype	37	10	
	All	Mutant	6	11	0.287
		Wildtype	43	39	

Table 4.9. Frequency and association of ploidy status, microsatellite instability and various hotspots of driver gene mutations in the Nottingham cohort of colorectal cancer

			Ploidy		**Fisher's exact test Exact significance (2-sided)**
			Aneuploid (n=12)	**Diploid (n=26)**	
***KRAS* exon 2**	MSI	Mutant	0	4	1.000
		Wildtype	0	14	
	MSS (CIN vs MACS)	Mutant	5	1	0.340
		Wildtype	7	7	
	All	Mutant	5	5	0.269
		Wildtype	7	21	
***KRAS* exon 3**	MSI	Mutant	0	0	NA
		Wildtype	0	18	
	MSS (CIN vs MACS)	Mutant	1	2	0.211
		Wildtype	11	6	
	All	Mutant	1	2	0.490
		Wildtype	11	24	
***KRAS* exon 4**	MSI	Mutant	0	0	1.000
		Wildtype	0	18	
	MSS (CIN vs MACS)	Mutant	0	0	0.340
		Wildtype	12	8	
	All	Mutant	0	0	0.269
		Wildtype	12	26	

			Ploidy		Fisher's exact test Exact significance (2-sided)
			Aneuploid (n=12)	Diploid (n=26)	
***PIK3CA* exon 1**	MSI	Mutant	0	1	0.409
		Wildtype	0	17	
	MSS (CIN vs MACS)	Mutant	0	0	NA
		Wildtype	12	8	
	All	Mutant	0	1	0.384
		Wildtype	12	25	
***PIK3CA* exon 9**	MSI	Mutant	0	0	0.068
		Wildtype	0	18	
	MSS (CIN vs MACS)	Mutant	2	2	0.358
		Wildtype	10	6	
	All	Mutant	2	2	0.662
		Wildtype	10	24	
***PIK3CA* exon 20**	MSI	Mutant	0	2	1.000
		Wildtype	0	16	
	MSS (CIN vs MACS)	Mutant	0	1	0.145
		Wildtype	12	7	
	All	Mutant	0	3	0.219
		Wildtype	12	23	
***BRAF* exon 11**	MSI	Mutant	0	1	0.409
		Wildtype	0	17	
	MSS (CIN vs MACS)	Mutant	0	0	1.000
		Wildtype	12	8	
	All	Mutant	0	1	0.623
		Wildtype	12	25	
***BRAF* exon 15**	MSI	Mutant	0	12	0.227
		Wildtype	0	6	
	MSS (CIN vs MACS)	Mutant	0	1	0.515
		Wildtype	12	7	
	All	Mutant	0	13	0.003*
		Wildtype	12	13	
MSI status		MSI	0	18	<0.0001*
		MSS	12	8	

Table 4.10. Frequency and association of ploidy status and combined mutations of the driver genes in the Nottingham cohort of colorectal cancer

			Ploidy		Fisher's exact test Exact significance (2-sided)
			Aneuploid (n=12)	Diploid (n=26)	
***KRAS* Combined**	MSI	Mutant	0	4	1.000
		Wildtype	0	14	
	MSS (CIN vs MACS)	Mutant	6	3	0.927
		Wildtype	6	5	
	All	Mutant	6	7	0.414
		Wildtype	6	19	
***BRAF* Combined**	MSI	Mutant	0	12	0.227
		Wildtype	0	6	
	MSS (CIN vs MACS)	Mutant	0	1	0.454
		Wildtype	12	7	
	All	Mutant	0	13	0.004*
		Wildtype	12	13	
***PIK3CA* Combined**	MSI	Mutant	0	2	0.270
		Wildtype	0	16	
	MSS (CIN vs MACS)	Mutant	2	3	0.087
		Wildtype	10	5	
	All	Mutant	2	5	0.925
		Wildtype	10	21	

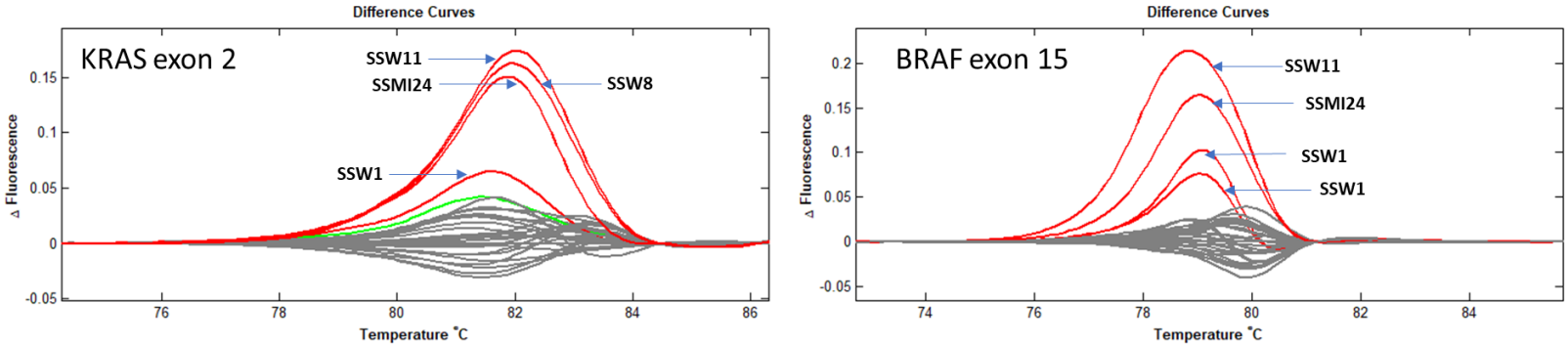


Figure 4.3. The derivative melting plot of colorectal tumour that showed double mutation in *KRAS* exon 2 and *BRAF* exon 15. The difference curves have clearly distinguished the four mutant cases from the wildtype cases. The PCR was carried out and the amplification plot was derived from the FAST 7500 Real-Time PCR (Applied Biosystem, USA). The HRMA was carried out using the LightScanner HRM system (Idaho Technology, USA). The temperature shift was performed following the normalization of the fluorescence (Y) axis onto a 0 to 100% scale followed by auto scanning analysis with the "common vs variant" grouping to determine mutant and wildtype samples. The internal instrument-sensitivity setting was set as normal with the threshold of 4%. Each sample was run in duplicate however, only one representative different curve was shown for each sample.

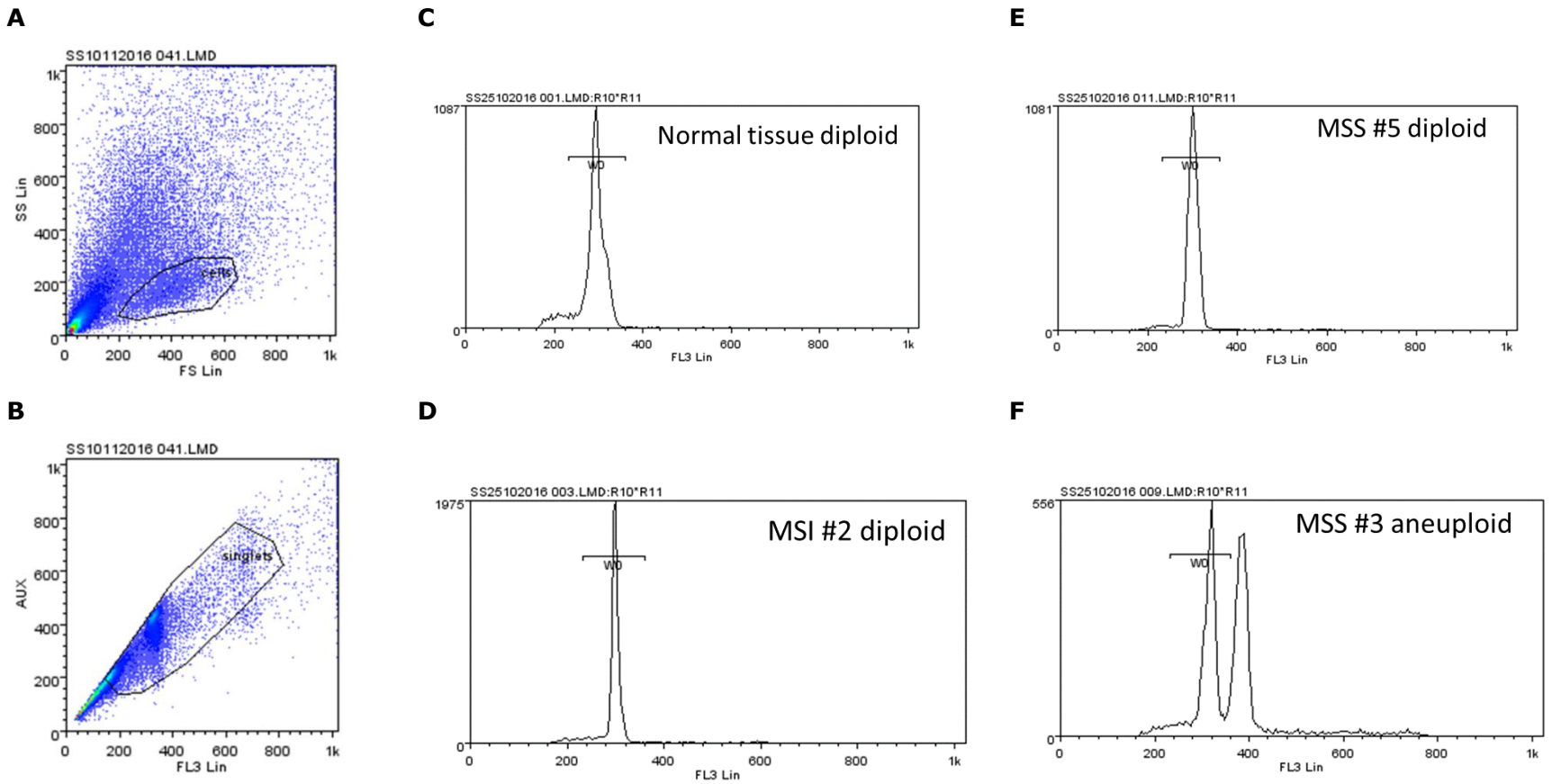


Figure 4.4. Flowcytometry analysis of DNA content (ploidy) on microsatellite instable (MSI) and microsatellite stable (MSS) of colorectal cancer. (A) & (B) The dot plots describe the gating strategies for debris, apoptotic and aggregates exclusion. (C) The G0/G1 peak on the normal colon tissue was used as reference for ploidy determination. (D) & (E) The diploid pattern of the MSI and MSS tumour, respectively. (F) The aneuploid pattern of MSS tumour shows additional peak that is clearly discernible from the dominant G0/G1 peak with the DNA index of this is less than 1.1. The diploid G0/G1 peak reflects the population of stromal population and serves as internal control. The histogram displays the relative fluorescence intensity of PI (propidium Iodide) nucleus staining against the total count/ event. Flowcytometry analysis was carried out using the WEASEL software v3.6 (The Walter and Eliza Hall Institute, Australia).

4.3. Discussion

This chapter described the genetic features of CRC and their associations. We performed a low-throughput yet robust genotyping of the CRC cases within the Nottingham cohort using the well-established HRMA-based QMC-PCR method. The focus of mutation detection was on the most common oncogenes altered in CRC carcinogenesis, which were *KRAS*, *BRAF* and *PIK3CA*.

Differential mutational profiling of CRC with or without MSI has been reported in a large cohort of CRC (TCGA, 2012). Later study confirmed the higher APC, *KRAS* and *TP53* mutations in MSS tumours and the higher mutation on *BRAF*, *PIK3CA*, and *PTEN* genes as well as mutations in the RTK gene family in MSI tumours (Vilar & Gruber, 2010; Lin, et al, 2015). Similarly, in this study, distinct profiles of important driver gene mutation in CRC with MSI and MSS were confirmed, in which, *KRAS* mutation was found slightly more frequent on the MSS cases although the difference was not statistically significant. The *TP53* and *BRAF* exon 15 (V600E) mutation were significantly more common on the MSS and MSI cases, respectively.

The majority of *TP53* mutations are predominantly single base-pair substitutions/ missense hotspots mutation, clustered in the DNA binding domain within exon 5 to 8 (codon 175, 245, 248, 249, 273 and 282) thus usually produce full-length proteins and resulted in IHC positivity. Meanwhile, frequent nonsense mutations such as at codon 213, 196, 306, 146, and 298 and frameshift mutations and deletions were immunonegative, resulted in IHC negativity (Murnyak & Hortobágyi, 2014; Kaye, 2015). Our data showed that the majority (~60%) of the mutant cases showed strong positive immunostaining, indicating the missense mutation while the remaining (~40%) showed the negative immunostaining, suggesting either nonsense, frameshift

or deleting mutation. Similar to findings from this project, it has been reported that in non-hypermutated CRC (~MSS), the mutation rate of *TP53* is about 55%–60%, which is the second-most frequent mutation observed in colorectal cancer (APC mutation is found >80%), whereas the mutation rate of *TP53* is significantly decreased to ~20% in hypermutated CRC (~MSI) (TCGA, 2012; Kandoth et al., 2013; Giannakis et al., 2016).

We found significant association between *TP53* mutation and *KRAS* exon 2 and combined *PIK3CA* mutations among the MSS subgroup but not in the MSI. This suggested the positive selections between *TP53, KRAS* (in particular exon 2) and *PIK3CA* mutations within the CIN/ MSS tumorigenesis as suggested by the classical Fearon and Vogelstein model (Vogelstein, et al, 1988; Nakayama & Oshima, 2019).

Both *KRAS* and *BRAF* are part of the RAS-RAF-MAPK pathway and downstream of the EGFR signalling that is commonly upregulated in CRC. Because of this, co-mutations in the MAPK signalling cascade offers no selective advantage for developing tumours and therefore *BRAF* mutations are mutually exclusive with *KRAS* or NRAS mutations (Nicolantonio et al, 2008; Tie, et al, 2011). We also confirm the significant negative association in this study. Interestingly, 4 cases of MSI that have concomitant *KRAS* and *BRAF* mutation were found. Although this could be the case of false positivity or polymorphism, the co-existence of *KRAS* and *BRAF* has been reported, highlighting the possibility of intratumoural heterogeneity arises from different clonal origins (Phipps,et al, 2013; Sahin, et al, 2013; Larki, et al, 2017). Few case studies have shown the association of double mutation of *KRAS* and *BRAF* with more severe and progressive disease (Larki, et al, 2017; Deshwar, et al, 2018; Vittal, et al, 2019).

We also found few cases that showed mutations on different hotspots of one driver gene, such as double mutation of *KRAS* at exon 2 and 3. Although

uncommon as it offers lack of selection benefit, previous studies has reported the similar findings and showed the association with more aggressive form of tumour (Moerkerk, et al, 1994; Jonsson, et al, 2009; Macedo, et al, 2011). Nonetheless, another possibility such as the existence of SNP (single nucleotide polymorphism) or intratumoral heterogeneity should be considered as possible causes.

PIK3CA forms part of the PI3K (phosphatidylinositide- 3-kinase) signalling pathway, and several studies have shown a significant association of *KRAS* and *PIK3CA* mutation in several cancer types including CRC (Nosho, et al, 2008; De Roock, et al, 2010; Rosty, et al, 2013). This could suggest the positive co-selection of MAPK and PI3K signalling activation implying synergy between these two pathways. If this is the case, then similar positive association would be expected between mutation of *BRAF* and *PIK3CA*. However, to date, less consistent or no association of *BRAF* and *PIK3CA* mutation has been reported (Nosho, et al, 2008; De Roock, et al, 2010; Day, et al, 2013).

Since it is well established that *BRAF* mutation is strongly associated with MSI in CRC, the association between mutation of *BRAF* and *PIK3CA* in a series of CRC enriched for MSI was therefore tested in order to have sufficient number of cases with *BRAF* mutation. Our data demonstrate that *PIK3CA* mutation, in particular, mutation of exon 9, has a significant positive association with *KRAS* mutation. The strength of the association is weak but supports published data. The negative association of *PIK3CA* mutation with *BRAF* mutation was observed, suggests that there is no generic co-selection of disrupted *PIK3CA* and MAPK pathways. Instead, it would seem that the *KRAS*/*PIK3CA* mutation co-selection is due to gene-specific synergy.

Mutations in *PIK3CA* occur far more frequently in exon 9 than in exon 20, and this may explain the lack of association between *KRAS* mutation and *PIK3CA*

exon 20 mutation. The nature and the biological significance of the putative interaction between *KRAS*/*PIK3CA* mutation remains unknown. Both genes are responsible for the transduction of signals from molecules on the cell surface, especially growth factor receptors, to modulate a number of biological functions including proliferation, apoptosis, stemness and motility (Asati, et al, 2016). As well as activating their cognate pathways, these mutations may result in other effects, and it is possible that the synergistic interaction between these other effects results in boosting of the survival advantage. Alternatively, it is possible that co-incidence of both mutations results in acquisition of new properties, which give a selective advantage over cells in which only one of the genes is mutated.

About 85% of sporadic CRC cases follow the classical Faeron and Vogelstein model of CRC tumorigenesis and were categorized as CIN (chromosomal instability) as they showed frequent structural changes of the chromosomes that led to aneuploidy (Lengauer, et al, 1997; Grady, 2004). A meta-analysis estimated that, of 5478 CRC patients, 42% showed a diploid genotype (Araujo, et al, 2007). However, smaller proportion of tumours were reported as MSI as opposed to the CIN/MSS (Pino & Chung, et al, 2010). If the cases with probable MSI are removed, then the data would suggest that a significant proportion of all CRC have neither MSI nor CIN.

More recently, our group and others have identified a subgroup within the non MSI CRC. These tumours (which are MSS) can be then classified into two subgroups i.e., those which are characterised by aneuploidy (termed here chromosomal instability in colorectal cancers, CIN-CRC) and those characterised by diploidy (termed here microsatellite and chromosomal stable colorectal cancers, MACS-CRC) (Georgiades, et al, 1999; Hawkins, et al, 2011; Silver, et al, 2011, Fadhil, et al, 2014).

Although performed on limited number of samples, using flow cytometry analysis on the FFPE tissues, this project was able to validate the previous study by showing a proportion of the MSS cases (40%) that were diploid. The proportion was similar to the percentage of MACS reported in the previous study (Fadhi, et al, 2014). These findings challenge the dogma that CRC could be dichotomised into tumours that progress along either the MSI or CIN pathway (Fearon, 2011, Pritchard and Grady, 2011). We have shown that a significant proportion of CRC belong to a third group which involves neither CIN nor MSI that may not have any genomic instability, or they may have another form of genomic instability, such as that caused by POLE mutations (Muzny et al., 2012, Palles et al., 2012). Speculatively, MACS maybe enriched in the mesenchymal-CMS3 subtype of CRC that were MSS and showed low somatic CNA (copy number alteration) (Guinney, et al, 2015).

Previous studies of tumour ploidy have found a significant association of diploid tumours with the right side of the colon and with better prognosis which would have been obviously confounded by the enrichment of the MSI tumours. Some studies have reported a left sided predominance of the MACS-CRC with a poor prognosis whilst others found that MACS associated with *BRAF* mutation and better survival (Hawkins et al., 2001, Kakar, et al, 2008; Banerjea, et al, 2009; Silver et al., 2011). Previous study from our group showed there was no significant difference of driver genes mutation, including *KRAS*, *BRAF*, *PIK3CA* and *TP53*, between the CIN and MACS CRC. It also been reported that diploid genotype does not predict the responsiveness to radiotherapy (Fadhil et al., 2014). This study found that *BRAF* mutation is associated with diploid tumour, which is not surprising consider the significant association between *BRAF* mutation and MSI tumour. Association study within the MSS cases that comprised the CIN-and MACS-CRC showed no significant different in mutational profile of driver genes including *KRAS*, *BRAF*, *PIK3CA* and *TP53*.

Nonetheless, as shown in this study, MACS form a significant group in the MSS CRC, that may represent the alternative route of CRC carcinogenesis thus represents a distinct subtype in addition to well-established MSI and CIN groups. The biological, mechanistic, and clinical importance of the different patterns of chromosomal alterations among the MSS tumours observed in this study needs to be established in a larger tumour set with known outcomes and warrant further investigations.

5. Cellular Community Profiling of Colorectal Cancer Tumour Microenvironment

5.1. Introduction

Colorectal cancer (CRC) is globally the third most diagnosed and second leading cause of cancer-related deaths for both sexes (Bray, et al, 2018). The commonly used TNM (Tumour-Node-Metastasis) staging does not incorporate the emerging role of the molecular and tumour microenvironment (TME) heterogeneity (Turley, et al, 2015; Dienstmann, et al, 2017). Nevertheless, WHO (World Health Organization) has published the 5th Classification of Digestive System Tumours that includes the molecular biomarker testing and assessment of immune response (WHO, 2019).

It is well regarded that different molecular features in CRC have been linked to distinct TME landscape. The recently described CMS (consensus molecular subtypes) classification of CRC displays differential TME features. The CMS1 that is enriched for MSI and *BRAF* mutation has been linked to high immune infiltrate composed of Th1 and cytotoxic T cells, with reasonably good prognosis. In contrast, the poor-prognosis mesenchymal subgroup, CMS4, is MSS-enriched and characterized by a high density of CAF and immunosuppressive lymphocytes and of cells of monocytic origin with prominent angiogenic and inflammatory signatures. The canonical CMS2 that involved Wnt signalling activation and metabolic CMS3 subtypes that enriched for *KRAS* mutation show intermediate prognosis and exhibit low immune and inflammatory signatures (Becht, et al, 2016; Colangelo, et al, 2017).

In a landmark study, Galon et al. (2014) showed that infiltration of tumours by cells of the immune system, in particular CD3+ and CD8+ T cells, was a more powerful prognostic factor than classical pathological staging, known as Immunoscore. The majority of MSI tumours had increased frameshift mutations, showed genetic evidence of immunoediting, had higher densities of

Th1, effector-memory T cells, in situ proliferating T cells, and inhibitory PD1-PDL1 cells, had high Immunoscore, and were infiltrated with mutation-specific cytotoxic T cells. Nonetheless, these immunogenic features are also shared by a subgroup of microsatellite-stable (MSS) tumours. Hence, it was reported that Immunoscore is superior to MSI status in predicting patients' disease-specific recurrence and survival and could be an important guide for immunotherapy strategies (Mlecnik, et al, 2016; Pages, et al, 2018).

Overall, multiple studies have demonstrated that MSI-driven highly immunogenic and inflamed TME enhances immune response and improves patient survival (Guastadisegni, et al, 2010; Maby, et al, 2015; Lockhead, et al, 2013; Goldstein, et al, 2014). MSI tumours were shown to be enriched with checkpoint proteins as PD-1, PD-L1, and CTLA-4, that determine objective and durable response to immunotherapies in mCRC (Llosa, et al, 2015; Rosenbaum, et al, 2016; Overman, et al, 2018; Narayanan, et al, 2019). However, immune profiling studies reveal the heterogeneity in immune-microenvironment and outcome variations both in MSI and MSS (microsatellite stable)-CRC (Becht, et al, 2015; Giannini, et al, 2020).

Some independent features of TME discussed above, such as number of infiltrating lymphocytes and cells expressing immune check-point molecules, provide important insight on CRC carcinogenesis and serve as prognostic and predictive markers. However, it is worth noting that TME consists of several interacting cellular subpopulations. Thus, studying multiple features of the TME, and their interactions, may better describe the effect of TME in CRC biology than by reporting single elements in isolation. This has been enabled by the rise of multiplex immunostaining and enhanced by the automatic image analysis for the classification and quantification of all cells and features within the TME. Moreover, the advancement of digital pathology has also enabled the

spatial analysis of the TME (Heindl, et al, 2015).

Digital image analysis (DIA) is the emerging field that been used to harness the importance of spatial aspects of immune cell subsets' distribution in TME of lung, breast, melanoma, CRC and other cancers (McIntire, et al, 2018; Saltz, et al, 2018; Enfiled, et al, 2019, Massi, et al, 2019; Yoon, et al, 2019). Among the first was the Immunoscore (IS) consensus that estimates CD3+ and CD8+ T cell densities in the IM and the CT to predict the risk of recurrence assessment superior the TNM-staging and MSI status in CRC (Galon, et al, 2012; Galon, et al, 2014; Pages, et al, 2018). Recently, another DIA-based computational Immunogradient indicators within the tumour-stroma interface zone (IZ) were proposed to quantify the CD8+ cell densities across the IZ and provide independent prognostic value in CRC and hormone receptor positive breast cancer patients (Rasmusson, et al, 2020).

The introduction of the molecular pathways and genetic markers to CRC classification, in addition to the morphological features, has opened a plethora of new potential biomarkers. Furthermore, as the tumours are usually surrounded by non-neoplastic cells from the microenvironment, the new platform of that enable the spatial landscape of TME to be capture in parallel with transcriptomic or genomic data should be envisaged to be incorporated into the search of useful biomarkers with the feasibility of translation to the clinical practice (Lee, et al, 2017; Newell & Becht, 2018; Demirkan, et al, 2019; Chuah & Chew, 2020).

Conventional IHC (immunohistochemistry) or IF (immunofluorescent) enables the detection of cellular antigens within tissue sections using enzyme-labelled or fluorochrome-labelled antibodies and is useful for identifying cell types and their spatial location within tissues (Tsurui, et al, 2000). Recent advances in multiple immunolabeling and multispectral imaging have enabled simultaneous

analysis of more than three markers within a single FFPE (formalin-fixed paraffin-embedded) tissue section, with accurate cell discrimination and spatial information. However, there are still limitations on the maximal number of markers that can be used simultaneously due to chromogenic or fluorescent spectra overlap and antibodies cross reactivity (Stack, et al, 2014).

This chapter discusses the molecular makeup of the two main subtypes of CRC, the MSI and MSS, and describe the TME composition associated with these molecular features by mapping the geographical expression pattern and the co-localisation of biomarkers within the tumour. In this project, a novel DIA registration algorithm named HMM (histogenic molecular mapping) was employed to establish *fm*-IHC (faux multiplex-immunohistochemistry) as a novel approach for multiple biomarker analysis to delineate the activated pathway.

5.2. Results

5.2.1. Principles of faux multiplex immunohistochemistry (fm-IHC)

5.2.1.1. The rationale of sequential sections and choice of biomarkers

In order to profile the cancer community and spatially map the tumour microenvironment for expression of biomarker, a novel in-house methodology called fm-IHC was employed. This method works on the assumption that since the histological sections are only 4µm thick, there is very little difference in the architectural appearance between adjacent sections. Figure 5.1 is an example of two adjacent sections and it can be seen that the spatial location of the various cellular populations is virtually identical in each section. If several sequential sections are cut, the same consideration applies to any two adjacent sections but the distance between the first and last section will be (n-1) X 4µm,

with n being the number of sections cut. With increasing distance, the chances of the architecture becoming different increases and thus there is a play-off between the numbers of biomarkers interrogated (with one biomarker tested per slide) and the risk of loss of spatial homology. For the purposes of this study, as depicted in Figure 5.2, 9 sequential sections were cut and section no. 5 was chosen as the reference section. This was to be stained for an epithelial marker (BerEP4) to identify the tumour areas and the maximum distance of any other section from the reference point was 16μm. This was deemed as low risk for change in architecture.

This part of the study aimed to evaluate the cancer community. Cellular populations in the tissue were to be detected by IHC for biomarkers used to identify the cellular populations. A total of 20 cases of MSI-CRC and 24 cases of MSS-CRC underwent immunostaining for all the biomarkers. A list of biomarkers and the rationale for their inclusion is detailed in Table 5.1.

5.2.1.2. Image scanning and pre-processing

After immunostaining, each side was scanned using an automatic slide scanner (Aperio AT2, Leica Biosystems, USA). The images were capture in RGB format and each scan was performed at 20x magnification. Scanning at this magnification gave images with a pixel size of 0.5μm X 0.5μm and pixel dimensions of 70,000 pixels X 35,000 pixels. The images were down-sampled using an open image viewer and analysis software called Qupath (Bankhead, et al, 2017) to facilitate manipulation of the image and to alleviate the effect of any local mis-correspondence. The down-sampling resulting in an image in which the pixel size was increased 2μm X 2μm (equivalent to 5x magnification).

The down-samples images were imported into bespoke software created by Dr Alain Pitiot (Ilixa Ltd, London, UK). Next, the pixels were merged to create

"super-pixels" measuring 10X10 pixels each and the images were converted from RGB to grey-scale images. These were 8-bit images meaning the images were stored simply by assigning 3 bits to red, 3 to green and 2 to blue to create a 3-3-2 8-bit colour image, with the maximum number of colours that can be displayed at any one time is 256 or 2^8 (Fisher, et al, 2003 retrieved from https://homepages.inf.ed.ac.uk/rbf/HIPR2/8bitcol.htm in August 2020).

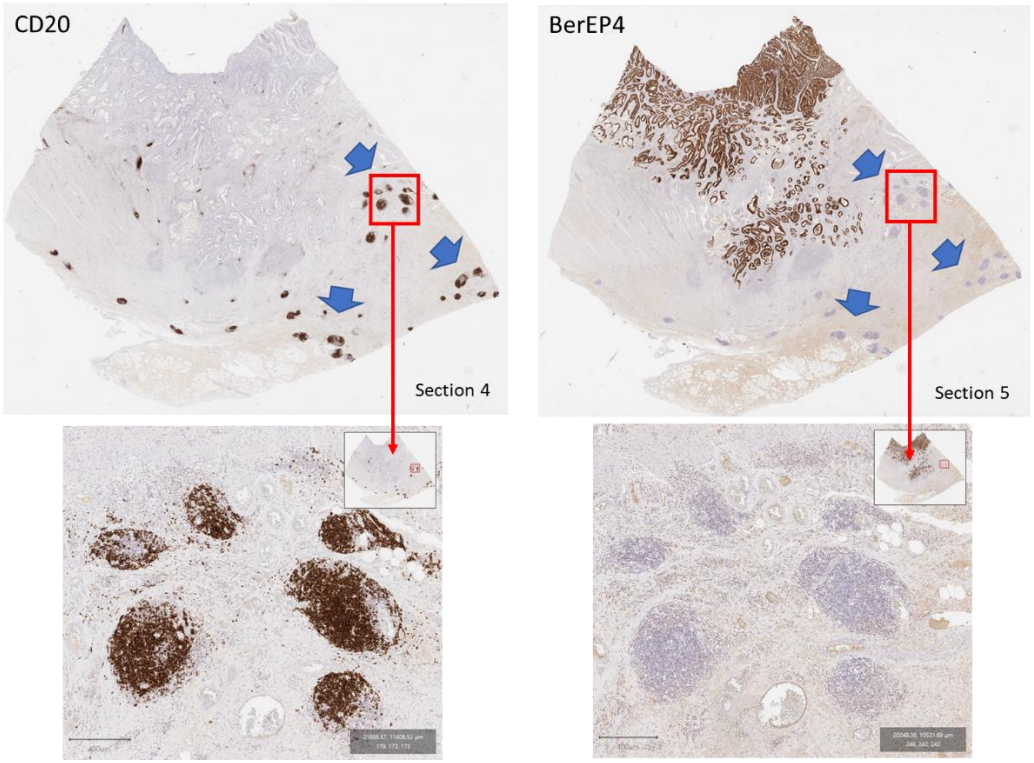


Figure 5.1. Representative images of two adjacent sections of series of sequential sections used for the faux multiplex immunohistochemistry (fm-IHC). Top panel displays the low power view of section 4 (stained for CD20) and section 5 (stained for BerEP4). The blue arrows indicated several tissue landmarks, indicating that the two sections are virtually identical. The below panel shows the high-power images of lymphocyte aggregates at the two corresponding sections stained positively for CD20 but not BerEP4, highlighting the spatially mirror topology between the sections. The digital images were produced by automatic slide scanner (Aperio AT2, Leica Biosystems, USA) at 20x magnification.

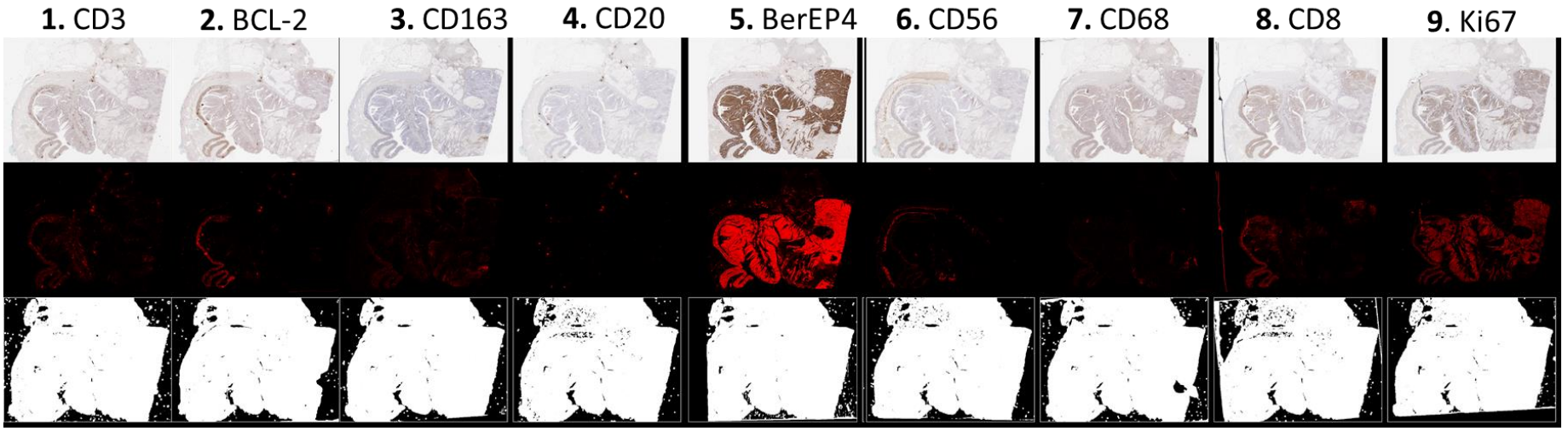


Figure 5.2. Representative images of Histogenic Molecular Mapping (HMM) used in the faux multiplex immunohistochemistry (fm-IHC). A precise image registration algorithm was developed by Dr. Alain Pitiot. Digital images of series of stained sequential sections were aligned based on several tissue landmarks that is independent of colour such as shape and texture. The middle section (section number 5, stained for BerEp4) was used as reference for alignment. The images were then being threshold and false colours can be generated for each biomarker and a visual representation of the location of the biomarkers can be generated.

Table 5.1. Cellular and functional markers to map tumour microenvironment in the Nottingham cohort of colorectal cancer

Marker	Cellular Type/ Functional	Rationale	References
CD3	Pan T-cell	Part of adaptive immune response. Evidence of high infiltration on MSI tumour and *BRAF* mutant, lower T-cell signatures on *KRAS* mutant	Schwitalle, et al, 2008; LIosa, et al, 2015; Becht, et al, 2016; Kwak, et al, 2016; Hamada, et al, 2017; Lal, et al, 2018
CD8	Cytotoxic T-cell		
CD20	B-lymphocyte	Part of adaptive immune response. Less reported type of lymphocyte, evidence of similar infiltration on MSI and MSS tumour, positively correlates to CD8+ T-lymphocytes, higher infiltration in *KRAS* wildtype	Mlecnik et al., 2016; Berntsson, et al, 2016, Edin, et al, 2019
CD68	Pan macrophages	Part of innate immune response. Most prominent immune cell infiltrating stromal tissue. Evidence of higher infiltration at the invasive front of the MSI	Mlecnik et al., 2016; Korehisa, et al, 2018; Edin, et al, 2019; Alexander, et al, 2020
CD163	M2 macrophages	Subset of macrophages that is enriched within the tumour, high density within the invasive margin, especially of *KRAS* mutant	Kwak, et al, 2016, Pinto, et al, 2019, Zhang, et al, 2019
CD56	Natural killer (NK) cells	Part of innate immune response. Less reported in CRC. Evidence of very low presence in CRC tissue and correlation with CD8+ T-lymphocytes infiltration	Halama, et al, 2011; Sconocchia, et al, 2014
BerEp4	Epithelial	To virtually segment the epithelial and stromal component of the tumour	
BCL-2	Mature B-cell and anti-apoptotic	Apoptotic functionally of the cellular community	
Ki67	Proliferative cell	Proliferative functionally of the cellular community; evidence of high proliferative T-lymphocytes within the MSI tumour	Mlecnik et al., 2016

Grey scale images usually have an intensity value of 0 – 2^8 (255) with 0 representing black and 255 representing white. The images were inverted so that white had a value of 0 whilst black had a value of 255. With this transformation, the intensity of the immunostaining could be quantified with more intense staining being denoted by a higher value. As well continuous values for intensity of staining, the super-pixels could be allocated a positive/negative value using an automated thresholding algorithm within the software.

5.2.1.3. Precise image registration and data collection

The next step in fm-IHC requires for the images of the different sections to undergo registration i.e. identical parts of the images are aligned with each other. In principle, the registration of two sequentially cut images should be straightforward since architectural features can be identified and these "landmarks" in the images should be near-identical. However, there are several confounders. Firstly, the location and orientation of consecutive sections will not be the same. The sections may be located on different part of the slide, they may be rotated in relation to each other and one may be flipped over compared to the other. In addition, the sections are prone to artefact due to the nature of the specimen and the technical methodology behind section cutting. Thus, the tissue is located in a wax block and a 4μm slice is cut with a microtome blade and stretched out over water before being put onto a glass slide. During this process, the tissue section is susceptible to excessive stretching, tearing and folding over. The "local" artefacts can alter the spatial location of the landmarks thereby making registration more difficult.

Dr Pitiot has developed a proprietary algorithm which was used for the image registration. Of two images, one is chosen as a "reference" image whilst the other is the "test" image. The algorithm will automatically correct any flipped

images and it will choose several landmarks in the reference and test section. The landmarks are colour independent and are based on features such as texture, shape etc. For each landmark, the amount to rotation and movement will be calculated to align features in the test image to those in the reference image. Since hundreds of landmarks are chosen, image registration is still possible even if there are large artefacts present. The image registration of the series of biomarkers are depicted in Figure 5.2.

Once the images are aligned, false colours can be used for each biomarker and a visual representation of the location of the biomarkers can be generated. Multiple images can be registered and thus several populations can be mapped simultaneously as shown in Figure 5.3-5.5. However, in order to precisely assess whether biomarkers are co-localised, it was necessary to refine the registration process. Once the images were in perfect alignment with the reference image, all were cropped to be exactly the same size and to have exactly the same co-ordinates for each super-pixel. Thus, for any particular landmark, the co-ordinates of the super-pixels relating to that landmark would be the same for every biomarker image. In this way, any specific location (or landmark) on the image could be evaluated for expression of multiple biomarkers.

5.2.1.4. Data analysis

Approximately 200,000 super-pixels were collected for each image. Since the super-pixels in each image had exactly the same co-ordinates, it allowed for a variety of different types of data analysis.

a. **Virtual segmentation**. The precise registration allowed examination all the pixels in the WTS (whole tissue section) or individual tissue compartments through "virtual segmentation". Each super-pixel had an intensity value for each biomarker; it could be used as a raw value or it

could be dichotomised into a positive/negative value based on a threshold. For the purposes of dichotomisation, the threshold was set at 30% (i.e., 0.3 X 255) to allow for the fact the some super-pixels would lie on the boundaries between cellular communities and thus may not be fully occupied by one population type. This dichotomisation also allowed virtual segmentation of the images. Thus, BerEP4 is a marker of epithelium and would be expected to be positively expressed in the tumour epithelium. After dichotomisation of this marker, all the positive pixels would represent tumour epithelium whilst the negative pixels would represent tumour stroma and tissue mesenchyme (such as smooth muscle). By interrogating only those pixels which are BerEP4 positive, it is possible to investigate the biomarkers expressed in the tumour epithelium compartment of the tissue section. Similarly, by removing super-pixels positive for mesenchymal markers (such as desmin-not used in this project) and epithelial markers (such as BerEP4), the residual super-pixels would represent the stromal areas of the tumour.

b. **Correlation analysis**. As a result of the precise registration, it was possible, for any pair of biomarkers, to perform pairwise correlation on either the WTS or within individual compartments. There were subgroups within the overall data set (e.g., MSI-CRC and MSS-CRC, *KRAS* mutant and *KRAS* wild type) and, in order to ascertain any differences in correlation between the groups, the Pearson correlation coefficient of paired biomarkers were established for each sample. The Fisher "z" transformation was the applied to the Pearson's "r" value followed by the unpaired/ independent T-test to compare the means between two groups.

c. **Density distribution**. In order to evaluate the density of different cellular subpopulations within either the WTS or the individual compartments, the positive super-pixels were calculated as a proportion of the super-pixels in the WTS or target compartment. The subgroups could then be examined by simple comparison of ratios using either the unpaired T-test or the Man-Whitney U test (depending on the normality parameter of the data).

   Using the 30% cut-off for the intensity value to determine the positivity, the density for each biomarker (for instance marker A) was calculated based on the equations:

   1) In the WTS= number of super-pixel positive for marker A/ total number of super-pixels
   2) In the Epithelial= number of super-pixels that were positive for marker A and BerEP4/ total number of BerEP4 positive super-pixels
   3) In the stroma (non-epithelial) = number of super-pixels that were positive for marker A but negative for BerEP4/ total number of BerEP4 negative super-pixels

d. **Functional analysis**: Cellular number may give some indication of the presence of a community, but cells may also exist in different states of "activity". Thus, it is possible that, between any two conditions, the cellular numbers may not be different but the "activation" state in one condition may be different to the other condition. We sought to interrogate the functional properties of each cellular population by looking at expression of markers associated with the processes of proliferation (using the marker Ki67) and apoptosis (using the marker BCL-2). Thus, for any specific population (such CD3+ T lymphocytes), the state of activity of that population could be assessed by comparing super-pixels which are positive for both the community marker and the

function marker (i.e., CD3+Ki67+/total CD3+ super-pixels would indicate the proportion of CD3+ cells undergoing proliferation). By virtual segmentation, the activity of any particular population in any particular compartment could be analysed.

Meanwhile, using the similar 30% cut off for positivity, the density of each functional (Ki67+ or BCL-2+) cellular biomarkers (for instance marker A) was calculated based on the equations:

1) In the WTS= number of super-pixel positive for marker A and Ki67 or BCL-2/ total number of super-pixels
2) In the Epithelial= number of super-pixels that were positive for marker A, Ki67 or BCL-2 and BerEP4/ total number of BerEP4 positive super-pixels
3) In the stroma (non-epithelial) = number of super-pixels that were positive for marker A and Ki67 or BCL-2 but negative for BerEP4/ total number of BerEP4 negative super-pixels

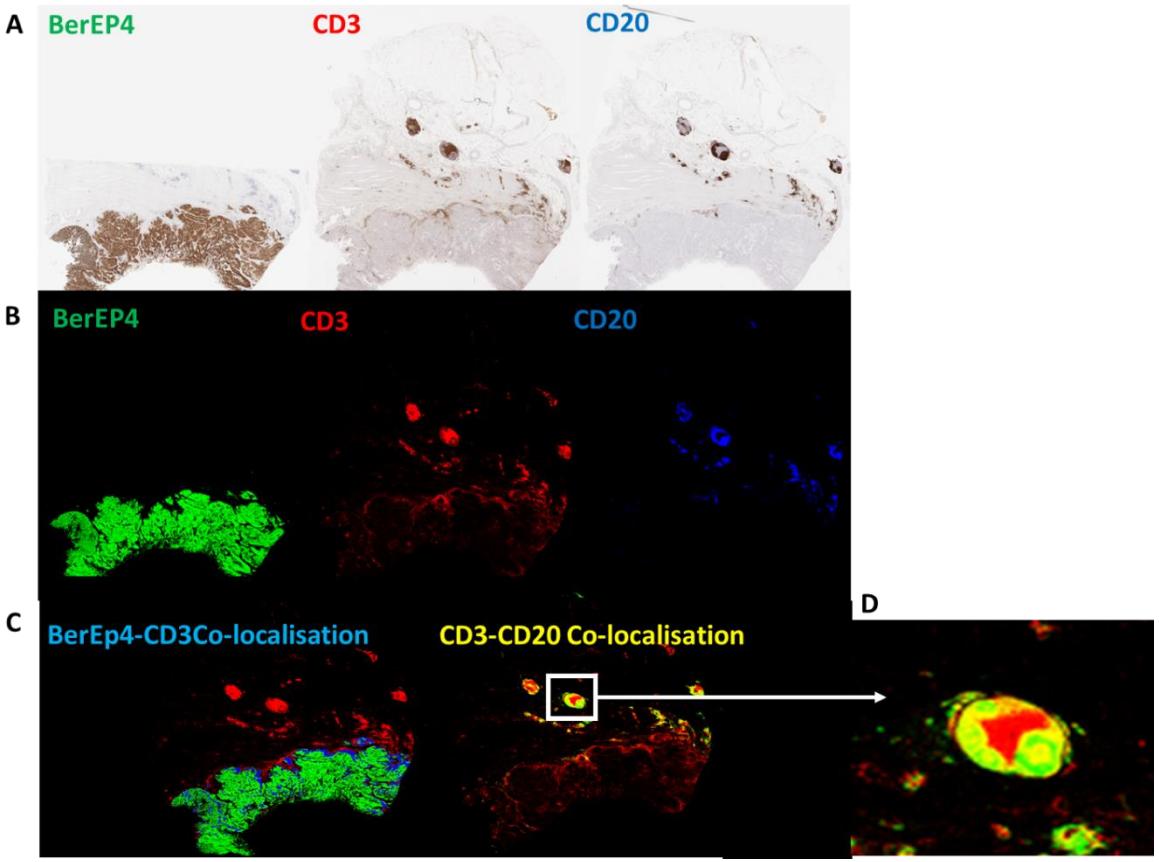


Figure 5.3. Faux multiplex immunohistochemistry (fm-IHC) using histology molecular mapping (HMM) for pairwise biomarker co-localization. (A) Immunohistochemistry (IHC) staining for BerEP4 (epithelial), CD3 (T-lymphocyte) and CD20 (B-lymphocyte). (B) The feature extraction of the IHC staining for each biomarker. (C) The tissue registration using HMM and fm-IHC for BerEP4-CD3 and CD3-CD20. The blue areas in the middle panel show intra-epithelial T cells. (D) The precision of the registration is exemplified in the CD3/CD20 panel on the right. A high-power view of a lymph node shows delineated T cell rich medulla (red), B cell rich mantle (green) and mixed T & B cell germinal centres (yellow).

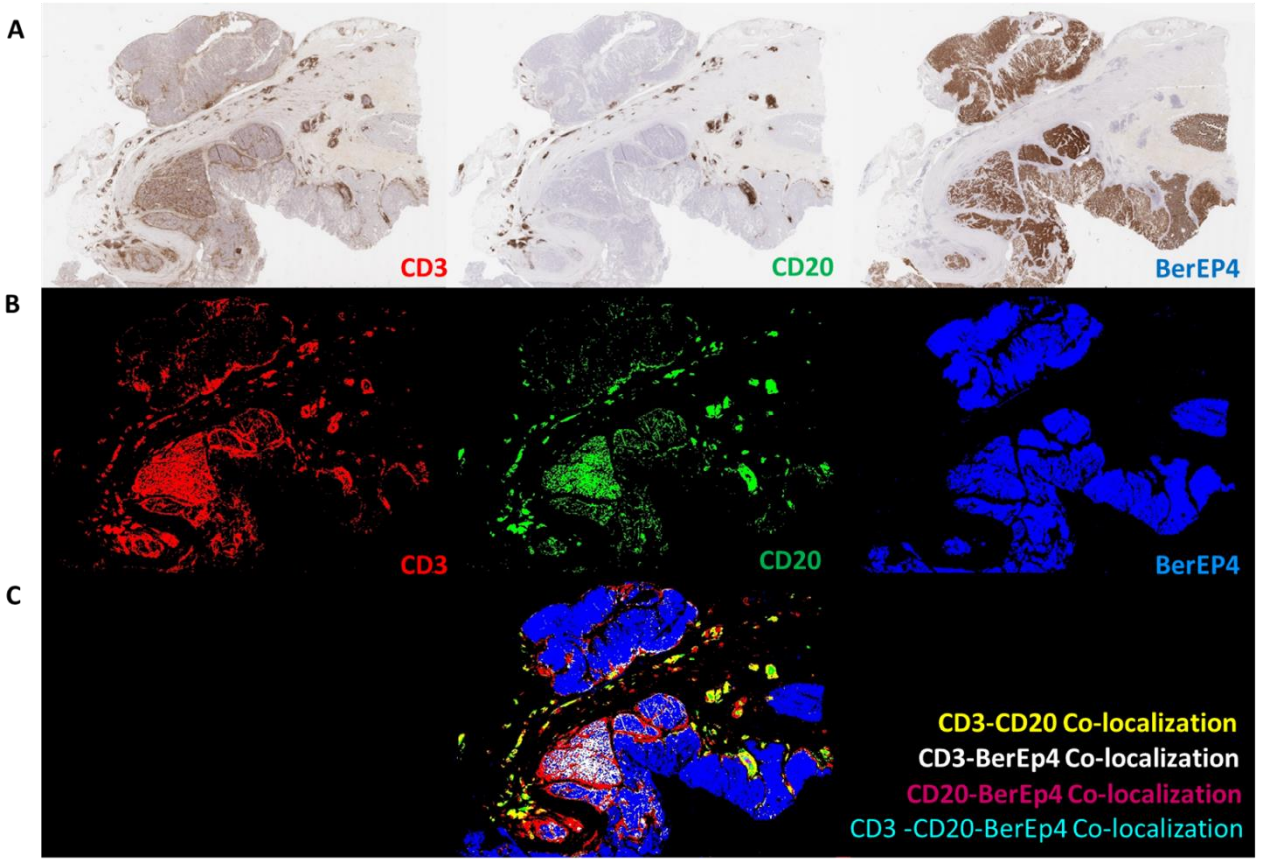


Figure 5.4. Faux multiplex immunohistochemistry (fm-IHC) using histology molecular mapping (HMM) for three biomarkers co-localization on microsatellite instable (MSI) colorectal cancer. (A) Immunohistochemistry (IHC) staining for CD3 (T-lymphocyte), CD20 (B-lymphocyte) and BerEP4 (epithelial). (B) The feature extraction of the IHC staining for each biomarker. (C) The tissue registration using HMM and fm-IHC for pairwise and three biomarkers co-localization. The white areas in the middle panel show high number of intra-epithelial T cells on the MSI case.

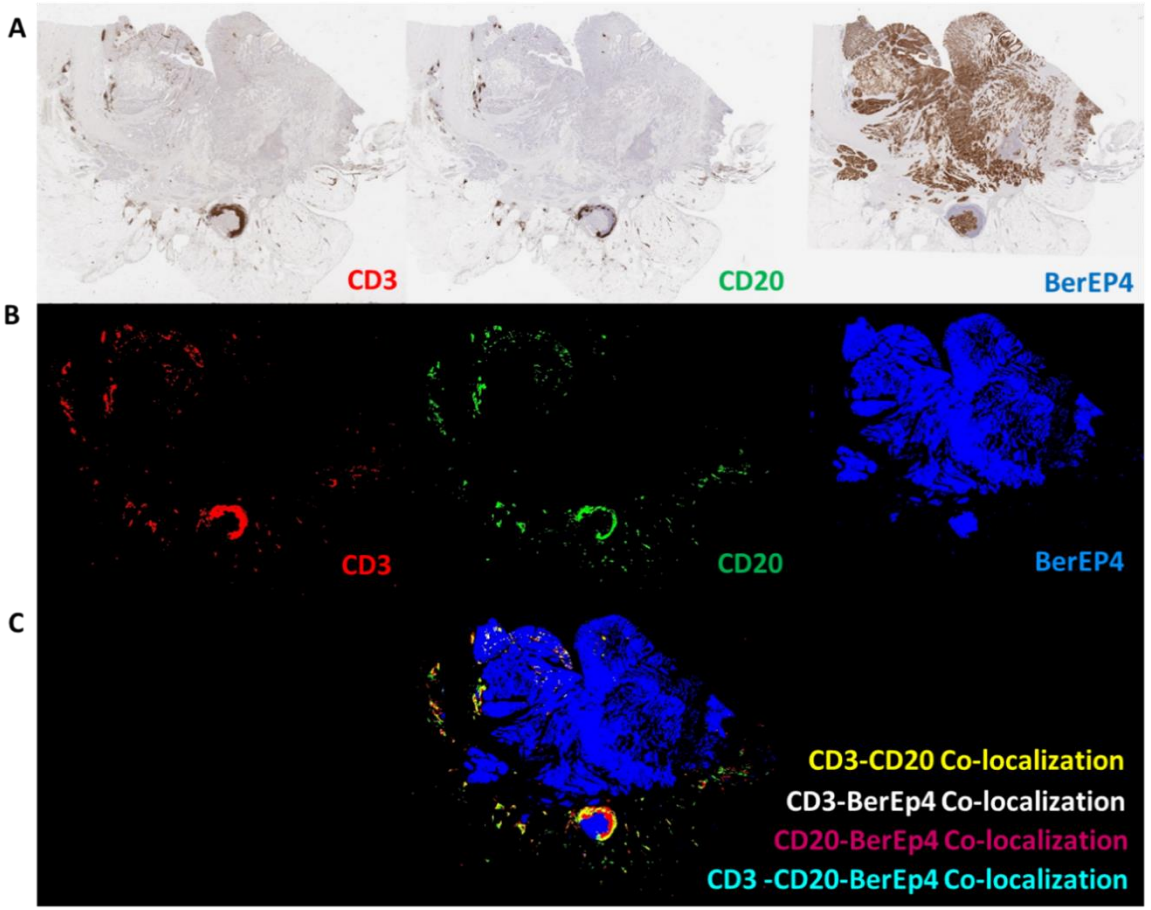


Figure 5.5. Faux multiplex immunohistochemistry (fm-IHC) using histology molecular mapping (HMM) for three biomarkers co-localization on microsatellite stable (MSS) colorectal cancer. (A) Immunohistochemistry (IHC) staining for CD3 (T-lymphocyte), CD20 (B-lymphocyte) and BerEP4 (epithelial). (B) The feature extraction of the IHC staining for each biomarker. (C) The tissue registration using HMM and fm-IHC for pairwise and three biomarkers co-localization. There are very few intraepithelial lymphocytes on the MSS case as compare to the microsatellite instable (MSI), including in the area of lymph node with a tumour metastasis.

5.2.2. Cellular community mapping of the colorectal cancer tumour microenvironment.

The TME characteristics including the density of cellular markers and their functional state as well as the correlation between the cellular markers were investigated on different compartment of the tissues (WTS, epithelial and stroma) based on the molecular features characterised in the chapter 4 of this thesis. The significant features were detailed in table 5.2 and 5.3.

Nonetheless, one of the limitations of the fm-IHC is it could not register the sections into the single cell level (instead using the spatial fragments of super-pixels of 10 x 10 pixels at the size of 2μm X 2μm per pixel). The fact that both cell functional markers, Ki67 and BCL-2, are also expressed by the epithelial/ tumour cells would confound the interpretation of the co-existence of Ki67+/ BCL-2+ with cellular marker within the epithelial and the WTS. Thus, although quite a few of significant features the Ki67+/ BCL-2+ cellular population within the epithelial and WTS of the tissue were found, only findings on the stroma compartment were discussed.

5.2.2.1. MSI and MSS

In this project, it was found that the MSI cases showed higher density of all TME cellular communities in WTS, epithelial and stroma compartments, however, the differences were not statistically significant on Mann-Whitney non-parametric analysis. There was a significantly higher proliferating (Ki67+) CD3+ lymphocytes on the stroma of the MSI tumour. The low apoptotic (BCL-2+) CD20+ B-lymphocytes was also found higher in the MSI tumour (Table 5.2). Further, there was higher correlation between cytotoxic T-lymphocytes and pan macrophages (CD8-CD68) in the epithelial and WTS of the MSI.

Meanwhile, higher correlation between T and B-lymphocytes (CD3-CD20) and between M2 macrophages and NK cell (CD163-CD56) were found in epithelial the MSS tumour (Table 5.3).

5.2.2.2. *BRAF* mutant and wildtype

When the analysis was carried based on *BRAF* mutation status, the mutant cases showed statistically significantly higher density of CD3+ T-lymphocytes on both the WTS and stroma compartments. In the WTS, there was also significantly higher density of CD20+ B-lymphocytes in the *BRAF* mutant. Similar to the MSI, there were significantly higher density of proliferating CD3+ lymphocytes in the stroma of *BRAF* mutant, in addition to higher density of proliferating CD163+ M2-macrophages. The co-existence of BCL-2 was found significantly higher in the T-lymphocytes (both CD3+ and CD8+), B-lymphocytes (CD20+), M2-macropahes (CD163+) and NK-cell (CD56+) on the *BRAF* mutant (Table 5.2). Also, similar to the MSI, there was higher correlation between cytotoxic T-lymphocytes and pan macrophages (CD8-CD68) in the epithelial and WTS of *BRAF* mutant, in addition to higher correlation between the cytotoxic T-lymphocytes and M2-macrophages (CD8-CD163). Conversely, the pan macrophages were associated with higher B-lymphocytes (CD8-CD20) and NK cell (CD8-CD56) in the epithelial of *BRAF* wildtype (Table 5.3).

5.2.2.3. *KRAS* mutation

No statistically significant differences of cellular community density were observed between mutant and wildtype of *KRAS*. Similar features of BCL-2 association with several cellular markers (CD3, CD8, CD20, CD163 and CD56) were found in *KRAS* wildtype as in *BRAF* mutant (Table 5.2). There was higher correlation between cytotoxic lymphocytes and both pan (CD8-CD68) and M2 macrophages (CD8-CD163) in the epithelial of *KRAS* wildtype similar to what

was observed with *BRAF* mutant (table 5.3). These findings highlight the exclusivity between the mutations of the *KRAS* and *BRAF*.

5.2.2.4. *PIK3CA* mutation

No statistically significant differences of cellular community density and their functional properties were observed between mutant and wildtype of *PIK3CA*. There was only significant correlation between T-lymphocytes with M2-macrophages (CD3-CD163) in the epithelial of *PIK3CA* mutant (Table 5.3).

5.2.2.5. *TP53* mutation

We found higher density of CD3+ T-lymphocytes, CD68+ macrophages and CD56+NK cells on the epithelial areas of the *TP53* mutant cases. There was also higher density of the proliferating NK cells among the *TP53* mutant (Table 5.2). Similar to the *PIK3CA* mutant, there was strong correlation between T-lymphocytes and M2-macrophages (CD3-CD163) in epithelial and WTS of *TP53* mutant. However, higher correlation between T- and B-lymphocytes (CD3-CD20) was found in the WTS of *TP53* wildtype (Table 5.3).

5.2.2.6. Diploid vs aneuploid

As described in the chapter 4 of this thesis, the MSI tumour was all diploid while some MSS shown to be diploid, known as CIN (chromosomal instable) and some were aneuploid, known as MACS (microsatellite and chromosomal stable). No statistically significant differences of cellular community density were observed between diploid and aneuploid tumour. However, there was a significantly higher proliferating CD3+ lymphocytes in the stroma of diploid tumour, which is similar to what been observed in the MSI and *BRAF* mutant (Table 5.2). Also similar to *BRAF* mutant, diploid tumour showed higher stromal density of proliferating CD163+ M2-macrophages (table 5.2) and higher correlation

between cytotoxic T-lymphocytes and the M2-macrophages (CD8-CD163) in the epithelial and WTS. Meanwhile, similar to the MSS, there was higher correlation between M2 macrophages and NK cell (CD163-CD56) were found in epithelial the MSS tumour (Table 5.3).

When subgroup analysis of MACS (microsatellite and chromosomal stable) and CIN (chromosomal instable) tumour was carried out, no significant difference on the density of all cellular communities were found, except for higher CD56+ NK cell density within the stroma and WTS of the MACS. The MACS tumour also showed higher stromal density of proliferating CD163+ M2-macrophages similar to what been within the diploid tumour (Table 5.3).

5.3. Discussions

In this project a digital pathology platform were utilised to analysis the cancer community of CRC. The fm-IHC approach utilised a bespoke precise image registration built by Dr. Alain Pitiot to align series of sequential IHC stained section into spatially corresponding images, which then segmented into approximately 200,000 super-pixels that allow several analysis to be taken, including the density and correlation analysis of the cellular and functional markers.

Table 5.2. Significant spatial density of cellular community and their functional properties of tumour microenvironment in the Nottingham cohort of colorectal cancer

Genetic features	Cellular community	Spatial Distribution	Density (Mean ± SD)		Exact Sig. (2 sided)
MSI/MSS	**Ki67+ Pan T-lymphocytes (CD3)**	Stroma	MSI (n=19)	0.0062±0.0031	0.040*
			MSS (n=24)	0.0005±0.0001	
	BCL-2+ B-lymphocytes (CD20)	Stroma	MSI (n=19)	0.0096±0.0028	0.047*
			MSS (n=24)	0.0043±0.0015	
BRAF	**Pan T-lymphocytes (CD3)**	Stroma	Mutant (n=14)	0.0552±0.0138	0.013*
			Wildtype (n=29)	0.0217±0.0056	
		WTS	Mutant (n=14)	0.0656±0.0195	0.007*
			Wildtype (n=29)	0.0237±0.0061	
	B-lymphocytes (CD20)	WTS	Mutant (n=14)	0.0351±0.0080	0.041*
			Wildtype (n=29)	0.0162±0.036	
	Ki67+ Pan T-lymphocytes (CD3)	Stroma	Mutant (n=14)	0.0069±0.0039	0.015*
			Wildtype (n=29)	0.0011±0.0007	
	Ki67+ M2-macrophages (CD163)	Stroma	Mutant (n=14)	0.0023±0.0012	0.040*
			Wildtype (n=29)	0.0009±0.0005	
	BCL-2+Pan T-lymphocytes (CD3)	Stroma	Mutant (n=14)	0.0100±0.0025	0.015*
			Wildtype (n=29)	0.0038±0.0014	
	BCL-2+ Cytotoxic T-lymphocytes (CD8)	Stroma	Mutant (n=14)	0.0036±0.0011	0.003*
			Wildtype (n=29)	0.0007±0.0002	
	BCL-2+ B-lymphocytes (CD20)	Stroma	Mutant (n=14)	0.0115±0.0032	0.013*
			Wildtype (n=29)	0.0044±0.0015	
	BCL-2+ M2-macrophages (CD163)	Stroma	Mutant (n=14)	0.0011±0.0005	0.006*
			Wildtype (n=29)	0.0002±0.0001	
	BCL-2+ NK cells (CD56)	Stroma	Mutant (n=14)	0.0002±0.00005	0.009*
			Wildtype (n=29)	0.00004±0.00001	
KRAS	**BCL-2+Pan T-lymphocytes (CD3)**	Stroma	Mutant (n=15)	0.0019±0.0009	0.019*
			Wildtype (n=28)	0.0080±0.0019	
	BCL-2+ Cytotoxic T-lymphocytes (CD8)	Stroma	Mutant (n=15)	0.0018±0.00009	0.007*
			Wildtype (n=28)	0.0024±0.0006	

Genetic features	Cellular community	Spatial Distribution	Density (Mean ± SD)		Exact Sig. (2 sided)
	BCL-2+ B-lymphocytes (CD20)	Stroma	Mutant (n=15)	0.0021±0.0010	0.025*
			Wildtype (n=28)	0.0091±0.0022	
	BCL-2+ M2-macrophages (CD163)	Stroma	Mutant (n=15)	0.00006±0.00003	0.009*
			Wildtype (n=28)	0.0007±0.0003	
	BCL-2+ NK cells (CD56)	Stroma	Mutant (n=15)	0.00003±0.00001	0.027
			Wildtype (n=28)	0.0001±0.00003	
TP53	**Pan T-lymphocytes (CD3)**	Epithelial	Mutant (n=20)	0.0504±0.0223	0.017*
			Wildtype (n=23)	0.0211±0.0091	
	Pan Macrophages (CD68)	Epithelial	Mutant (n=20)	0.1620±0.0757	0.049*
			Wildtype (n=23)	0.0144±0.0040	
	NK cells (CD56)	Epithelial	Mutant (n=20)	0.0039±0.014	0.013*
			Wildtype (n=23)	0.0009±0.0004	
	Ki67+ NK cells (CD56)	Stroma	Mutant (n=20)	0.00009±0.00003	0.004*
			Wildtype (n=23)	0.00009±0.00004	
Ploidy	**Ki67+ Pan T-lymphocytes (CD3)**	Stroma	Diploid (n=26)	0.0047±0.0022	0.021*
			Aneuploid (n=11)	0.0003±0.0001	
	Ki67+ M2-macrophages (CD163)	Stroma	Diploid (n=26)	0.0022±0.0010	0.012*
			Aneuploid (n=11)	0.0001±0.00004	
CIN vs MACS	**NK cells (CD56)**	Stroma	CIN (n=11)	0.0056±0.0022	0.044*
			MACS (n=7)	0.0259±0.0119	
		WTS	CIN (n=11)	0.0056±0.0021	0.044*
			MACS (n=7)	0.0207±0.0090	
	Ki67+ M2-macrophages (CD163)	Stroma	CIN (n=11)	0.0001±0.00004	0.044*
			MACS (n=7)	0.0010±0.0005	

Mann–Whitney U test. P<0.05. WTS, whole tissue section.

Table 5.3. Significant spatial pairwise correlation of cellular community of tumour microenvironment in the Nottingham cohort of colorectal cancer

Cell Type	Pairwise Correlation of cellular community		Molecular Features
Between Lymphocytes	Pan T-lymphocytes (CD3)	Cytotoxic T-lymphocytes (CD8)	Higher in epithelial and WTS of diploid tumour
		B-lymphocytes (CD20)	Higher in epithelial of MSS Higher in WTS of *TP53* wildtype
Macrophages-Lymphocytes and NK cells	Pan Macrophages (CD68)	Cytotoxic T-lymphocytes (CD8)	Higher in epithelial and WTS of MSI Higher in epithelial and WTS of *BRAF* mutant Higher in epithelial of *KRAS* wildtype
		B-lymphocytes (CD20)	Higher in epithelial of *BRAF* wildtype
		NK cells (CD56)	Higher in epithelial of *BRAF* wildtype
	M2-macrophages (CD163)	Pan T-lymphocytes (CD3)	Higher in epithelial of *PIK3CA* mutant Higher in epithelial and WTS of *TP53* mutant
		Cytotoxic T-lymphocytes (CD8)	Higher in epithelial and WTS of *BRAF* mutant Higher in epithelial of *KRAS* wildtype Higher in epithelial and WTS of diploid
		NK cells (CD56)	Higher in epithelial of MSS Higher in epithelial of aneuploid

WTS, whole tissue section.

Many studies have shown that MSI CRC has higher number/ density of CD3+, CD8+, and CD20+ infiltrating lymphocytes and CD68+ macrophages, mainly within the tumour glands (intraepithelial) (Michael-Robinson, et al, 2001; Bindea, et al, 2013; Galon, et al, 2014; Mlecnik, et al, 2016; Williams, et al, 2019). In this study, although higher density of T- and B-cell lymphocytes, macrophages and other immune biomarkers were observed, the differences were not reached statistical significance, perhaps due to the small number of samples being analysed. However, a significantly higher density of proliferating (Ki67+) CD3+ T-lymphocytes was found within the stroma of the MSI and diploid tumour (which enriched for MSI), suggesting the more active state of stromal lymphocytes of the MSI compare to the MSS. This finding is similar to the previous study that showed MSI patients had a significantly higher density of proliferating T cells, marked as CD3+Ki67+ than MSS patients in the invasive margin (part of tumour stroma) and core of the tumour (Mlecnik, et al, 2016). Also, similar to the finding in this project, the study by Mlecnik, et al (2016) also shown that the density of proliferating B cells (CD20+) within various compartments of the tissues was similar in MSI and MSS tumours. Interestingly, higher density of BCL-2+ CD20+ B-lymphocytes was found in the stroma of MSI tumour, suggesting the maintenance of low-apoptotic cell state. We also found significant correlation of CD8+ cytotoxic T-lymphocytes with CD68+ macrophages in the epithelial of MSI tumour. Altogether, these findings imply that the MSI tumour being more immunogenic could maintain the more functional stromal T- and B-lymphocytes and presumably attract other immune cells like macrophages into the cancerous epithelium. Alternatively, macrophages may regulate the function of the lymphocytes through the release of various cytokines. It has been reported that M1 macrophages produce immune stimulatory cytokines, like IL (interleukin)-6, -12 and CXCL (CXC-

chemokine ligand)-9, that promote recruitment of cytotoxic T-lymphocytes, while M2 macrophages exhibit an immune suppressive signature and support tumour growth by release of angiogenic factors, like IL-10 and CCL22, matrix remodelling mediated by proteases, and inhibit the cytotoxic T-lymphocytes activity (Franklin, et al, 2014; Kzhyshkowska, et al, 2014; Seliger, et al, 2019).

We further explored the association of other molecular features of CRC with the density of cancer community. There was significantly higher density of CD3+ T-lymphocytes within the stroma and WTS of *BRAF* mutant and also higher density of CD20+ B-lymphocytes on the WTS of the mutant. Density of proliferating (Ki67+) CD3+ lymphocytes and CD163+ M2-macrophages were also higher within the stroma of *BRAF* mutant and diploid tumour, which enriched for MSI. The *BRAF* mutant and *KRAS* wildtype (*KRAS* and *BRAF* mutations are exclusive) tumour had higher density of cellular community expressing BCL-2, which includes CD3+ and CD8+ T-lymphocytes, CD20+ B-lymphocytes, CD163+ M2- macrophages and CD56+ NK cells, indicating the low-apoptosis property.

Previous studies have shown that the presence of TIL (tumour-infiltrating lymphocytes) signature was associated with *BRAF* mutation, although not solely as an independent factor but related to high-level MSI, high-degree CIMP and higher amounts of neoantigens (Hamada, et al, 2018; Zhang, et al, 2018). In contrast to the MSI, data form this project were able to show that *BRAF* mutant CRC has higher stromal density of functional (highly proliferative and low-apoptotic) immune cellular populations, suggesting that *BRAF* may be stronger feature (as compare to MSI) to facilitate immune activation within the CRC TME.

BRAF mutation is associated with poor prognosis in advance and metastatic disease among MSS but not in the MSI cases (Taieb, et al, 2016; Lockhead, et

al, 2013; Pietrantonio et al, 2015; Yuan, et al, 2013; Balker, et al, 2018; Yang, et al, 2018; Renaud, et al, 2015; Schmoll,et al, 2012; Yokota, et al, 2011; Domingo, et al, 2018). In paradox, MSI tumour, which has been shown in this study and other to be enriched for *BRAF* mutation, has been associated with good prognosis for stage II and III (Popat, et al, 2005; Lockhead, et al, 2013; Goldstein, et al, 2014). It would be of interest to determine if *BRAF* mutation would be associated with enhanced immune landscape within the MSS only group. Nonetheless, in this project, the number of MSS tumour with *BRAF* mutation was too small (n=2) to be properly analysed.

Whether or not the finding with regard to *BRAF* mutation is associated with MSI, the significant functionally active T- and B-lymphocytes, macrophages and NK-cell observed in the mutant cases suggests that *BRAF* could be explored as a predictive biomarker for immunotherapy such as the check point inhibitors. In fact, *BRAF* mutation was linked to enhanced immune infiltrates through generation of MHC class II and checkpoint ligand molecules COX-2, PD-L1 and PD-L2 (Thorsson, et al, 2018).

Similar to the MSI tumour, *BRAF* mutant and *KRAS* wildtype showed higher correlation of CD8+ cytotoxic T-cell with CD68+ macrophages in the epithelium. Similar correlation was also found with CD163+ M2-macrophages. Together with higher density of Ki67+ and BCL-2+ of CD163+ M2-macropahes within the stroma of *BRAF* mutant, it seems that immunogenic type of CRC (ie. MSI and or *BRAF* mutant) could attract more macrophages including the pro-tumoural M2-macropahes (CD163+) that is enriched within the TAM (tumour associated macrophages). At the face value, this seems contra intuitive as immunogenic CRC has been linked to better prognosis (Gallon, et al, 2014; Becht, et al, 2016; Mlecnik, et al, 2016; Colangelo, et al, 2017; Pages, et al, 2018).

Further studies were required to study the prognostic and predictive significant of these macrophages as conflicting results has been reported so far (Gulubova et al., 2013; Marech et al., 2016; Mlecnik et al., 2016; Wei, et al, 2019). Despite the numerous literatures found on TAM pro-tumoural function and poor prognosis, some studies have shown that TAM in CRC was linked with enhanced disease-free survival and demonstrated antitumour activity by showing that the macrophages found in the tumour margin and less hypoxic areas were able to induce cell death in Fas ligand-dependent manner (Sugita, et al, 2002; Yahaya, et al, 2019). We investigated further the role of monocytic cell including the peripheral monocytes and macrophages in modulating CRC biology using 3D (three dimensional) multicellular co-culture model as describe in the next chapter (chapter 6) of this thesis.

In this study, *TP53* mutation was associated with higher intratumoural (epithelial) density of CD3+ T-lymphocytes, CD68+ macrophages, and CD56+ NK cells. There was also higher density of proliferating (Ki67+) NK cells within the stroma of *TP53* mutant tumour. To our knowledge, these are novel findings that have not been reported before and indicate that *TP53* mutation could, to certain degree, facilitate immune activation. Although, studies in other cancer entities and mouse model have also suggested that PTEN loss and *TP53* mutation may contribute to the less effective priming of T-cell and some innate immune cells including dendritic and NK cells, resulting in non-inflamed tumour phenotype (Spanger, et al, 2018; Tumeh, et al, 2014; Dientsmans, et al, 2017).

We have also explored the significance features of TME landscape of the diploid subtype of MSS tumour, namely MACS (microsatellite and chromosomal stable), which differs from the CIN (chromosomal instable) that were aneuploid. There was higher density of CD56+ NK cells within the stroma and WTS of MACS tumour. The stroma MACS also had significantly higher density of

proliferating (Ki67+) macrophages. These findings suggest that MACS tumour may trigger partial immune response as compare to relatively immune-inactive CIN counterpart. So far, although they were described about a decade ago, few studies are found with regard to MACS and no distinctive mutational profile are reported (Georgiades, et al, 1999; Hawkins, et al, 2011; Silver, et al, 2011, Fadhil, et al, 2014). Thus, the current findings with regard to the TME signatures of MACS warrant further investigation.

In summary, findings of this project suggest distinctive topology of TME in CRC in association of molecular characteristics defined by MSI and important driver gene mutation. Consistent with prior literature, the data support the role of TIL, macrophages and less described NK cells as an important effector in tumour-immune interactions. Our findings would likely inform future studies to better understand tumour-immune microenvironment of colorectal carcinomas in the era of precision therapy.

6. Three-dimensional (3D) Spheroid Co-Culture Model to Study the Interaction of Cancer Cells with Non-Neoplastic Cells in CRC.

6.1. Introduction

In recent years, one cellular community within the TME (tumour microenvironment) has become particularly prominent in the understanding of tumour biology. Galon et al. (2014) showed that infiltration of tumours by cells of the immune system, in particular CD3+ and CD8+ T cells, was a more powerful prognostic factor than classical pathological staging. Since then, the exquisite nature of the interaction between the epithelium and the stroma in regulating tumour growth has become apparent. Molecules such as CTLA4 and PD-L1 – expressed in both the epithelium and stroma – help tumour cells evade the immune responses (Llosa, et al, 2015). Conversely, tumours with a high mutation rate (such as mismatch repair deficient CRCs) appear to evoke a stronger immune response through generation of neo-antigens (Xiao, et al, 2015; Germano, et al, 2017). Although most attention has been focussed on T cells, other cells of both the adaptive and innate immune system, such as B cells, NK cells and macrophages may also influence tumour biology. Furthermore, the interaction between immune cells and other cellular components present within the tumour microenvironment such as fibroblasts and endothelial cells in modulating tumour progression is also warrant further investigation.

Tumour-associated Macrophages (TAMs) exist in close proximity to or within tumour networks. TAMs derive from circulating monocytes and are recruited to tumour sites by schemo-attractants such as CCL2 (chemokine ligand-2), CCL5, VEGF (vascular endothelial growth factor) and TGF-β (transforming growth factor- β) (Allavena, et al, 2008; Erreni et al., 2011; Komohara et al., 2016). In complex pathologic conditions such as cancer, as a response to the presence of multiple stimuli, macrophages may acquire dedicated phenotypes with

specific functions (Martinez and Gordon, 2014). It is now well accepted that TAMs demonstrate a range of polarized phenotypes, with the classical M1 that shows anti-tumour properties and M2 that exhibits pro-tumour activity, at the extremes, although generally TAMs are mostly M2-like (Biswas, et al, 2006; Erreni et al., 2011; Mantovani, 2014; Komohara et al., 2016).

Macrophages are characterised distinctively depending on the growth factors and chemokines present in its TME. For example, M1 macrophage will be polarised if there are any inducers (e.g., IFN-γ (interferon-γ), lipopolysaccharides (LPS), or TNF- α (tumour necrosis factor α) present in the TME. On the other hand, in the presence of interleukin (IL)- 4 and -13, the monocytes will be polarised into M2 macrophages. The inducers can either independently or coincide the monocyte to become M1 or M2 macrophage. The polarisation of M1 macrophage from monocyte is often referred to as classical activation, whereas alternative activation is frequently referred to the polarisation of M2 macrophage (Mantovani & Locati, 2013; Yahaya, et al, 2019). It is well accepted that CD68 is a pan-macrophagic marker that ubiquitously expressed both in M1 and in M2 groups. Although it may not be considered as conclusive markers, CD86 is highly expressed in M1 cells, whereas CD163 is commonly associated to M2 polarization (Vogel, et al, 2014; Bertani, et al, 2017).

To date, studies on the role of TAMs within the CRC microenvironment have yielded conflicting results. A recent study showed that CD68+ and CD163+ macrophages were associated with poor prognosis of CRC. These cells were mainly expressed at the tumour invasive front and stroma and associated with epithelial cells displaying a phenotype associated with reduced EMT (epithelial-mesenchymal transition) indicated by reduced E-cadherin and increased Vimentin (Wei, et al, 2019). Other studies have shown similar results. The CD68+ macrophages have been significantly linked to a more pro-angiogenic

environment in locally advance CRC indicated by increasing VEGF-A levels, microvascular density and endothelial area, thus, favouring cancer metastasis (Marech et al., 2016). Furthermore, a higher frequency of CD163+ macrophages was found to correlate with advanced tumour stage and shorter survival, in which the prognostic relevance was independent of the tumour stage (Shabo et al., 2014; Herrera, et al, 2013). In contrast, low levels of CD68+ macrophages have been linked to the activation of TGF-β signalling and unfavourable survival of CRC patients (Gulubova et al., 2013). Similarly, infiltration of CD68+ macrophages in colorectal tumours (both CT and IM areas) was significantly higher in the MSI patients that generally have better prognosis (Mlecnik et al., 2016). Together, these findings suggest that different subsets within the complex polarizing spectrum of macrophages may affect cancer growth in a distinctive manner.

Previous study by Wei et al. (2019) utilised a non-contact co-culture Transwell system (Corning, USA) to show that TAMs induced epithelial-mesenchymal transition (EMT) in CRC, resulting in increased cell migration and invasion through upregulation of IL-6 produced by the TAMs. This study suggested that IL6 activated the JAK2/STAT3 pathway and activated STAT3 transcriptionally inhibited the tumour suppressor miR-506-3p in CRC cells. miR-506-3p, a key miRNA regulating FoxQ1, was downregulated in CRC cells, resulting in increased FoxQ1 expression, which in turn led to the production of CCL2 that promoted monocyte recruitment. Another study by Zhang et al (2019) also utilised the Transwell co-culture system to study the interaction of CAFs (cancer-associated fibroblasts) and TAM in CRC biology and revealed that CAFs can promote the recruitment of monocytes by secreting IL-8 (interleukin-8) and up-regulating VCAM-1 expression in colorectal cancer cells and subsequently promote M2 polarization of macrophages, marked as CD206+ and CD163+. M2 macrophages then synergize with CAF in suppressing the functioning of natural

killer (NK) cells.

Within the TME of CRC, CAFs (cancer-associated fibroblasts) are the main cellular components both in the primary and metastatic diseases (Mueller, et al, 2007; Herrera, et al, 2013). In general, CAFs are more metabolically active and exhibit tumour-promoting properties (Tommelein, et al, 2015). CAFs secrete cytokines such as HGF (hepatocyte growth factor), IL-6 (interleukin-6), and SDF-1 (stromal cell-derived factor 1), which have a variety of effects on cancer cells and stroma, including angiogenesis, tumour growth, migration, and are an alternative source for extracellular matrix (Shiga, et al, 2015; Karakasheva, et al, 2018, Zhang, et al, 2019). Recently, numerous studies have demonstrated that CAFs play an important role in disruption of the anti-tumour immune response (Lambrechts, et al, 2018; Ziani, et al, 2018). Nonetheless, although limited, the tumour-inhibiting properties of CAF have been reported (Yamanashi, et al, 2009; Özdemir, et al, 2014).

Studies to dissect the mechanism of action of different components of tumour microenvironment to modulate cancer growth will provide information on potential tumour treatments. Nevertheless, a major challenge is the development of relevant models that reflect the human pathologies. Interactions between tumour and stroma are difficult to study *in-vivo* due to limitations in tissue accessibility, *in-vivo* monitoring and selection of specific intercellular interactions (Cattin, et al, 2018). Thus, recently, 3D (three-dimensional) tumour cell cultures under non-adherent conditions, called tumour spheroids/ organoids, have been developed from tumour primary cells and cell lines (Katt, et al, 2016; Sato, et al, 2011; Weiswald, et al, 2015; Clevers, 2016). A typical model incorporates co-existence of ex-vivo epithelial cancer cells with other cellular components of the tumour microenvironment such as immune cells and fibroblasts, embedded in synthetic extracellular matrix which may mimic in-vivo conditions (Bullock et al, 2014; Lazzari, et al, 2018).

Establishment of the co-culture model will allow various downstream applications such as genotype and phenotype profiling of tumour, stroma and infiltrating immune cells as well as some functional studies, for instance tumour growth and invasiveness. Using this approach, possible treatment with chemical inhibitors and targeted gene alteration using the CRISPR/CAS-9 system can also be applied (Lee, et al, 2018; Driehuis and Clevers, 2017; Courau, et al, 2019).

Amongst the 3D in vitro models available for CRC, recellularized CRC scaffolds have been suggested as a useful preclinical patient-derived tool that could predict in vitro the success of future therapies administered to the patient (Sensi, et al, 2020). However, due to its uniqueness and complexity, this method may not be as practical as heterotypic spheroids for drug screening. Addition of stromal cell types such as CAF to 3D models substantially supports growth of cancer cell lines and may also promote invasion and metastasis by guiding cancer cells at the invasive edge (Labernadie, et al, 2017).

CD24 is a highly glycosylated, mucin-like glycosylphosphatidylinositol-anchored surface protein that is linked to the membrane via glycosylphosphatidylinositol (GPI)-anchor and is exclusively localised in membrane lipid raft domains (Kay et al, 1991; Schabath et al, 2006). In humans, CD24 has a protein core of only 31 amino acids with 16 potential O- and N-glycosylation sites. (Kay et al, 1991). In normal tissue, CD24 is expressed predominantly on cells of the hematopoietic lineage such as B lymphocytes, monocytes, granulocytes and activated T lymphocytes yet CD24 is also overexpressed in many human cancers and its expression is associated with poor prognosis including in CRC (Kristiansen et al, 2004; Fang et al, 2010; Wang, et al, 2018).

CD24 overexpression reported to occur at early stage in cell carcinogenesis and was identified as a marker for cancer stem cells for a variety of cancer types

(Woodward and Sulman, 2008). In tumour cells, CD24 was identified as a ligand of P-selectin that supports the rolling of cancer cells on endothelial cells and adhesion to platelets, therefore might facilitate the metastatic spread of tumour cells (Aigner et al, 1997; Friederichs et al, 2000; Kristiansen et al, 2004; Baumann et al, 2005). Other ligands have been identified for CD24 including L-, and E- Selectin, HMGB1 (High Mobility Group Box 1), L1CAM (L1 cell adhesion molecule), NCAM1 (Neural cell adhesion molecule) and Siglec-G (Aigner et al., 1997; Myung et al., 2011; Tan et al., 2016). Several signal transduction proteins are associated with CD24 activity. The best-described are the Src-family protein tyrosine kinases Lyn, Fyn, Fgr, Lck and Hck but how these are activated is unknown (Sammar et al., 1997; Fang et al., 2010; Su et al., 2012).

CD24 expression has been shown to regulate tumour cell proliferation, migration, invasion and angiogenesis, in a variety of cancers including CRC (Baumann et al, 2005; Smith et al, 2006; Runz et al, 2008; Sagiv et al, 2008; Wang et al, 2010; Mierke et al, 2011; Bretz et al, 2012; Wang, et al, 2016) and was found to affect gene expression in colon and pancreatic cell lines (Sagiv et al, 2008). Previous study from our group has also showed that transient CD24 overexpression increased CRC cell, HCT116, migration, invasion, and colony formation but have no effect on cell proliferation in 2D culture (Ahmed, et al, 2010).

This chapter discusses the development of a 3D multicellular co-culture spheroid model of CRC to study the effect of CAF and cells of monocytic lineage ie. monocytes and macrophages, on tumour growth. It is hypothesized that signals from the cancer cell dictate the stromal cells to respond in regulating tumour biology. Colorectal cancer cell lines with different molecular background were used and the effect of stromal cell components on the growth of CRC cell lines were observed. We also used the 3D co-culture model to investigate the role of CD24 in CRC growth/proliferation to see if there is distinctive role from

what been observed in 2D culture of previous studies in our group.

6.2. Results

6.2.1. Three-dimensional (3D) spheroid culture of CRC cell lines

Fibroblasts are one of the most abundant stromal cells within the CRCs. Initial experiments involved the construction of 3D co-culture spheroids of CRC-CAF as the basic model to study cancer-stromal cells interactions. CAFs were isolated from the tumour tissue of one patient donor, according to the protocol established within the Cancer Biology Unit, School of Medicine, University of Nottingham (Prof. Anna Grabowska's group). Following isolation, CAF were expanded as 2D culture and maintained using appropriate growth media enriched with supplements before being harvested for 3D co-culture. To minimise the potential changes of these primary cells following *in-vitro* culture, the passage number was kept to 8 and the morphology of the cells was monitored in each passage.

The initial experiments were set up to determine the ability of five CRC cell line, which were HCT116, DLD-1, SW480, SW620 and LS1034, to form spheroid and the optimal seeding density. The CRC cell lines expressing td-Tomato, were seeded onto 96-well ultralow attachment culture plate (Corning, Cat: CLS4515) at different cell numbers, 2000; 4000; and 8000 cells/well. The growth of the spheroids was followed by volumetric and fluorescence measurements. The spheroid formation method used in this project revealed different morphologies between CRC cell lines. Whilst DLD1 and HCT116 formed compact spheroids of round uniform shape, SW480 and SW620 produced loose aggregates and LS1034 produced a globous irregular shape, as depicted in Figure 6.1. Thus, only data from HCT116 and DLD-1 spheroids were analysed further.

As shown in Figure 6.2 and 6.3. The volume of the spheroid was presented as

percent growth after normalization to the value the spheroid at day 2 after seeding, when the spheroids started to form sphere-like shape. The relative fluorescence readings were normalised to the fluorescence measured immediately (1 hour) after seeding at day 0. As depicted in Figure 6.4, there was only slight fluorescence reading difference for different seeding density at day 0 due to relatively small cell numbers used (maximum of 8000 cells/well). Nonetheless, the difference was become more prominent following the 7 days of culture and the RFU (relative fluorescence unit) were proportional to the seeding number in which the seeding number of 8000 cells/well showing the highest fluorescence reading.

As expected, the higher cell seeding number resulted in bigger spheroids in size as measured by the volume approximation. There was significant difference on the growth rate of different seeding numbers, with bigger spheroids showing the lowest growth in size from day 4 onward. Interestingly, when the growth rate was measured by the fluorescence reading of the Td-Tomato expressed by the CRC cells, no significant differences were observed between the different seeding numbers. Thus, it is likely that seeding the spheroid at higher number of cells would result in more compact spheroids, yet the cells proliferated at the similar rate as cells seeded at lower density. This suggests that the physical size of the spheroid was not necessarily related to the cell number in the spheroid.

Further in this project, the total of 2000 cells/ well was used as the optimal seeding number of spheroid culture. As presented in the supplementary materials, the lower seeding number at 1000 cells/well was also explored. Nonetheless, as also reported by others, lower seeding number would result in much smaller-sized and difficult to handle spheroids whereas the higher seeding number would result in larger-sized spheroid with the higher chance of forming larger necrotic core (Daster, et al, 2016; Barisma, et al, 2018).

6.2.2. CRC cell lines and CAF 3D spheroid co-culture

For optimisation of a co-culture model, HCT116 and DLD-1 cells tagged with Td-Tomato were co-cultured with CAF tagged with GFP. The cancer cells and CAF were seeded at different ratio (1:1 and 1:2) with total cell numbers maintained at 2000 cells/ well. The growth of the spheroid were assessed by volumetric measurements based on the brightfield images and fluorescence readings, with red fluorescence of Td-tomato (544 nm excitation and 590 nm emission) reflecting the growth of the cancer cells and green fluorescence of GFP (488 nm excitation and 520 nm emission) reflecting the growth of the CAF, as shown in Figure 6.5.

As depicted in figure 6.6, the sphere-like structure was observed on day 2 after the seeding of HCT116 cells with and without different proportion of CAF on the ultra-low attachment plate. Whereas the mono- and co-culture of DLD-1 formed sphere-like structure earlier at day 1, as shown in Figure 6.8. The fluorescence image shown in figure 6.7 and 6.9 details that the CAF congregated in the core of the spheroids. The Td-Tomato and GFP transduction of the cancer cells and CAF, respectively allowed us to measure the growth of both cell types within the spheroids. As shown in Figure 6.10, the co-culture of HCT116 with CAF, particularly at 1:1 ratio, showed a significant increase in spheroid growth as measured by the total volume of the spheroid. The proliferation of the HCT116 cells also increased significantly when co-cultured withs CAF at both 1:1 and 1:2 ratio. Interestingly, the CAF numbers in this co-culture model decreased each day, most probably due to cell death with approximately 20% decline after 7 days of seeding. However, the possibility of loss of fluorescence signal in the co-cultured CAF following the lentivirus transduction could not be ruled out. When grown in low adherence conditions, CAF form small spheroids that do not increase in volume, apparently in a quiescent state as depicted in Figure 6.5.

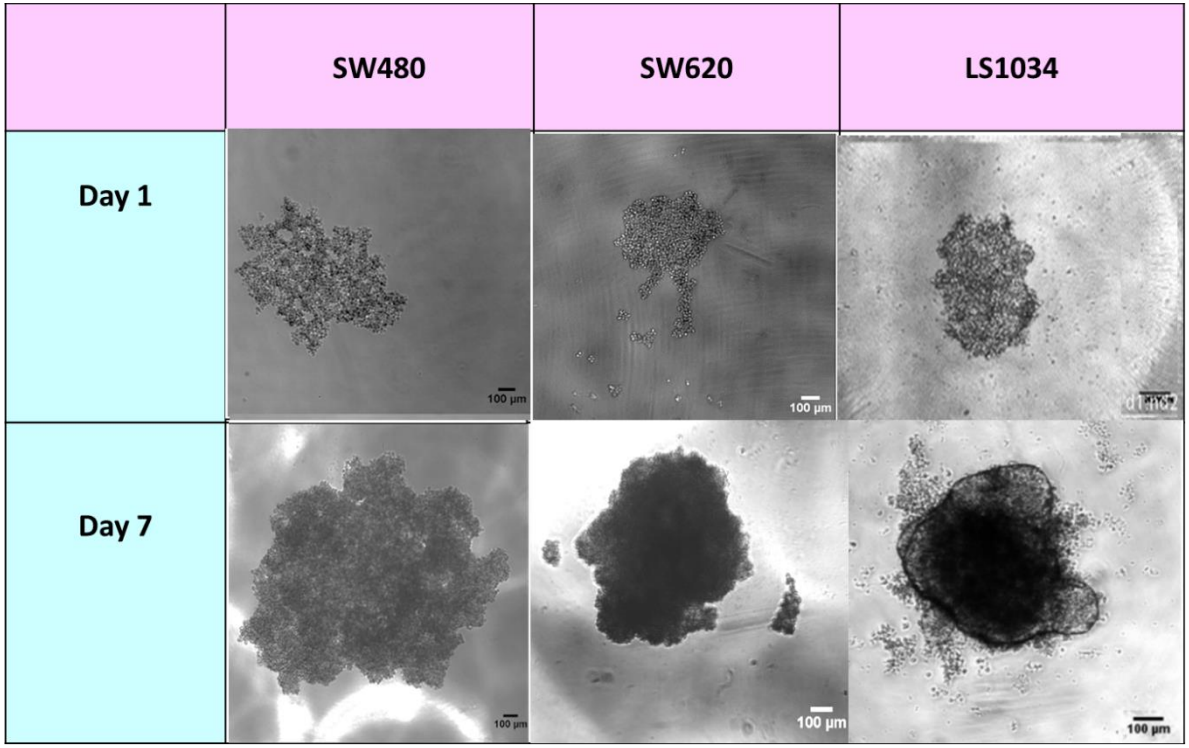
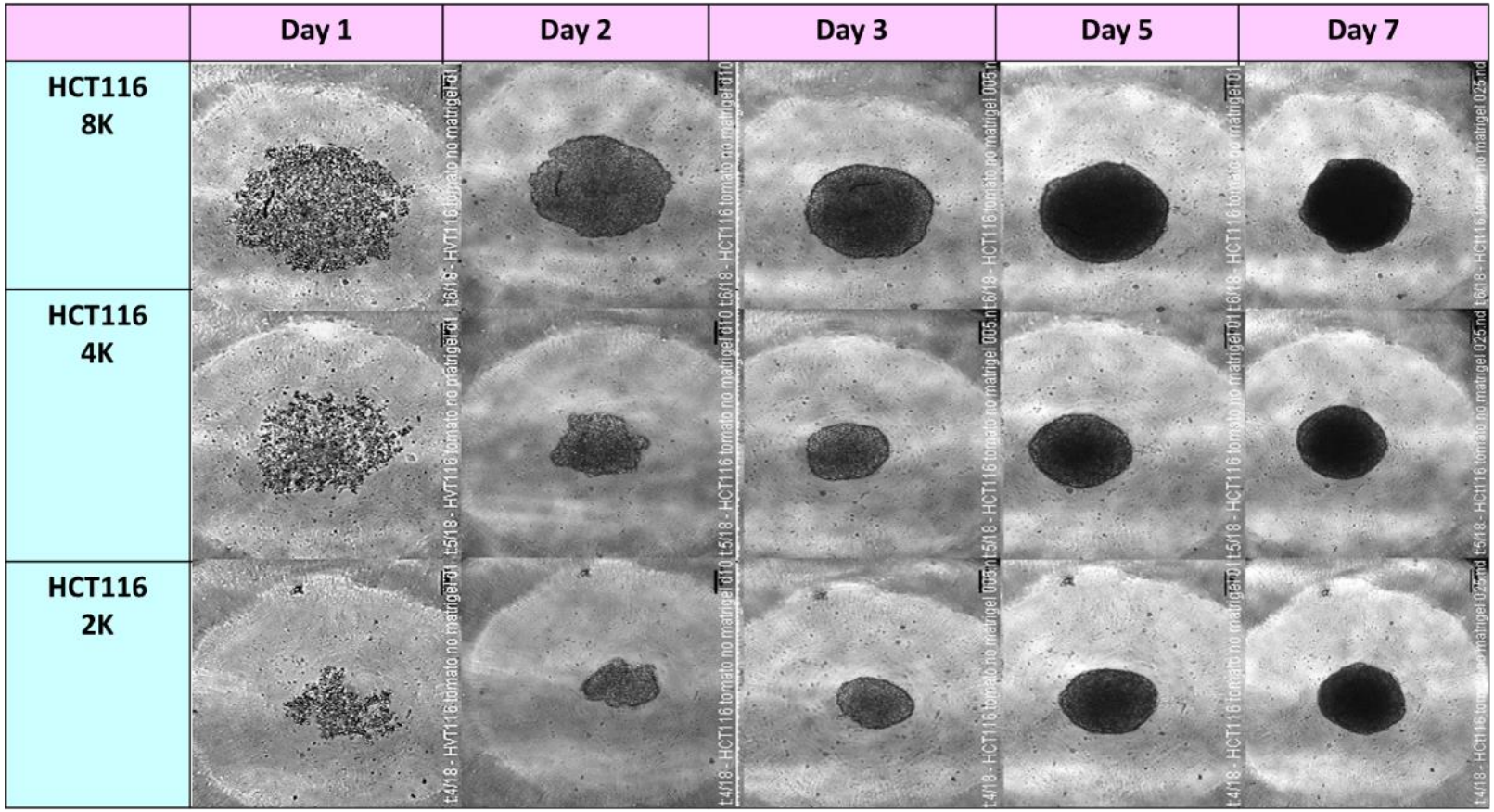
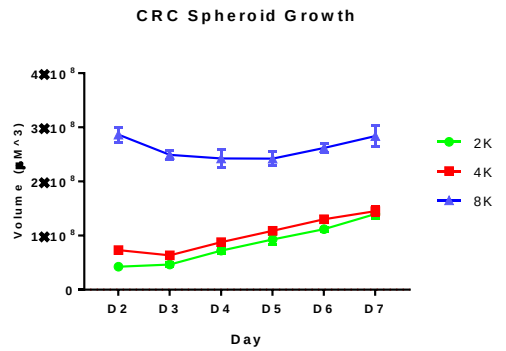


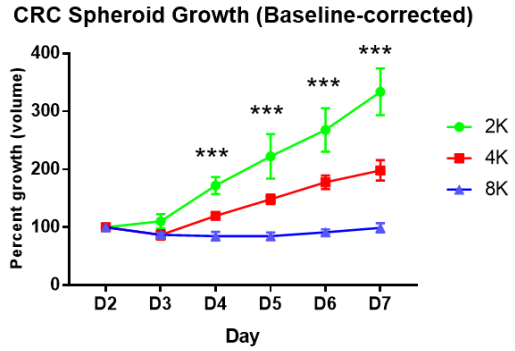
Figure 6.1. Live cell brightfield imaging of three-dimensional (3D) co-culture spheroid of colorectal cancer (CRC) cell line, SW480, SW620 and LS1034. The images were taken at 4x magnification using a widefield inverted microscope (Nikon TiE). The CRC cells were seeded as monoculture with total number of 2000 cell/well on a 96-well black ultralow attachment plate (Corning, Cat: CLS4515). The scale bar indicates 100 µM. After 7 days of culture, these cells formed looser or even irregularly shaped aggregates, which confounded the volumetric measurement of the spheroid.

A

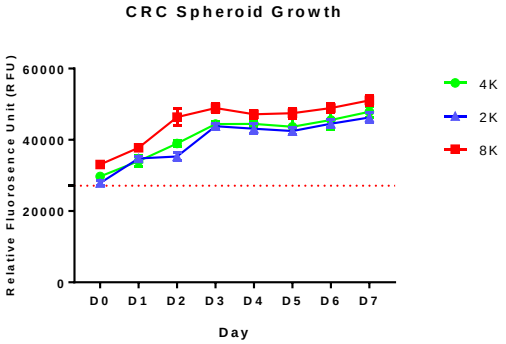


B





C



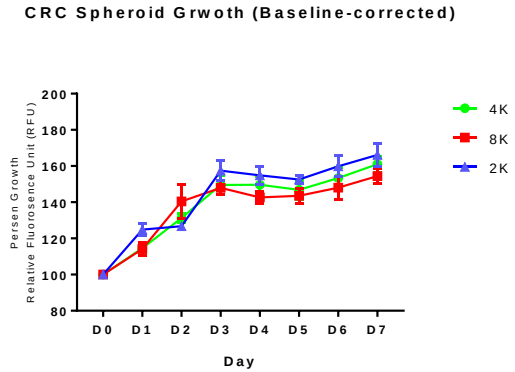
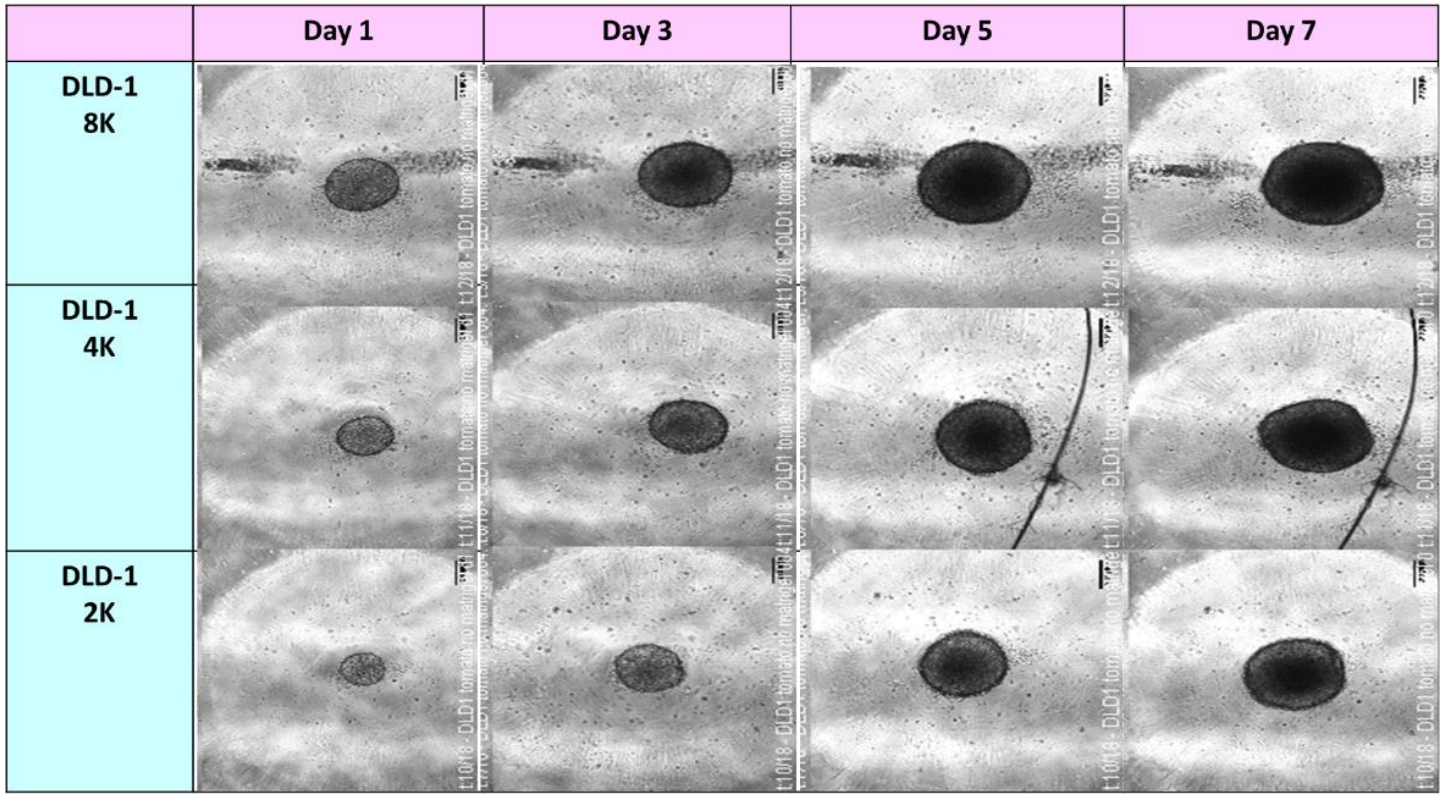
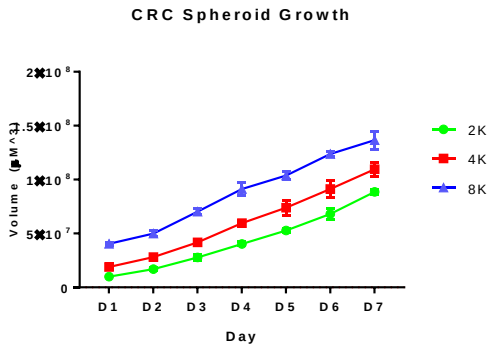


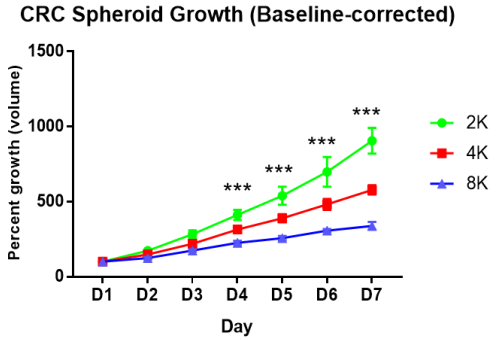
Figure 6.2. Three-dimensional (3D) mono-culture spheroid of colorectal cancer (CRC) cell line, HCT116 expressing Td-Tomato. A. The live cell brightfield images of the spheroids were taken at 4x magnification using a widefield inverted microscope (Nikon TiE). The CRC cells were seeded at total number of 8000 (8K), 4000 (4K) and 2000 (2K) cells/well on a 96-well black ultralow attachment plate (Corning, Cat: CLS4515). The compact spheroids were observed since day 2 after seeding. B. The images were used to calculate the mean spheroid radius by assuming an approximation to the area of the circle and from there inferred the volume of the spheroid, as an approximation to the volume of a sphere (left). The relative percent growth represents the normalised values with respect to the volume of spheroids measured at Day 2 after seeding (right). C. The Td-Tomato fluorescence signal was measured (left) and normalised to the value obtained on the day of seeding (D0) as the relative percent growth (right). Graphs are representative of 6 replicates per condition results shown are representative of 2 independent experiments. ***, $P \leq 0.001$ based on Two-Way ANOVA test performed on GraphPad Prism v.7.03.

A

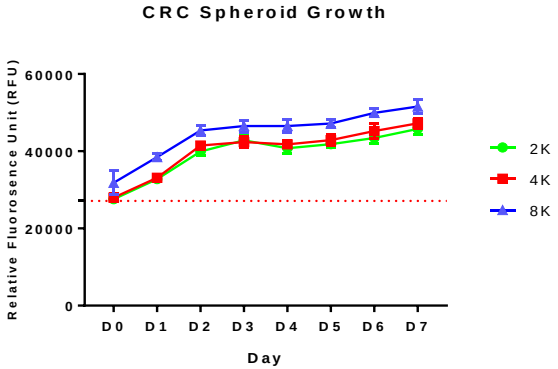


B





C



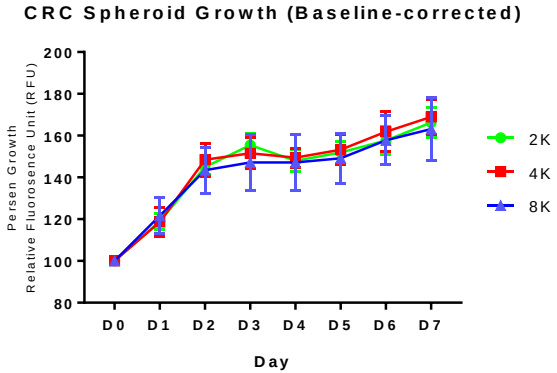
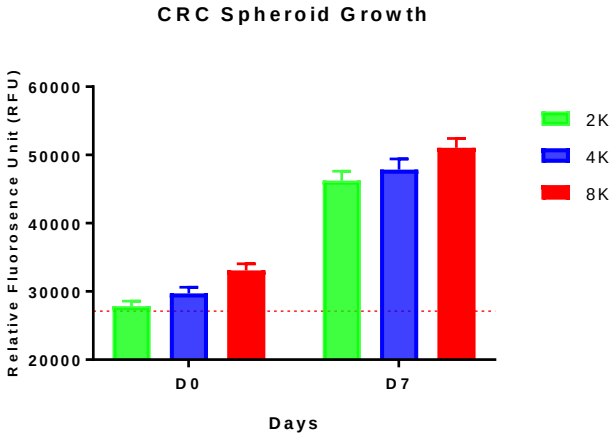


Figure 6.3. Three-dimensional (3D) mono-culture spheroid of colorectal cancer (CRC) cell line, DLD-1 expressing Td-Tomato. A. The live cell brightfield images of the spheroids were taken at 4x magnification using a widefield inverted microscope (Nikon TiE). The CRC cells were seeded at total number of 8000 (8K), 4000 (4K) and 2000 (2K) cells/well on a 96-well black ultralow attachment plate (Corning, Cat: CLS4515). The compact spheroids were observed since day 2 after seeding. B. The images were used to calculate the mean spheroid radius by assuming an approximation to the area of the circle and from there inferred the volume of the spheroid, as an approximation to the volume of a sphere (left). The relative percent growth represents the normalised values with respect to the volume of spheroids measured at Day 2 after seeding (right). C. The Td-Tomato fluorescence signal was measured (left) and normalised to the value obtained on the day of seeding (D0) as the relative percent growth (right). Graphs are representative of 6 replicates per condition results shown are representative of 2 independent experiments. ***, $P \leq 0.001$ based on Two-Way ANOVA test performed on GraphPad Prism v.7.03.

A



B

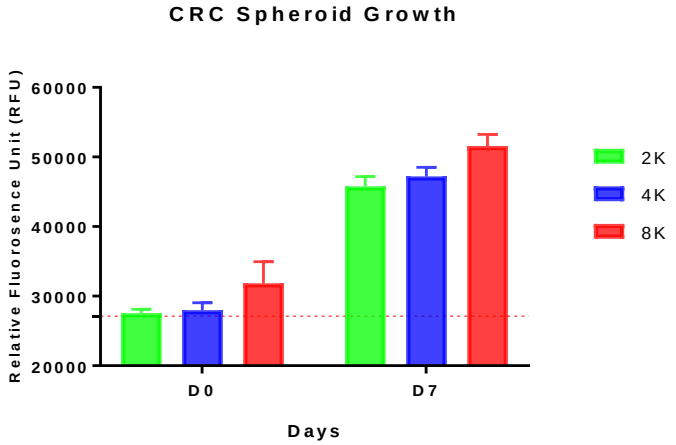


Figure 6.4. The growth of three-dimensional (3D) mono-culture spheroid of colorectal cancer (CRC) cell line measured as relative fluorescence unit (RFU). A. HCT116. B. DLD-1. The CRC cells were seeded at total number of 8000 (8K), 4000 (4K) and 2000 (2K) cells/well on a 96-well black ultralow attachment plate (Corning, Cat: CLS4515). The Td-Tomato fluorescence signal was measured at day 0 (1 hour) and day 7 after seeding. The increase of fluorescence reading corresponded with the increase of seeding number. The RFU differences among different seeding density become more prominent after 7 days of culture. Graphs are representative of 6 replicates per condition results shown are representative of 2 independent experiments.

A similar co-culture setup was applied to the CRC cell line, DLD-1. Interestingly as shown in Figure 6.11, co-culture with CAF resulted in smaller growth of spheroids based on total volume compared to DLD-1 cells monocultures. However, there was no significant differences on the proliferation of the cancer cells measured by Td-Tomato fluorescence readings on both co- and monocultures. This suggests that co-culture of DLD-1 with CAF did not resulted in stimulation of cancer cell growth as observed in co-culture with HCT116, instead there was increased in the spheroid compactness as shown by the decreased of spheroid volume. Similar to previous findings from the co-cultures of HCT116 and CAF, the proliferation of the CAF in the co-culture model was also found to be decreased by 20% after day 7 of seeding.

In conclusion, HCT116 and DLD-1 have responded differently to the stimuli of CAF in the 3D co-culture model been used in this project. In addition, the CAF was found to be localised at the core of the spheroid for both HCT116 and DLD-1, as depicted in Figure 6.7 and 6.9, possibly due to the stronger cell to cell adhesion between CAF. A previous study showed that hypoxic and necrotic areas are found within spheroids with diameter larger than 200 μm due to the decreased concentration of oxygen and glucose (Daster, et al, 2016; Barisma, et al, 2018). Based on the calculations from the brightfield images of the spheroids, the diameter of the CRC spheroids both in mono-and co-culture with initial seeding number at 2000 cells/well were within the 300-800 μm range during the 7 days of culture (data not shown). Based on the findings it appears that CAFs were not proliferating in this co-culture model.

6.2.3. The role of monocytes and macrophages 3D spheroid co-culture of CRC- CAF

Using the optimised model of CRC-CAF co-culture at 1:1 ratio, in which optimal response of cancer cells growth toward CAF stimuli was observed on HCT116 (CAF-responder), further studies were performed on to study the effect immune cells of monocytic lineage, monocytes and macrophages on the CRC tumour growth using both HCT116 and DLD-1 (CAF- non responder) . The monocytes were isolated from buffy coats from healthy volunteers and macrophages were differentiated from monocytes in the presence of M-CSF. The preparation of monocytes and macrophages was carried out by Dr. Sirina Muntaka from Dr. Luisa Martinez-Pomares's group (School of Life Science, University of Nottingham, UK)

Immediately after the isolation, monocytes were added at different cell number, ie 100, 250 and 500 cells/ well into the mixture of 2000 cells/ well of CRC-CAF at 1:1 ratio on 96-well low attachment culture plate. Similar to previous experiments, the multicellular spheroids were cultured for 7 days and the brightfield images and fluorescence readings were taken every day to follow the growth kinetics. As shown in Figure 6.12, there was no significant differences on the total volume of the HCT116-CAF spheroids with the presence of different numbers of monocytes during the 7 days of culture. Particularly, there was also no significant difference on the proliferation of the HCT116 as reflected by the fluorescence signals of the Td-Tomato. Figure 6.13 described the similar experiments with DLD-1. As what been observed with the HCT116, there was no significant differences on the total volume of the spheroids and the proliferation of the CRC within the multicellular culture.

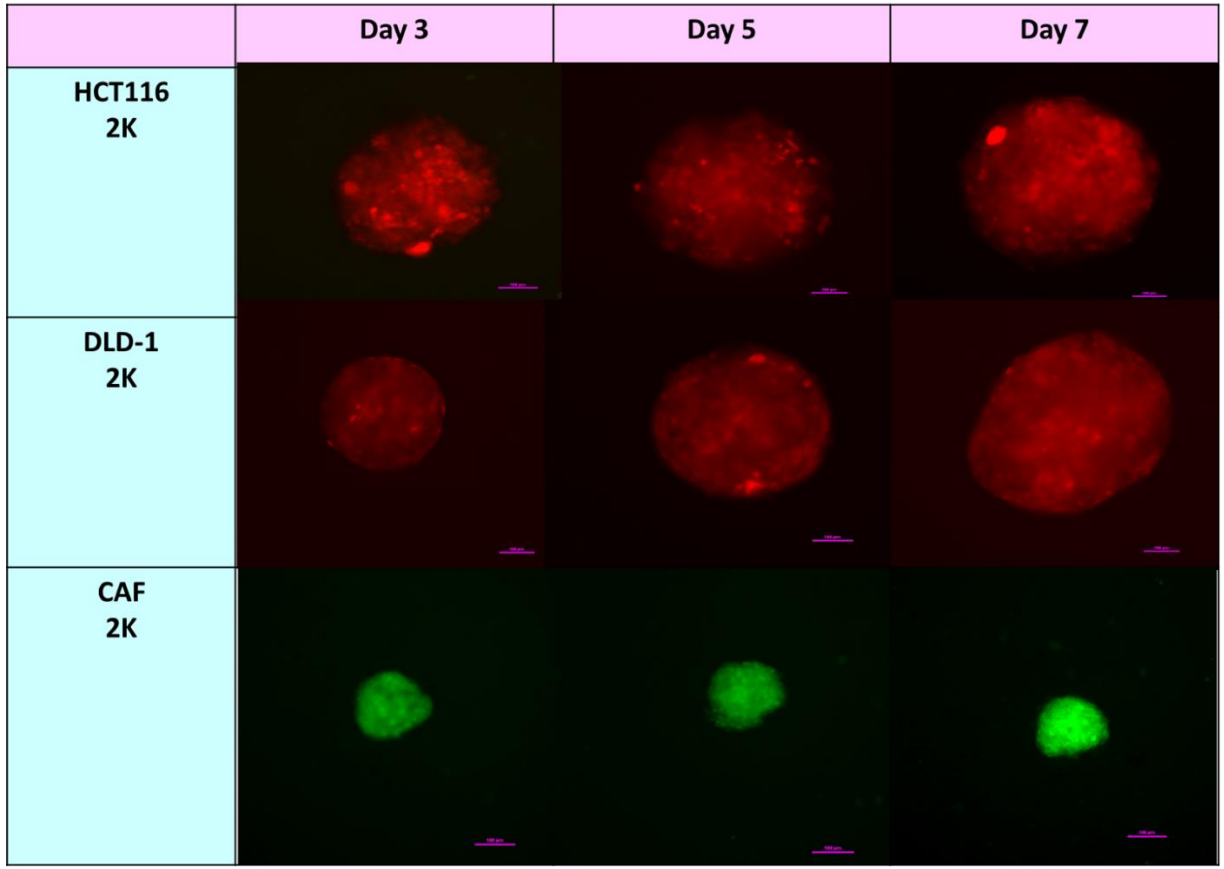


Figure 6.5. Live-cell fluorescence imaging of three-dimensional (3D) mono-culture spheroids of colorectal cancer (CRC) cell line, HCT116 and DLD-1, and cancer-associated fibroblast (CAF). The images were taken at 10x magnification using a widefield inverted microscope (Nikon TiE). The CRC and CAF cells were seeded alone at the total number of 2000 cells/well on a 96-well black ultralow attachment plate (Corning, Cat: CLS4515). The HCT116 and DLD-1 were transduced with tdTomato (red) and the CAF were transduced with GFP (green). The scale bar indicates 100 μM. The CAF spheroid was found to be much smaller and quiescent compare to the CRC spheroid.

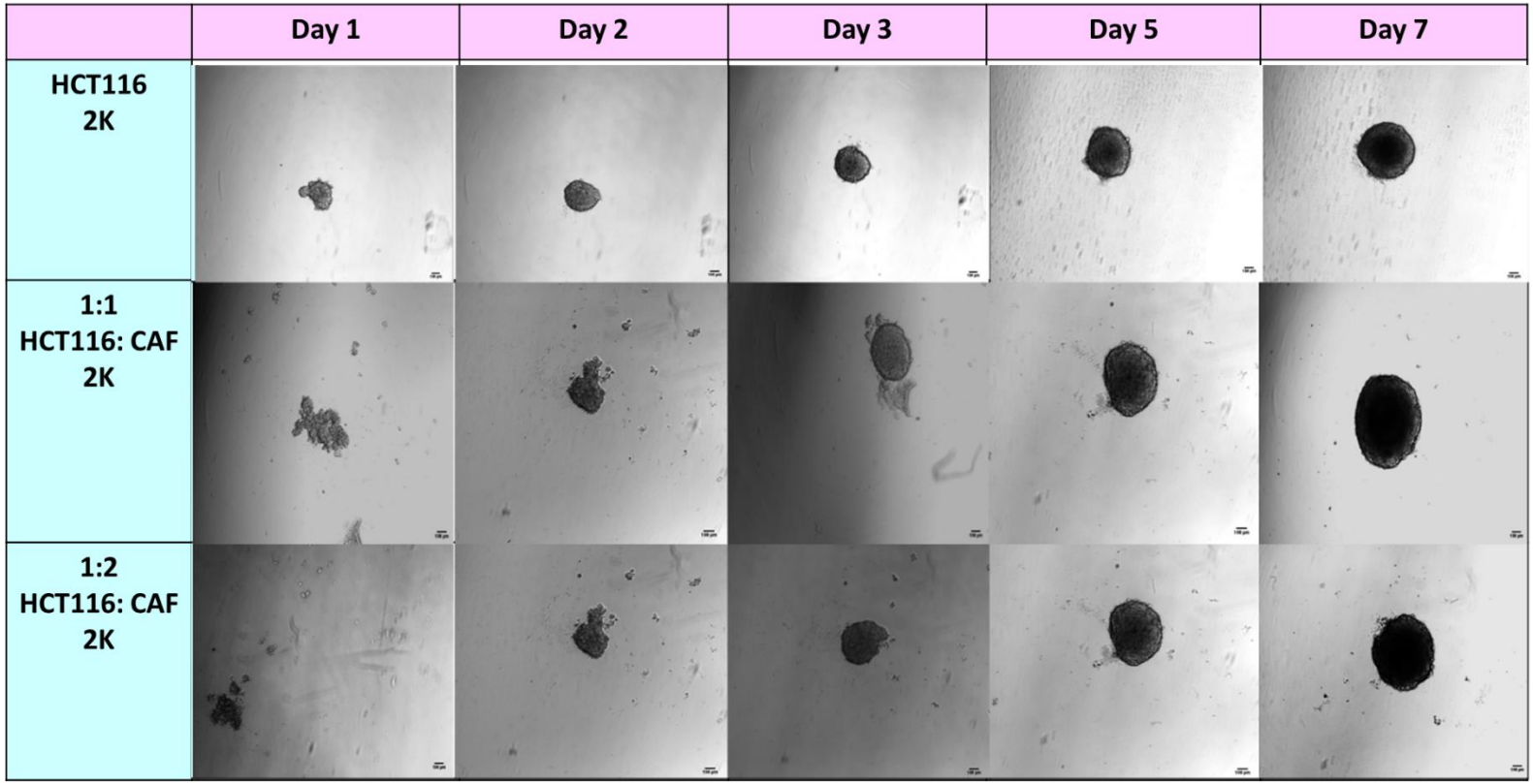


Figure 6.6. Live-cell brightfield imaging of three-dimensional (3D) co-culture spheroid of colorectal cancer (CRC) cell line, HCT116, and cancer-associated fibroblast (CAF). The images were taken at 4x magnification using a widefield inverted microscope (Nikon TiE). The CRC cells were seeded alone and with CAF at 1:1 and 1:2 ratio at total number of 2000 cell/well on a 96-well black ultralow attachment plate (Corning, Cat: CLS4515). The scale bar indicates 100 µM. The compact spheroids were observed since day 2 after seeding for mono and co-culture.

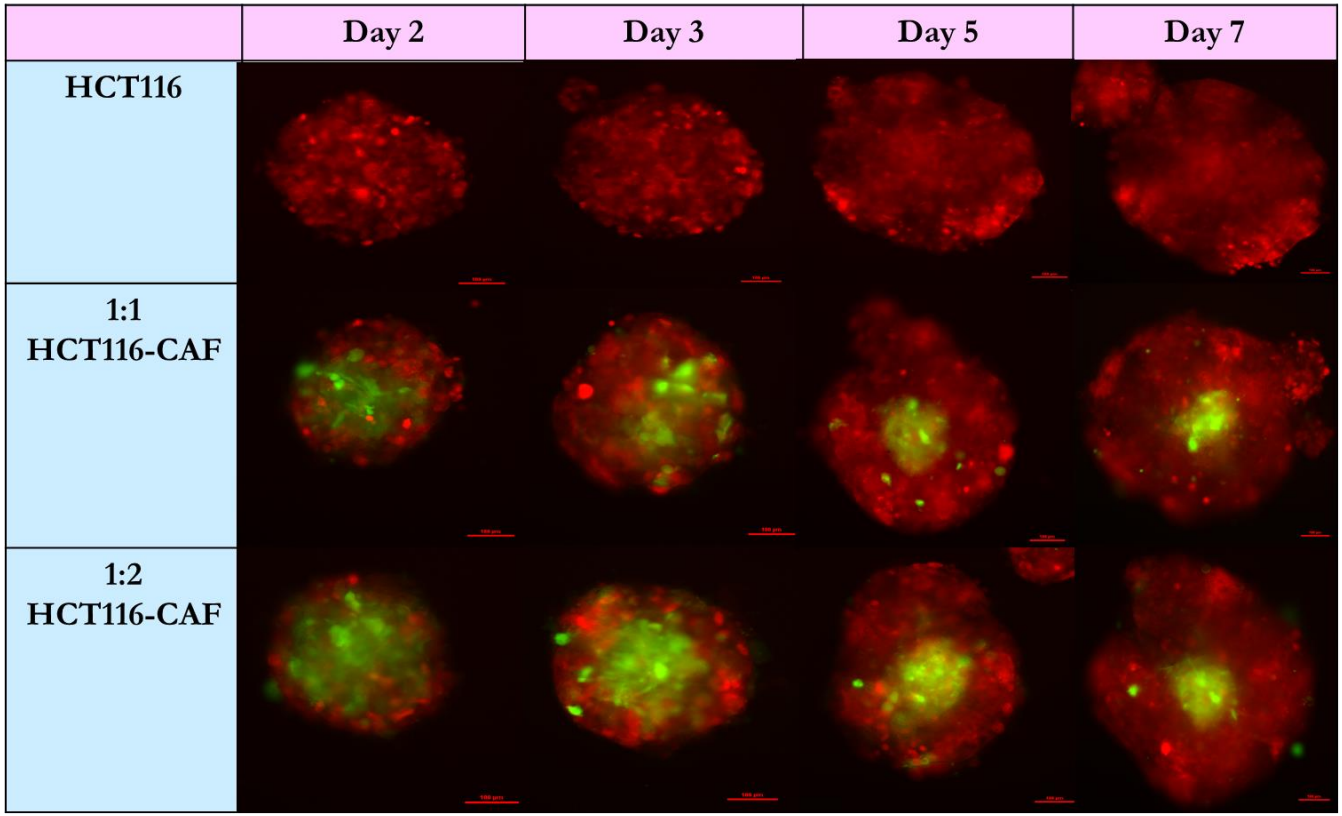


Figure 6.7. Live-cell fluorescence imaging of three-dimensional (3D) co-culture spheroid of colorectal cancer (CRC) cell line, HCT116, and cancer-associated fibroblast (CAF). The images were taken at 10x magnification using a widefield inverted microscope (Nikon TiE). The CRC cells were seeded alone and with CAF at 1:1 and 1:2 ratio at total number of 2000 cell/well on a 96-well black ultralow attachment plate (Corning, Cat: CLS4515). The HCT116 and CAF were transduced with tdTomato (red) and GFP (green) proteins, respectively. The scale bar indicates 100 µM. The compact spheroids were observed since day 2 after seeding for mono and co-culture. In this co-culture model, the CAF was found to congregate in the core area as the spheroids growing in size.

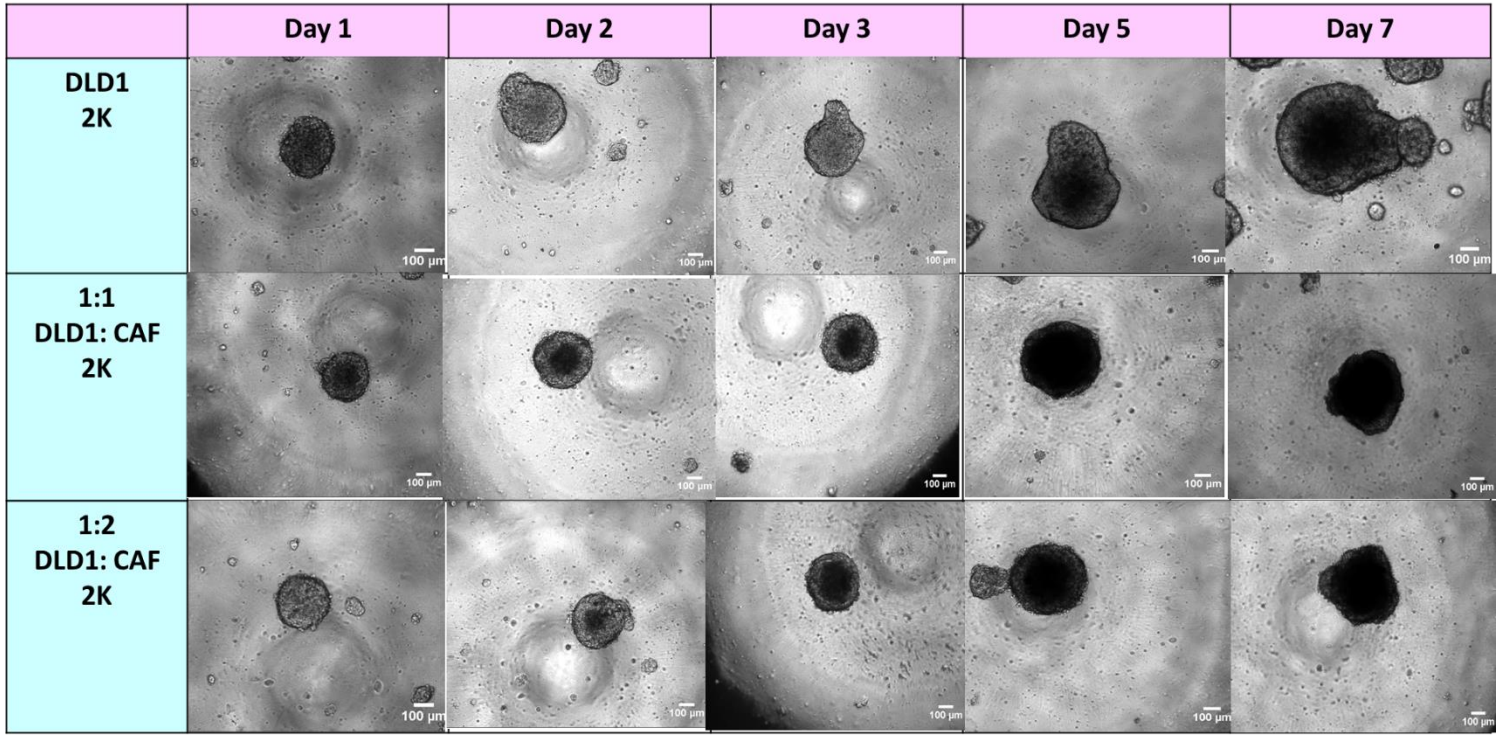


Figure 6.8. Live-cell brightfield imaging of three-dimensional (3D) co-culture spheroid of colorectal cancer (CRC) cell line, DLD-1, and cancer-associated fibroblast (CAF). The images were taken at 4x magnification using a widefield inverted microscope (Nikon TiE). The CRC cells were seeded alone and with CAF at 1:1 and 1:2 ratio at total number of 2000 cell/well on a 96-well black ultralow attachment plate (Corning, Cat: CLS4515). The scale bar indicates 100 µM. The compact spheroids were observed since day 1 after seeding for mono and co-culture.

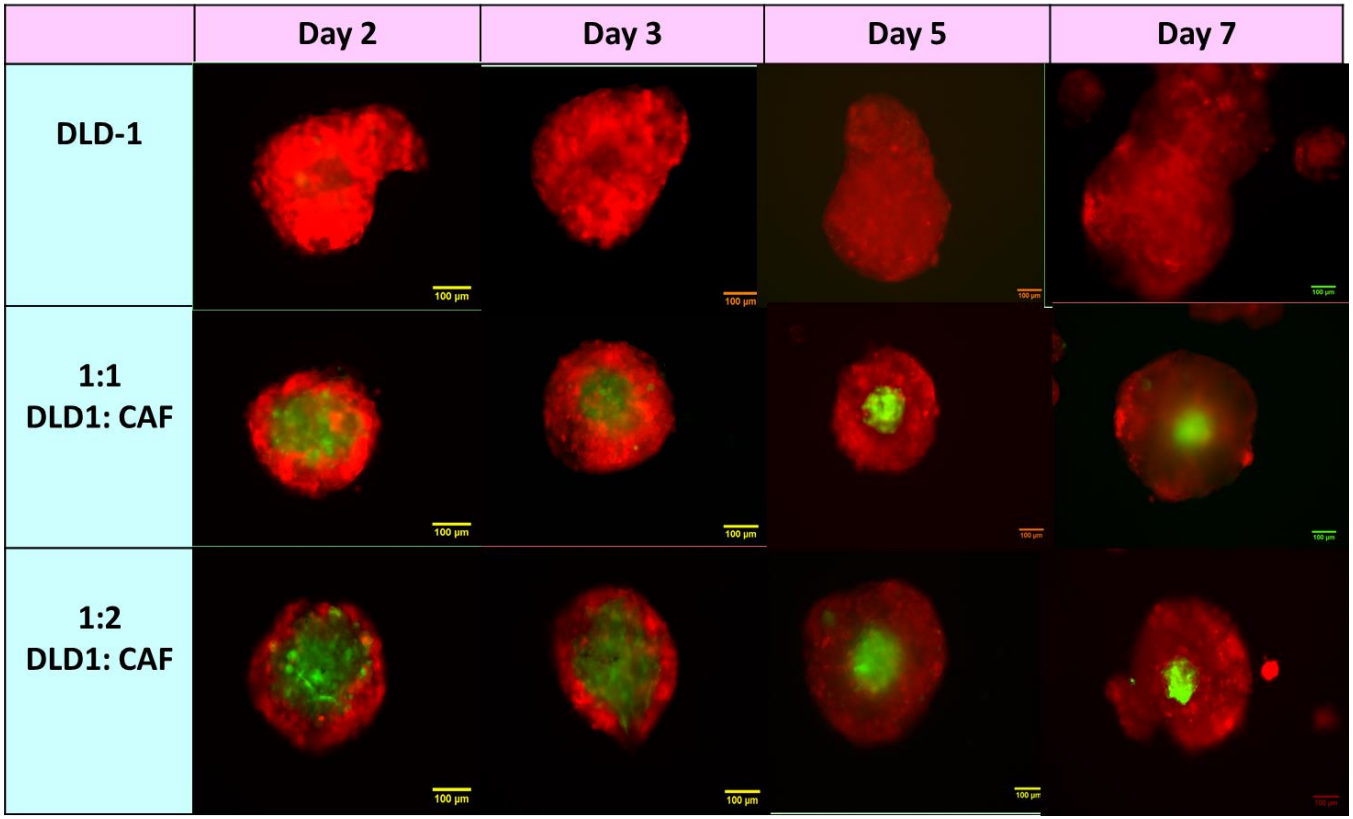


Figure 6.9. Live-cell fluorescence imaging of three-dimensional (3D) co-culture spheroid of colorectal cancer (CRC) cell line, DLD-1, and cancer-associated fibroblast (CAF). The images were taken at 10x magnification using a widefield inverted microscope (Nikon TiE). The CRC cells were seeded alone and with CAF at 1:1 and 1:2 ratio at total number of 2000 cell/well on a 96-well black ultralow attachment plate (Corning, Cat: CLS4515). The HCT116 and CAF were transduced with tdTomato (red) and GFP (green) proteins, respectively. The scale bar indicates 100 µM. The compact spheroids were observed at day 2 to 7 after seeding for mono and co-culture. In this co-culture model, the CAF was found to congregate in the core area as the spheroids growing in size.

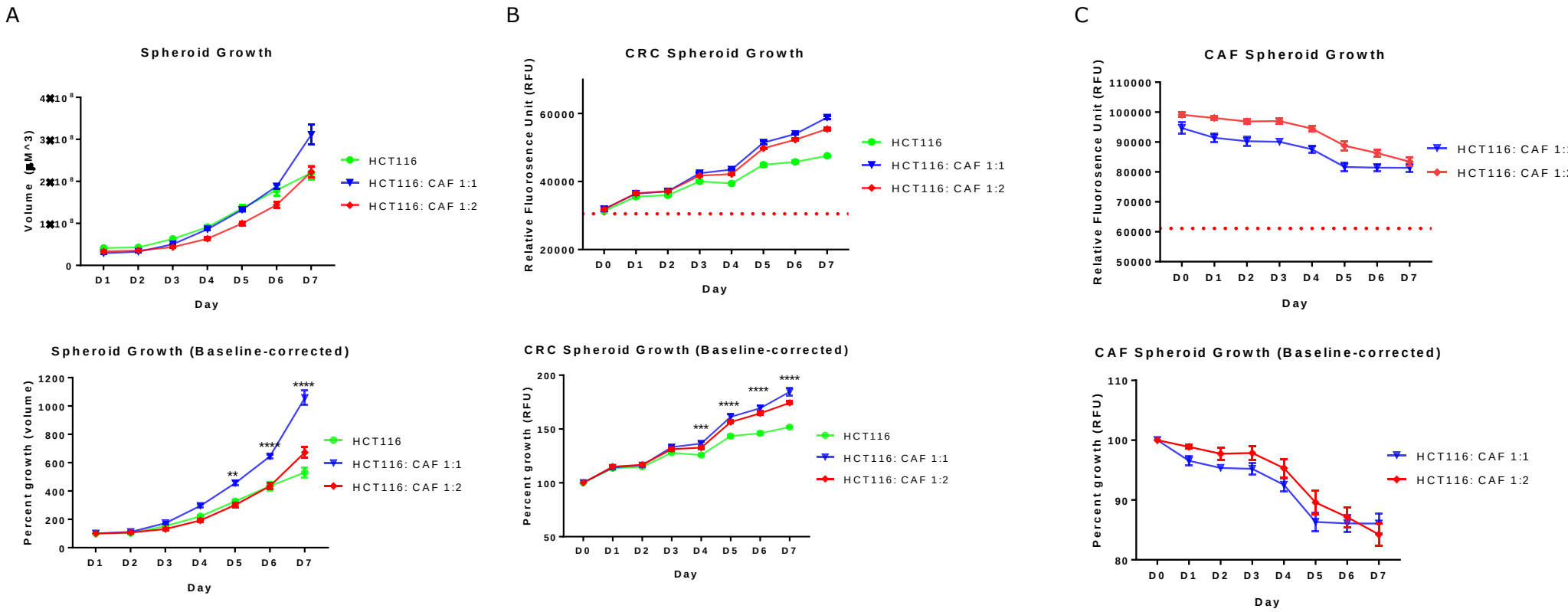


Figure 6.10. Growth of three-dimensional (3D) co-culture spheroid of colorectal cancer (CRC) cell line, HCT116, and cancer-associated fibroblast (CAF). The CRC cells, expressing Td-Tomato were seeded alone and with CAF, expressing GFP at 1:1 and 1:2 ratio at total number of 2000 cell/well on a 96-well black ultralow attachment plate (Corning, Cat: CLS4515). A. The brightfield images of the spheroid were used to calculate the mean spheroid radius by assuming an approximation to the area of the circle and from there inferred the volume of the spheroid, as an approximation to the volume of a sphere (above). The relative percent growth represents the normalised values with respect to the volume of spheroids measured at Day 1 after seeding (below). C. The Td-Tomato fluorescence signal was measured (above) to represent the growth of the CRC cells and normalised to the value obtained on the day of seeding (D0) as the relative percent growth (below). D. The GFP fluorescence signal was measured (above) to represent the growth of the CAF cells and normalised to the value obtained on the day of seeding (D0) as the relative percent growth (below). Graphs are representative of 6 replicates per condition results shown are representative of 2 independent experiments. Red dot line represents the relative fluorescence unit (RFU) for the culture media as the background reading. **, P ≤ 0.01; ***, P ≤ 0.001 and ****, P ≤ 0.0001 based on Two-Way ANOVA test performed on GraphPad Prism v.7.03.

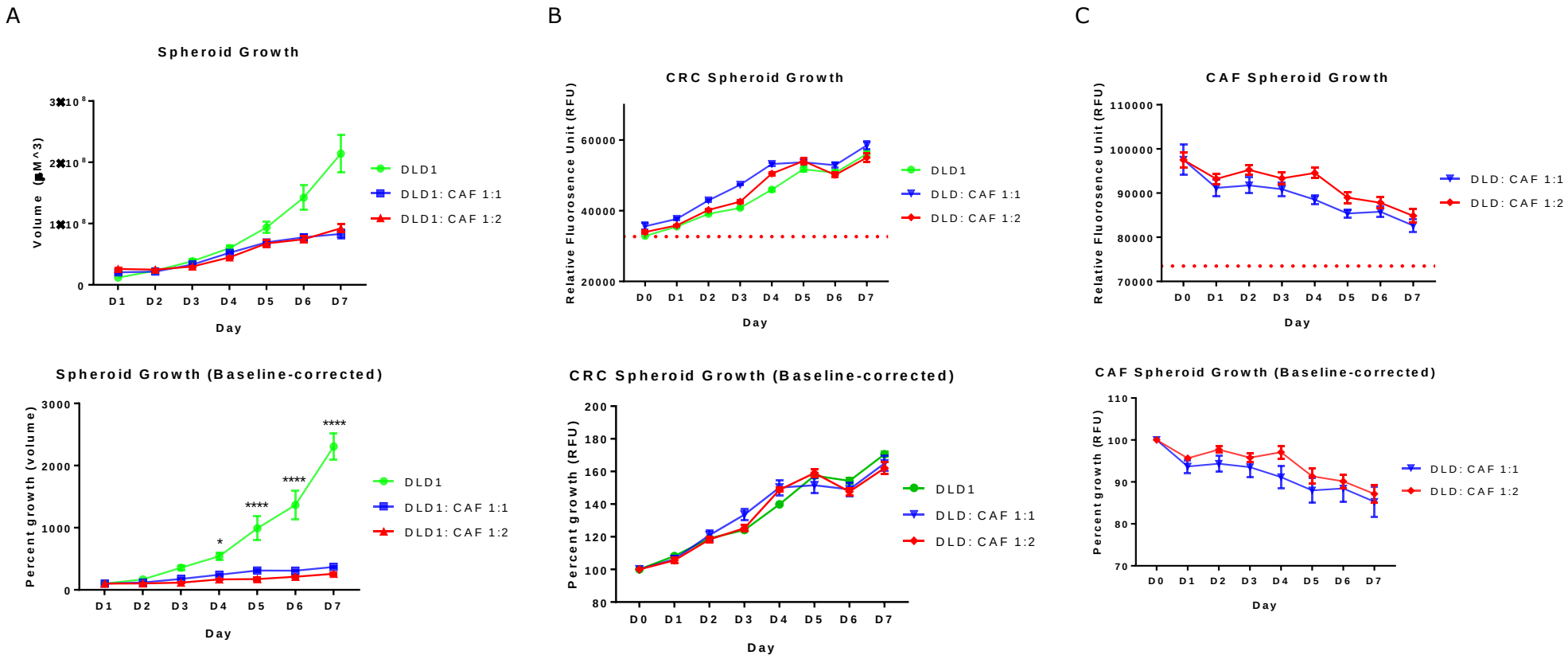


Figure 6.11. Growth of three-dimensional (3D) co-culture spheroid of colorectal cancer (CRC) cell line, DLD-1, and cancer-associated fibroblast (CAF). The CRC cells, expressing Td-Tomato were seeded alone and with CAF, expressing GFP at 1:1 and 1:2 ratio at total number of 2000 cell/well on a 96-well black ultralow attachment plate (Corning, Cat: CLS4515). A. The brightfield images of the spheroid were used to calculate the mean spheroid radius by assuming an approximation to the area of the circle and from there inferred the volume of the spheroid, as an approximation to the volume of a sphere (above). The relative percent growth represents the normalised values with respect to the volume of spheroids measured at Day 1 after seeding (below). B. The Td-Tomato fluorescence signal was measured (above) to represent the growth of the CRC cells and normalised to the value obtained on the day of seeding (D0) as the relative percent growth (below). C. The GFP fluorescence signal was measured (above) to represent the growth of the CAF cells and normalised to the value obtained on the day of seeding (D0) as the relative percent growth (below). Graphs are representative of 6 replicates per condition results shown are representative of 2 independent experiments. Red dot line represents the relative fluorescence unit (RFU) for the culture media as the background reading. *, $P \leq 0.05$; ****, $P \leq 0.0001$ based on Two-Way ANOVA test performed on GraphPad Prism v.7.03.

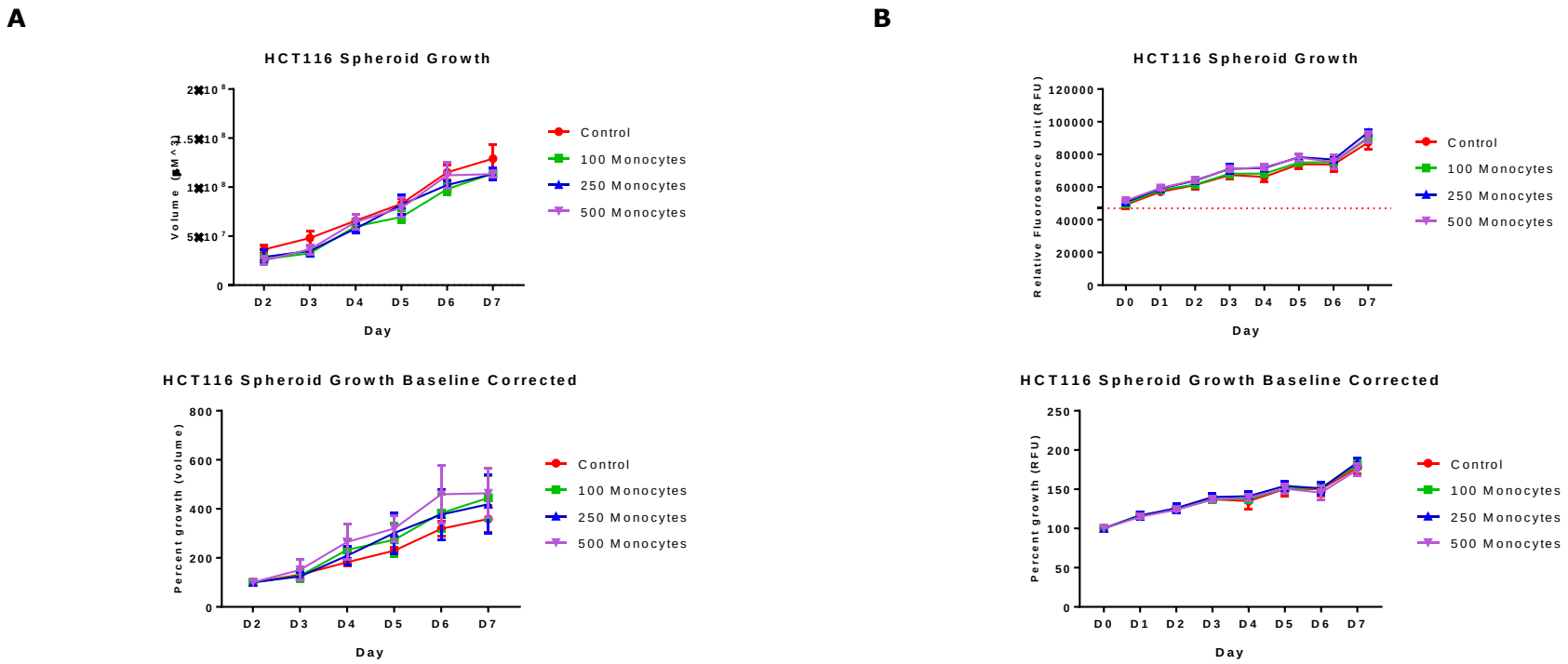


Figure 6.12. Growth of three-dimensional (3D) co-culture spheroid of colorectal cancer (CRC) cell line, HCT116, and cancer-associated fibroblast (CAF) in the present of monocytes. The CRC cells, expressing Td-Tomato were seeded alone and with CAF, expressing GFP at 1:1 ratio at total number of 2000 cells/well on a 96-well black ultralow attachment plate (Corning, Cat: CLS4515) without and with the present monocytes isolated from human buffy coat. A. The brightfield images of the spheroid were used to calculate the mean spheroid radius by assuming an approximation to the area of the circle and from there inferred the volume of the spheroid, as an approximation to the volume of a sphere (above). The relative percent growth represents the normalised values with respect to the volume of spheroids measured at Day 2 after seeding (below). B. The Td-Tomato fluorescence signal was measured (above) to represent the growth of the CRC cells and normalised to the value obtained on the day of seeding (D0) as the relative percent growth (below). Graphs are representative of 6 replicates per condition results shown are representative of 2 independent experiments. Red dot line represents the relative fluorescence unit (RFU) for the culture media as the background reading. No significance difference was observed between the experimental groups based on Two-Way ANOVA test performed on GraphPad Prism v.7.03

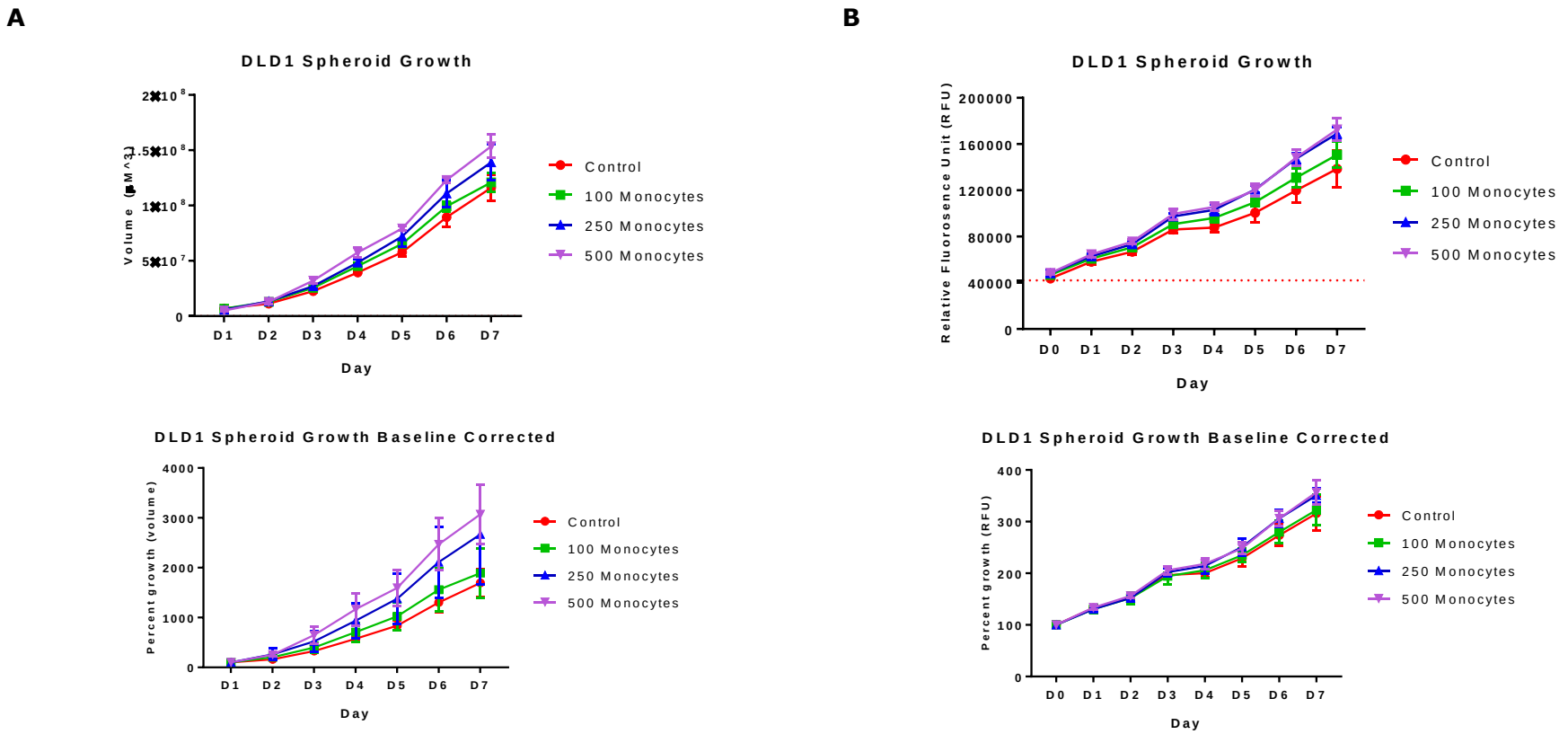


Figure 6.13. Growth of three-dimensional (3D) co-culture spheroid of colorectal cancer (CRC) cell line, DLD-1, and cancer-associated fibroblast (CAF) in the present of monocytes. The CRC cells, expressing Td-Tomato were seeded alone and with CAF, expressing GFP at 1:1 ratio at total number of 2000 cells/well on a 96-well black ultralow attachment plate (Corning, Cat: CLS4515) without and with the present monocytes isolated from human buffy coat. A. The brightfield images of the spheroid were used to calculate the mean spheroid radius by assuming an approximation to the area of the circle and from there inferred the volume of the spheroid, as an approximation to the volume of a sphere (above). The relative percent growth represents the normalised values with respect to the volume of spheroids measured at Day 2 after seeding (below). B. The Td-Tomato fluorescence signal was measured (above) to represent the growth of the CRC cells and normalised to the value obtained on the day of seeding (D0) as the relative percent growth (below). Graphs are representative of 6 replicates per condition results shown are representative of 2 independent experiments. Red dot line represents the relative fluorescence unit (RFU) for the culture media as the background reading. No significance difference was observed between the experimental groups based on Two-Way ANOVA test performed on GraphPad Prism v.7.03

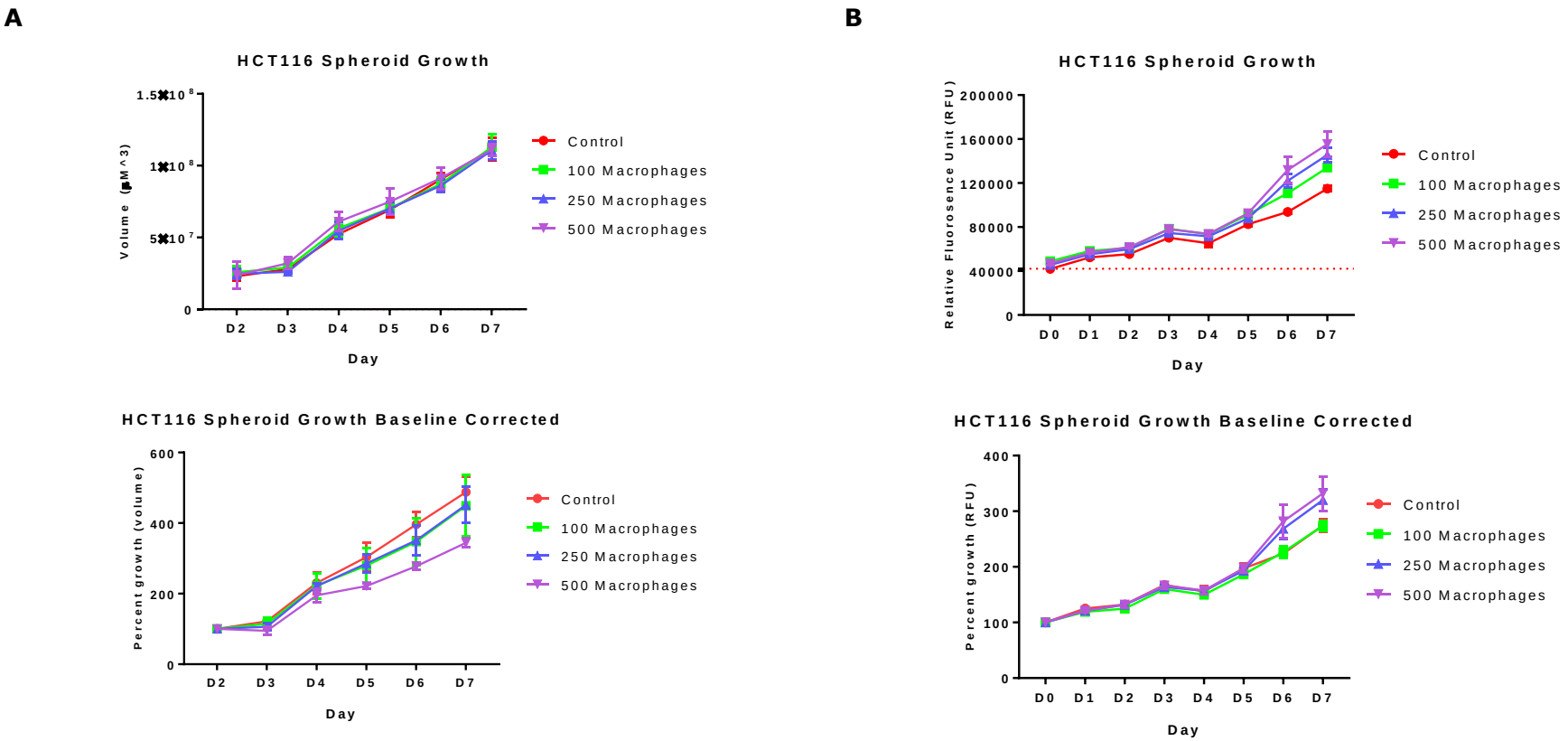


Figure 6.14. Growth of three-dimensional (3D) co-culture spheroid of colorectal cancer (CRC) cell line, HCT116, and cancer-associated fibroblast (CAF) in the present of macrophages. The CRC cells, expressing Td-Tomato were seeded alone and with CAF, expressing GFP at 1:1 ratio at total number of 2000 cells/well on a 96-well black ultralow attachment plate (Corning, Cat: CLS4515) without and with the present macrophages, differentiated from the monocytes isolated from human buffy coat. A. The brightfield images of the spheroid were used to calculate the mean spheroid radius by assuming an approximation to the area of the circle and from there inferred the volume of the spheroid, as an approximation to the volume of a sphere (above). The relative percent growth represents the normalised values with respect to the volume of spheroids measured at Day 2 after seeding (below). B. The Td-Tomato fluorescence signal was measured (above) to represent the growth of the CRC cells and normalised to the value obtained on the day of seeding (D0) as the relative percent growth (below). Graphs are representative of 6 replicates per condition results shown are representative of 2 independent experiments. Red dot line represents the relative fluorescence unit (RFU) for the culture media as the background reading. No significance difference was observed between the experimental groups based on Two-Way ANOVA test performed on GraphPad Prism v.7.03

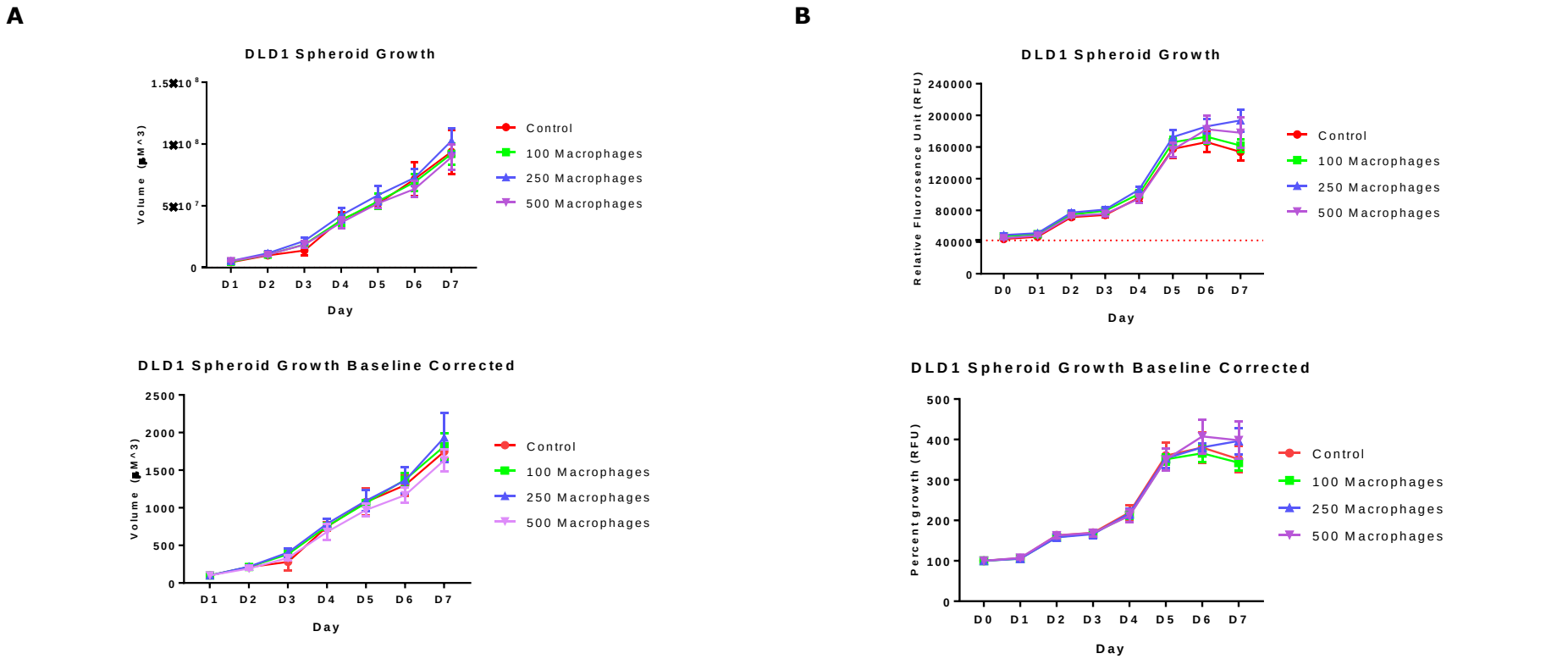


Figure 6.15. Growth of three-dimensional (3D) co-culture spheroid of colorectal cancer (CRC) cell line, DLD-1, and cancer-associated fibroblast (CAF) in the present of macrophages. The CRC cells, expressing Td-Tomato were seeded alone and with CAF, expressing GFP at 1:1 ratio at total number of 2000 cells/well on a 96-well black ultralow attachment plate (Corning, Cat: CLS4515) without and with the present macrophages, differentiated from the monocytes isolated from human buffy coat. A. The brightfield images of the spheroid were used to calculate the mean spheroid radius by assuming an approximation to the area of the circle and from there inferred the volume of the spheroid, as an approximation to the volume of a sphere (above). The relative percent growth represents the normalised values with respect to the volume of spheroids measured at Day 2 after seeding (below). B. The Td-Tomato fluorescence signal was measured (above) to represent the growth of the CRC cells and normalised to the value obtained on the day of seeding (D0) as the relative percent growth (below). Graphs are representative of 6 replicates per condition results shown are representative of 2 independent experiments. Red dot line represents the relative fluorescence unit (RFU) for the culture media as the background reading. No significance difference was observed between the experimental groups based on Two-Way ANOVA test performed on GraphPad Prism v.7.03

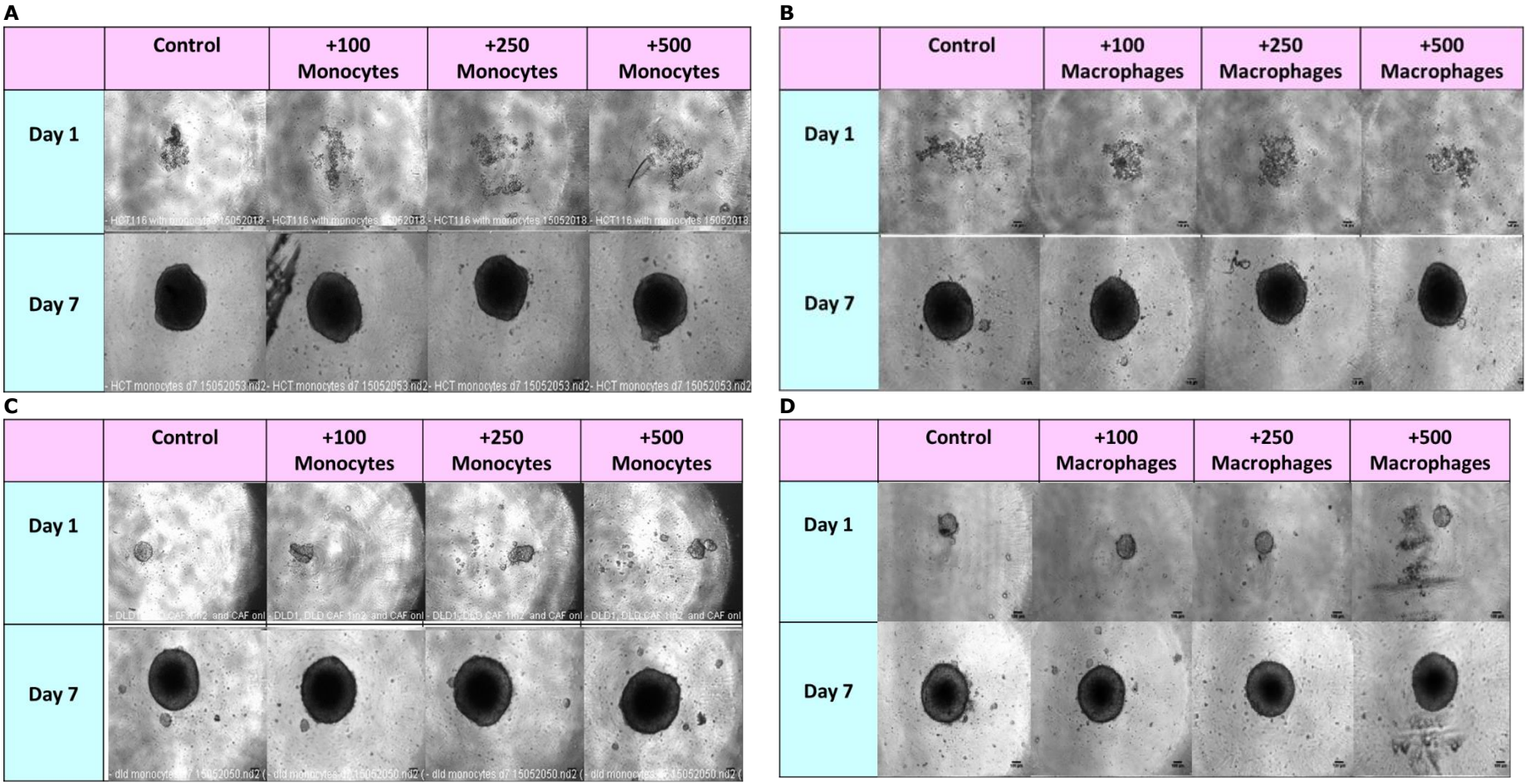


Figure 6.16.Live cell brightfield imaging of three-dimensional (3D) multicellular co-culture spheroid of colorectal cancer (CRC) cell line with cancer-associated fibroblast (CAF) and monocytic cells. HCT116 (A & B) and DLD-1 (C & D) were co-culture with CAF at 1:1 ratio at total number of 2000 cells/ well on a 96-well black ultralow attachment plate (Corning, Cat: CLS4515) with the present of different number of monocytes (A & C) and macrophages (B & D). The images were taken at 4x magnification using a widefield inverted microscope (Nikon TiE). No disruption of spheroid structure was observed when the monocytic cells were added into the co-culture of CRC-CAF.

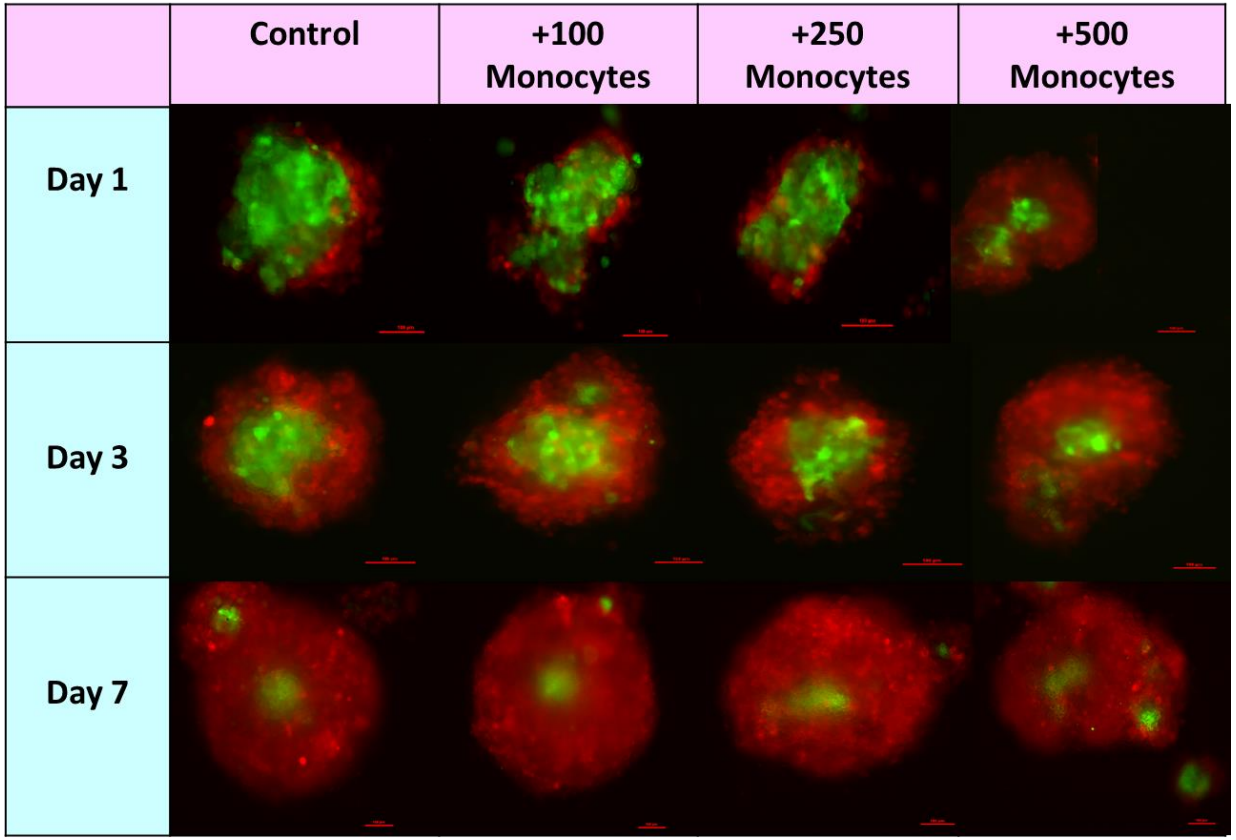


Figure 6.17. Live-cell fluorescence imaging of three-dimensional (3D) multicellular co-culture spheroid of colorectal cancer (CRC) cell line, HCT116, with cancer-associated fibroblast (CAF) and monocytes. The images were taken at 10x magnification using a widefield inverted microscope (Nikon TiE). DLD-1 was co-culture with CAF at 1:1 ratio at total number of 2000 cells/ well on a 96-well black ultralow attachment plate (Corning, Cat: CLS4515) with the present of different number of monocytes. The DLD-1 and CAF were transduced with tdTomato (red) and GFP (green), respectively. The scale bar indicates 100 μM. No disruption of spheroid structure was observed when the monocytes cells were added into the co-culture of CRC-CAF in which the CAF was found to congregate at the core area as the spheroids growing.

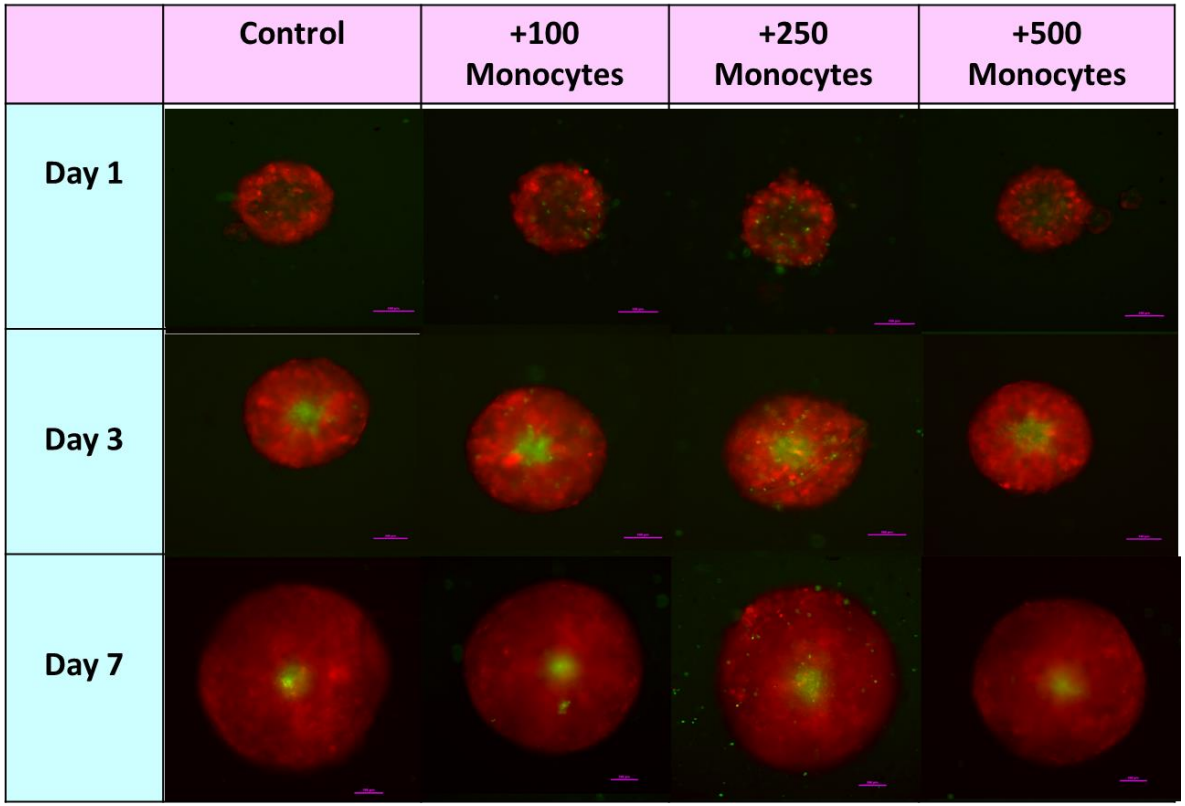


Figure 6.18. Live-cell fluorescence imaging of three-dimensional (3D) multicellular co-culture spheroid of colorectal cancer (CRC) cell line, DLD-1, with cancer-associated fibroblast (CAF) and monocytes. The images were taken at 10x magnification using a widefield inverted microscope (Nikon TiE). DLD-1 was co-culture with CAF at 1:1 ratio at total number of 2000 cells/ well on a 96-well black ultralow attachment plate (Corning, Cat: CLS4515) with the present of different number of monocytes. The DLD-1 and CAF were transduced with tdTomato (red) and GFP (green), respectively. The scale bar indicates 100 μM. No disruption of spheroid structure was observed when the monocytes cells were added into the co-culture of CRC-CAF in which the CAF was found to congregate at the core area as the spheroids growing.

Following the isolation from human buffy coat, some of the monocytes, maintained in M-CSF were cultured and differentiated into macrophages. After 7 days of culture, the macrophages were then subjected to the similar multicellular culture with CRC and CAF as described earlier for monocytes. As depicted in figure 6.14 and 6.15, there was no statistically significant difference on the growth kinetics of the co-culture of CRC, both HCT116 and DLD-1 with CAF, in the presence of different numbers of macrophages. Similarly, to previous experiments with monocytes, the growth of the spheroid was measured as total volume and Td-Tomato fluorescence signals representing specifically the proliferation of the CRC cells.

We gathered previously that HCT116 was the responder cell of CAF stimuli whereas DLD-1 was the non-responder. Nonetheless, the findings showed no effect of monocytes and macrophages on the growth on both CRC cell lines, HCT116 and DLD-1, with the presence of CAF. There is a possibility, however, that the co-culture model was not robust enough to capture the subtle effect of the monocytic cells on the CRC proliferation. No disruption of the spheroid formation was observed when the monocytic cells were added into the co-culture of CRC-CAF as shown on Figure 6.16. Furthermore, in the experiments with monocytes and macrophages, the proliferation of the CAF was not followed as it has been shown during the optimisation of the CRC-CAF co-culture model that CAF were assembled in the core of the spheroid and were not proliferating. As represented in Figure 6.17 and 6.18, the similar observation with CAF being aggregated within the core area of the spheroid was also seen on the multicellular culture of CRC (DLD-1) with addition of monocytes or macrophages.

6.2.4. Utilising the CRC- CAF 3D co-culture to study the role of CD24 in tumour growth

The 3D co-culture model developed in this project was used further to study the role of CD24 in cancer biology. Addition of stromal components ie. CAF will allow the heterotypic interaction to be studied in more simplistic manner compare to in vivo models that have several limitation including tissue accessibilities, biological parameters monitoring and selection of specific intercellular interactions (Cattin, et al, 2018). This part of the project focused on the use of the CAF co-culture model to study the role of CD24 in CRC proliferation. To this end stable lentiviral CD24 overexpression and FUGW control in HCT116 cells expressing GFP fluorescent protein were used, cultured in isolation or with CAFs in co-culture spheroids. Expression of fluorescent GFP was used to measure the growth of CRC cells within the spheroid. The HCT116 was used in this experiment because intrinsically, this cell line expresses low levels of CD24. The relative expression of CD24 protein following the lentivirus transduction is depicted in Figure 6.19. The western blot was carried out by another member of the group, Mr. Zaki Hakami.

As described in Figure 6.20, similar to the findings of previous experiments, there were significant differences in the total volume of the spheroids and the proliferation of the CRC, when the HCT116 was co-cultured with CAF in the normal FUGW control and overexpressed condition of CD24. Interestingly, the overexpression of CD24 resulted in significantly smaller spheroids as measured as total spheroid volume with and without CAF stimulation. However, CD24 overexpressed CRC showed significantly higher proliferation compared to the normal control as reflected by the fluorescence measurement. These results were observed consistently in two independent experiments

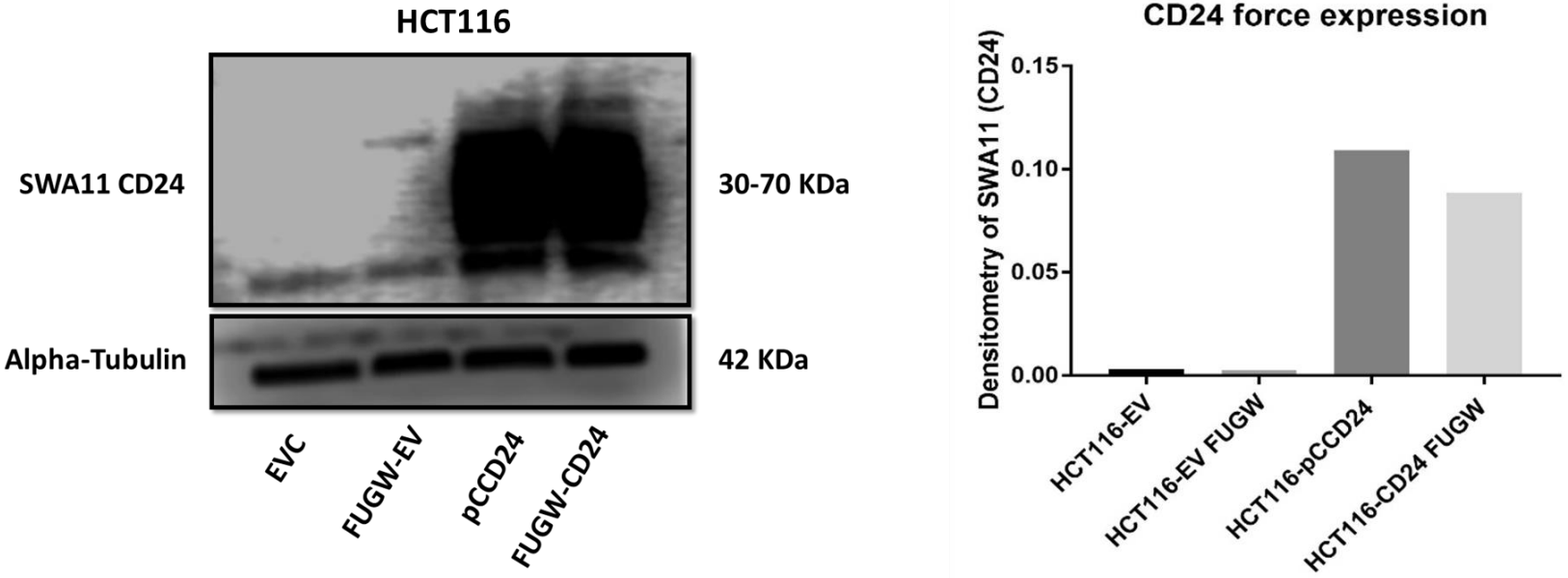


Figure 6.19. Expression of CD24 protein following the lentivirus transduction. Immunoblots are shown on the left, showing increased expression of CD24 on HCT116 cell stably transduced with FUGW insert plasmid (FUGW-CD24), comparable to the transient transfection (pCCD24). Molecular weight markers are indicated in kilo Daltons (kDa). The graphs on the right show relative CD24 levels calculated by densitometric analysis of the immunoreactive bands normalised against the EV (empty vector) control and adjusted against β actin loading control. The western blot was carried out by another member of the lab, Mr. Zaki Hakami.

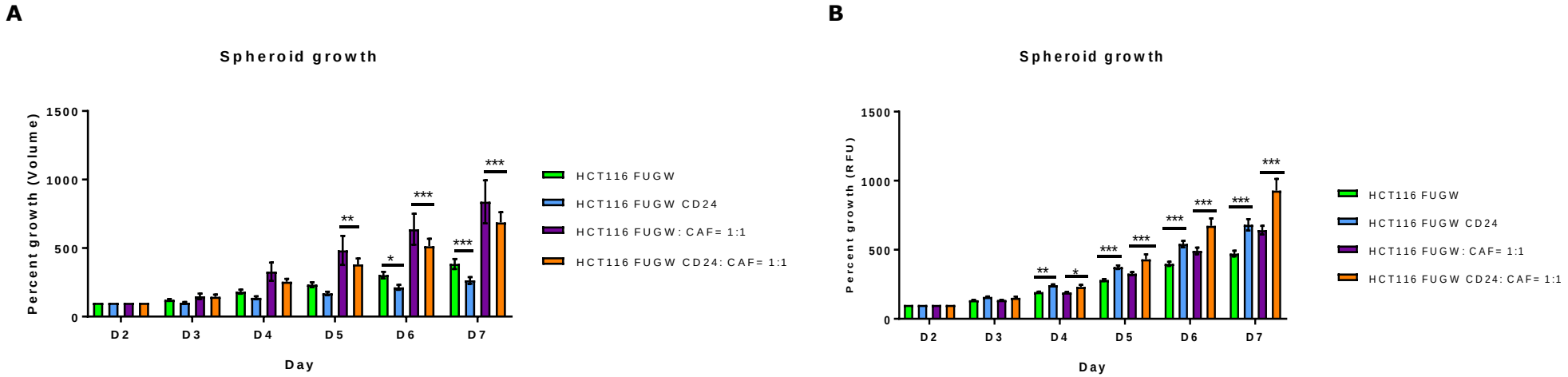


Figure 6.20. The role of CD24 on the growth of spheroids of CRC cell line, HCT116 with and without cancer-associated fibroblast (CAF). The CRC cells were stably transduced by lentivirus with FUGW plasmid (control) and CD24 gene overexpression. The HCT116, expressing GFP, were seeded alone and with CAF at 1:1 ratio at total number of 2000 cells/well on a 96-well black ultralow attachment plate (Corning, Cat: CLS4515). A. The brightfield images of the spheroid were used to calculate the mean spheroid radius by assuming an approximation to the area of the circle and from there inferred the volume of the spheroid, as an approximation to the volume of a sphere. The relative percent growth represents the normalised values with respect to the volume of spheroids measured at Day 2 after seeding. B. The GFP fluorescence signal was measured to represent the growth of the CRC cells and normalised to the value obtained on the day of seeding (D0) as the relative percent growth. Graphs are representative of 6 replicates per condition results shown are representative of 2 independent experiments. *, $P \leq 0.05$; **, $P \leq 0.01$; ***, $P \leq 0.001$ based on Two-Way ANOVA test performed on GraphPad Prism v.7.03. The volumes and the fluorescence data show opposite effects.

6.3. Discussion

This chapter described the efforts to develop a 3D co-culture model that better represents the tumour microenvironment as a means to investigate cancer development. The 3D culture was established using low attachment surface that allows the seeded cells to form spheroid-shaped aggregates. The growth kinetics of the spheroids were followed as total volume measurements, based on brightfield images, and fluorescence, based on the expression of Td-tomato or GFP by the stably transduced cells.

The initial experiments involved the seeding of different numbers of CRC cells on the 96-well low attachment plates. We found that some CRC cell lines, such as HCT116 and DLD-1, form compact ball-shaped aggregates (Figure 6.2-6.3) while others, such as SW480, SW620 and LS1034 form looser or even irregularly shaped aggregates (Figure 6.1). Thus, for further experiments HCT116 and DLD-1 were used to facilitate the volumetric measurement of the spheroid growth assuming ball-shaped structures. This was done in addition to the monitoring of the proliferation of CRC cells through fluorescence quantification. By comparing the volumetric and fluorescence measurements, it has been demonstrated that there were no differences in CRC proliferation rate between different seeding densities, yet the higher seeding numbers resulted in bigger spheroids with reduced growth in the spheroid size suggesting more compactness in higher density spheroids.

Various studies have described the stages of spheroid development. At the earliest stages, spheroids consist of proliferating cancer cells, followed by an intermediate stage when the proliferating cells form an outer layer and there is an inner core that consists of live cells that are not actively dividing, which referred to as “quiescent.” At later stages, the inner core of the spheroid will

become necrotic and will be surrounded by a shell of quiescent cells, and an outermost layer of live, proliferating cells (Wallace and Guo, 2013; Horman, et al, 2017). The necrotic core has been implicated as the main factor for the cessation of the spheroid growth, mainly due to the lack of access to oxygen and nutrients such as glucose (Daster, et al, 2016; Barisma, et al, 2018). The size of the spheroid is correlated with the size of the necrotic core (Freyer, 1988). However, as it was observed that spheroids at different seeding numbers has similar growth rate based on the fluorescence signals, it is unlikely that necrosis of the centre is the cause of the observation on the slower volume growth of the spheroids at the higher seeding number. It is possible that levels of contact-inhibition between cell are affected by the cell density.

Within the CRC stromal communities, CAFs are the most abundant cells and the number of α-SMA (smooth muscle action) and or FAP (fibroblast-associated protein) positive CAFs and its' gene signatures have been reported to be associated with poor prognosis, chemoresistance and angiogenesis (Tsujino, et al, 2007; Wikberk, et al, 2013; Berdiel-acel, et al, 2015; Calon, et al, 2015; Guinney et al., 2015; Dunne, et al, 2015; Hu, et al, 2015). A study by Horman et al. (2017) reported that the interaction between the CRC cell line HCT116 with normal human colon fibroblast cells CCD-18Co at 1:1000 fibroblast-CRC cell ratio, was enough to initiate the differentiation of the normal fibroblast cell line into a CAF-like phenotype, determined by distinct gene signatures that was similar to canonical patients' CAFs signature (including TGF-β, CCL2 and FAP), in 3D but not 2D co-cultures.

A similar result was also observed using another CRC cell line, HT-29. The HCT116 cell line harbour *KRAS* pG13D and *PIK3CA* p.H1047R mutation while HT-29 is a mutant for *BRAF* V600E and *TP53* p.R273H. Thus, the study suggested the cancer cell induced- CAF signature was not exclusively *KRAS*-driven. Instead, activation of the classical WNT signalling, COL3A1 and OGR1

were reported to be responsible for the changes in fibroblast phenotype when in contact with the CRC cells.

Our findings suggest that although CAFs were quiescent within the co-culture, its presence enhanced the growth of HCT116 spheroids as measured by the total volume and the cancer cell proliferation as measured by the fluorescence read-out. Interestingly, it was found that DLD-1, another CRC cell line that harbour *KRAS* p.G13D (similar to HCT116), *PIK3CA* p.E545K and p.D549N and *TP53* p.S241F mutations, did not respond to CAF stimulation. Although both cell lines are categorised as MSI, it has been suggested that HCT116 shows the signature of CMS-4 (Consensus Molecular Sub-type-4) whereas DLD-1 shows the signature of CMS-1 CRC. The CMS-4 tumour has been described as the subtype of CRC with enhanced EMT and TGF-β signature and the most prominent stromal infiltration, including fibroblast and inflammatory cells for instance monocytic cells, while CMS-1 is the immunogenic type with high lymphocyte infiltration. This CMS distinction may explain the distinct response of HCT116 and DLD-1 towards CAF stimulation.

We further used the CRC-CAF co-culture model at 1:1 ratio with total seeding number at 2000 cells/well to study the effect of monocytic cells on CRC proliferation. The monocytes and macrophages were derived and differentiated from healthy human blood and added at different cell numbers into the CRC-CAF co-culture mixture to form the multicellular spheroid culture. We found that adding the monocytes or macrophages into CRC-CAF co-culture did not alter the integrity of the spheroids; both HCT116 and DLD-1 co-cultures still formed tight and compact sphere-like structures. In this project, no significance effect was found of monocytes and macrophages on the proliferation of either HCT116 and DLD-1, the CAF responder and non-responder CRC cells, respectively.

It is less likely that undifferentiated monocytes would be found within the

tumour, nonetheless, the more differentiated form of the monocytic cells, which is the tumour-associated macrophage has been associated with both bad and good prognosis in CRC (Gulubova et al., 2013; Herrera, et al, 2013; Shabo et al., 2014; Marech et al., 2016; Mlecnik et al., 2016; Wei, et al, 2019). This may be due the wide polarizing spectrum of macrophages, with the anti-tumour, M1 and pro-tumour, M2 phenotypes at both opposite ends (Erreni et al., 2011; Mantovani, 2014; Komohara et al., 2016). In this project, M-CSF (macrophage colony-stimulating factor), also known as CSF-1, was used to stimulate the differentiation of monocytes to macrophages. M-CSF is an important chemoattractant and functional regulator of macrophages. High expression of CSF-1 has been associated with higher density of CD68+ macrophages within the CRC tumour and correlated with better patient outcome through the production of IL-8 (Wang, et al, 2016). This may explain the findings in which there was no enhancement of CRC proliferation in the multicellular culture with macrophages.

Further, it been reported previously that in CRC, fibroblast abundance correlates with myeloid cells abundance and CAF promoted the recruitment of monocytes by secreting IL-8 and up-regulating VCAM-1 expression and subsequently promote pro-tumoural M2 polarization of macrophages (Herrera, et al, 2013, Becht, et al, 2016; Zhang, et al, 2019). Thus, it would be expected that CRC co-culture with CAF and monocytes/ macrophages would induce cancer cell growth, especially on the CAF-responder, HCT116. Nonetheless, there is also a possibility that this co-culture model was not robust enough to capture any subtle changes.

Similarly, the CRC-CAF co-culture model was used to study the role of CD24 in CRC proliferation. This molecule has been a long interest of our research group. Some studies have shown that CD24 is an oncogene reported to be overexpressed in CRC. CD24 expression is associated with poor prognosis and

promotion of the tumour growth by enhancing metastasis and angiogenesis (Kristiansen, et al, 2004; Sagiv, et al, 2006; Lee, et al, 2009; Eyvazy, et al, 2018; Wang, et al, 2018). Our group was among the firsts to report that transient CD24 overexpression increased CRC cell, HCT116, migration, invasion, and colony formation but have no effect on cell proliferation. These findings were validated using transient knockdown of high CD24 expressor CRC cell, HT29 (Ahmed, et al, 2010). However, another study has shown that the treatment with anti-CD24 blocking mAb (monoclonal antibody), SWA11, in a time- and dose-dependent manner could inhibit the growth of HT29 and COLO-357 cells, high expressors of CD24, up to 90%, whereas the lower inhibition rate was observed on SW480 and PANC1 cells that have low expression of CD24 (Sagiv, et al, 2006). Different approaches in modulating the expression of CD24 in the two studies may contributes to the contradicting observation with regard to the role of CD24 in CRC cell proliferation. The possibility of SWA11 mAb in inducing other signalling pathways independent to CD24 should also be consider as feasible cause of the differential results. It has been reported that SWA11 mAb treatment resulted in changes in the intratumoural cytokine levels such as CXCL9 and CCL2, increased macrophage infiltration and reduced angiogenesis, in addition to its direct effect on direct effects on the CD24-positive tumour cells (validated by transduction of CD25 shRNA) (Salnikov, et al, 2013).

The concept of 3D spheres is based on the creation of spheroid structures in which cells form various layers and mimics the physical and biochemical features of a solid tumour mass as the result of the proper cell-cell and cell-environment interactions (Kapalczynska, et al, 2016). It has been shown by many studies that cell proliferation within the spheroid depends on cell location and is higher in the peripheral part of the 3D structures, with the hypoxic and necrotic area located within the core (Daster, et al, 2016; Barisma, et al, 2018).

It is not surprising that tumour cells are less sensitive to radiation and drugs in 3D than in 2D cultures due reduced access to the radiation and compounds in the medium, or by pathophysiological differences due to hypoxia, or by changes in the cell cycle, in which quiescent cells would be less sensitive (Griffith, et al, 2006; Cawkill, et al, 2007; Kapalczynska, et al, 2016). Thus, in this project, it is of interest to explore the effect of CD24 in CRC proliferation using the 3D co-culture model that arguably represent better the *in-vivo* condition of tumour.

We overexpressed the CD24 gene through lentivirus stable transduction of FUGW plasmid on HCT116 cell line, which is normally a low expressor of this surface molecule. The insertion of the FUGW plasmid allows the cells to also express the GFP fluorescence protein that can be detected by a plate reader at the at 488 nm excitation and 520 nm emission wavelength. This will provide an idea of cell proliferation. Compared to the FUGW-transduced HCT116 as controls, CD24 overexpressing cells showed higher rate of proliferation as measured by the GFP fluorescence read-out. Further, as known from the other experiments that HCT116 responded well to CAF stimulation, the CD24 overexpression in the CRC-CAF co-culture resulted in the highest proliferation of CRC cells among the experimental groups. These findings suggested that CD24 induced CRC proliferation and does not interfere with, or possibly enhances, the response of the CRC cells toward the CAF stimulus. This is a very interesting finding as previous studies in our laboratory showed no effect of CD24 in CRC proliferation using the 2D culture system. Furthermore, it was observed that with and without CAFs, overexpression of CD24 resulted in the smaller size and arguably more compact spheroids despite showing the higher proliferation, indicating that CD24 may play a role in modulating cell to cell adhesion, given the fact that CD24 is a cell-surface protein. Currently in CRC biology, CD24 is known as an alternative ligand for P-selectin, an adhesion receptor expressed on activated endothelial cells and platelets and could thus

enhance the metastatic potential of CD24-expressing tumour cells (Aigner, et al, 1997; Weichert, et al, 2005). Nonetheless, the role of CD24 in cell-to-cell interaction both within the cancer cells and between the cancer cells and CAFs warrants further investigation. Furthermore, as CD24 is heavily glycosylated it would be of interest to know if its sugars change depending on 3D vs 2D cultures and if the change, if any, effect CD24 interaction with P-selectin, a member of lectin family that binds to carbohydrates.

Altogether, a 3D co-culture model of CRC has been developed and demonstrated the utility of this model to study CRC biology. With the ability to incorporate different cellular components of the tumour microenvironment, such as the fibroblast and immune cells, the 3D models are potentially a better approach in the search for new biomarkers and new treatment strategies, leading us closer to the goal of personalized medicine.

7. Final Discussion

7.1. Introduction

The overall aim of this thesis is to investigate the interaction between cancer cells and non-cancerous cellular community within the TME (tumour microenvironment) of CRC (colorectal cancer). This was investigated by mapping the TME using IHC (immunohistochemistry) of several cellular biomarkers on serial sections of the FFPE (formalin-fixed paraffin-embedded) tissues, followed by novel digital image analysis called HMM (histogenic molecular mapping) to produce fm-IHC (faux multiplex IHC). The associations between the TME and important genetic markers were then investigated. The *in-vitro* 3D (three dimensional) multicellular spheroid model was then optimised and employed to study to role of some cellular components of TME, in particular CAF (cancer associated fibroblasts) and monocytic cells on CRC biology. In addition, the new panel of robust and low-cost molecular test for MSI (microsatellite instability) has also been validated. This study has made a number of novel observations regarding the genetic and TME biomarkers, the findings of which need to be consolidated and extended in the future.

7.2. Cardinal Findings

7.2.1. Simple and rapid molecular test to detect microsatellite instability (MSI)

Testing for the MSI has been arguably beneficial as prognostic marker to indicate the likelihood of better survival and as predictive marker for good response for immunotherapy and poor response to 5-FU. Currently, the MSI testing kit commercially offered by Promega (Madison, USA) utilises the fluorescence-based CE/ fragment length analysis (FLA) and includes five

quasi monomorphic mononucleotide markers, including NR-21, BAT-25, MONO-27, NR-24, BAT-26, and 2 pentanucleotide repeats, involving penta C and penta D as controls (Bacher, et al, 2004). However, this technique is expensive, laborious, and difficult to optimize (Deschoolmeester, et al, 2006). Moreover, the LOD of FLA for MSI detection can vary (from 1 to 10%) according to the length of the mutant alleles and the WT genotype, so that large deletions present a lower LOD than small deletions due to the presence of stutter peaks which mask mutant alleles (How-kit, et al, 2018). Thus, to date, in the clinical practice, the IHC for MMR protein is widely used as a surrogate method to determine the MSI. The IHC for MMR has been proven to be highly concordance with the MSI testing. This study also highlighted the high concordance (100%) between the IHC of MMR protein with the PCR-based MSI testing (Susanti, et al, 2018). Nonetheless, testing MSI by IHC has some caveat of false positivity on MSI-low subtype, in which only one microsatellite locus shows instability (Lindor, et al, 2002; Umar, et al, 2004; Babaei, et al, 2017).

Our research group are among the few that utilise the high-resolution melting analysis (HRMA), a relatively low-cost technology, for MSI detection on the FFPE tissues (Janavicius, et al, 2010; Fadhil, et al, 2012; Fadhil, et al, 2014). This PhD project has successfully curated a new panel of MSI markers that is robust and easy to implement in the clinical setting. Despite some attempt to simplify the MSI testing by using only one MSI marker (Babaei, et al, 2017; How-kit, et al, 2018), to anticipate the high polymorphism levels of microsatellite sequences in the different human populations and the errors induced by PCR slippage during amplification of microsatellite sequences, in this project, 5 MSI markers were included, although the data suggested that the MSI detection could be done with only

three or even 2 markers only.

7.2.2. Positive association of *PIK3CA* mutation with *KRAS* mutation but not *BRAF* mutation in colorectal cancer suggests co-selection is gene specific but not pathway specific

As shown in this project and also by others, *KRAS* and *BRAF* mutations are usually exclusive (Nicolantonio et al, 2008; De Roock, et al, 2010; Tie, et al, 2011). The concomitant mutations of *KRAS* and *BRAF* are rare as *BRAF* and *KRAS* both lie at the MAPK pathway thus co-mutation arguably offers no selective advantages for tumour carcinogenesis. A significant association of *KRAS* and *PIK3CA* mutation in several cancer types including CRC has been reported, suggesting the co-selection and synergy between the MAPK and PI3K signalling (Nosho, et al, 2008; De Roock, et al, 2010; Rosty, et al, 2013; Thariq & Ghias, 2016). In this study, the significant positive association between *KRAS* exon 2 mutation and *PIK3CA* exon 9 was confirmed

It is well established that *BRAF* mutation is predominantly associated with the MSI status, therefore, to gain the adequate power in the association test, it was necessary to enriched for the MSI tumour to get sufficient cases with *BRAF* mutation. We investigated the association between *BRAF* exon 15 (V600E) mutation with *PIK3CA* common mutation on both exon 9 and 20 in the MSI-enriched Nottingham and Edinburgh cohort of CRC. The negative association that was observed of *PIK3CA* mutation with *BRAF* mutation suggests that there is no generic co-selection of disrupted PI3K/AKT and MAPK pathways. Instead, it would seem that the *KRAS*/*PIK3CA* mutation co-

selection is due to gene-specific synergy.

Mutation in *KRAS*, *BRAF* and *PIK3CA*, have been linked with the low response to anti-EGFR treatments such as cetuximab and panitumumab (De Roock, et al, 2010), suggesting that oncogenic mutation in either MAPK or PI3K/AKT is sufficient in providing the escape mechanism for the EGFR signalling inhibition. Altogether, these and findings of this project support the rationale of combination therapy targeting both MAPK and PI3K/AKT pathways (Shimizu, et al, 2012).

7.2.3. Genetic features of colorectal cancer associate with distinct spatial tumour microenvironment landscape

In this project a novel approach called fm-IHC (faux-multiples immunohistochemistry) was employed to study the interaction between TME biomarkers in spatial manner on archived FFPE tissue. Utilising the emerging field of digital pathology, the fm-IHC applied precise image registration algorithm (developed by Dr. Alain Pitiot), named HMM (Histogenic Molecular Mapping).

The fm-IHC method described in this project offers an alternative to multiplex immunostaining. Recent advances in multiple immunolabeling and multispectral imaging have enabled simultaneous analysis of more than three markers within a single FFPE tissue section, with accurate cell discrimination and spatial information. However, maximising the number of markers presents multiple difficulties, including antibodies cross reactivity, spectral mixing and epitope degradation following subsequent wash, thus, so far, the optimal multiplex IF (immunofluorescence) protocol has just able to incorporate up to six markers simultaneously (Stack, et al, 2014). The

fm-IHC can be used to study as many as markers as possible as long as the sequential sections of the FPPE block used for the IHC still hold high similarity on the corresponding tissue landmarks. However, it is anticipated that the more sections being cut the much more difference between sections would be observed.

Immunoscore introduced by Galon, et al (2014) has set a momentum on the role of infiltrating T-lymphocytes as prognostic factor that is superior to the classical TNM pathological staging and independent to MSI status, although it is well reported that MSI tumour, due to the generation of neoantigens resulted from the frameshift mutations, are enriched with high immune cell intrusion and increased immune check point molecules, including PD-1 and PDL-1 (Schwitalle, et al, 2008; Angelove, et al, 2015; Liosa, et al, 2015; Mlecnik, et al, 2016; Becht, et al, 2016; Lal, et al, 2018; Pages, et al, 2018). In this study, although higher density of T- and B-cell lymphocytes, macrophages and other immune biomarkers were observed, the differences did not reach statistical significance, perhaps due to the small number of samples being analysed. However, few significant features that indicates active stage of TME of MSI tumour were found such as higher density of proliferating (Ki67+) CD3+ T-lymphocytes, that is similar to the report from another study (Mlecnik, et al, 2016) and low-apoptotic (BCL-2+) CD20+ B-lymphocytes within the stroma as well as high correlation of CD8+ cytotoxic T-lymphocytes with CD68+ macrophages in the epithelial.

Consensus molecular subtypes (CMS) of CRC is strongly associated with different immune and stromal contextures. Not surprisingly, the MSI-like group CMS1 which is enriched with *BRAF* mutation and associated with high immune infiltrate composed of Th1 and cytotoxic T cells, showing good

prognosis, similar to what been shown by the Immunoscore studies It is important to note, however, although showing the similar feature of higher lymphocytes infiltration, the mesenchymal-subtype CMS4, had the worst prognosis of the four subgroups. This subtype is also characterized by a high density of CAF and of cells of monocytic origin with prominent angiogenic and inflammatory signatures that arguably hampers the anti-tumour value of the Th1/CD8+ T cells (Galon, et al, 2014; Mlecnik, et al, 2016; Becht, et al, 2016).

We found more significant TME features within the *BRAF* mutant as compare to MSI. This includes higher density of CD3+ T-lymphocytes within the stroma and WTS (whole tissue section) of *BRAF* mutant and also higher density of CD20+ B-lymphocytes on the WTS of the mutant. In the stroma, more proliferating (Ki67+) CD3+ lymphocytes and CD163+ M2-macrophages and BCL2+ (low apoptotic) cellular community were also found, which includes CD3+ and CD8+ T-lymphocytes, CD20+ B-lymphocytes, CD163+ M2- macrophages and CD56+ NK cells. *BRAF* mutant also showed higher correlation between CD8+ cytotoxic T-cell with CD68+ macrophages and CD163+ M2-macrophages in the epithelial. Collectively, these findings suggest highly functional immune cellular community associated with *BRAF* mutation.

Several novel findings were observed in this study, including the significance of *TP53* mutation in inducing immune activation within the TME of CRC, indicated by higher intratumoural (epithelial) density of CD3+ T-lymphocytes, CD68+ macrophages, and CD56+ NK cells. There was also higher density of proliferating (Ki67+) NK cells within the stroma of *TP53* mutant tumour. Furthermore, further study would be essential to study the

mechanism and biological importance of distinctive TME feature of MACS (microsatellite and chromosomal stable) within the MSS tumour, showing higher density of CD56+ NK cells and proliferating (Ki67+) macrophages in the stroma. In this study as well as previous study from our group, there was no difference in driver genes mutation between MACS and CIN (chromosomal instable) tumour.

7.2.4. Three-dimensional (3D) co-culture model reveals differential response of CRC toward stimuli of CAF and the role of CD24 in modulating CRC proliferation

Cancer-associated fibroblasts (CAF) are highly abundant in CRC, recruited from local tissue-resident fibroblasts or pericryptal fibroblasts and distant fibroblast precursors and generally promoting the tumour growth and metastasis (Tommelein, et al, 2015). Utilising the three-dimensional (3D) spheroid co-culture model that arguably better mimic the in-vivo tumour arrangement, it is found that there was a differential CRC cells response toward CAF stimuli, showing HCT116 as CAF-responder and DLD-1 as non-responder.

Both cell lines are MSI and CIMP+ yet have different mutational profile on driver oncogenes. Both cell lines are *BRAF*-wild-type and harbour *KRAS* p.G13D mutation, but exhibit *PIK3CA* mutation on different sites, which are at p.H1047R for HCT116 and p.E545K and p.D549N for DLD-1. Multi-omics study has classified HCT116 and DLD-1 into CMS-4 and CMS-1 subtypes respectively (Ahmed, et al, 2013; Berg, et al, 2017). It is well reported that CMS1, called as MSI-like, represents the majority of MSI tumours with high hypermethylation status, frequent *BRAF* mutation, low level of somatic copy

number alteration (SCNA) and high immune cell (lymphocytes) infiltration. Whereas CMS4, called as mesenchymal type, exhibits more complex carcinogenesis with activation of TGF-β, EMT, angiogenesis, inflammation and stromal infiltration, including high density of CAF within the TME (Guinney, et al, 2015; Becht, et al, 2016). Partially, this may explain the findings that HCT116, which is considered as CMS-4 subtype, responded to the stimulation by CAF but not the DLD-1 which represent the CMS-1. Differential effect of CAF on HCT116 and DLD-1 was also observed in another study with similar 3D co-culture method, showing that the addition of fibroblasts at various ratios and EC increased the resistance to some drug combinations in SW620 and DLD1 cells, but not in HCT116 (Zoetemelk, et al, 2019).

Tumour-TME crosstalk regulates, either positively or negatively, cancer progression. While the TME of early-stage tumours confers anti-malignancy functions, some cancer cells can tolerate the suppression and, in turn, reprogram the TME into one exerting pro-malignancy functions (Maman & Witz, 2018). One of the examples of this is the initiation the normal fibroblast polarization into CAF-like phenotype by very small number of CRC cells in 3D co-culture (Horman, et al, 2017). Although there was no direct evidence whether CAF could induce somatic mutation and tumorigenesis, the pancreatic adenocarcinoma data demonstrated differential expression level of ACTA2 (α-SMA) among different *KRAS* status, suggesting that CAF in TME may play a role in selecting tumour cells with specified driver mutation (Wang, et al, 2018; Liu, et al, 2019)

The crosstalk between CAF and monocytic cells, especially the tumour associated macrophages (TAM) has been reported in supporting the CRC

growth by escaping the immune regulations and promoting metastasis and chemoresistance (Ireland & Mielgo, 2018). Using multi-omics analysis, Becht, et al (2016) showed that fibroblast abundance correlates with endothelial and myeloid cells abundance CRC and other cancers. Another study also showed CAFs can promote the recruitment of monocytes by secreting interleukin-8 (IL-8) and up-regulating VCAM-1 expression in colorectal cancer cells and subsequently promote pro-tumoural M2 polarization of macrophages, marked as CD206+ and CD163+ (Zhang, et al, 2019).

Nonetheless, in this project, utilising the spheroid multicellular co-culture model, no effect of CAF and monocytes or macrophages interactions on CRC growth was observed, both on HCT116 (CAF responding) and DLD-1 (CAF non-responding) cells. It is important to note that M-CSF was used in this project and the high expression of CSF-1 has been associated with higher density and co-localisation with the CD68+ macrophages within the CRC tumour and correlated with better patient outcome through the production of IL-8 (Wang, et al, 2016). Although, it may be speculated that CRC-CAF crosstalk may induce the differentiation of the monocytes toward M2-like phenotype/ TAM that support tumour growth, thus, there is also a possibility that the co-culture model, in particular with the addition of the un-differentiated monocytes, was not robust enough to capture any subtle changes on the CRC proliferation.

Spheroid culture in which cells form various layers and mimics the physical and biochemical features of a solid tumour mass as the result of the proper cell-cell and cell-environment interactions (Kapalczynska, et al, 2016; Young & Reed, 2016). Using the 3D spheroid model, this project abled to describe

the oncogenic effect of CD24 in inducing CRC growth, which previously was not observed in the conventional 2D culture (Ahmed, et al, 2010) and potentially modulate cell to cell adhesion reflecting in smaller yet more proliferative spheroids. Although not describe in this thesis, the 3D co-culture spheroid model also have been employed to study the role of another oncogene, named TNS4 (Tensin 4 or Cten) in CRC biology (Raposo, et al, 2020).

7.3. Future perspective

The work presented in this thesis has demonstrated that the cellular community in within the TME of CRC is non-random and is dictated by signals from the epithelium and reciprocally, the cellular community can influence tumour kinetics. However, this understanding would be enhanced with future studies.

The first part of this study has resulted in simple and robust molecular test to detect MSI which led to the development of Lynch Syndrome (LS) called N_LyST (Susanti, et al, 2018). Despite the benefit to inform the management of CRC, such as the use of 5-FU, the implementation of MSI testing (and LS screening) in clinical setting is still relatively limited.

The potential of this test to be translated into clinical practise is warrant further investigation. Validation in larger cohort of samples and ideally in multiple laboratories are required to assess if the test performance, as compare to the gold standard, is at suitable level of accuracy for diagnostic purpose and if the level of accuracy is routinely maintained. Furthermore, as HRMA is a relatively cheap and easy-to use method, thus suitable for implementation in resource limited setting such as in low- and middle-

income countries (LMIC), where cutting edge technology such as NGS may still be limited due to technology cost, the infrastructure and skills required. Thus, validation of this test using the clinical samples from these countries are critical to check if the test performance is impended when applied to people with different genetic background. In fact, further funding has been secured to validate this test in Indonesia.

Given that the MSI in also found to be a genetic phenomenon on other types of cancer, including gastric cancer, endometrium cancer, ovarian cancer, hepatobiliary tract cancer, urinary tract cancer, brain cancer, and skin cancers, it would be of interest to validate the novel panel of MSI markers and develop it further as a highly sensitive pan-cancer panel for MSI diagnosis. Further, the improvement of LOD, including the enrichment of mutant alleles, may enable the MSI detection to be performed by liquid biopsy. Although to date, MSI determination using NGS is often hampered by the errors induced during the sequencing-by-synthesis of homopolymers, the difficulties of alignment of repetitive DNA sequences due to the short read length, and the low accuracy of indel calling, the recent and future advancement of the NGS technology may provide more reliable approach in the field.

We have shown, using low throughput mutation detection methodology previously developed in the group called QMC (quick multiplex consensus)-PCR, the genetic alteration of the important driver genes in CRC are similar to the previously reported studies. The negative association of *BRAF* mutation with *PIK3CA* mutation as oppose to co-selection of *KRAS* and *PIK3CA* mutations, is critical to be explored further as this may have important clinical implication on the use of anti-EGFR therapy. Detailed

analysis on these genes and their interaction using NGS on larger cohort of CRC particularly with *BRAF* and *PIK3CA*- mutant enrichment, would provide an insight on the extent of the mutation interaction beyond the hotspots that were covered in this thesis. The association with clinicopathological, response to therapy and survival data is required to assess the clinical importance of the disrupted PI3K/AKT and MAPK pathways in CRC carcinogenesis. Genetic editing of the CRC cell using CRISPR-Cas9 and its derivatives can be useful to study the mechanistic effect of the targeted mutations on CRC biology including its interaction with TME components though 3D multicellular co-culture model. Similar approach could be applied to further study the co-occurrence of *BRAF* and *KRAS* mutation. Although considered to be rare, the co-existence of mutation on both genes has been *KRAS* has been reported on more severe and progressive diseases. Larger cohort with complete clinical data is required to amplify this observation. Single cell sequencing could be employed to examine the possibility of this occurrence arises from intra-tumoural heterogeneity of different clonal origins.

In this project, a novel digital pathology analysis platform called fm-IHC have been described to map the TME using conventional IHC staining of several cellular biomarkers on serial sections of the FFPE tissues. The non-linear image registration algorithm called HMM should be validated further on more series of cases, preferably covering different type of cancer, and then packaged into a stand-alone non-specialist user-friendly software. The automatic computation of spatial quantification of biomarker density and co-existence could be incorporated. The development of automatic segmentation of epithelial and stroma compartment may also be beneficial to speed up the analysis workflow.

Our findings showing that *BRAF* mutation and *TP53* could evoke significant immune activation within the TME of CRC should be validated in larger cohort of CRC as these may indicate that there could be other pathways involved in evoking the immunogenicity of CRC tumour in addition to well-described MSI-induced neoantigens. The biological mechanism of these finding can be addressed by CRISPR-Cas9 facilitation of gene editing to produce the cancer cells that harbour specifically *BRAF* and *TP53* mutation combined with multicellular co-culture system. Furthermore, although not the focus of this thesis, the association of the molecular and immune features with clinicopathological data is important to establish the clinical importance of the findings. Future analysis can be directed to study the TME map of less defined subset of CRC such as the MACS (microsatellite and chromosomal stable) group.

Utilising the 3D spheroid multicellular model, the differential response of different subtype of CRC toward CAF stimuli was revealed and the effect of the oncogene, CD24 on CRC proliferation was demonstrated. Nonetheless, there was possibility that the system was not sufficient to capture the effect of the monocytic cells on the growth of the cancer cells perhaps due to subtle changes. In this project, although the CAF and the monocytes were isolated as primary culture from human specimen, the CRC cell line was used instead of primary cancer cells isolated from patients' tumour. It would be of interest to established multicellular spheroid co-culture model that consists of fully primary cells. Future efforts can also focus on refining the model, for instance to use scaffolds or matrixes such as hydrogel, preferably using 3D printing approach, to enable the 3D culture of cell subtypes that not normally growth

as tight aggregate such as SW480 and SW620. The possibility to incorporates more cellular component into the co-culture, such as endothelial cells should be explored to closely mimic the biological complexity of the TME. The refinement of downstream application following the co-culture beyond the growth kinetics should be explored, including the IHC for different biomarkers, western blot for protein expression and qPCR or RNAseq for quantitative analysis of interest genes expression. These will allow in-depth analysis of the current findings such as differential expression between CAF-responding and non-responding tumour cells, crosstalk between CAF and monocytic cells and oncogenic downstream signalling of CD24. The expression profiling on co-culture would require some sort spheroid disintegration techniques and cell sorting, to study in details which cell population give rise to certain gene expression. Nonetheless, the spheroid disintegration followed by cell sorting could badly effect cell viability and damage the membrane protein of some important biomarkers, thus, further enhancement to navigate these issues is critical. Finally, it would be interesting to validate the findings using the cutting-edge techniques such as microfluid-based 3D models of cancer or known as organ-o-chip.

References

The Association of Methylation in the Promoter of APC and MGMT and the Prognosis of Taiwanese CRC Patients. (2009). Genetic Testing and Molecular Biomarkers, 13(1), 67-71. doi:10.1089/gtmb.2008.0045

Abumaree, M. H., Al Harthy, S., Al Subayyil, A. M., Alshabibi, M. A., Abomaray, F. M., Khatlani, T., . . . AlAskar, A. S. (2019). Decidua Basalis Mesenchymal Stem Cells Favor Inflammatory M1 Macrophage Differentiation In Vitro. Cells, 8(2), 173. doi:10.3390/cells8020173

Abumaree, M. H., Al Jumah, M. A., Kalionis, B., Jawdat, D., Al Khaldi, A., Abomaray, F. M., . . . Knawy, B. A. (2013). Human placental mesenchymal stem cells (pMSCs) play a role as immune suppressive cells by shifting macrophage differentiation from inflammatory M1 to anti-inflammatory M2 macrophages. Stem Cell Rev Rep, 9(5), 620-641. doi:10.1007/s12015-013-9455-2

Adami, H.-O., Bretthauer, M., Emilsson, L., Hernán, M. A., Kalager, M., Ludvigsson, J. F., & Ekbom, A. (2016). The continuing uncertainty about cancer risk in inflammatory bowel disease. Gut, 65(6), 889-893. doi:10.1136/gutjnl-2015-311003

Adegboyega, P. A., Mifflin, R. C., DiMari, J. F., Saada, J. I., & Powell, D. W. (2002). Immunohistochemical study of myofibroblasts in normal colonic mucosa, hyperplastic polyps, and adenomatous colorectal polyps. Arch Pathol Lab Med, 126(7), 829-836. doi:10.1043/0003-9985(2002)126<0829:Isomin>2.0.Co;2

Ahmed, M. A. H., Jackson, D., Seth, R., Robins, A., Lobo, D. N., Tomlinson, I. P. M., & Ilyas, M. (2010). CD24 is upregulated in inflammatory bowel disease and stimulates cell motility and colony formation. Inflammatory Bowel Diseases, 16(5), 795-803. doi:10.1002/ibd.21134

Aigner, S., Sthoeger, Z. M., Fogel, M., Weber, E., Zarn, J., Ruppert, M., . . . Altevogt, P. (1997). CD24, a mucin-type glycoprotein, is a ligand for P-selectin on human tumor cells. Blood, 89(9), 3385-3395.

Akkoca, A. N., Yanık, S., Ozdemir, Z. T., Cihan, F. G., Sayar, S., Cincin, T. G., . . . Ozer, C. (2014). TNM and Modified Dukes staging along with the demographic characteristics of patients with colorectal carcinoma. International journal of clinical and experimental medicine, 7(9), 2828-2835. Retrieved from https://pubmed.ncbi.nlm.nih.gov/25356145 https://www.ncbi.nlm.nih.gov/pmc/articles/PMC4211795/

Alexander, P. G., McMillan, D. C., & Park, J. H. (2020). The local inflammatory response in colorectal cancer – Type, location or density? A systematic review and meta-analysis. Cancer Treatment Reviews, 83, 101949. doi:https://doi.org/10.1016/j.ctrv.2019.101949

Amado, R. G., Wolf, M., Peeters, M., Van Cutsem, E., Siena, S., Freeman, D. J., . . . Chang, D. D. (2008). Wild-type *KRAS* is required for panitumumab efficacy in patients with metastatic colorectal cancer. J Clin Oncol, 26(10), 1626-1634. doi:10.1200/jco.2007.14.7116

American Joint Committee for Cancer Staging and End Results Reporting. (2017). Cancer Staging Manual. 8th edition. American Joint Committee. Chicago, USA.

Araujo, S. E. A., Bernardo, W. M., Habr-Gama, A., Kiss, D. R., & Cecconello, I. (2007). DNA Ploidy Status and Prognosis in Colorectal Cancer: A Meta-Analysis of Published Data. Diseases of the Colon & Rectum, 50(11), 1800-1810. doi:10.1007/s10350-007-9013-6

Arnold, M., Sierra, M. S., Laversanne, M., Soerjomataram, I., Jemal, A., & Bray, F. (2017). Global patterns and trends in colorectal cancer incidence and mortality. Gut, 66(4), 683-691. doi:10.1136/gutjnl-2015-310912

Arriba, M., Sánchez, R., Rueda, D., Gómez, L., García, J. L., Rodríguez, Y., . . . Perea, J. (2017). Toward a Molecular Classification of Synchronous Colorectal Cancer: Clinical and Molecular Characterization. Clinical Colorectal Cancer, 16(1), 31-37. doi:https://doi.org/10.1016/j.clcc.2016.07.014

Arthofer, W., Steiner, F. M., & Schlick-Steiner, B. C. (2011). Rapid and cost-effective screening of newly identified microsatellite loci by high-resolution melting analysis. Molecular Genetics and Genomics, 286(3), 225. doi:10.1007/s00438-011-0641-0

Asati, V., Mahapatra, D. K., & Bharti, S. K. (2016). PI3K/Akt/mTOR and Ras/Raf/MEK/ERK signaling pathways inhibitors as anticancer agents: Structural and pharmacological perspectives. European Journal of Medicinal Chemistry, 109, 314-341. doi:https://doi.org/10.1016/j.ejmech.2016.01.012

Astler, V. B., & Coller, F. A. (1954). The prognostic significance of direct extension of carcinoma of the colon and rectum. Annals of surgery, 139(6), 846-852. doi:10.1097/00000658-195406000-00015

Babaei, H., Zeinalian, M., Emami, M. H., Hashemzadeh, M., Farahani, N., & Salehi, R. (2017). Simplified microsatellite instability detection protocol provides equivalent sensitivity to robust detection strategies in Lynch syndrome patients. Cancer biology & medicine, 14(2), 142-150. doi:10.20892/j.issn.2095-3941.2016.0091

Bacher, J. W., Flanagan, L. A., Smalley, R. L., Nassif, N. A., Burgart, L. J., Halberg, R. B., . . . Thibodeau, S. N. (2004). Development of a fluorescent multiplex assay for detection of MSI-High tumors. Dis Markers, 20(4-5), 237-250. doi:10.1155/2004/136734

Baeten, C. I. M., Castermans, K., Hillen, H. F. P., & Griffioen, A. W. (2006). Proliferating Endothelial Cells and Leukocyte Infiltration as Prognostic Markers in Colorectal Cancer. Clinical Gastroenterology and Hepatology, 4(11), 1351-1357. doi:10.1016/j.cgh.2006.08.005

Bakhoum, S. F., & Cantley, L. C. (2018). The Multifaceted Role of Chromosomal Instability in Cancer and Its Microenvironment. Cell, 174(6), 1347-1360. doi:https://doi.org/10.1016/j.cell.2018.08.027

Banerjea, A., Hands, R. E., Powar, M. P., Bustin, S. A., & Dorudi, S. (2009). Microsatellite and chromosomal stable colorectal cancers demonstrate

poor immunogenicity and early disease recurrence. Colorectal Dis, 11(6), 601-608. doi:10.1111/j.1463-1318.2008.01639.x

Bankhead, P., Loughrey, M. B., Fernández, J. A., Dombrowski, Y., McArt, D. G., Dunne, P. D., . . . Hamilton, P. W. (2017). QuPath: Open source software for digital pathology image analysis. Sci Rep, 7(1), 16878. doi:10.1038/s41598-017-17204-5

Bardhan, K., & Liu, K. (2013). Epigenetics and colorectal cancer pathogenesis. Cancers, 5(2), 676-713. doi:10.3390/cancers5020676

Baudrin, L. G., Deleuze, J.-F., & How-Kit, A. (2018). Molecular and Computational Methods for the Detection of Microsatellite Instability in Cancer. Frontiers in Oncology, 8(621). doi:10.3389/fonc.2018.00621

Baumann, P., Cremers, N., Kroese, F., Orend, G., Chiquet-Ehrismann, R., Uede, T., . . . Sleeman, J. P. (2005). CD24 Expression Causes the Acquisition of Multiple Cellular Properties Associated with Tumor Growth and Metastasis. Cancer Research, 65(23), 10783. doi:10.1158/0008-5472.CAN-05-0619

Becht, E., de Reyniès, A., Giraldo, N. A., Pilati, C., Buttard, B., Lacroix, L., . . . Fridman, W. H. (2016). Immune and Stromal Classification of Colorectal Cancer Is Associated with Molecular Subtypes and Relevant for Precision Immunotherapy. Clin Cancer Res, 22(16), 4057-4066. doi:10.1158/1078-0432.Ccr-15-2879

Beeram, M., Patnaik, A., & Rowinsky, E. K. (2005). Raf: A Strategic Target for Therapeutic Development Against Cancer. Journal of Clinical Oncology, 23(27), 6771-6790. doi:10.1200/jco.2005.08.036

Behrens, J. (2005). The role of the Wnt signalling pathway in colorectal tumorigenesis. Biochemical Society Transactions, 33(4), 672-675. doi:10.1042/bst0330672

Bellizzi, A. M. (2015). Update on immunohistochemistry to identify colorectal tumours with deficient DNA mismatch repair function. Diagnostic Histopathology, 21(3), 122-130. doi:10.1016/j.mpdhp.2015.04.002

Berdiel-Acer, M., Sanz-Pamplona, R., Calon, A., Cuadras, D., Berenguer, A., Sanjuan, X., . . . Molleví, D. G. (2014). Differences between CAFs and their paired NCF from adjacent colonic mucosa reveal functional heterogeneity of CAFs, providing prognostic information. Molecular oncology, 8(7), 1290-1305. doi:10.1016/j.molonc.2014.04.006

Berretta, M., Alessandrini, L., De Divitiis, C., Nasti, G., Lleshi, A., Di Francia, R., . . . Canzonieri, V. (2017). Serum and tissue markers in colorectal cancer: State of art. Critical Reviews in Oncology/Hematology, 111, 103-116. doi:https://doi.org/10.1016/j.critrevonc.2017.01.007

Bertani, F. R., Mozetic, P., Fioramonti, M., Iuliani, M., Ribelli, G., Pantano, F., . . . Rainer, A. (2017). Classification of M1/M2-polarized human macrophages by label-free hyperspectral reflectance confocal microscopy and multivariate analysis. Sci Rep, 7(1), 8965. doi:10.1038/s41598-017-08121-8

Berthel, A., Zoernig, I., Valous, N. A., Kahlert, C., Klupp, F., Ulrich, A., . . . Halama, N. (2017). Detailed resolution analysis reveals spatial T cell

heterogeneity in the invasive margin of colorectal cancer liver metastases associated with improved survival. Oncoimmunology, 6(3), e1286436-e1286436. doi:10.1080/2162402X.2017.1286436

Beswick, E. J., Johnson, J. R., Saada, J. I., Humen, M., House, J., Dann, S., . . . Pinchuk, I. V. (2014). TLR4 activation enhances the PD-L1-mediated tolerogenic capacity of colonic CD90+ stromal cells. Journal of immunology (Baltimore, Md. : 1950), 193(5), 2218-2229. doi:10.4049/jimmunol.1203441

Bhalla, A., Zulfiqar, M., & Bluth, M. H. (2018). Molecular Diagnostics in Colorectal Carcinoma: Advances and Applications for 2018. Clinics in Laboratory Medicine, 38(2), 311-342. doi:https://doi.org/10.1016/j.cll.2018.02.008

Bindea, G., Mlecnik, B., Tosolini, M., Kirilovsky, A., Waldner, M., Obenauf, Anna C., . . . Galon, J. (2013). Spatiotemporal Dynamics of Intratumoral Immune Cells Reveal the Immune Landscape in Human Cancer. Immunity, 39(4), 782-795. doi:https://doi.org/10.1016/j.immuni.2013.10.003

Birk, J. W., Tadros, M., Moezardalan, K., Nadyarnykh, O., Forouhar, F., Anderson, J., & Campagnola, P. (2014). Second harmonic generation imaging distinguishes both high-grade dysplasia and cancer from normal colonic mucosa. Dig Dis Sci, 59(7), 1529-1534. doi:10.1007/s10620-014-3121-7

Biswas, S., Holyoake, D., & Maughan, T. S. (2016). Molecular Taxonomy and Tumourigenesis of Colorectal Cancer. Clinical Oncology, 28(2), 73-82. doi:https://doi.org/10.1016/j.clon.2015.11.001

Bläker, H., Alwers, E., Arnold, A., Herpel, E., Tagscherer, K. E., Roth, W., . . . Hoffmeister, M. (2019). The Association Between Mutations in *BRAF* and Colorectal Cancer-Specific Survival Depends on Microsatellite Status and Tumor Stage. Clin Gastroenterol Hepatol, 17(3), 455-462.e456. doi:10.1016/j.cgh.2018.04.015

Blazer, D. G., 3rd, Kishi, Y., Maru, D. M., Kopetz, S., Chun, Y. S., Overman, M. J., . . . Vauthey, J. N. (2008). Pathologic response to preoperative chemotherapy: a new outcome end point after resection of hepatic colorectal metastases. J Clin Oncol, 26(33), 5344-5351. doi:10.1200/jco.2008.17.5299

Bokemeyer, C., Kohne, C.-H., Ciardiello, F., Lenz, H.-J., Heinemann, V., Klinkhardt, U., . . . Tejpar, S. (2014). Treatment outcome according to tumor RAS mutation status in OPUS study patients with metastatic colorectal cancer (mCRC) randomized to FOLFOX4 with/without cetuximab. Journal of Clinical Oncology, 32(15_suppl), 3505-3505. doi:10.1200/jco.2014.32.15_suppl.3505

Boland, C. R., & Goel, A. (2010). Microsatellite instability in colorectal cancer. Gastroenterology, 138(6), 2073-2087.e2073. doi:10.1053/j.gastro.2009.12.064

Boland, C. R., Thibodeau, S. N., Hamilton, S. R., Sidransky, D., Eshleman, J. R., Burt, R. W., . . . Srivastava, S. (1998). A National Cancer Institute Workshop on Microsatellite Instability for Cancer Detection and Familial

Predisposition: Development of International Criteria for the Determination of Microsatellite Instability in Colorectal Cancer. Cancer Research, 58(22), 5248. Retrieved from http://cancerres.aacrjournals.org/content/58/22/5248.abstract

Bouchalova, P., Nenutil, R., Muller, P., Hrstka, R., Appleyard, M. V., Murray, K., . . . Coates, P. J. (2014). Mutant p53 accumulation in human breast cancer is not an intrinsic property or dependent on structural or functional disruption but is regulated by exogenous stress and receptor status. The Journal of pathology, 233(3), 238-246. doi:10.1002/path.4356

Boulay, J. L., Mild, G., Lowy, A., Reuter, J., Lagrange, M., Terracciano, L., . . . Rochlitz, C. (2002). SMAD4 is a predictive marker for 5-fluorouracil-based chemotherapy in patients with colorectal cancer. British Journal of Cancer, 87(6), 630-634. doi:10.1038/sj.bjc.6600511

Bouzourene, H., Hutter, P., Losi, L., Martin, P., & Benhattar, J. (2010). Selection of patients with germline MLH1 mutated Lynch syndrome by determination of MLH1 methylation and *BRAF* mutation. Fam Cancer, 9(2), 167-172. doi:10.1007/s10689-009-9302-4

Bramsen, J. B., Rasmussen, M. H., Ongen, H., Mattesen, T. B., Ørntoft, M.-B. W., Árnadóttir, S. S., . . . Andersen, C. L. (2017). Molecular-Subtype-Specific Biomarkers Improve Prediction of Prognosis in Colorectal Cancer. Cell Reports, 19(6), 1268-1280. doi:https://doi.org/10.1016/j.celrep.2017.04.045

Braster, R., Bögels, M., Beelen, R. H. J., & van Egmond, M. (2017). The delicate balance of macrophages in colorectal cancer; their role in tumour development and therapeutic potential. Immunobiology, 222(1), 21-30. doi:https://doi.org/10.1016/j.imbio.2015.08.011

Bray, F., Ferlay, J., Soerjomataram, I., Siegel, R. L., Torre, L. A., & Jemal, A. (2018). Global cancer statistics 2018: GLOBOCAN estimates of incidence and mortality worldwide for 36 cancers in 185 countries. CA: A Cancer Journal for Clinicians, 68(6), 394-424. doi:10.3322/caac.21492

Brennen, W. N., Denmeade, S. R., & Isaacs, J. T. (2013). Mesenchymal stem cells as a vector for the inflammatory prostate microenvironment. 20(5), R269. doi:10.1530/erc-13-0151

Brennen, W. N., Isaacs, J. T., & Denmeade, S. R. (2012). Rationale behind targeting fibroblast activation protein-expressing carcinoma-associated fibroblasts as a novel chemotherapeutic strategy. Molecular cancer therapeutics, 11(2), 257-266. doi:10.1158/1535-7163.MCT-11-0340

Brenner, H., Kloor, M., & Pox, C. P. (2014). Colorectal cancer. The Lancet, 383(9927), 1490-1502. doi:10.1016/S0140-6736(13)61649-9

Bröker, M. E. E., Lalmahomed, Z. S., Roest, H. P., van Huizen, N. A., Dekker, L. J. M., Calame, W., . . . Luider, T. M. (2013). Collagen Peptides in Urine: A New Promising Biomarker for the Detection of Colorectal Liver Metastases. PloS one, 8(8), e70918. doi:10.1371/journal.pone.0070918

Bronte, V., Brandau, S., Chen, S.-H., Colombo, M. P., Frey, A. B., Greten, T. F., . . . Gabrilovich, D. I. (2016). Recommendations for myeloid-derived suppressor cell nomenclature and characterization standards. Nature Communications, 7(1), 12150. doi:10.1038/ncomms12150

Bullock, M. D., Mellone, M., Pickard, K. M., Sayan, A. E., Mitter, R., Primrose, J. N., . . . Mirnezami, A. H. (2014). Molecular profiling of the invasive tumor microenvironment in a 3-dimensional model of colorectal cancer cells and ex vivo fibroblasts. Journal of visualized experiments : JoVE(86), 51475. doi:10.3791/51475

Calon, A., Lonardo, E., Berenguer-Llergo, A., Espinet, E., Hernando-Momblona, X., Iglesias, M., . . . Batlle, E. (2015). Stromal gene expression defines poor-prognosis subtypes in colorectal cancer. Nat Genet, 47(4), 320-329. doi:10.1038/ng.3225

Campbell, F. C., Loughrey, M. B., McClements, J., Deevi, R. K., Javadi, A., & Rainey, L. (2018). Mechanistic Insights into Colorectal Cancer Phenomics from Fundamental and Organotypic Model Studies. The American Journal of Pathology, 188(9), 1936-1948. doi:https://doi.org/10.1016/j.ajpath.2018.05.021

Cancer Research United Kingdom (2020), Colorectal cancer. www.cancerresearchuk.org/health-professional/cancer-statistics/statistics-by-cancer-type/bowel-cancer. Retrieved in May 2020

Cao, H., Xu, Z., Wang, J., Cigliano, A., Pilo, M. G., Ribback, S., . . . Chen, X. (2019). Functional role of SGK3 in PI3K/Pten driven liver tumor development. BMC cancer, 19(1), 343. doi:10.1186/s12885-019-5551-2

Cao, P., Liu, B., Du, F., Li, D., Wang, Y., Yan, X., . . . Li, Y. (2019). Scutellarin suppresses proliferation and promotes apoptosis in A549 lung adenocarcinoma cells via AKT/mTOR/4EBP1 and STAT3 pathways. Thoracic Cancer, 10(3), 492-500. doi:10.1111/1759-7714.12962

Cattin, S., Ramont, L., & Rüegg, C. (2018). Characterization and In Vivo Validation of a Three-Dimensional Multi-Cellular Culture Model to Study Heterotypic Interactions in Colorectal Cancer Cell Growth, Invasion and Metastasis. Frontiers in bioengineering and biotechnology, 6, 97. doi:10.3389/fbioe.2018.00097

Cawkill, D., & Eaglestone, S. S. (2007). Evolution of cell-based reagent provision. Drug Discov Today, 12(19-20), 820-825. doi:10.1016/j.drudis.2007.08.014

Cha, Y., Kim, K.-J., Han, S.-W., Rhee, Y. Y., Bae, J. M., Wen, X., . . . Kim, T.-Y. (2016). Adverse prognostic impact of the CpG island methylator phenotype in metastatic colorectal cancer. British Journal of Cancer, 115(2), 164-171. doi:10.1038/bjc.2016.176

Chang, D. T., Pai, R. K., Rybicki, L. A., Dimaio, M. A., Limaye, M., Jayachandran, P., . . . Pai, R. K. (2012). Clinicopathologic and molecular features of sporadic early-onset colorectal adenocarcinoma: an adenocarcinoma with frequent signet ring cell differentiation, rectal

and sigmoid involvement, and adverse morphologic features. Mod Pathol, 25(8), 1128-1139. doi:10.1038/modpathol.2012.61

Chen, S. P., Chiu, S. C., Wu, C. C., Lin, S. Z., Kang, J. C., Chen, Y. L., . . . Harn, H. J. (2009). The association of methylation in the promoter of APC and MGMT and the prognosis of Taiwanese CRC patients. Genet Test Mol Biomarkers, 13(1), 67-71. doi:10.1089/gtmb.2008.0045

Chen, T.-H., Chang, S.-W., Huang, C.-C., Wang, K.-L., Yeh, K.-T., Liu, C.-N., . . . Cheng, Y.-W. (2013). The prognostic significance of APC gene mutation and miR-21 expression in advanced-stage colorectal cancer. Colorectal Disease, 15(11), 1367-1374. doi:10.1111/codi.12318

Chen, Y., Yuan, R., Wu, X., He, X., Zeng, Y., Fan, X., . . . Wu, X. (2016). A Novel Immune Marker Model Predicts Oncological Outcomes of Patients with Colorectal Cancer. Annals of Surgical Oncology, 23(3), 826-832. doi:10.1245/s10434-015-4889-1

Chiaravalli, A. M., Furlan, D., Facco, C., Tibiletti, M. G., Dionigi, A., Casati, B., . . . Capella, C. (2001). Immunohistochemical pattern of hMSH2/hMLH1 in familial and sporadic colorectal, gastric, endometrial and ovarian carcinomas with instability in microsatellite sequences. Virchows Arch, 438(1), 39-48. doi:10.1007/s004280000325

Chin, Y. R., Yuan, X., Balk, S. P., & Toker, A. (2014). PTEN-deficient tumors depend on AKT2 for maintenance and survival. Cancer Discov, 4(8), 942-955. doi:10.1158/2159-8290.Cd-13-0873

Chinnadurai, R., Copland, I. B., Patel, S. R., & Galipeau, J. (2014). IDO-independent suppression of T cell effector function by IFN-γ-licensed human mesenchymal stromal cells. Journal of immunology (Baltimore, Md.: 1950), 192(4), 1491-1501. doi:10.4049/jimmunol.1301828

Cho, D. I., Kim, M. R., Jeong, H. Y., Jeong, H. C., Jeong, M. H., Yoon, S. H., . . . Ahn, Y. (2014). Mesenchymal stem cells reciprocally regulate the M1/M2 balance in mouse bone marrow-derived macrophages. Exp Mol Med, 46(1), e70. doi:10.1038/emm.2013.135

Chuah, S., & Chew, V. (2020). High-dimensional immune-profiling in cancer: implications for immunotherapy. Journal for Immunotherapy of Cancer, 8(1). doi:10.1136/jitc-2019-000363

Ciardiello, F., Lenz, H.-J., Kohne, C.-H., Heinemann, V., Tejpar, S., Melezinek, I., . . . Cutsem, E. V. (2014). Treatment outcome according to tumor RAS mutation status in CRYSTAL study patients with metastatic colorectal cancer (mCRC) randomized to FOLFIRI with/without cetuximab. Journal of Clinical Oncology, 32(15_suppl), 3506-3506. doi:10.1200/jco.2014.32.15_suppl.3506

Cima, I., Kong, S. L., Sengupta, D., Tan, I. B., Phyo, W. M., Lee, D., . . . Tan, M. H. (2016). Tumor-derived circulating endothelial cell clusters in colorectal cancer. Sci Transl Med, 8(345), 345ra389. doi:10.1126/scitranslmed.aad7369

Clevers, H. (2016). Modeling Development and Disease with Organoids. Cell, 165(7), 1586-1597. doi:10.1016/j.cell.2016.05.082

Colangelo, T., Polcaro, G., Muccillo, L., D'Agostino, G., Rosato, V., Ziccardi, P., . . . Colantuoni, V. (2017). Friend or foe?: The tumour microenvironment dilemma in colorectal cancer. Biochimica et Biophysica Acta (BBA) - Reviews on Cancer, 1867(1), 1-18. doi:https://doi.org/10.1016/j.bbcan.2016.11.001

Colotta, F., Allavena, P., Sica, A., Garlanda, C., & Mantovani, A. (2009). Cancer-related inflammation, the seventh hallmark of cancer: links to genetic instability. Carcinogenesis, 30(7), 1073-1081. doi:10.1093/carcin/bgp127

Conti, J., & Thomas, G. (2011). The role of tumour stroma in colorectal cancer invasion and metastasis. Cancers, 3(2), 2160-2168. doi:10.3390/cancers3022160

Correia, A. L., & Bissell, M. J. (2012). The tumor microenvironment is a dominant force in multidrug resistance. Drug Resistance Updates, 15(1), 39-49. doi:https://doi.org/10.1016/j.drup.2012.01.006

Cortés-Ciriano, I., Lee, S., Park, W.-Y., Kim, T.-M., & Park, P. J. (2017). A molecular portrait of microsatellite instability across multiple cancers. Nature Communications, 8.

Courau, T., Bonnereau, J., Chicoteau, J., Bottois, H., Remark, R., Assante Miranda, L., . . . Le Bourhis, L. (2019). Cocultures of human colorectal tumor spheroids with immune cells reveal the therapeutic potential of MICA/B and NKG2A targeting for cancer treatment. Journal for Immunotherapy of Cancer, 7(1), 74. doi:10.1186/s40425-019-0553-9

Cross, W., Kovac, M., Mustonen, V., Temko, D., Davis, H., Baker, A. M., . . . Tomlinson, I. P. M. (2018). The evolutionary landscape of colorectal tumorigenesis. Nat Ecol Evol, 2(10), 1661-1672. doi:10.1038/s41559-018-0642-z

Crotti, S., Piccoli, M., Rizzolio, F., Giordano, A., Nitti, D., & Agostini, M. (2017). Extracellular Matrix and Colorectal Cancer: How Surrounding Microenvironment Affects Cancer Cell Behavior? J Cell Physiol, 232(5), 967-975. doi:10.1002/jcp.25658

Cunningham, J. M., Christensen, E. R., Tester, D. J., Kim, C. Y., Roche, P. C., Burgart, L. J., & Thibodeau, S. N. (1998). Hypermethylation of the hMLH1 promoter in colon cancer with microsatellite instability. Cancer Res, 58(15), 3455-3460.

Cutsem, E. V., Lang, I., D'haens, G., Moiseyenko, V., Zaluski, J., Folprecht, G., . . . Rougier, P. (2008). *KRAS* status and efficacy in the first-line treatment of patients with metastatic colorectal cancer (mCRC) treated with FOLFIRI with or without cetuximab: The CRYSTAL experience. Journal of Clinical Oncology, 26(15_suppl), 2-2. doi:10.1200/jco.2008.26.15_suppl.2

Czabotar, P. E., Lessene, G., Strasser, A., & Adams, J. M. (2014). Control of apoptosis by the BCL-2 protein family: implications for physiology and therapy. Nat Rev Mol Cell Biol, 15(1), 49-63. doi:10.1038/nrm3722

Dallol, A., Buhmeida, A., Al-Ahwal, M. S., Al-Maghrabi, J., Bajouh, O., Al-Khayyat, S., . . . Abuzenadah, A. M. (2016). Clinical significance of

frequent somatic mutations detected by high-throughput targeted sequencing in archived colorectal cancer samples. Journal of translational medicine, 14(1), 118-118. doi:10.1186/s12967-016-0878-9

Das, M., & Law, S. (2018). Role of tumor microenvironment in cancer stem cell chemoresistance and recurrence. The International Journal of Biochemistry & Cell Biology, 103, 115-124. doi:https://doi.org/10.1016/j.biocel.2018.08.011

Däster, S., Amatruda, N., Calabrese, D., Ivanek, R., Turrini, E., Droeser, R. A., . . . Muraro, M. G. (2017). Induction of hypoxia and necrosis in multicellular tumor spheroids is associated with resistance to chemotherapy treatment. Oncotarget, 8(1), 1725-1736. doi:10.18632/oncotarget.13857

Day, F., Jorissen, R., Lipton, L., Mouradov, D., Sakthianandeswaren, A., Christie, M., . . . Sieber, O. (2013). *PIK3CA* and PTEN Gene and Exon Mutation-Specific Clinicopathologic and Molecular Associations in Colorectal Cancer. Clinical Cancer Research, 19, 3285 - 3296.

De Roock, W., Claes, B., Bernasconi, D., De Schutter, J., Biesmans, B., Fountzilas, G., . . . Tejpar, S. (2010). Effects of *KRAS*, *BRAF*, NRAS, and *PIK3CA* mutations on the efficacy of cetuximab plus chemotherapy in chemotherapy-refractory metastatic colorectal cancer: a retrospective consortium analysis. Lancet Oncol, 11(8), 753-762. doi:10.1016/s1470-2045(10)70130-3

De Roock, W., Piessevaux, H., De Schutter, J., Janssens, M., De Hertogh, G., Personeni, N., . . . Tejpar, S. (2008). *KRAS* wild-type state predicts survival and is associated to early radiological response in metastatic colorectal cancer treated with cetuximab. Ann Oncol, 19(3), 508-515. doi:10.1093/annonc/mdm496

de Visser, K. E., Eichten, A., & Coussens, L. M. (2006). Paradoxical roles of the immune system during cancer development. Nat Rev Cancer, 6(1), 24-37. doi:10.1038/nrc1782

Delektorskaya, V. V., & Kushlinskii, N. E. (2011). Clinical Significance of the Content of Biomolecular Markers in Invasive Front of Colon Carcinomas. Bulletin of Experimental Biology and Medicine, 150(3), 368-371. doi:10.1007/s10517-011-1144-z

Demirkan, G., Merritt, C., Hinerfeld, D., Ong, G., Sorg, K., Balasundaram, G., . . . Beechem, J. M. (2019). Spatially-resolved, multiplexed quantification of protein and mRNA distribution and abundance in colorectal cancer tumor microenvironment with multiple modalities of NanoString GeoMx Digital Spatial Profiler. Journal of Clinical Oncology, 37(15_suppl), e14218-e14218. doi:10.1200/JCO.2019.37.15_suppl.e14218

Deng, G., Bell, I., Crawley, S., Gum, J., Terdiman, J. P., Allen, B. A., . . . Kim, Y. S. (2004). *BRAF* Mutation Is Frequently Present in Sporadic Colorectal Cancer with Methylated hMLH1, But Not in Hereditary Nonpolyposis Colorectal Cancer. Clinical Cancer Research, 10(1), 191. doi:10.1158/1078-0432.CCR-1118-3

Des Guetz, G., Uzzan, B., Nicolas, P., Schischmanoff, O., & Morere, J. F. (2009). Microsatellite instability: a predictive marker in metastatic colorectal cancer? Target Oncol, 4(1), 57-62. doi:10.1007/s11523-008-0103-8

Deschoolmeester, V., Baay, M., Lardon, F., Pauwels, P., & Peeters, M. (2011). Immune Cells in Colorectal Cancer: Prognostic Relevance and Role of MSI. Cancer microenvironment : official journal of the International Cancer Microenvironment Society, 4(3), 377-392. doi:10.1007/s12307-011-0068-5

Deshwar, A., Margonis, G. A., Andreatos, N., Barbon, C., Wang, J., Buettner, S., . . . Weiss, M. J. (2018). Double *KRAS* and *BRAF* Mutations in Surgically Treated Colorectal Cancer Liver Metastases: An International, Multi-institutional Case Series. Anticancer Res, 38(5), 2891-2895. doi:10.21873/anticanres.12535

Di Bartolomeo, M., Pietrantonio, F., Perrone, F., Dotti, K. F., Lampis, A., Bertan, C., . . . on behalf of Italian Trials in Medical Oncology, G. (2014). Lack of *KRAS*, NRAS, *BRAF* and *TP53* mutations improves outcome of elderly metastatic colorectal cancer patients treated with cetuximab, oxaliplatin and UFT. Targeted Oncology, 9(2), 155-162. doi:10.1007/s11523-013-0283-8

Di Nicolantonio, F., Martini, M., Molinari, F., Sartore-Bianchi, A., Arena, S., Saletti, P., . . . Bardelli, A. (2008). Wild-type *BRAF* is required for response to panitumumab or cetuximab in metastatic colorectal cancer. J Clin Oncol, 26(35), 5705-5712. doi:10.1200/jco.2008.18.0786

Dienstmann, R., Vermeulen, L., Guinney, J., Kopetz, S., Tejpar, S., & Tabernero, J. (2017). Consensus molecular subtypes and the evolution of precision medicine in colorectal cancer. Nat Rev Cancer, 17(2), 79-92. doi:10.1038/nrc.2016.126

Diep, C. B., Thorstensen, L., Meling, G. I., Skovlund, E., Rognum, T. O., & Lothe, R. A. (2003). Genetic Tumor Markers With Prognostic Impact in Dukes' Stages B and C Colorectal Cancer Patients. Journal of Clinical Oncology, 21(5), 820-829. doi:10.1200/jco.2003.05.190

Dietmaier, W., & Hofstädter, F. (2001). Detection of microsatellite instability by real time PCR and hybridization probe melting point analysis. Lab Invest, 81(10), 1453-1456. doi:10.1038/labinvest.3780358

DiPiro, J.T.; Talbert, R.L.; Yee, G.C.; Matzke, G.R.; Wells, B.G.; LPosey, L.M. (2014). Pharmacotherapy: A Pathophysiologic Approach, 9th edition; McGraw-Hill: New York, USA,.

Direkze, N. C., Hodivala-Dilke, K., Jeffery, R., Hunt, T., Poulsom, R., Oukrif, D., . . . Wright, N. A. (2004). Bone marrow contribution to tumor-associated myofibroblasts and fibroblasts. Cancer Res, 64(23), 8492-8495. doi:10.1158/0008-5472.Can-04-1708

Distefano, G., Caruso, M., La Malfa, S., Gentile, A., & Wu, S.-B. (2012). High resolution melting analysis is a more sensitive and effective alternative to gel-based platforms in analysis of SSR--an example in citrus. PloS one, 7(8), e44202-e44202. doi:10.1371/journal.pone.0044202

Domingo, E., Camps, C., Kaisaki, P. J., Parsons, M. J., Mouradov, D., Pentony, M. M., . . . Tomlinson, I. (2018). Mutation burden and other molecular markers of prognosis in colorectal cancer treated with curative intent: results from the QUASAR 2 clinical trial and an Australian community-based series. The Lancet Gastroenterology & Hepatology, 3(9), 635-643. doi:10.1016/S2468-1253(18)30117-1

Domingo, E., Laiho, P., Ollikainen, M., Pinto, M., Wang, L., French, A. J., . . . Schwartz, S., Jr. (2004). *BRAF* screening as a low-cost effective strategy for simplifying HNPCC genetic testing. Journal of medical genetics, 41(9), 664-668. doi:10.1136/jmg.2004.020651

Driehuis, E., & Clevers, H. (2017). CRISPR/Cas 9 genome editing and its applications in organoids. Am J Physiol Gastrointest Liver Physiol, 312(3), G257-g265. doi:10.1152/ajpgi.00410.2016

Dudley, A. C. (2012). Tumor endothelial cells. Cold Spring Harbor perspectives in medicine, 2(3), a006536-a006536. doi:10.1101/cshperspect.a006536

Dukes, C. E. (1932). The classification of cancer of the rectum. The Journal of Pathology and Bacteriology, 35(3), 323-332. doi:10.1002/path.1700350303

Dunne, P. D., Alderdice, M., O'Reilly, P. G., Roddy, A. C., McCorry, A. M. B., Richman, S., . . . Lawler, M. (2017). Cancer-cell intrinsic gene expression signatures overcome intratumoural heterogeneity bias in colorectal cancer patient classification. Nature Communications, 8(1), 15657. doi:10.1038/ncomms15657

Dunne, P. D., McArt, D. G., Bradley, C. A., O'Reilly, P. G., Barrett, H. L., Cummins, R., . . . Van Schaeybroeck, S. (2016). Challenging the Cancer Molecular Stratification Dogma: Intratumoral Heterogeneity Undermines Consensus Molecular Subtypes and Potential Diagnostic Value in Colorectal Cancer. Clin Cancer Res, 22(16), 4095-4104. doi:10.1158/1078-0432.Ccr-16-0032

E, J., Yan, F., Kang, Z., Zhu, L., Xing, J., & Yu, E. (2018). CD8+CXCR5+ T cells in tumor-draining lymph nodes are highly activated and predict better prognosis in colorectal cancer. Human Immunology, 79(6), 446-452. doi:https://doi.org/10.1016/j.humimm.2018.03.003

Eaden, J. A., Abrams, K. R., & Mayberry, J. F. (2001). The risk of colorectal cancer in ulcerative colitis: a meta-analysis. Gut, 48(4), 526-535. doi:10.1136/gut.48.4.526

East, J. E., Saunders, B. P., & Jass, J. R. (2008). Sporadic and Syndromic Hyperplastic Polyps and Serrated Adenomas of the Colon: Classification, Molecular Genetics, Natural History, and Clinical Management. Gastroenterology Clinics of North America, 37(1), 25-46. doi:https://doi.org/10.1016/j.gtc.2007.12.014

Ebili, H. O., Hassall, J., Asiri, A., Ham-Karim, H., Fadhil, W., Agboola, A. J., & Ilyas, M. (2017). QMC-PCRx: a novel method for rapid mutation detection. Journal of clinical pathology, jclinpath-2016-204264. doi:10.1136/jclinpath-2016-204264

Edin, S., Kaprio, T., Hagström, J., Larsson, P., Mustonen, H., Böckelman, C., . . . Palmqvist, R. (2019). The Prognostic Importance of CD20+ B lymphocytes in Colorectal Cancer and the Relation to Other Immune Cell subsets. Scientific Reports, 9(1), 19997. doi:10.1038/s41598-019-56441-8

Edwards, B. K., Ward, E., Kohler, B. A., Eheman, C., Zauber, A. G., Anderson, R. N., . . . Ries, L. A. (2010). Annual report to the nation on the status of cancer, 1975-2006, featuring colorectal cancer trends and impact of interventions (risk factors, screening, and treatment) to reduce future rates. Cancer, 116(3), 544-573. doi:10.1002/cncr.24760

Elez, E., Schellens, J., van Geel, R., Bendell, J., Spreafico, A., Schuler, M., . . . Tabernero, J. (2015). LBA-08 Results of a phase 1b study of the selective *BRAF* V600 inhibitor encorafenib in combination with cetuximab alone or cetuximab + alpelisib for treatment of patients with advanced *BRAF*-mutant metastatic colorectal cancer. Annals of Oncology, 26, iv120. doi:10.1093/annonc/mdv262.08

Enfield, K. S. S., Martin, S. D., Marshall, E. A., Kung, S. H. Y., Gallagher, P., Milne, K., . . . Guillaud, M. (2019). Hyperspectral cell sociology reveals spatial tumor-immune cell interactions associated with lung cancer recurrence. Journal for Immunotherapy of Cancer, 7(1), 13. doi:10.1186/s40425-018-0488-6

Erreni, M., Mantovani, A., & Allavena, P. (2011). Tumor-associated Macrophages (TAM) and Inflammation in Colorectal Cancer. Cancer microenvironment : official journal of the International Cancer Microenvironment Society, 4(2), 141-154. doi:10.1007/s12307-010-0052-5

Eshleman, J. R., Lang, E. Z., Bowerfind, G. K., Parsons, R., Vogelstein, B., Willson, J. K., . . . Markowitz, S. D. (1995). Increased mutation rate at the hprt locus accompanies microsatellite instability in colon cancer. Oncogene, 10(1), 33-37.

Eshleman, J. R., & Markowitz, S. D. (1996). Mismatch repair defects in human carcinogenesis. Human Molecular Genetics, 5(Supplement_1), 1489-1494. doi:10.1093/hmg/5.Supplement_1.1489

Eyvazi, S., Kazemi, B., Dastmalchi, S., & Bandehpour, M. (2018). Involvement of CD24 in Multiple Cancer Related Pathways Makes It an Interesting New Target for Cancer Therapy. Curr Cancer Drug Targets, 18(4), 328-336. doi:10.2174/1570163814666170818125036

Fadhil, W., Ibrahem, S., Seth, R., AbuAli, G., Ragunath, K., Kaye, P., & Ilyas, M. (2012). The utility of diagnostic biopsy specimens for predictive molecular testing in colorectal cancer. Histopathology, 61(6), 1117-1124. doi:10.1111/j.1365-2559.2012.04321.x

Fadhil, W., Ibrahem, S., Seth, R., & Ilyas, M. (2010). Quick-multiplex-consensus (QMC)-PCR followed by high-resolution melting: a simple and robust method for mutation detection in formalin-fixed paraffin-embedded tissue. Journal of clinical pathology, 63(2), 134. doi:10.1136/jcp.2009.070508

Fadhil, W., Kindle, K., Jackson, D., Zaitoun, A., Lane, N., Robins, A., & Ilyas, M. (2014). DNA content analysis of colorectal cancer defines a distinct 'microsatellite and chromosome stable' group but does not predict response to radiotherapy. International journal of experimental pathology, 95(1), 16-23. doi:10.1111/iep.12070

Fan, H., Zhao, G., Liu, L., Liu, F., Gong, W., Liu, X., . . . Hou, Y. (2012). Pre-treatment with IL-1β enhances the efficacy of MSC transplantation in DSS-induced colitis. Cellular & Molecular Immunology, 9(6), 473-481. doi:10.1038/cmi.2012.40

Fang, X., Zheng, P., Tang, J., & Liu, Y. (2010). CD24: from A to Z. Cellular & Molecular Immunology, 7(2), 100-103. doi:10.1038/cmi.2009.119

Fariña Sarasqueta, A., Forte, G. I., Corver, W. E., de Miranda, N. F., Ruano, D., van Eijk, R., . . . Morreau, H. (2013). Integral analysis of p53 and its value as prognostic factor in sporadic colon cancer. BMC cancer, 13(1), 277. doi:10.1186/1471-2407-13-277

Fariña Sarasqueta, A., Zeestraten, E. C. M., van Wezel, T., van Lijnschoten, G., van Eijk, R., Dekker, J. W. T., . . . van den Brule, A. J. C. (2011). *PIK3CA* kinase domain mutation identifies a subgroup of stage III colon cancer patients with poor prognosis. Cellular Oncology, 34(6), 523-531. doi:10.1007/s13402-011-0054-4

Fearon, E. R., & Vogelstein, B. (1990). A genetic model for colorectal tumorigenesis. Cell, 61(5), 759-767. doi:https://doi.org/10.1016/0092-8674(90)90186-I

Fernández-Peralta, A. M., Daimiel, L., Nejda, N., Iglesias, D., Medina Arana, V., & González-Aguilera, J. J. (2010). Association of polymorphisms MTHFR C677T and A1298C with risk of colorectal cancer, genetic and epigenetic characteristic of tumors, and response to chemotherapy. International Journal of Colorectal Disease, 25(2), 141-151. doi:10.1007/s00384-009-0779-y

Fernández-Peralta, A. M., Nejda, N., Oliart, S., Medina, V., Azcoita, M. M., & González-Aguilera, J. J. (2005). Significance of mutations in TGFBR2 and BAX in neoplastic progression and patient outcome in sporadic colorectal tumors with high-frequency microsatellite instability. Cancer Genetics and Cytogenetics, 157(1), 18-24. doi:https://doi.org/10.1016/j.cancergencyto.2004.05.008

Fitzgerald, R. H., Jr. (1982). What is the Dukes' system for carcinoma of the rectum? Dis Colon Rectum, 25(5), 474-477. doi:10.1007/bf02553661

Flaherty, D. C., Lavotshkin, S., Jalas, J. R., Torisu-Itakura, H., Kirchoff, D. D., Sim, M. S., . . . Bilchik, A. J. (2016). Prognostic Utility of Immunoprofiling in Colon Cancer: Results from a Prospective, Multicenter Nodal Ultrastaging Trial. Journal of the American College of Surgeons, 223(1), 134-140. doi:https://doi.org/10.1016/j.jamcollsurg.2016.03.003

Fletcher, R., Wang, Y.-J., Schoen, R. E., Finn, O. J., Yu, J., & Zhang, L. (2018). Colorectal cancer prevention: Immune modulation taking the stage. Biochimica et Biophysica Acta (BBA) - Reviews on Cancer, 1869(2), 138-148. doi:https://doi.org/10.1016/j.bbcan.2017.12.002

Foell, D., Wittkowski, H., Vogl, T., & Roth, J. (2007). S100 proteins expressed in phagocytes: a novel group of damage-associated molecular pattern molecules. Journal of Leukocyte Biology, 81(1), 28-37. doi:10.1189/jlb.0306170

Foltran, L., De Maglio, G., Pella, N., Ermacora, P., Aprile, G., Masiero, E., . . . Fasola, G. (2015). Prognostic role of *KRAS*, NRAS, *BRAF* and *PIK3CA* mutations in advanced colorectal cancer. Future Oncol, 11(4), 629-640. doi:10.2217/fon.14.279

Font, A., Abad, A., Monzó, M., Sanchez, J. J., Guillot, M., Manzano, J. L., . . . Rosell, R. (2001). Prognostic value of K-ras mutations and allelic imbalance on chromosome 18q in patients with resected colorectal cancer. Dis Colon Rectum, 44(4), 549-557. doi:10.1007/bf02234328

Förster, I., Brockmann, M., Schildgen, O., & Schildgen, V. (2018). Microsatellite instability testing in colorectal cancer using the QiaXcel advanced platform. BMC cancer, 18(1), 484-484. doi:10.1186/s12885-018-4400-z

Franklin, R. A., Liao, W., Sarkar, A., Kim, M. V., Bivona, M. R., Liu, K., . . . Li, M. O. (2014). The cellular and molecular origin of tumor-associated macrophages. Science, 344(6186), 921. doi:10.1126/science.1252510

Frattini, M., Saletti, P., Romagnani, E., Martin, V., Molinari, F., Ghisletta, M., . . . Mazzucchelli, L. (2007). PTEN loss of expression predicts cetuximab efficacy in metastatic colorectal cancer patients. British Journal of Cancer, 97(8), 1139-1145. doi:10.1038/sj.bjc.6604009

Freeman, H.-J. (2008). Colorectal cancer risk in Crohn's disease. World journal of gastroenterology, 14(12), 1810-1811. doi:10.3748/wjg.14.1810

Freyer, J. P. (1988). Role of necrosis in regulating the growth saturation of multicellular spheroids. Cancer Res, 48(9), 2432-2439.

Fridman, W. H., Pagès, F., Sautès-Fridman, C., & Galon, J. (2012). The immune contexture in human tumours: impact on clinical outcome. Nat Rev Cancer, 12(4), 298-306. doi:10.1038/nrc3245

Friederichs, J., Zeller, Y., Hafezi-Moghadam, A., Gröne, H. J., Ley, K., & Altevogt, P. (2000). The CD24/P-selectin binding pathway initiates lung arrest of human A125 adenocarcinoma cells. Cancer Res, 60(23), 6714-6722.

Fu, J., Yang, J., Tan, Y., Jiang, M., Wen, F., Huang, Y., . . . Yuan, Y. (2014). Young patients (≤ 35 years old) with colorectal cancer have worse outcomes due to more advanced disease: a 30-year retrospective review. Medicine, 93(23), e135-e135. doi:10.1097/MD.0000000000000135

Gabrilovich, D. I., Bronte, V., Chen, S.-H., Colombo, M. P., Ochoa, A., Ostrand-Rosenberg, S., & Schreiber, H. (2007). The Terminology Issue for Myeloid-Derived Suppressor Cells. Cancer Research, 67(1), 425. doi:10.1158/0008-5472.CAN-06-3037

Gabrilovich, D. I., Ostrand-Rosenberg, S., & Bronte, V. (2012). Coordinated regulation of myeloid cells by tumours. Nature reviews. Immunology, 12(4), 253-268. doi:10.1038/nri3175

Galluzzi, L., Buqué, A., Kepp, O., Zitvogel, L., & Kroemer, G. (2017). Immunogenic cell death in cancer and infectious disease. Nature Reviews Immunology, 17(2), 97-111. doi:10.1038/nri.2016.107

Galon, J., Costes, A., Sanchez-Cabo, F., Kirilovsky, A., Mlecnik, B., Lagorce-Pagès, C., . . . Pagès, F. (2006). Type, density, and location of immune cells within human colorectal tumors predict clinical outcome. Science, 313(5795), 1960-1964. doi:10.1126/science.1129139

Galon, J., Mlecnik, B., Bindea, G., Angell, H. K., Berger, A., Lagorce, C., . . . Pagès, F. (2014). Towards the introduction of the 'Immunoscore' in the classification of malignant tumours. The Journal of pathology, 232(2), 199-209. doi:10.1002/path.4287

Gan, C., Love, C., Beshay, V., Macrae, F., Fox, S., Waring, P., & Taylor, G. (2015). Applicability of next generation sequencing technology in microsatellite instability testing. Genes (Basel), 6(1), 46-59. doi:10.3390/genes6010046

Ganopoulos, I., Tsaballa, A., Xanthopoulou, A., Madesis, P., & Tsaftaris, A. (2013). Sweet Cherry Cultivar Identification by High-Resolution-Melting (HRM) Analysis Using Gene-Based SNP Markers. Plant Molecular Biology Reporter, 31(3), 763-768. doi:10.1007/s11105-012-0538-z

Georgiades, I. B., Curtis, L. J., Morris, R. M., Bird, C. C., & Wyllie, A. H. (1999). Heterogeneity studies identify a subset of sporadic colorectal cancers without evidence for chromosomal or microsatellite instability. Oncogene, 18(56), 7933-7940. doi:10.1038/sj.onc.1203368

Germano, G., Amirouchene-Angelozzi, N., Rospo, G., & Bardelli, A. (2018). The Clinical Impact of the Genomic Landscape of Mismatch Repair-Deficient Cancers. Cancer Discov, 8(12), 1518-1528. doi:10.1158/2159-8290.Cd-18-0150

Giannakis, M., Mu, X. J., Shukla, S. A., Qian, Z. R., Cohen, O., Nishihara, R., . . . Garraway, L. A. (2016). Genomic Correlates of Immune-Cell Infiltrates in Colorectal Carcinoma. Cell Reports, 15(4), 857-865. doi:10.1016/j.celrep.2016.03.075

Giardiello, F. M., Allen, J. I., Axilbund, J. E., Boland, C. R., Burke, C. A., Burt, R. W., . . . Rex, D. K. (2014). Guidelines on genetic evaluation and management of Lynch syndrome: a consensus statement by the US Multi-Society Task Force on colorectal cancer. Gastroenterology, 147(2), 502-526. doi:10.1053/j.gastro.2014.04.001

Goel, A., Arnold, C. N., Niedzwiecki, D., Chang, D. K., Ricciardiello, L., Carethers, J. M., . . . Boland, C. R. (2003). Characterization of sporadic colon cancer by patterns of genomic instability. Cancer Res, 63(7), 1608-1614.

Goldstein, J., Tran, B., Ensor, J., Gibbs, P., Wong, H. L., Wong, S. F., . . . Overman, M. J. (2014). Multicenter retrospective analysis of metastatic

colorectal cancer (CRC) with high-level microsatellite instability (MSI-H). Ann Oncol, 25(5), 1032-1038. doi:10.1093/annonc/mdu100

Goldstein, N. S., & Armin, M. (2001). Epidermal growth factor receptor immunohistochemical reactivity in patients with American Joint Committee on Cancer Stage IV colon adenocarcinoma. Cancer, 92(5), 1331-1346. doi:10.1002/1097-0142(20010901)92:5<1331::Aid-cncr1455>3.0.Co;2-m

Gong, Y., Scott, E., Lu, R., Xu, Y., Oh, W. K., & Yu, Q. (2013). TIMP-1 promotes accumulation of cancer associated fibroblasts and cancer progression. PloS one, 8(10), e77366. doi:10.1371/journal.pone.0077366

Gonzalez, H., Hagerling, C., & Werb, Z. (2018). Roles of the immune system in cancer: from tumor initiation to metastatic progression. Genes & Development, 32(19-20), 1267-1284. doi:10.1101/gad.314617.118

Grady, W. M. (2004). Genomic instability and colon cancer. Cancer Metastasis Rev, 23(1-2), 11-27. doi:10.1023/a:1025861527711

Griffith, L. G., & Swartz, M. A. (2006). Capturing complex 3D tissue physiology in vitro. Nature Reviews Molecular Cell Biology, 7(3), 211-224. doi:10.1038/nrm1858

Grosse, S. D. (2015). When is Genomic Testing Cost-Effective? Testing for Lynch Syndrome in Patients with Newly-Diagnosed Colorectal Cancer and Their Relatives. Healthcare (Basel, Switzerland), 3(4), 860-878. doi:10.3390/healthcare3040860

Guastadisegni, C., Colafranceschi, M., Ottini, L., & Dogliotti, E. (2010). Microsatellite instability as a marker of prognosis and response to therapy: a meta-analysis of colorectal cancer survival data. Eur J Cancer, 46(15), 2788-2798. doi:10.1016/j.ejca.2010.05.009

Guda, K., Veigl, M. L., Varadan, V., Nosrati, A., Ravi, L., Lutterbaugh, J., . . . Willis, J. E. (2015). Novel recurrently mutated genes in African American colon cancers. Proceedings of the National Academy of Sciences, 112(4), 1149. doi:10.1073/pnas.1417064112

Guidoboni, M., Gafà, R., Viel, A., Doglioni, C., Russo, A., Santini, A., . . . Dolcetti, R. (2001). Microsatellite instability and high content of activated cytotoxic lymphocytes identify colon cancer patients with a favorable prognosis. Am J Pathol, 159(1), 297-304. doi:10.1016/s0002-9440(10)61695-1

Guinney, J., Dienstmann, R., Wang, X., de Reyniès, A., Schlicker, A., Soneson, C., . . . Tejpar, S. (2015). The consensus molecular subtypes of colorectal cancer. Nature medicine, 21(11), 1350-1356. doi:10.1038/nm.3967

Gulubova, M., Ananiev, J., Yovchev, Y., Julianov, A., Karashmalakov, A., & Vlaykova, T. (2013). The density of macrophages in colorectal cancer is inversely correlated to TGF-β1 expression and patients' survival. J Mol Histol, 44(6), 679-692. doi:10.1007/s10735-013-9520-9

Haggar, F. A., & Boushey, R. P. (2009). Colorectal cancer epidemiology: incidence, mortality, survival, and risk factors. Clinics in colon and rectal surgery, 22(4), 191-197. doi:10.1055/s-0029-1242458

Hahn, S. A., Schutte, M., Hoque, A. T., Moskaluk, C. A., da Costa, L. T., Rozenblum, E., . . . Kern, S. E. (1996). DPC4, a candidate tumor suppressor gene at human chromosome 18q21.1. Science, 271(5247), 350-353. doi:10.1126/science.271.5247.350

Halama, N., Braun, M., Kahlert, C., Spille, A., Quack, C., Rahbari, N., . . . Falk, C. S. (2011). Natural Killer Cells are Scarce in Colorectal Carcinoma Tissue Despite High Levels of Chemokines and Cytokines. Clinical Cancer Research, 17(4), 678. doi:10.1158/1078-0432.CCR-10-2173

Halama, N., Michel, S., Kloor, M., Zoernig, I., Benner, A., Spille, A., . . . Jaeger, D. (2011). Localization and density of immune cells in the invasive margin of human colorectal cancer liver metastases are prognostic for response to chemotherapy. Cancer Res, 71(17), 5670-5677. doi:10.1158/0008-5472.Can-11-0268

Hamada, T., Cao, Y., Qian, Z. R., Masugi, Y., Nowak, J. A., Yang, J., . . . Ogino, S. (2017). Aspirin Use and Colorectal Cancer Survival According to Tumor CD274 (Programmed Cell Death 1 Ligand 1) Expression Status. Journal of clinical oncology : official journal of the American Society of Clinical Oncology, 35(16), 1836-1844. doi:10.1200/JCO.2016.70.7547

Hamada, T., Soong, T. R., Masugi, Y., Kosumi, K., Nowak, J. A., da Silva, A., . . . Ogino, S. (2018). TIME (Tumor Immunity in the MicroEnvironment) classification based on tumor CD274 (PD-L1) expression status and tumor-infiltrating lymphocytes in colorectal carcinomas. Oncoimmunology, 7(7), e1442999-e1442999. doi:10.1080/2162402X.2018.1442999

Hamm, A., Prenen, H., Van Delm, W., Di Matteo, M., Wenes, M., Delamarre, E., . . . Mazzone, M. (2016). Tumour-educated circulating monocytes are powerful candidate biomarkers for diagnosis and disease follow-up of colorectal cancer. Gut, 65(6), 990. doi:10.1136/gutjnl-2014-308988

Hanahan, D., & Weinberg, R. A. (2000). The Hallmarks of Cancer. Cell, 100(1), 57-70. doi:10.1016/S0092-8674(00)81683-9

Hanahan, D., & Weinberg, Robert A. (2011). Hallmarks of Cancer: The Next Generation. Cell, 144(5), 646-674. doi:10.1016/j.cell.2011.02.013

Hao, H. X., Jiang, X., & Cong, F. (2016). Control of Wnt Receptor Turnover by R-spondin-ZNRF3/RNF43 Signaling Module and Its Dysregulation in Cancer. Cancers, 8(6). doi:10.3390/cancers8060054

Haq, A. I., Schneeweiss, J., Kalsi, V., & Arya, M. (2009). The Dukes staging system: a cornerstone in the clinical management of colorectal cancer. Lancet Oncol, 10(11), 1128. doi:10.1016/s1470-2045(09)70157-3

HARA, M., NAGASAKI, T., SHIGA, K., & TAKEYAMA, H. (2016). Suppression of Cancer-associated Fibroblasts and Endothelial Cells by Itraconazole in Bevacizumab-resistant Gastrointestinal Cancer. Anticancer

Research, 36(1), 169-177. Retrieved from http://ar.iiarjournals.org/content/36/1/169.abstract

Haraldsdottir, S., Hampel, H., Tomsic, J., Frankel, W. L., Pearlman, R., de la Chapelle, A., & Pritchard, C. C. (2014). Colon and endometrial cancers with mismatch repair deficiency can arise from somatic, rather than germline, mutations. Gastroenterology, 147(6), 1308-1316.e1301. doi:10.1053/j.gastro.2014.08.041

Harati, M. D., Amiri, F., Jaleh, F., Mehdipour, A., Harati, M. D., Molaee, S., . . . Roudkenar, M. H. (2015). Targeting delivery of lipocalin 2-engineered mesenchymal stem cells to colon cancer in order to inhibit liver metastasis in nude mice. Tumor Biology, 36(8), 6011-6018. doi:10.1007/s13277-015-3277-6

Harper, J., & Sainson, R. C. (2014). Regulation of the anti-tumour immune response by cancer-associated fibroblasts. Semin Cancer Biol, 25, 69-77. doi:10.1016/j.semcancer.2013.12.005

Harper, J., & Sainson, R. C. A. (2014). Regulation of the anti-tumour immune response by cancer-associated fibroblasts. Seminars in Cancer Biology, 25, 69-77. doi:https://doi.org/10.1016/j.semcancer.2013.12.005

Hawinkels, L. J., Paauwe, M., Verspaget, H. W., Wiercinska, E., van der Zon, J. M., van der Ploeg, K., . . . Sier, C. F. (2014). Interaction with colon cancer cells hyperactivates TGF-β signaling in cancer-associated fibroblasts. Oncogene, 33(1), 97-107. doi:10.1038/onc.2012.536

Hawkins, N. J., Tomlinson, I., Meagher, A., & Ward, R. L. (2001). Microsatellite-stable diploid carcinoma: a biologically distinct and aggressive subset of sporadic colorectal cancer. British Journal of Cancer, 84(2), 232-236. doi:10.1054/bjoc.2000.1554

Hedley, D. W., Friedlander, M. L., Taylor, I. W., Rugg, C. A., & Musgrove, E. A. (1983). Method for analysis of cellular DNA content of paraffin-embedded pathological material using flow cytometry. Journal of Histochemistry & Cytochemistry, 31(11), 1333-1335. doi:10.1177/31.11.6619538

Heemskerk, B., Kvistborg, P., & Schumacher, T. N. M. (2013). The cancer antigenome. The EMBO journal, 32(2), 194-203. doi:10.1038/emboj.2012.333

Heindl, A., Nawaz, S., & Yuan, Y. (2015). Mapping spatial heterogeneity in the tumor microenvironment: a new era for digital pathology. Laboratory Investigation, 95(4), 377-384. doi:10.1038/labinvest.2014.155

Heindl, A., Sestak, I., Naidoo, K., Cuzick, J., Dowsett, M., & Yuan, Y. (2017). Relevance of Spatial Heterogeneity of Immune Infiltration for Predicting Risk of Recurrence After Endocrine Therapy of ER+ Breast Cancer. JNCI: Journal of the National Cancer Institute, 110(2), 166-175. doi:10.1093/jnci/djx137

Herman, J. G., Umar, A., Polyak, K., Graff, J. R., Ahuja, N., Issa, J.-P. J., . . . Baylin, S. B. (1998). Incidence and functional consequences of hMLH1 promoter hypermethylation in colorectal

carcinoma. Proceedings of the National Academy of Sciences, 95(12), 6870. doi:10.1073/pnas.95.12.6870

Hermsen, M., Postma, C., Baak, J., Weiss, M., Rapallo, A., Sciutto, A., . . . Meijer, G. (2002). Colorectal adenoma to carcinoma progression follows multiple pathways of chromosomal instability. Gastroenterology, 123(4), 1109-1119. doi:10.1053/gast.2002.36051

Herrera, M., Herrera, A., Domínguez, G., Silva, J., García, V., García, J. M., . . . Peña, C. (2013). Cancer-associated fibroblast and M2 macrophage markers together predict outcome in colorectal cancer patients. Cancer Sci, 104(4), 437-444. doi:10.1111/cas.12096

Hof-Nahor, I., Leshansky, L., Shivtiel, S., Eldor, L., Aberdam, D., Itskovitz-Eldor, J., & Berrih-Aknin, S. (2012). Human mesenchymal stem cells shift CD8+ T cells towards a suppressive phenotype by inducing tolerogenic monocytes. Journal of Cell Science, 125(19), 4640. doi:10.1242/jcs.108860

Horman, S. R., To, J., Lamb, J., Zoll, J. H., Leonetti, N., Tu, B., . . . Orth, A. P. (2017). Functional profiling of microtumors to identify cancer associated fibroblast-derived drug targets. Oncotarget, 8(59), 99913-99930. doi:10.18632/oncotarget.21915

How-Kit, A., Daunay, A., Buhard, O., Meiller, C., Sahbatou, M., Collura, A., . . . Deleuze, J.-F. (2018). Major improvement in the detection of microsatellite instability in colorectal cancer using HSP110 T17 E-ice-COLD-PCR. Human Mutation, 39(3), 441-453. doi:10.1002/humu.23379

Hu, X., Li, Y.-Q., Li, Q.-G., Ma, Y.-L., Peng, J.-J., & Cai, S.-J. (2018). ITGAE Defines CD8+ Tumor-Infiltrating Lymphocytes Predicting a better Prognostic Survival in Colorectal Cancer. EBioMedicine, 35, 178-188. doi:https://doi.org/10.1016/j.ebiom.2018.08.003

Hu, Y., Yan, C., Mu, L., Huang, K., Li, X., Tao, D., . . . Qin, J. (2015). Fibroblast-Derived Exosomes Contribute to Chemoresistance through Priming Cancer Stem Cells in Colorectal Cancer. PloS one, 10(5), e0125625. doi:10.1371/journal.pone.0125625

Huang, Q., Li, S., Cheng, P., Deng, M., He, X., Wang, Z., . . . Huang, J. (2017). High expression of anti-apoptotic protein Bcl-2 is a good prognostic factor in colorectal cancer: Result of a meta-analysis. World journal of gastroenterology, 23(27), 5018-5033. doi:10.3748/wjg.v23.i27.5018

Huang, W. H., Chang, M. C., Tsai, K. S., Hung, M. C., Chen, H. L., & Hung, S. C. (2013). Mesenchymal stem cells promote growth and angiogenesis of tumors in mice. Oncogene, 32(37), 4343-4354. doi:10.1038/onc.2012.458

Huang, Y., Bharill, S., Karandur, D., Peterson, S. M., Marita, M., Shi, X., . . . Kuriyan, J. (2016). Molecular basis for multimerization in the activation of the epidermal growth factor receptor. eLife, 5, e14107. doi:10.7554/eLife.14107

Hühns, M., Krohn, S., Murua Escobar, H., & Prall, F. (2018). Genomic heterogeneity in primary colorectal carcinomas and their metastases: born bad or brought up a villain? Human Pathology, 74, 54-63. doi:https://doi.org/10.1016/j.humpath.2017.12.015

Hynes, N. E., & Lane, H. A. (2005). Correction: ERBB Receptors and Cancer: The Complexity of Targeted Inhibitors. Nature Reviews Cancer, 5(7), 580-580. doi:10.1038/nrc1667

Iacopetta, B. (2003). *TP53* mutation in colorectal cancer. Human Mutation, 21(3), 271-276. doi:10.1002/humu.10175

Iacopetta, B., Russo, A., Bazan, V., Dardanoni, G., Gebbia, N., Soussi, T., . . . Ishioka, C. (2006). Functional categories of *TP53* mutation in colorectal cancer: results of an International Collaborative Study. Annals of Oncology, 17(5), 842-847. doi:https://doi.org/10.1093/annonc/mdl035

Iacopetta, B. J., Welch, J., Soong, R., House, A. K., Zhou, X.-P., & Hamelin, R. (1998). Mutation of the transforming growth factor-β type II receptor gene in right-sided colorectal cancer: relationship to clinicopathological features and genetic alterations. The Journal of pathology, 184(4), 390-395. doi:10.1002/(sici)1096-9896(199804)184:4<390::Aid-path1230>3.0.Co;2-q

Ibrahem, S., Seth, R., O'Sullivan, B., Fadhil, W., Taniere, P., & Ilyas, M. (2010). Comparative analysis of pyrosequencing and QMC-PCR in conjunction with high resolution melting for *KRAS*/*BRAF* mutation detection. International journal of experimental pathology, 91(6), 500-505. doi:10.1111/j.1365-2613.2010.00733.x

Ilyas, M., Tomlinson, I. P., Hanby, A. M., Yao, T., Bodmer, W. F., & Talbot, I. C. (1996). Bcl-2 expression in colorectal tumors: evidence of different pathways in sporadic and ulcerative-colitis-associated carcinomas. The American Journal of Pathology, 149(5), 1719-1726. Retrieved from https://pubmed.ncbi.nlm.nih.gov/8909260

https://www.ncbi.nlm.nih.gov/pmc/articles/PMC1865256/

Inamoto, S., Itatani, Y., Yamamoto, T., Minamiguchi, S., Hirai, H., Iwamoto, M., . . . Kawada, K. (2016). Loss of SMAD4 Promotes Colorectal Cancer Progression by Accumulation of Myeloid-Derived Suppressor Cells through the CCL15-CCR1 Chemokine Axis. Clin Cancer Res, 22(2), 492-501. doi:10.1158/1078-0432.Ccr-15-0726

Ireland, L. V., & Mielgo, A. (2018). Macrophages and Fibroblasts, Key Players in Cancer Chemoresistance. Frontiers in cell and developmental biology, 6, 131-131. doi:10.3389/fcell.2018.00131

Isella, C., Brundu, F., Bellomo, S. E., Galimi, F., Zanella, E., Porporato, R., . . . Bertotti, A. (2017). Selective analysis of cancer-cell intrinsic transcriptional traits defines novel clinically relevant subtypes of colorectal cancer. Nature Communications, 8(1), 15107. doi:10.1038/ncomms15107

Isella, C., Terrasi, A., Bellomo, S. E., Petti, C., Galatola, G., Muratore, A., . . . Medico, E. (2015). Stromal contribution to the colorectal cancer transcriptome. Nature Genetics, 47(4), 312-319. doi:10.1038/ng.3224

Janavicius, R., Matiukaite, D., Jakubauskas, A., & Griskevicius, L. (2010). Microsatellite Instability Detection by High-Resolution Melting Analysis. Clinical Chemistry, 56(11), 1750-1757. doi:10.1373/clinchem.2010.150680

Jasperson, K. W., Tuohy, T. M., Neklason, D. W., & Burt, R. W. (2010). Hereditary and familial colon cancer. Gastroenterology, 138(6), 2044-2058. doi:10.1053/j.gastro.2010.01.054

Jass, J. R., Biden, K. G., Cummings, M. C., Simms, L. A., Walsh, M., Schoch, E., . . . Leggett, B. A. (1999). Characterisation of a subtype of colorectal cancer combining features of the suppressor and mild mutator pathways. Journal of clinical pathology, 52(6), 455-460. doi:10.1136/jcp.52.6.455

Jass, J. R., & Stewart, S. M. (1992). Evolution of hereditary non-polyposis colorectal cancer. Gut, 33(6), 783. doi:10.1136/gut.33.6.783

Jia, X., Shanmugam, C., Paluri, R. K., Jhala, N. C., Behring, M. P., Katkoori, V. R., . . . Manne, U. (2017). Prognostic value of loss of heterozygosity and sub-cellular localization of SMAD4 varies with tumor stage in colorectal cancer. Oncotarget, 8(12), 20198-20212. doi:10.18632/oncotarget.15560

Jiang, S., Good, D., & Wei, M. Q. (2019). Vaccinations for Colorectal Cancer: Progress, Strategies, and Novel Adjuvants. International journal of molecular sciences, 20(14), 3403. doi:10.3390/ijms20143403

Jinushi, M., & Komohara, Y. (2015). Tumor-associated macrophages as an emerging target against tumors: Creating a new path from bench to bedside. Biochimica et Biophysica Acta (BBA) - Reviews on Cancer, 1855(2), 123-130. doi:https://doi.org/10.1016/j.bbcan.2015.01.002

Johnson, C. M., Wei, C., Ensor, J. E., Smolenski, D. J., Amos, C. I., Levin, B., & Berry, D. A. (2013). Meta-analyses of colorectal cancer risk factors. Cancer Causes Control, 24(6), 1207-1222. doi:10.1007/s10552-013-0201-5

Johnson, S. M., Gulhati, P., Rampy, B. A., Han, Y., Rychahou, P. G., Doan, H. Q., . . . Evers, B. M. (2010). Novel expression patterns of PI3K/Akt/mTOR signaling pathway components in colorectal cancer. Journal of the American College of Surgeons, 210(5), 767-778. doi:10.1016/j.jamcollsurg.2009.12.008

Jokinen, E., & Koivunen, J. P. (2015). MEK and PI3K inhibition in solid tumors: rationale and evidence to date. Ther Adv Med Oncol, 7(3), 170-180. doi:10.1177/1758834015571111

Jonker, D. J., O'Callaghan, C. J., Karapetis, C. S., Zalcberg, J. R., Tu, D., Au, H.-J., . . . Moore, M. J. (2007). Cetuximab for the Treatment of Colorectal Cancer. New England Journal of Medicine, 357(20), 2040-2048. doi:10.1056/NEJMoa071834

Jönsson, M., Ekstrand, A., Edekling, T., Eberhard, J., Grabau, D., Borg, D., & Nilbert, M. (2009). Experiences from treatment-predictive *KRAS* testing; high mutation frequency in rectal cancers from females and concurrent mutations in the same tumor. BMC Clin Pathol, 9, 8. doi:10.1186/1472-6890-9-8

Jorissen, R. N., Christie, M., Mouradov, D., Sakthianandeswaren, A., Li, S., Love, C., . . . Sieber, O. M. (2015). Wild-type APC predicts poor prognosis in microsatellite-stable proximal colon cancer. British Journal of Cancer, 113(6), 979-988. doi:10.1038/bjc.2015.296

Jover, R., Zapater, P., Castells, A., Llor, X., Andreu, M., Cubiella, J., . . . Alenda, C. (2009). The efficacy of adjuvant chemotherapy with 5-fluorouracil in colorectal cancer depends on the mismatch repair status. Eur J Cancer, 45(3), 365-373. doi:10.1016/j.ejca.2008.07.016

Jung, Y., Kim, J. K., Shiozawa, Y., Wang, J., Mishra, A., Joseph, J., . . . Taichman, R. S. (2013). Recruitment of mesenchymal stem cells into prostate tumours promotes metastasis. Nature Communications, 4, 1795-1795. doi:10.1038/ncomms2766

Juo, Y. Y., Johnston, F. M., Zhang, D. Y., Juo, H. H., Wang, H., Pappou, E. P., . . . Ahuja, N. (2014). Prognostic value of CpG island methylator phenotype among colorectal cancer patients: a systematic review and meta-analysis. Annals of Oncology, 25(12), 2314-2327. doi:https://doi.org/10.1093/annonc/mdu149

Kakar, S., Deng, G., Sahai, V., Matsuzaki, K., Tanaka, H., Miura, S., & Kim, Y. S. (2008). Clinicopathologic Characteristics, CpG Island Methylator Phenotype, and *BRAF* Mutations in Microsatellite-Stable Colorectal Cancers Without Chromosomal Instability. Archives of Pathology & Laboratory Medicine, 132(6), 958-964. doi:10.1043/1543-2165(2008)132[958:CCCIMP]2.0.CO;2

Kaler, P., Owusu, B. Y., Augenlicht, L., & Klampfer, L. (2014). The Role of STAT1 for Crosstalk between Fibroblasts and Colon Cancer Cells. Frontiers in Oncology, 4, 88-88. doi:10.3389/fonc.2014.00088

Kalimuthu, S., Gangadaran, P., Rajendran, R. L., Zhu, L., Oh, J. M., Lee, H. W., . . . Ahn, B.-C. (2018). A New Approach for Loading Anticancer Drugs Into Mesenchymal Stem Cell-Derived Exosome Mimetics for Cancer Therapy. Frontiers in pharmacology, 9, 1116-1116. doi:10.3389/fphar.2018.01116

Kandoth, C., McLellan, M. D., Vandin, F., Ye, K., Niu, B., Lu, C., . . . Ding, L. (2013). Mutational landscape and significance across 12 major cancer types. Nature, 502(7471), 333-339. doi:10.1038/nature12634

Kang, Y. J., Killen, J., Caruana, M., Simms, K., Taylor, N., Frayling, I. M., . . . Canfell, K. (2020). The predicted impact and cost-effectiveness of systematic testing of people with incident colorectal cancer for Lynch syndrome. Med J Aust, 212(2), 72-81. doi:10.5694/mja2.50356

Kapałczyńska, M., Kolenda, T., Przybyła, W., Zajączkowska, M., Teresiak, A., Filas, V., . . . Lamperska, K. (2018). 2D and 3D cell cultures - a comparison of different types of cancer cell cultures. Archives of

medical science : AMS, 14(4), 910-919. doi:10.5114/aoms.2016.63743

Kather, J. N., Suarez-Carmona, M., Charoentong, P., Weis, C. A., Hirsch, D., Bankhead, P., . . . Halama, N. (2018). Topography of cancer-associated immune cells in human solid tumors. eLife, 7. doi:10.7554/eLife.36967

Katt, M. E., Placone, A. L., Wong, A. D., Xu, Z. S., & Searson, P. C. (2016). In Vitro Tumor Models: Advantages, Disadvantages, Variables, and Selecting the Right Platform. Frontiers in bioengineering and biotechnology, 4, 12-12. doi:10.3389/fbioe.2016.00012

Kay, R., Rosten, P. M., & Humphries, R. K. (1991). CD24, a signal transducer modulating B cell activation responses, is a very short peptide with a glycosyl phosphatidylinositol membrane anchor. Journal of immunology (Baltimore, Md. : 1950), 147(4), 1412-1416.

Kaye, P. V. (2015). p53 Immunohistochemistry as a biomarker of dysplasia and neoplastic progression in Barrett's oesophagus. Diagnostic Histopathology, 21(3), 89-98. doi:10.1016/j.mpdhp.2015.04.001

Khan, K., Valeri, N., Dearman, C., Rao, S., Watkins, D., Starling, N., . . . Cunningham, D. (2019). Targeting EGFR pathway in metastatic colorectal cancer- tumour heterogeniety and convergent evolution. Critical Reviews in Oncology/Hematology, 143, 153-163. doi:https://doi.org/10.1016/j.critrevonc.2019.09.001

Khan, S. A., Morris, M., Idrees, K., Gimbel, M. I., Rosenberg, S., Zeng, Z., . . . Paty, P. B. (2016). Colorectal cancer in the very young: a comparative study of tumor markers, pathology and survival in early onset and adult onset patients. Journal of pediatric surgery, 51(11), 1812-1817. doi:10.1016/j.jpedsurg.2016.07.015

Kikuchi, H., Yagi, H., Hasegawa, H., Ishii, Y., Okabayashi, K., Tsuruta, M., . . . Kitagawa, Y. (2014). Therapeutic potential of transgenic mesenchymal stem cells engineered to mediate anti–high mobility group box 1 activity: targeting of colon cancer. Journal of Surgical Research, 190(1), 134-143. doi:https://doi.org/10.1016/j.jss.2014.02.047

Kikuchi, Y., Kashima, T. G., Nishiyama, T., Shimazu, K., Morishita, Y., Shimazaki, M., . . . Fukayama, M. (2008). Periostin is expressed in pericryptal fibroblasts and cancer-associated fibroblasts in the colon. The journal of histochemistry and cytochemistry : official journal of the Histochemistry Society, 56(8), 753-764. doi:10.1369/jhc.2008.951061

Kim, E. R., & Chang, D. K. (2014). Colorectal cancer in inflammatory bowel disease: the risk, pathogenesis, prevention and diagnosis. World journal of gastroenterology, 20(29), 9872-9881. doi:10.3748/wjg.v20.i29.9872

Kim, W. G., Kim, J. Y., & Park, D. Y. (2017). Simple classifiers for molecular subtypes of colorectal cancer. Arab Journal of Gastroenterology, 18(4), 191-200. doi:https://doi.org/10.1016/j.ajg.2017.11.007

Kitaeva, M. N., Grogan, L., Williams, J. P., Dimond, E., Nakahara, K., Hausner, P., . . . Kirsch, I. R. (1997). Mutations in beta-catenin are uncommon in colorectal cancer occurring in occasional replication error-positive tumors. Cancer Res, 57(20), 4478-4481.

Klingbiel, D., Saridaki, Z., Roth, A. D., Bosman, F. T., Delorenzi, M., & Tejpar, S. (2015). Prognosis of stage II and III colon cancer treated with adjuvant 5-fluorouracil or FOLFIRI in relation to microsatellite status: results of the PETACC-3 trial. Ann Oncol, 26(1), 126-132. doi:10.1093/annonc/mdu499

Knoop, K., Schwenk, N., Schmohl, K., Müller, A., Zach, C., Cyran, C., . . . Spitzweg, C. (2015). Mesenchymal Stem Cell–Mediated, Tumor Stroma–Targeted Radioiodine Therapy of Metastatic Colon Cancer Using the Sodium Iodide Symporter as Theranostic Gene. Journal of Nuclear Medicine, 56(4), 600-606. doi:10.2967/jnumed.114.146662

Komohara, Y., Fujiwara, Y., Ohnishi, K., & Takeya, M. (2016). Tumor-associated macrophages: Potential therapeutic targets for anti-cancer therapy. Adv Drug Deliv Rev, 99(Pt B), 180-185. doi:10.1016/j.addr.2015.11.009

Kondelin, J., Tuupanen, S., Gylfe, A. E., Aavikko, M., Renkonen-Sinisalo, L., Järvinen, H., . . . Aaltonen, L. A. (2015). 3′-UTR poly(T/U) repeat of EWSR1 is altered in microsatellite unstable colorectal cancer with nearly perfect sensitivity. Familial Cancer, 14(3), 449-453. doi:10.1007/s10689-015-9804-1

Korehisa, S., Oki, E., Iimori, M., Nakaji, Y., Shimokawa, M., Saeki, H., . . . Maehara, Y. (2018). Clinical significance of programmed cell death-ligand 1 expression and the immune microenvironment at the invasive front of colorectal cancers with high microsatellite instability. Int J Cancer, 142(4), 822-832. doi:10.1002/ijc.31107

Kotelevets, L., Scott, M. G. H., & Chastre, E. (2018). Targeting PTEN in Colorectal Cancers. Adv Exp Med Biol, 1110, 55-73. doi:10.1007/978-3-030-02771-1_5

Kraman, M., Bambrough, P. J., Arnold, J. N., Roberts, E. W., Magiera, L., Jones, J. O., . . . Fearon, D. T. (2010). Suppression of antitumor immunity by stromal cells expressing fibroblast activation protein-alpha. Science, 330(6005), 827-830. doi:10.1126/science.1195300

Krampera, M., Pasini, A., Pizzolo, G., Cosmi, L., Romagnani, S., & Annunziato, F. (2006). Regenerative and immunomodulatory potential of mesenchymal stem cells. Curr Opin Pharmacol, 6(4), 435-441. doi:10.1016/j.coph.2006.02.008

*KRAS*inskas, A. M. (2011). EGFR Signaling in Colorectal Carcinoma. Patholog Res Int, 2011, 932932. doi:10.4061/2011/932932

Kristiansen, G., Sammar, M., & Altevogt, P. (2004). Tumour Biological Aspects of CD24, A Mucin-Like Adhesion Molecule. Journal of Molecular Histology, 35(3), 255-262. doi:10.1023/B:HIJO.0000032357.16261.c5

Kucerova, L., Altanerova, V., Matuskova, M., Tyciakova, S., & Altaner, C. (2007). Adipose Tissue–Derived Human Mesenchymal Stem Cells Mediated Prodrug Cancer Gene Therapy. Cancer Research, 67(13), 6304. doi:10.1158/0008-5472.CAN-06-4024

Kumar, V., Donthireddy, L., Marvel, D., Condamine, T., Wang, F., Lavilla-Alonso, S., . . . Gabrilovich, D. I. (2017). Cancer-Associated Fibroblasts Neutralize the Anti-tumor Effect of CSF1 Receptor Blockade by Inducing PMN-MDSC Infiltration of Tumors. Cancer Cell, 32(5), 654-668.e655. doi:https://doi.org/10.1016/j.ccell.2017.10.005

Kwak, E. L., & Chung, D. C. (2007). Hereditary Colorectal Cancer Syndromes: An Overview. Clinical Colorectal Cancer, 6(5), 340-344. doi:https://doi.org/10.3816/CCC.2007.n.002

Kwak, Y., Koh, J., Kim, D.-W., Kang, S.-B., Kim, W. H., & Lee, H. S. (2016). Immunoscore encompassing CD3+ and CD8+ T cell densities in distant metastasis is a robust prognostic marker for advanced colorectal cancer. Oncotarget, 7(49), 81778-81790. doi:10.18632/oncotarget.13207

Kzhyshkowska, J., Riabov, V., Gudima, A., Wang, N., Orekhov, A., & Mickley, A. (2014). Role of tumor associated macrophages in tumor angiogenesis and lymphangiogenesis. Frontiers in Physiology, 5(75). doi:10.3389/fphys.2014.00075

Labernadie, A., Kato, T., Brugués, A., Serra-Picamal, X., Derzsi, S., Arwert, E., . . . Trepat, X. (2017). A mechanically active heterotypic E-cadherin/N-cadherin adhesion enables fibroblasts to drive cancer cell invasion. Nat Cell Biol, 19(3), 224-237. doi:10.1038/ncb3478

Labianca, R., Beretta, G. D., Kildani, B., Milesi, L., Merlin, F., Mosconi, S., . . . Wils, J. (2010). Colon cancer. Crit Rev Oncol Hematol, 74(2), 106-133. doi:10.1016/j.critrevonc.2010.01.010

Lal, N., White, B. S., Goussous, G., Pickles, O., Mason, M. J., Beggs, A. D., . . . Middleton, G. W. (2018). *KRAS* Mutation and Consensus Molecular Subtypes 2 and 3 Are Independently Associated with Reduced Immune Infiltration and Reactivity in Colorectal Cancer. Clinical cancer research : an official journal of the American Association for Cancer Research, 24(1), 224-233. doi:10.1158/1078-0432.CCR-17-1090

Larki, P., Gharib, E., Yaghoob Taleghani, M., Khorshidi, F., Nazemalhosseini-Mojarad, E., & Asadzadeh Aghdaei, H. (2017). Coexistence of *KRAS* and *BRAF* Mutations in Colorectal Cancer: A Case Report Supporting The Concept of Tumoral Heterogeneity. Cell journal, 19(Suppl 1), 113-117. doi:10.22074/cellj.2017.5123

Laurent-Puig, P., Cayre, A., Manceau, G., Buc, E., Bachet, J. B., Lecomte, T., . . . Penault-Llorca, F. (2009). Analysis of PTEN, *BRAF*, and EGFR status in determining benefit from cetuximab therapy in wild-type *KRAS* metastatic colon cancer. J Clin Oncol, 27(35), 5924-5930. doi:10.1200/jco.2008.21.6796

Lawes, D. A., SenGupta, S., & Boulos, P. B. (2003). The clinical importance and prognostic implications of microsatellite instability in sporadic

cancer. Eur J Surg Oncol, 29(3), 201-212. doi:10.1053/ejso.2002.1399

Lazaris, A., Tzoumani, A. N., Thimara, I., Theodoropoulos, G. E., Thomopoulou, G., Dicoglou, C., . . . Davaris, P. (2003). Immunohistochemical assessment of basement membrane components in colorectal cancer: prognostic implications. J Exp Clin Cancer Res, 22(4), 599-606.

Lazzari, G., Nicolas, V., Matsusaki, M., Akashi, M., Couvreur, P., & Mura, S. (2018). Multicellular spheroid based on a triple co-culture: A novel 3D model to mimic pancreatic tumor complexity. Acta Biomater, 78, 296-307. doi:10.1016/j.actbio.2018.08.008

Le, D. T., Durham, J. N., Smith, K. N., Wang, H., Bartlett, B. R., Aulakh, L. K., . . . Diaz, L. A. (2017). Mismatch repair deficiency predicts response of solid tumors to PD-1 blockade. Science, 357(6349), 409. doi:10.1126/science.aan6733

Le, D. T., Uram, J. N., Wang, H., Bartlett, B. R., Kemberling, H., Eyring, A. D., . . . Diaz, L. A., Jr. (2015). PD-1 Blockade in Tumors with Mismatch-Repair Deficiency. The New England journal of medicine, 372(26), 2509-2520. doi:10.1056/NEJMoa1500596

Lee, J.-H., Kim, S.-H., Lee, E.-S., & Kim, Y.-S. (2009). CD24 overexpression in cancer development and progression: A meta-analysis. Oncol Rep, 22(5), 1149-1156. doi:10.3892/or_00000548

Lee, J. M., Park, D. Y., Yang, L., Kim, E.-J., Ahrberg, C. D., Lee, K.-B., & Chung, B. G. (2018). Generation of uniform-sized multicellular tumor spheroids using hydrogel microwells for advanced drug screening. Scientific Reports, 8(1), 17145. doi:10.1038/s41598-018-35216-7

Lee, S. S.-Y., Bindokas, V. P., & Kron, S. J. (2017). Multiplex three-dimensional optical mapping of tumor immune microenvironment. Scientific Reports, 7(1), 17031. doi:10.1038/s41598-017-16987-x

Leenen, C. H. M., Goverde, A., de Bekker-Grob, E. W., Wagner, A., van Lier, M. G. F., Spaander, M. C. W., . . . on behalf of the, L. s. g. (2016). Cost-effectiveness of routine screening for Lynch syndrome in colorectal cancer patients up to 70 years of age. Genetics in Medicine, 18(10), 966-973. doi:10.1038/gim.2015.206

Lengauer, C., Kinzler, K. W., & Vogelstein, B. (1997). Genetic instability in colorectal cancers. Nature, 386(6625), 623-627. doi:10.1038/386623a0

Leslie, A., Carey, F. A., Pratt, N. R., & Steele, R. J. C. (2002). The colorectal adenoma–carcinoma sequence. British Journal of Surgery, 89(7), 845-860. doi:10.1046/j.1365-2168.2002.02120.x

Li, C., Luo, X., Lin, Y., Tang, X., Ling, L., Wang, L., & Jiang, Y. (2015). A Higher Frequency of CD14+ CD169+ Monocytes/Macrophages in Patients with Colorectal Cancer. PloS one, 10(10), e0141817-e0141817. doi:10.1371/journal.pone.0141817

Li, H.-T., Lu, Y.-Y., An, Y.-X., Wang, X., & Zhao, Q.-C. (2011). *KRAS*, *BRAF* and *PIK3CA* mutations in human colorectal cancer: Relationship with

metastatic colorectal cancer. Oncol Rep, 25(6), 1691-1697. doi:10.3892/or.2011.1217

Li, Q., & Lozano, G. (2013). Molecular pathways: targeting Mdm2 and Mdm4 in cancer therapy. Clinical cancer research : an official journal of the American Association for Cancer Research, 19(1), 34-41. doi:10.1158/1078-0432.CCR-12-0053

Li, W. Q., Kawakami, K., Ruszkiewicz, A., Bennett, G., Moore, J., & Iacopetta, B. (2006). *BRAF* mutations are associated with distinctive clinical, pathological and molecular features of colorectal cancer independently of microsatellite instability status. Molecular cancer, 5, 2-2. doi:10.1186/1476-4598-5-2

Li, X.-L., Zhou, J., Chen, Z.-R., & Chng, W.-J. (2015). P53 mutations in colorectal cancer - molecular pathogenesis and pharmacological reactivation. World journal of gastroenterology, 21(1), 84-93. doi:10.3748/wjg.v21.i1.84

Li, Y., Xu, X., Wang, L., Liu, G., Li, Y., Wu, X., . . . Wang, G. (2015). Senescent mesenchymal stem cells promote colorectal cancer cells growth via galectin-3 expression. Cell & bioscience, 5, 21-21. doi:10.1186/s13578-015-0012-3

Limagne, E., Euvrard, R., Thibaudin, M., Rébé, C., Derangère, V., Chevriaux, A., . . . Ghiringhelli, F. (2016). Accumulation of MDSC and Th17 Cells in Patients with Metastatic Colorectal Cancer Predicts the Efficacy of a FOLFOX-Bevacizumab Drug Treatment Regimen. Cancer Res, 76(18), 5241-5252. doi:10.1158/0008-5472.Can-15-3164

Lin, E. I., Tseng, L.-H., Gocke, C. D., Reil, S., Le, D. T., Azad, N. S., & Eshleman, J. R. (2015). Mutational profiling of colorectal cancers with microsatellite instability. Oncotarget, 6(39), 42334-42344. doi:10.18632/oncotarget.5997

Lindor, N. M., Burgart, L. J., Leontovich, O., Goldberg, R. M., Cunningham, J. M., Sargent, D. J., . . . Thibodeau, S. N. (2002). Immunohistochemistry versus microsatellite instability testing in phenotyping colorectal tumors. J Clin Oncol, 20(4), 1043-1048. doi:10.1200/jco.2002.20.4.1043

Liu, B., Nicolaides, N. C., Markowitz, S., Willson, J. K., Parsons, R. E., Jen, J., . . . et al. (1995). Mismatch repair gene defects in sporadic colorectal cancers with microsatellite instability. Nat Genet, 9(1), 48-55. doi:10.1038/ng0195-48

Liu, J., Lu, C.-x., Zhang, F., Lv, W., & Liu, C. (2018). Expression of ILT3 predicts poor prognosis and is inversely associated with infiltration of CD45RO+ T cells in patients with colorectal cancer. Pathology - Research and Practice, 214(10), 1621-1625. doi:https://doi.org/10.1016/j.prp.2018.07.026

Liu, T., Han, C., Wang, S., Fang, P., Ma, Z., Xu, L., & Yin, R. (2019). Cancer-associated fibroblasts: an emerging target of anti-cancer immunotherapy. Journal of hematology & oncology, 12(1), 86. doi:10.1186/s13045-019-0770-1

Liu, T., Zhou, L., Li, D., Andl, T., & Zhang, Y. (2019). Cancer-Associated Fibroblasts Build and Secure the Tumor Microenvironment. Frontiers in cell and developmental biology, 7, 60-60. doi:10.3389/fcell.2019.00060

Liu, Y., Han, Z.-p., Zhang, S.-s., Jing, Y.-y., Bu, X.-x., Wang, C.-y., . . . Wei, L.-x. (2011). Effects of inflammatory factors on mesenchymal stem cells and their role in the promotion of tumor angiogenesis in colon cancer. The Journal of biological chemistry, 286(28), 25007-25015. doi:10.1074/jbc.M110.213108

Liu, Y.-P., Wu, H.-Y., Yang, X., Xu, H.-Q., Chen, D., Huang, Q., & Fu, W.-L. (2014). Diagnostic accuracy of high resolution melting analysis for detection of *KRAS* mutations: a systematic review and meta-analysis. Scientific Reports, 4(1), 7521. doi:10.1038/srep07521

Llosa, N. J., Cruise, M., Tam, A., Wicks, E. C., Hechenbleikner, E. M., Taube, J. M., . . . Housseau, F. (2015). The Vigorous Immune Microenvironment of Microsatellite Instable Colon Cancer Is Balanced by Multiple Counter-Inhibitory Checkpoints. Cancer Discovery, 5(1), 43. doi:10.1158/2159-8290.CD-14-0863

Llosa, N. J., Housseau, F., Wick, E., Hechenbleikner, L., Cruise, M., Anders, R., . . . Pardoll, D. (2013). Immune checkpoints in MSI and CSI colorectal cancers and their translational implications. Journal for Immunotherapy of Cancer, 1(Suppl 1), P161-P161. doi:10.1186/2051-1426-1-S1-P161

Lochhead, P., Kuchiba, A., Imamura, Y., Liao, X., Yamauchi, M., Nishihara, R., . . . Ogino, S. (2013). Microsatellite Instability and *BRAF* Mutation Testing in Colorectal Cancer Prognostication. JNCI: Journal of the National Cancer Institute, 105(15), 1151-1156. doi:10.1093/jnci/djt173

López, I., L, P. O., Tucci, P., Alvarez-Valín, F., R, A. C., & Marín, M. (2012). Different mutation profiles associated to P53 accumulation in colorectal cancer. Gene, 499(1), 81-87. doi:10.1016/j.gene.2012.02.011

López, P. J. T., Albero, J. S., & Rodríguez-Montes, J. A. (2014). Primary and Secondary Prevention of Colorectal Cancer. Clinical Medicine Insights: Gastroenterology, 7, CGast.S14039. doi:10.4137/CGast.S14039

Loupakis, F., Ruzzo, A., Cremolini, C., Vincenzi, B., Salvatore, L., Santini, D., . . . Graziano, F. (2009). *KRAS* codon 61, 146 and *BRAF* mutations predict resistance to cetuximab plus irinotecan in *KRAS* codon 12 and 13 wild-type metastatic colorectal cancer. British Journal of Cancer, 101(4), 715-721. doi:10.1038/sj.bjc.6605177

Lu, J., Ye, X., Fan, F., Xia, L., Bhattacharya, R., Bellister, S., . . . Ellis, L. M. (2013). Endothelial cells promote the colorectal cancer stem cell phenotype through a soluble form of Jagged-1. Cancer Cell, 23(2), 171-185. doi:10.1016/j.ccr.2012.12.021

Luca, A. C., Mersch, S., Deenen, R., Schmidt, S., Messner, I., Schäfer, K.-L., . . . Stoecklein, N. H. (2013). Impact of the 3D Microenvironment on Phenotype, Gene Expression, and EGFR Inhibition of Colorectal

Cancer Cell Lines. PloS one, 8(3), e59689. doi:10.1371/journal.pone.0059689

Luke, J. J., Bao, R., Spranger, S., Sweis, R. F., & Gajewski, T. (2016). Correlation of WNT/β-catenin pathway activation with immune exclusion across most human cancers. Journal of Clinical Oncology, 34(15_suppl), 3004-3004. doi:10.1200/JCO.2016.34.15_suppl.3004

Lynch, H. T., & de la Chapelle, A. (1999). Genetic susceptibility to non-polyposis colorectal cancer. Journal of medical genetics, 36(11), 801-818. Retrieved from https://pubmed.ncbi.nlm.nih.gov/10544223

https://www.ncbi.nlm.nih.gov/pmc/articles/PMC1734258/

Ma, X. T., Wang, S., Ye, Y. J., Du, R. Y., Cui, Z. R., & Somsouk, M. (2004). Constitutive activation of Stat3 signaling pathway in human colorectal carcinoma. World journal of gastroenterology, 10(11), 1569-1573. doi:10.3748/wjg.v10.i11.1569

Maby, P., Tougeron, D., Hamieh, M., Mlecnik, B., Kora, H., Bindea, G., . . . Latouche, J.-B. (2015). Correlation between Density of CD8⁺ T-cell Infiltrate in Microsatellite Unstable Colorectal Cancers and Frameshift Mutations: A Rationale for Personalized Immunotherapy. Cancer Research, 75(17), 3446. doi:10.1158/0008-5472.CAN-14-3051

Macedo, M. P., Andrade, L. D. B., Coudry, R., Crespo, R., Gomes, M., Lisboa, B. C. G., . . . Cunha, I. W. (2011). Multiple mutations in the *KRAS* gene in colorectal cancer: review of the literature with two case reports. International Journal of Colorectal Disease, 26(10), 1241-1248. doi:10.1007/s00384-011-1238-0

Mackay, J. F., Wright, C. D., & Bonfiglioli, R. G. (2008). A new approach to varietal identification in plants by microsatellite high resolution melting analysis: application to the verification of grapevine and olive cultivars. Plant Methods, 4, 8. doi:10.1186/1746-4811-4-8

Mader, E., Lukas, B., & Novak, J. (2008). A Strategy to Setup Codominant Microsatellite Analysis for High-Resolution-Melting-Curve-Analysis (HRM). BMC Genetics, 9(1), 69. doi:10.1186/1471-2156-9-69

Maley, C. C., Aktipis, A., Graham, T. A., Sottoriva, A., Boddy, A. M., Janiszewska, M., . . . Shibata, D. (2017). Classifying the evolutionary and ecological features of neoplasms. Nature Reviews Cancer, 17(10), 605-619. doi:10.1038/nrc.2017.69

Maman, S., & Witz, I. P. (2018). A history of exploring cancer in context. Nat Rev Cancer, 18(6), 359-376. doi:10.1038/s41568-018-0006-7

Manning, B. D., & Toker, A. (2017). AKT/PKB Signaling: Navigating the Network. Cell, 169(3), 381-405. doi:10.1016/j.cell.2017.04.001

Mantovani, A. (2014). Macrophages, Neutrophils, and Cancer: A Double Edged Sword. New Journal of Science, 2014, 271940. doi:10.1155/2014/271940

Mantovani, A., Allavena, P., Sica, A., & Balkwill, F. (2008). Cancer-related inflammation. Nature, 454(7203), 436-444. doi:10.1038/nature07205

Mao, C., Yang, Z. Y., Hu, X. F., Chen, Q., & Tang, J. L. (2012). *PIK3CA* exon 20 mutations as a potential biomarker for resistance to anti-EGFR monoclonal antibodies in *KRAS* wild-type metastatic colorectal cancer: a systematic review and meta-analysis. Annals of Oncology, 23(6), 1518-1525. doi:https://doi.org/10.1093/annonc/mdr464

Marech, I., Ammendola, M., Sacco, R., Sammarco, G., Zuccalà, V., Zizzo, N., . . . Ranieri, G. (2016). Tumour-associated macrophages correlate with microvascular bed extension in colorectal cancer patients. Journal of cellular and molecular medicine, 20(7), 1373-1380. doi:10.1111/jcmm.12826

Martin, M., Pujuguet, P., & Martin, F. (1996). Role of stromal myofibroblasts infiltrating colon cancer in tumor invasion. Pathol Res Pract, 192(7), 712-717. doi:10.1016/s0344-0338(96)80093-8

Martinez, F. O., & Gordon, S. (2014). The M1 and M2 paradigm of macrophage activation: time for reassessment. F1000Prime Rep, 6, 13. doi:10.12703/p6-13

Marx, J. (2008). Cancer immunology. Cancer's bulwark against immune attack: MDS cells. Science, 319(5860), 154-156. doi:10.1126/science.319.5860.154

Marzouk, O., & Schofield, J. (2011). Review of histopathological and molecular prognostic features in colorectal cancer. Cancers, 3(2), 2767-2810. doi:10.3390/cancers3022767

Massi, D., Rulli, E., Cossa, M., Valeri, B., Rodolfo, M., Merelli, B., . . . on behalf of the Italian Melanoma, I. (2019). The density and spatial tissue distribution of CD8+ and CD163+ immune cells predict response and outcome in melanoma patients receiving MAPK inhibitors. Journal for Immunotherapy of Cancer, 7(1), 308. doi:10.1186/s40425-019-0797-4

Matevska-Geshkovska, N., Staninova-Stojovska, M., Kapedanovska-Nestorovska, A., Petrushevska-Angelovska, N., Panovski, M., Grozdanovska, B., . . . Dimovski, A. (2018). Influence of MSI and 18q LOH markers on capecitabine adjuvant monotherapy in colon cancer patients. Pharmacogenomics and personalized medicine, 11, 193-203. doi:10.2147/PGPM.S172467

Matsuzaki, K., Deng, G., Tanaka, H., Kakar, S., Miura, S., & Kim, Y. S. (2005). The Relationship between Global Methylation Level, Loss of Heterozygosity, and Microsatellite Instability in Sporadic Colorectal Cancer. Clinical Cancer Research, 11(24), 8564. doi:10.1158/1078-0432.CCR-05-0859

Mayer, A., Takimoto, M., Fritz, E., Schellander, G., Kofler, K., & Ludwig, H. (1993). The prognostic significance of proliferating cell nuclear antigen, epidermal growth factor receptor, and mdr gene expression in colorectal cancer. Cancer, 71(8), 2454-2460. doi:10.1002/1097-0142(19930415)71:8<2454::aid-cncr2820710805>3.0.co;2-2

Mazzoni, S. M., & Fearon, E. R. (2014). AXIN1 and AXIN2 variants in gastrointestinal cancers. Cancer letters, 355(1), 1-8. doi:10.1016/j.canlet.2014.09.018

McCleary, N. J., Sato, K., Nishihara, R., Inamura, K., Morikawa, T., Zhang, X., . . . Meyerhardt, J. A. (2016). Prognostic Utility of Molecular Factors by Age at Diagnosis of Colorectal Cancer. Clinical Cancer Research, 22(6), 1489. doi:10.1158/1078-0432.CCR-15-0946

McCubrey, J. A., Steelman, L. S., Chappell, W. H., Abrams, S. L., Wong, E. W., Chang, F., . . . Franklin, R. A. (2007). Roles of the Raf/MEK/ERK pathway in cell growth, malignant transformation and drug resistance. Biochim Biophys Acta, 1773(8), 1263-1284. doi:10.1016/j.bbamcr.2006.10.001

McIntire, P. J., Irshaid, L., Liu, Y., Chen, Z., Menken, F., Nowak, E., . . . Ginter, P. S. (2018). Hot Spot and Whole-Tumor Enumeration of CD8(+) Tumor-Infiltrating Lymphocytes Utilizing Digital Image Analysis Is Prognostic in Triple-Negative Breast Cancer. Clin Breast Cancer, 18(6), 451-458.e451. doi:10.1016/j.clbc.2018.04.019

Mei, Z., Shao, Y. W., Lin, P., Cai, X., Wang, B., Ding, Y., . . . Gu, Y. (2018). SMAD4 and NF1 mutations as potential biomarkers for poor prognosis to cetuximab-based therapy in Chinese metastatic colorectal cancer patients. BMC cancer, 18(1), 479. doi:10.1186/s12885-018-4298-5

Meisel, R., Zibert, A., Laryea, M., Göbel, U., Däubener, W., & Dilloo, D. (2004). Human bone marrow stromal cells inhibit allogeneic T-cell responses by indoleamine 2,3-dioxygenase-mediated tryptophan degradation. Blood, 103(12), 4619-4621. doi:10.1182/blood-2003-11-3909

Mendoza, M. C., Er, E. E., & Blenis, J. (2011). The Ras-ERK and PI3K-mTOR pathways: cross-talk and compensation. Trends in Biochemical Sciences, 36(6), 320-328. doi:https://doi.org/10.1016/j.tibs.2011.03.006

Messa, C., Russo, F., Caruso, M. G., & Di Leo, A. (1998). EGF, TGF-alpha, and EGF-R in human colorectal adenocarcinoma. Acta Oncol, 37(3), 285-289. doi:10.1080/028418698429595

Michael-Robinson, J. M., Biemer-Hüttmann, A., Purdie, D. M., Walsh, M. D., Simms, L. A., Biden, K. G., . . . Radford-Smith, G. L. (2001). Tumour infiltrating lymphocytes and apoptosis are independent features in colorectal cancer stratified according to microsatellite instability status. Gut, 48(3), 360-366. doi:10.1136/gut.48.3.360

Midthun, L., Shaheen, S., Deisch, J., Senthil, M., Tsai, J., & Hsueh, C.-T. (2019). Concomitant *KRAS* and *BRAF* mutations in colorectal cancer. Journal of gastrointestinal oncology, 10(3), 577-581. doi:10.21037/jgo.2019.01.10

Millis, S. Z., Ikeda, S., Reddy, S., Gatalica, Z., & Kurzrock, R. (2016). Landscape of Phosphatidylinositol-3-Kinase Pathway Alterations Across 19 784 Diverse Solid Tumors. JAMA Oncol, 2(12), 1565-1573. doi:10.1001/jamaoncol.2016.0891

Mlecnik, B., Bindea, G., Angell, H. K., Maby, P., Angelova, M., Tougeron, D., . . . Galon, J. (2016). Integrative Analyses of Colorectal Cancer Show Immunoscore Is a Stronger Predictor of Patient Survival Than

Microsatellite Instability. Immunity, 44(3), 698-711. doi:https://doi.org/10.1016/j.immuni.2016.02.025

Mlecnik, B., Bindea, G., Angell, H. K., Sasso, M. S., Obenauf, A. C., Fredriksen, T., . . . Galon, J. (2014). Functional Network Pipeline Reveals Genetic Determinants Associated with in Situ Lymphocyte Proliferation and Survival of Cancer Patients. Science Translational Medicine, 6(228), 228ra237. doi:10.1126/scitranslmed.3007240

Moerkerk, P., Arends, J. W., van Driel, M., de Bruïne, A., de Goeij, A., & ten Kate, J. (1994). Type and number of Ki-ras point mutations relate to stage of human colorectal cancer. Cancer Res, 54(13), 3376-3378.

Molinari, F., & Frattini, M. (2013). Functions and Regulation of the PTEN Gene in Colorectal Cancer. Front Oncol, 3, 326. doi:10.3389/fonc.2013.00326

Morikawa, T., Kuchiba, A., Yamauchi, M., Meyerhardt, J. A., Shima, K., Nosho, K., . . . Ogino, S. (2011). Association of CTNNB1 (beta-catenin) alterations, body mass index, and physical activity with survival in patients with colorectal cancer. Jama, 305(16), 1685-1694. doi:10.1001/jama.2011.513

Mueller, A., Bachmann, E., Linnig, M., Khillimberger, K., Schimanski, C. C., Galle, P. R., & Moehler, M. (2012). Selective PI3K inhibition by BKM120 and BEZ235 alone or in combination with chemotherapy in wild-type and mutated human gastrointestinal cancer cell lines. Cancer chemotherapy and pharmacology, 69(6), 1601-1615. doi:10.1007/s00280-012-1869-z

Multhaupt, H. A., Leitinger, B., Gullberg, D., & Couchman, J. R. (2016). Extracellular matrix component signaling in cancer. Adv Drug Deliv Rev, 97, 28-40. doi:10.1016/j.addr.2015.10.013

Mundi, P. S., Sachdev, J., McCourt, C., & Kalinsky, K. (2016). AKT in cancer: new molecular insights and advances in drug development. British journal of clinical pharmacology, 82(4), 943-956. doi:10.1111/bcp.13021

Munro, A. J., Lain, S., & Lane, D. P. (2005). P53 abnormalities and outcomes in colorectal cancer: a systematic review. British Journal of Cancer, 92(3), 434-444. doi:10.1038/sj.bjc.6602358

Murcia, O., Juárez, M., Rodríguez-Soler, M., Hernández-Illán, E., Giner-Calabuig, M., Alustiza, M., . . . Jover, R. (2018). Colorectal cancer molecular classification using *BRAF*, *KRAS*, microsatellite instability and CIMP status: Prognostic implications and response to chemotherapy. PloS one, 13(9), e0203051-e0203051. doi:10.1371/journal.pone.0203051

Murnyák, B., & Hortobágyi, T. (2016). Immunohistochemical correlates of *TP53* somatic mutations in cancer. Oncotarget, 7(40), 64910-64920. doi:10.18632/oncotarget.11912

Murphy, C. C., Sanoff, H. K., Stitzenberg, K. B., Baron, J. A., Lund, J. L., & Sandler, R. S. (2017). Patterns of Sociodemographic and Clinicopathologic Characteristics of Stages II and III Colorectal Cancer

Patients by Age: Examining Potential Mechanisms of Young-Onset Disease. Journal of cancer epidemiology, 2017, 4024580-4024580. doi:10.1155/2017/4024580

Mutoh, H., Sakurai, S., Satoh, K., Osawa, H., Tomiyama, T., Kita, H., . . . Sugano, K. (2005). Pericryptal fibroblast sheath in intestinal metaplasia and gastric carcinoma. Gut, 54(1), 33-39. doi:10.1136/gut.2004.042770

Muzny, D. M., Bainbridge, M. N., Chang, K., Dinh, H. H., Drummond, J. A., Fowler, G., . . . disease working, g. (2012). Comprehensive molecular characterization of human colon and rectal cancer. Nature, 487(7407), 330-337. doi:10.1038/nature11252

Myung, J. H., Gajjar, K. A., Pearson, R. M., Launiere, C. A., Eddington, D. T., & Hong, S. (2011). Direct Measurements on CD24-Mediated Rolling of Human Breast Cancer MCF-7 Cells on E-Selectin. Analytical Chemistry, 83(3), 1078-1083. doi:10.1021/ac102901e

Naba, A., Clauser, K. R., Hoersch, S., Liu, H., Carr, S. A., & Hynes, R. O. (2012). The Matrisome: In Silico Definition and In Vivo Characterization by Proteomics of Normal and Tumor Extracellular Matrices. Molecular & Cellular Proteomics, 11(4), M111.014647. doi:10.1074/mcp.M111.014647

Naba, A., Clauser, K. R., Lamar, J. M., Carr, S. A., & Hynes, R. O. (2014). Extracellular matrix signatures of human mammary carcinoma identify novel metastasis promoters. eLife, 3, e01308-e01308. doi:10.7554/eLife.01308

Nagasaki, T., Hara, M., Nakanishi, H., Takahashi, H., Sato, M., & Takeyama, H. (2014). Interleukin-6 released by colon cancer-associated fibroblasts is critical for tumour angiogenesis: anti-interleukin-6 receptor antibody suppressed angiogenesis and inhibited tumour-stroma interaction. Br J Cancer, 110(2), 469-478. doi:10.1038/bjc.2013.748

Nagtegaal, I. D., Odze, R. D., Klimstra, D., Paradis, V., Rugge, M., Schirmacher, P., . . . Board, W. H. O. C. o. T. E. (2020). The 2019 WHO classification of tumours of the digestive system. Histopathology, 76(2), 182-188. doi:10.1111/his.13975

Nakayama, M., & Oshima, M. (2018). Mutant p53 in colon cancer. Journal of Molecular Cell Biology, 11(4), 267-276. doi:10.1093/jmcb/mjy075

Narayanan, S., Kawaguchi, T., Peng, X., Qi, Q., Liu, S., Yan, L., & Takabe, K. (2019). Tumor Infiltrating Lymphocytes and Macrophages Improve Survival in Microsatellite Unstable Colorectal Cancer. Scientific Reports, 9(1), 13455. doi:10.1038/s41598-019-49878-4

Narra, K., Mullins, S. R., Lee, H. O., Strzemkowski-Brun, B., Magalong, K., Christiansen, V. J., . . . Cheng, J. D. (2007). Phase II trial of single agent Val-boroPro (Talabostat) inhibiting Fibroblast Activation Protein in patients with metastatic colorectal cancer. Cancer Biol Ther, 6(11), 1691-1699. doi:10.4161/cbt.6.11.4874

Naschberger, E., Liebl, A., Schellerer, V. S., Schütz, M., Britzen-Laurent, N., Kölbel, P., . . . Stürzl, M. (2016). Matricellular protein SPARCL1 regulates tumor microenvironment-dependent endothelial cell heterogeneity in colorectal carcinoma. The Journal of clinical investigation, 126(11), 4187-4204. doi:10.1172/JCI78260

Nassif, N. T., Lobo, G. P., Wu, X., Henderson, C. J. A., Morrison, C. D., Eng, C., . . . Segelov, E. (2004). PTEN mutations are common in sporadic microsatellite stable colorectal cancer. Oncogene, 23(2), 617-628. doi:10.1038/sj.onc.1207059

Nasuno, M., Arimura, Y., Nagaishi, K., Isshiki, H., Onodera, K., Nakagaki, S., . . . Shinomura, Y. (2014). Mesenchymal stem cells cancel azoxymethane-induced tumor initiation. Stem Cells, 32(4), 913-925. doi:10.1002/stem.1594

Natrajan, R., Sailem, H., Mardakheh, F. K., Arias Garcia, M., Tape, C. J., Dowsett, M., . . . Yuan, Y. (2016). Microenvironmental Heterogeneity Parallels Breast Cancer Progression: A Histology–Genomic Integration Analysis. PLOS Medicine, 13(2), e1001961. doi:10.1371/journal.pmed.1001961

Newell, E. W., & Becht, E. (2018). High-Dimensional Profiling of Tumor-Specific Immune Responses: Asking T Cells about What They "See" in Cancer. Cancer Immunol Res, 6(1), 2-9. doi:10.1158/2326-6066.Cir-17-0519

Niu, B., Ye, K., Zhang, Q., Lu, C., Xie, M., McLellan, M. D., . . . Ding, L. (2014). MSIsensor: microsatellite instability detection using paired tumor-normal sequence data. Bioinformatics, 30(7), 1015-1016. doi:10.1093/bioinformatics/btt755

Norton, S. E., Dunn, E. T., McCall, J. L., Munro, F., & Kemp, R. A. (2016). Gut macrophage phenotype is dependent on the tumor microenvironment in colorectal cancer. Clin Transl Immunology, 5(4), e76. doi:10.1038/cti.2016.21

Nosho, K., Kawasaki, T., Ohnishi, M., Suemoto, Y., Kirkner, G. J., Zepf, D., . . . Ogino, S. (2008). *PIK3CA* mutation in colorectal cancer: relationship with genetic and epigenetic alterations. Neoplasia, 10(6), 534-541. doi:10.1593/neo.08336

Nowak, J. A., Yurgelun, M. B., Bruce, J. L., Rojas-Rudilla, V., Hall, D. L., Shivdasani, P., . . . Dong, F. (2017). Detection of Mismatch Repair Deficiency and Microsatellite Instability in Colorectal Adenocarcinoma by Targeted Next-Generation Sequencing. The Journal of molecular diagnostics : JMD, 19(1), 84-91. doi:10.1016/j.jmoldx.2016.07.010

Ogino, S., Cantor, M., Kawasaki, T., Brahmandam, M., Kirkner, G. J., Weisenberger, D. J., . . . Fuchs, C. S. (2006). CpG island methylator phenotype (CIMP) of colorectal cancer is best characterised by quantitative DNA methylation analysis and prospective cohort studies. Gut, 55(7), 1000. doi:10.1136/gut.2005.082933

Ogino, S., & Goel, A. (2008). Molecular classification and correlates in colorectal cancer. The Journal of molecular diagnostics : JMD, 10(1), 13-27. doi:10.2353/jmoldx.2008.070082

Ogino, S., Kawasaki, T., Kirkner, G. J., Ohnishi, M., & Fuchs, C. S. (2007). 18q loss of heterozygosity in microsatellite stable colorectal cancer is correlated with CpG island methylator phenotype-negative (CIMP-0) and inversely with CIMP-low and CIMP-high. BMC cancer, 7, 72-72. doi:10.1186/1471-2407-7-72

Ogino, S., Liao, X., Imamura, Y., Yamauchi, M., McCleary, N. J., Ng, K., . . . Oncology, f. t. A. f. C. T. i. (2013). Predictive and Prognostic Analysis of *PIK3CA* Mutation in Stage III Colon Cancer Intergroup Trial. JNCI: Journal of the National Cancer Institute, 105(23), 1789-1798. doi:10.1093/jnci/djt298

O'Malley, G., Heijltjes, M., Houston, A. M., Rani, S., Ritter, T., Egan, L. J., & Ryan, A. E. (2016). Mesenchymal stromal cells (MSCs) and colorectal cancer: a troublesome twosome for the anti-tumour immune response? Oncotarget, 7(37), 60752-60774. doi:10.18632/oncotarget.11354

Ormerod, M. G., Tribukait, B., & Giaretti, W. (1998). Consensus report of the task force on standardisation of DNA flow cytometry in clinical pathology. DNA Flow Cytometry Task Force of the European Society for Analytical Cellular Pathology. Analytical cellular pathology: the journal of the European Society for Analytical Cellular Pathology, 17(2), 103-110. doi:10.1155/1998/842306

Ostrand-Rosenberg, S., & Sinha, P. (2009). Myeloid-derived suppressor cells: linking inflammation and cancer. Journal of immunology (Baltimore, Md.: 1950), 182(8), 4499-4506. doi:10.4049/jimmunol.0802740

OuYang, L.-Y., Wu, X.-J., Ye, S.-B., Zhang, R.-X., Li, Z.-L., Liao, W., . . . Li, J. (2015). Tumor-induced myeloid-derived suppressor cells promote tumor progression through oxidative metabolism in human colorectal cancer. Journal of translational medicine, 13, 47-47. doi:10.1186/s12967-015-0410-7

Overman, M. J., Lonardi, S., Leone, F., McDermott, R. S., Morse, M. A., Wong, K. Y. M., . . . Andre, T. (2017). Nivolumab in patients with DNA mismatch repair deficient/microsatellite instability high metastatic colorectal cancer: Update from CheckMate 142. Journal of Clinical Oncology, 35(4_suppl), 519-519. doi: 10.1200/JCO.2017.35.4_suppl.519

Overman, M. J., Lonardi, S., Wong, K. Y. M., Lenz, H. J., Gelsomino, F., Aglietta, M., . . . André, T. (2018). Durable Clinical Benefit with Nivolumab Plus Ipilimumab in DNA Mismatch Repair-Deficient/Microsatellite Instability-High Metastatic Colorectal Cancer. J Clin Oncol, 36(8), 773-779. doi:10.1200/jco.2017.76.9901

Özdemir, B. C., Pentcheva-Hoang, T., Carstens, J. L., Zheng, X., Wu, C. C., Simpson, T. R., . . . Kalluri, R. (2014). Depletion of carcinoma-associated fibroblasts and fibrosis induces immunosuppression and accelerates pancreas cancer with reduced survival. Cancer Cell, 25(6), 719-734. doi: 10.1016/j.ccr.2014.04.005

Pagès, F., Mlecnik, B., Marliot, F., Bindea, G., Ou, F. S., Bifulco, C., . . . Galon, J. (2018). International validation of the consensus Immunoscore for the classification of colon cancer: a prognostic and

accuracy study. Lancet, 391(10135), 2128-2139. doi:10.1016/s0140-6736(18)30789-x

Pai, S. G., Carneiro, B. A., Mota, J. M., Costa, R., Leite, C. A., Barroso-Sousa, R., . . . Giles, F. J. (2017). Wnt/beta-catenin pathway: modulating anticancer immune response. Journal of hematology & oncology, 10(1), 101-101. doi:10.1186/s13045-017-0471-6

Paleari, L., Puntoni, M., Clavarezza, M., DeCensi, M., Cuzick, J., & DeCensi, A. (2016). *PIK3CA* Mutation, Aspirin Use after Diagnosis and Survival of Colorectal Cancer. A Systematic Review and Meta-analysis of Epidemiological Studies. Clin Oncol (R Coll Radiol), 28(5), 317-326. doi: 10.1016/j.clon.2015.11.008

Palles, C., Cazier, J. B., Howarth, K. M., Domingo, E., Jones, A. M., Broderick, P., . . . Tomlinson, I. (2013). Germline mutations affecting the proofreading domains of POLE and POLD1 predispose to colorectal adenomas and carcinomas. Nat Genet, 45(2), 136-144. doi:10.1038/ng.2503

Pan, P.-Y., Ma, G., Weber, K. J., Ozao-Choy, J., Wang, G., Yin, B., . . . Chen, S.-H. (2010). Immune stimulatory receptor CD40 is required for T-cell suppression and T regulatory cell activation mediated by myeloid-derived suppressor cells in cancer. Cancer Research, 70(1), 99-108. doi:10.1158/0008-5472.CAN-09-1882

Pasqualone, A., Di Rienzo, V., Sabetta, W., Fanelli, V., Summo, C., Paradiso, V. M., . . . Caponio, F. (2016). Chemical and Molecular Characterization of Crude Oil Obtained by Olive-Pomace Recentrifugation. Journal of Chemistry, 2016, 4347207. doi:10.1155/2016/4347207

Patel, S. A., Meyer, J. R., Greco, S. J., Corcoran, K. E., Bryan, M., & Rameshwar, P. (2010). Mesenchymal stem cells protect breast cancer cells through regulatory T cells: role of mesenchymal stem cell-derived TGF-beta. Journal of immunology (Baltimore, Md. : 1950), 184(10), 5885-5894. doi:10.4049/jimmunol.0903143

Peddareddigari, V. G., Wang, D., & Dubois, R. N. (2010). The tumor microenvironment in colorectal carcinogenesis. Cancer microenvironment : official journal of the International Cancer Microenvironment Society, 3(1), 149-166. doi:10.1007/s12307-010-0038-3

Peeters, M., Oliner, K. S., Price, T. J., Cervantes, A., Sobrero, A. F., Ducreux, M., . . . Patterson, S. D. (2015). Analysis of *KRAS*/NRAS Mutations in a Phase III Study of Panitumumab with FOLFIRI Compared with FOLFIRI Alone as Second-line Treatment for Metastatic Colorectal Cancer. Clin Cancer Res, 21(24), 5469-5479. doi:10.1158/1078-0432.Ccr-15-0526

Peltomäki, P. (2003). Role of DNA mismatch repair defects in the pathogenesis of human cancer. J Clin Oncol, 21(6), 1174-1179. doi:10.1200/jco.2003.04.060

Pentheroudakis, G., Kotoula, V., De Roock, W., Kouvatseas, G., Papakostas, P., Makatsoris, T., . . . Fountzilas, G. (2013). Biomarkers of benefit from cetuximab-based therapy in metastatic colorectal cancer:

interaction of EGFR ligand expression with RAS/RAF, *PIK3CA* genotypes. BMC cancer, 13, 49-49. doi:10.1186/1471-2407-13-49

Phipps, A. I., Buchanan, D. D., Makar, K. W., Win, A. K., Baron, J. A., Lindor, N. M., . . . Newcomb, P. A. (2013). *KRAS*-mutation status in relation to colorectal cancer survival: the joint impact of correlated tumour markers. Br J Cancer, 108(8), 1757-1764. doi:10.1038/bjc.2013.118

Phipps, A. I., Limburg, P. J., Baron, J. A., Burnett-Hartman, A. N., Weisenberger, D. J., Laird, P. W., . . . Newcomb, P. A. (2015). Association between molecular subtypes of colorectal cancer and patient survival. Gastroenterology, 148(1), 77-87.e72. doi:10.1053/j.gastro.2014.09.038

Pietrantonio, F., Cremolini, C., Petrelli, F., Di Bartolomeo, M., Loupakis, F., Maggi, C., . . . Iacovelli, R. (2015). First-line anti-EGFR monoclonal antibodies in panRAS wild-type metastatic colorectal cancer: A systematic review and meta-analysis. Crit Rev Oncol Hematol, 96(1), 156-166. doi:10.1016/j.critrevonc.2015.05.016

Pino, M. S., & Chung, D. C. (2010). The chromosomal instability pathway in colon cancer. Gastroenterology, 138(6), 2059-2072. doi:10.1053/j.gastro.2009.12.065

Pinto, M. L., Rios, E., Durães, C., Ribeiro, R., Machado, J. C., Mantovani, A., . . . Oliveira, M. J. (2019). The Two Faces of Tumor-Associated Macrophages and Their Clinical Significance in Colorectal Cancer. Frontiers in immunology, 10, 1875-1875. doi:10.3389/fimmu.2019.01875

Polakis, P. (2007). The many ways of Wnt in cancer. Current Opinion in Genetics & Development, 17(1), 45-51. doi:https://doi.org/10.1016/j.gde.2006.12.007

Popat, S., & Houlston, R. S. (2005). A systematic review and meta-analysis of the relationship between chromosome 18q genotype, DCC status and colorectal cancer prognosis. European Journal of Cancer, 41(14), 2060-2070. doi:10.1016/j.ejca.2005.04.039

Poynter, J. N., Siegmund, K. D., Weisenberger, D. J., Long, T. I., Thibodeau, S. N., Lindor, N., . . . Laird, P. W. (2008). Molecular Characterization of MSI-H Colorectal Cancer by MLHI Promoter Methylation, Immunohistochemistry, and Mismatch Repair Germline Mutation Screening. Cancer Epidemiology Biomarkers & Prevention, 17(11), 3208. doi:10.1158/1055-9965.EPI-08-0512

Price, T. J., Peeters, M., Kim, T. W., Li, J., Cascinu, S., Ruff, P., . . . Sidhu, R. (2014). Panitumumab versus cetuximab in patients with chemotherapy-refractory wild-type *KRAS* exon 2 metastatic colorectal cancer (ASPECCT): a randomised, multicentre, open-label, non-inferiority phase 3 study. Lancet Oncol, 15(6), 569-579. doi:10.1016/s1470-2045(14)70118-4

Prior, I. A., Lewis, P. D., & Mattos, C. (2012). A comprehensive survey of Ras mutations in cancer. Cancer Research, 72(10), 2457-2467. doi:10.1158/0008-5472.CAN-11-2612

Quail, D. F., & Joyce, J. A. (2013). Microenvironmental regulation of tumor progression and metastasis. Nature medicine, 19(11), 1423-1437. doi:10.1038/nm.3394

Quante, M., Tu, S. P., Tomita, H., Gonda, T., Wang, S. S. W., Takashi, S., . . . Wang, T. C. (2011). Bone marrow-derived myofibroblasts contribute to the mesenchymal stem cell niche and promote tumor growth. Cancer Cell, 19(2), 257-272. doi:10.1016/j.ccr.2011.01.020

Rahbari, N. N., Bork, U., Motschall, E., Thorlund, K., Büchler, M. W., Koch, M., & Weitz, J. (2012). Molecular detection of tumor cells in regional lymph nodes is associated with disease recurrence and poor survival in node-negative colorectal cancer: a systematic review and meta-analysis. J Clin Oncol, 30(1), 60-70. doi:10.1200/jco.2011.36.9504

Rahbari, N. N., Schölch, S., Bork, U., Kahlert, C., Schneider, M., Rahbari, M., . . . Reissfelder, C. (2017). Prognostic value of circulating endothelial cells in metastatic colorectal cancer. Oncotarget, 8(23), 37491-37501. doi:10.18632/oncotarget.16397

Rajagopalan, H., Bardelli, A., Lengauer, C., Kinzler, K. W., Vogelstein, B., & Velculescu, V. E. (2002). RAF/RAS oncogenes and mismatch-repair status. Nature, 418(6901), 934-934. doi:10.1038/418934a

Raposo, T. P., Susanti, S., & Ilyas, M. (2020). Investigating TNS4 in the Colorectal Tumor Microenvironment Using 3D Spheroid Models of Invasion. Advanced Biosystems, 4(6), 2000031. doi:10.1002/adbi.202000031

Rasmusson, A., Zilenaite, D., Nestarenkaite, A., Augulis, R., Laurinaviciene, A., Ostapenko, V., . . . Laurinavicius, A. (2020). Immunogradient Indicators for Antitumor Response Assessment by Automated Tumor-Stroma Interface Zone Detection. The American Journal of Pathology, 190(6), 1309-1322. doi:https://doi.org/10.1016/j.ajpath.2020.01.018

Raut, C. P., Pawlik, T. M., & Rodriguez-Bigas, M. A. (2004). Clinicopathologic features in colorectal cancer patients with microsatellite instability. Mutat Res, 568(2), 275-282. doi:10.1016/j.mrfmmm.2004.05.025

Rawla, P., Sunkara, T., & Barsouk, A. (2019). Epidemiology of colorectal cancer: incidence, mortality, survival, and risk factors. Przeglad gastroenterologiczny, 14(2), 89-103. doi:10.5114/pg.2018.81072

Redford, L., Alhilal, G., Needham, S., O'Brien, O., Coaker, J., Tyson, J., . . . Burn, J. (2018). A novel panel of short mononucleotide repeats linked to informative polymorphisms enabling effective high volume low cost discrimination between mismatch repair deficient and proficient tumours. PloS one, 13(8), e0203052-e0203052. doi:10.1371/journal.pone.0203052

Reggiani Bonetti, L., Barresi, V., Maiorana, A., Manfredini, S., Caprera, C., & Bettelli, S. (2018). Clinical Impact and Prognostic Role of *KRAS*/*BRAF*/*PIK3CA* Mutations in Stage I Colorectal Cancer. Disease markers, 2018, 2959801-2959801. doi:10.1155/2018/2959801

Remark, R., Merghoub, T., Grabe, N., Litjens, G., Damotte, D., Wolchok, J. D., . . . Gnjatic, S. (2016). In-depth tissue profiling using multiplexed immunohistochemical consecutive staining on single slide. Science Immunology, 1(1), aaf6925. doi:10.1126/sciimmunol.aaf6925

Ren, G., Zhang, L., Zhao, X., Xu, G., Zhang, Y., Roberts, A. I., . . . Shi, Y. (2008). Mesenchymal stem cell-mediated immunosuppression occurs via concerted action of chemokines and nitric oxide. Cell Stem Cell, 2(2), 141-150. doi:10.1016/j.stem.2007.11.014

Ren, G., Zhao, X., Wang, Y., Zhang, X., Chen, X., Xu, C., . . . Shi, Y. (2012). CCR2-Dependent Recruitment of Macrophages by Tumor-Educated Mesenchymal Stromal Cells Promotes Tumor Development and Is Mimicked by TNFα. Cell Stem Cell, 11(6), 812-824. doi:https://doi.org/10.1016/j.stem.2012.08.013

Renaud, S., Falcoz, P.-E., Romain, B., Olland, A., Santelmo, N., Brigand, C., . . . Massard, G. (2015). Reply: Comment on '*KRAS* and *BRAF* mutations are prognostic biomarkers in patients undergoing lung metastasectomy of colo-rectal cancer'. British Journal of Cancer, 113(11), 1637-1638. doi:10.1038/bjc.2015.330

Resnick, M. B., Routhier, J., Konkin, T., Sabo, E., & Pricolo, V. E. (2004). Epidermal growth factor receptor, c-MET, beta-catenin, and p53 expression as prognostic indicators in stage II colon cancer: a tissue microarray study. Clin Cancer Res, 10(9), 3069-3075. doi:10.1158/1078-0432.ccr-03-0462

Rho, Y. S., Gilabert, M., Polom, K., Aladashvili, A., Kopeckova, K., Megdanova, V., . . . Kavan, P. (2017). Comparing Clinical Characteristics and Outcomes of Young-onset and Late-onset Colorectal Cancer: An International Collaborative Study. Clin Colorectal Cancer, 16(4), 334-342. doi:10.1016/j.clcc.2017.03.008

Ribic, C. M., Sargent, D. J., Moore, M. J., Thibodeau, S. N., French, A. J., Goldberg, R. M., . . . Gallinger, S. (2003). Tumor microsatellite-instability status as a predictor of benefit from fluorouracil-based adjuvant chemotherapy for colon cancer. The New England journal of medicine, 349(3), 247-257. doi:10.1056/NEJMoa022289

Ried, T., Meijer, G. A., Harrison, D. J., Grech, G., Franch-Expósito, S., Briffa, R., . . . Camps, J. (2019). The landscape of genomic copy number alterations in colorectal cancer and their consequences on gene expression levels and disease outcome. Mol Aspects Med, 69, 48-61. doi:10.1016/j.mam.2019.07.007

Riedl, A., Schlederer, M., Pudelko, K., Stadler, M., Walter, S., Unterleuthner, D., . . . Dolznig, H. (2017). Comparison of cancer cells in 2D vs 3D culture reveals differences in AKT-mTOR-S6K signaling and drug responses. J Cell Sci, 130(1), 203-218. doi:10.1242/jcs.188102

Rodriguez-Salas, N., Dominguez, G., Barderas, R., Mendiola, M., García-Albéniz, X., Maurel, J., & Batlle, J. F. (2017). Clinical relevance of colorectal cancer molecular subtypes. Critical Reviews in Oncology/Hematology, 109, 9-19. doi:https://doi.org/10.1016/j.critrevonc.2016.11.007

Romero-López, M., Trinh, A. L., Sobrino, A., Hatch, M. M. S., Keating, M. T., Fimbres, C., . . . Hughes, C. C. W. (2017). Recapitulating the human tumor microenvironment: Colon tumor-derived extracellular matrix promotes angiogenesis and tumor cell growth. Biomaterials, 116, 118-129. doi:10.1016/j.biomaterials.2016.11.034

Ronnekleiv-Kelly, S. M., Burkhart, R. A., & Pawlik, T. M. (2016). Molecular markers of prognosis and therapeutic targets in metastatic colorectal cancer. Surgical Oncology, 25(3), 190-199. doi:https://doi.org/10.1016/j.suronc.2016.05.018

Rosenbaum, M. W., Bledsoe, J. R., Morales-Oyarvide, V., Huynh, T. G., & Mino-Kenudson, M. (2016). PD-L1 expression in colorectal cancer is associated with microsatellite instability, *BRAF* mutation, medullary morphology and cytotoxic tumor-infiltrating lymphocytes. Mod Pathol, 29(9), 1104-1112. doi:10.1038/modpathol.2016.95

Rosty, C., Young, J. P., Walsh, M. D., Clendenning, M., Sanderson, K., Walters, R. J., . . . Buchanan, D. D. (2013). *PIK3CA* Activating Mutation in Colorectal Carcinoma: Associations with Molecular Features and Survival. PloS one, 8(6), e65479. doi:10.1371/journal.pone.0065479

Roth, A. D., Delorenzi, M., Tejpar, S., Yan, P., Klingbiel, D., Fiocca, R., . . . Van Cutsem, E. (2012). Integrated Analysis of Molecular and Clinical Prognostic Factors in Stage II/III Colon Cancer. JNCI: Journal of the National Cancer Institute, 104(21), 1635-1646. doi:10.1093/jnci/djs427

Rowan, A. J., Lamlum, H., Ilyas, M., Wheeler, J., Straub, J., Papadopoulou, A., . . . Tomlinson, I. P. (2000). APC mutations in sporadic colorectal tumors: A mutational "hotspot" and interdependence of the "two hits". Proc Natl Acad Sci U S A, 97(7), 3352-3357. doi:10.1073/pnas.97.7.3352

Royal Collage of Pathologist (2020). Dataset-for-histopathological-reporting-of-colorectal-cancer. https://www.rcpath.org/uploads/assets/c8b61ba0-ae3f-43f1 85ffd3ab9f17cfe6/G049-Dataset-for-histopathological-reporting-of-colorectal-cancer.pdf. Retrieved in August, 2020.

Runz, S., Mierke, C. T., Joumaa, S., Behrens, J., Fabry, B., & Altevogt, P. (2008). CD24 induces localization of β1 integrin to lipid raft domains. Biochemical and Biophysical Research Communications, 365(1), 35-41. doi:https://doi.org/10.1016/j.bbrc.2007.10.139

Rupp, C., Scherzer, M., Rudisch, A., Unger, C., Haslinger, C., Schweifer, N., . . . Garin-Chesa, P. (2015). IGFBP7, a novel tumor stroma marker, with growth-promoting effects in colon cancer through a paracrine tumor–stroma interaction. Oncogene, 34(7), 815-825. doi:10.1038/onc.2014.18

Russo, A., Bazan, V., Iacopetta, B., Kerr, D., Soussi, T., & Gebbia, N. (2005). The *TP53* colorectal cancer international collaborative study on the prognostic and predictive significance of p53 mutation: influence of tumor site, type of mutation, and adjuvant treatment. J Clin Oncol, 23(30), 7518-7528. doi:10.1200/jco.2005.00.471

Saada, J. I., Pinchuk, I. V., Barrera, C. A., Adegboyega, P. A., Suarez, G., Mifflin, R. C., . . . Powell, D. W. (2006). Subepithelial Myofibroblasts are Novel Nonprofessional APCs in the Human Colonic Mucosa. The Journal of Immunology, 177(9), 5968. doi:10.4049/jimmunol.177.9.5968

Sagiv, E., Memeo, L., Karin, A., Kazanov, D., Jacob-Hirsch, J., Mansukhani, M., . . . Arber, N. (2006). CD24 is a new oncogene, early at the multistep process of colorectal cancer carcinogenesis. Gastroenterology, 131(2), 630-639. doi:10.1053/j.gastro.2006.04.028

Sahin, I. H., Chen, W., Sonbol, M. B., Das, S., Chen, Z., Akce, M., . . . Wu, C. (2019). Analysis of age, tumor-sidedness, and mismatch repair (MMR) genes with response to immune checkpoint inhibitors (ICIs) in MMR-deficient (dMMR) colorectal cancer (CRC) patients (pts): A multi-institutional study. Journal of Clinical Oncology, 37(15_suppl), e15029-e15029. doi:10.1200/JCO.2019.37.15_suppl.e15029

Sahin, I. H., Kazmi, S. M. A., Yorio, J. T., Bhadkamkar, N. A., Kee, B. K., & Garrett, C. R. (2013). Rare Though Not Mutually Exclusive: A Report of Three Cases of Concomitant *KRAS* and *BRAF* Mutation and a Review of the Literature. Journal of Cancer, 4(4), 320-322. doi:10.7150/jca.3619

Salnikov, A. V., Bretz, N. P., Perne, C., Hazin, J., Keller, S., Fogel, M., . . . Altevogt, P. (2013). Antibody targeting of CD24 efficiently retards growth and influences cytokine milieu in experimental carcinomas. British Journal of Cancer, 108(7), 1449-1459. doi:10.1038/bjc.2013.102

Saltz, J., Gupta, R., Hou, L., Kurc, T., Singh, P., Nguyen, V., . . . Thorsson, V. (2018). Spatial Organization and Molecular Correlation of Tumor-Infiltrating Lymphocytes Using Deep Learning on Pathology Images. Cell Rep, 23(1), 181-193.e187. doi:10.1016/j.celrep.2018.03.086

Sammar, M., Gulbins, E., Hilbert, K., Lang, F., & Altevogt, P. (1997). Mouse CD24 as a Signaling Molecule for Integrin-Mediated Cell Binding: Functional and Physical Association with src-Kinases. Biochemical and Biophysical Research Communications, 234(2), 330-334. doi:https://doi.org/10.1006/bbrc.1997.6639

Samowitz, W. S., Powers, M. D., Spirio, L. N., Nollet, F., van Roy, F., & Slattery, M. L. (1999). β-Catenin Mutations Are More Frequent in Small Colorectal Adenomas Than in Larger Adenomas and Invasive Carcinomas. Cancer Research, 59(7), 1442. Retrieved from http://cancerres.aacrjournals.org/content/59/7/1442.abstract

Sanmamed, M. F., Rodriguez, I., Schalper, K. A., Oñate, C., Azpilikueta, A., Rodriguez-Ruiz, M. E., . . . Melero, I. (2015). Nivolumab and Urelumab Enhance Antitumor Activity of Human T Lymphocytes Engrafted in Rag2^{−/−}IL2Rγ^{null} Immunodeficient Mice. Cancer Research, 75(17), 3466-3478. doi:10.1158/0008-5472.Can-14-3510

Sartore-Bianchi, A., Martini, M., Molinari, F., Veronese, S., Nichelatti, M., Artale, S., . . . Bardelli, A. (2009). *PIK3CA* mutations in colorectal

cancer are associated with clinical resistance to EGFR-targeted monoclonal antibodies. Cancer Res, 69(5), 1851-1857. doi:10.1158/0008-5472.Can-08-2466

Sato, T., Stange, D. E., Ferrante, M., Vries, R. G. J., van Es, J. H., van den Brink, S., . . . Clevers, H. (2011). Long-term Expansion of Epithelial Organoids From Human Colon, Adenoma, Adenocarcinoma, and Barrett's Epithelium. Gastroenterology, 141(5), 1762-1772. doi:10.1053/j.gastro.2011.07.050

Sawai, H., Yasuda, A., Ochi, N., Ma, J., Matsuo, Y., Wakasugi, T., . . . Takeyama, H. (2008). Loss of PTEN expression is associated with colorectal cancer liver metastasis and poor patient survival. BMC gastroenterology, 8, 56-56. doi:10.1186/1471-230X-8-56

Scaltriti, M., & Baselga, J. (2006). The Epidermal Growth Factor Receptor Pathway: A Model for Targeted Therapy. Clinical Cancer Research, 12(18), 5268. doi:10.1158/1078-0432.CCR-05-1554

Schabath, H., Runz, S., Joumaa, S., & Altevogt, P. (2006). CD24 affects CXCR4 function in pre-B lymphocytes and breast carcinoma cells. Journal of Cell Science, 119(2), 314. doi:10.1242/jcs.02741

Schatoff, E. M., Leach, B. I., & Dow, L. E. (2017). Wnt Signaling and Colorectal Cancer. Current colorectal cancer reports, 13(2), 101-110. doi:10.1007/s11888-017-0354-9

Schell, M. J., Yang, M., Teer, J. K., Lo, F. Y., Madan, A., Coppola, D., . . . Yeatman, T. J. (2016). A multigene mutation classification of 468 colorectal cancers reveals a prognostic role for APC. Nature Communications, 7(1), 11743. doi:10.1038/ncomms11743

Schmoll, H. J., Van Cutsem, E., Stein, A., Valentini, V., Glimelius, B., Haustermans, K., . . . Cervantes, A. (2012). ESMO Consensus Guidelines for management of patients with colon and rectal cancer. A personalized approach to clinical decision making. Annals of Oncology, 23(10), 2479-2516. doi:https://doi.org/10.1093/annonc/mds236

Schwitalle, Y., Kloor, M., Eiermann, S., Linnebacher, M., Kienle, P., Knaebel, H. P., . . . von Knebel Doeberitz, M. (2008). Immune response against frameshift-induced neopeptides in HNPCC patients and healthy HNPCC mutation carriers. Gastroenterology, 134(4), 988-997. doi:10.1053/j.gastro.2008.01.015

Sconocchia, G., Eppenberger, S., Spagnoli, G. C., Tornillo, L., Droeser, R., Caratelli, S., . . . Ferrone, S. (2014). NK cells and T cells cooperate during the clinical course of colorectal cancer. Oncoimmunology, 3(8), e952197-e952197. doi:10.4161/21624011.2014.952197

Scott, A. M., Wiseman, G., Welt, S., Adjei, A., Lee, F.-T., Hopkins, W., . . . Old, L. J. (2003). A Phase I Dose-Escalation Study of Sibrotuzumab in Patients with Advanced or Metastatic Fibroblast Activation Protein-positive Cancer. Clinical Cancer Research, 9(5), 1639. Retrieved from http://clincancerres.aacrjournals.org/content/9/5/1639.abstract

Sefrioui, D., Vermeulin, T., Blanchard, F., Chapusot, C., Beaussire, L., Armengol-Debeir, L., . . . Di Fiore, F. (2017). Copy number variations

in DCC/18q and ERBB2/17q are associated with disease-free survival in microsatellite stable colon cancer. International Journal of Cancer, 140(7), 1653-1661. doi:10.1002/ijc.30584

Seliger, B. (2019). The Role of the Lymphocyte Functional Crosstalk and Regulation in the Context of Checkpoint Inhibitor Treatment—Review. Frontiers in immunology, 10(2043). doi:10.3389/fimmu.2019.02043

Sensi, F., D'Angelo, E., Piccoli, M., Pavan, P., Mastrotto, F., Caliceti, P., . . . Agostini, M. (2020). Recellularized Colorectal Cancer Patient-Derived Scaffolds as In Vitro Pre-Clinical 3D Model for Drug Screening. Cancers, 12(3), 681. Retrieved from https://www.mdpi.com/2072-6694/12/3/681

Sepulveda, A. R., Hamilton, S. R., Allegra, C. J., Grody, W., Cushman-Vokoun, A. M., Funkhouser, W. K., . . . Nowak, J. A. (2017). Molecular Biomarkers for the Evaluation of Colorectal Cancer: Guideline From the American Society for Clinical Pathology, College of American Pathologists, Association for Molecular Pathology, and American Society of Clinical Oncology. The Journal of molecular diagnostics : JMD, 19(2), 187-225. doi:10.1016/j.jmoldx.2016.11.001

Shabo, I., Olsson, H., Elkarim, R., Sun, X. F., & Svanvik, J. (2014). Macrophage Infiltration in Tumor Stroma is Related to Tumor Cell Expression of CD163 in Colorectal Cancer. Cancer microenvironment : official journal of the International Cancer Microenvironment Society, 7(1-2), 61-69. doi:10.1007/s12307-014-0145-7

Sharma, P., & Allison, James P. (2015). Immune Checkpoint Targeting in Cancer Therapy: Toward Combination Strategies with Curative Potential. Cell, 161(2), 205-214. doi:https://doi.org/10.1016/j.cell.2015.03.030

Sheffer, M., Bacolod, M. D., Zuk, O., Giardina, S. F., Pincas, H., Barany, F., . . . Domany, E. (2009). Association of survival and disease progression with chromosomal instability: a genomic exploration of colorectal cancer. Proc Natl Acad Sci U S A, 106(17), 7131-7136. doi:10.1073/pnas.0902232106

Shen, Y., Han, X., Wang, J., Wang, S., Yang, H., Lu, S.-H., & Shi, Y. (2016). Prognostic impact of mutation profiling in patients with stage II and III colon cancer. Scientific Reports, 6(1), 24310. doi:10.1038/srep24310

Shi, Y., Du, L., Lin, L., & Wang, Y. (2017). Tumour-associated mesenchymal stem/stromal cells: emerging therapeutic targets. Nature reviews. Drug discovery, 16(1), 35-52. doi:10.1038/nrd.2016.193

Shi, Y., Su, J., Roberts, A. I., Shou, P., Rabson, A. B., & Ren, G. (2012). How mesenchymal stem cells interact with tissue immune responses. Trends in immunology, 33(3), 136-143. doi:10.1016/j.it.2011.11.004

Shiga, K., Hara, M., Nagasaki, T., Sato, T., Takahashi, H., & Takeyama, H. (2015). Cancer-Associated Fibroblasts: Their Characteristics and Their Roles in Tumor Growth. Cancers, 7(4), 2443-2458. doi:10.3390/cancers7040902

Shima, K., Morikawa, T., Yamauchi, M., Kuchiba, A., Imamura, Y., Liao, X., . . . Ogino, S. (2011). TGFBR2 and BAX Mononucleotide Tract Mutations, Microsatellite Instability, and Prognosis in 1072 Colorectal Cancers. PloS one, 6(9), e25062. doi:10.1371/journal.pone.0025062

Shimizu, T., Tolcher, A. W., Papadopoulos, K. P., Beeram, M., Rasco, D. W., Smith, L. S., . . . Patnaik, A. (2012). The clinical effect of the dual-targeting strategy involving PI3K/AKT/mTOR and RAS/MEK/ERK pathways in patients with advanced cancer. Clin Cancer Res, 18(8), 2316-2325. doi:10.1158/1078-0432.Ccr-11-2381

Shinagawa, K., Kitadai, Y., Tanaka, M., Sumida, T., Kodama, M., Higashi, Y., . . . Chayama, K. (2010). Mesenchymal stem cells enhance growth and metastasis of colon cancer. Int J Cancer, 127(10), 2323-2333. doi:10.1002/ijc.25440

Silver, A., Sengupta, N., Propper, D., Wilson, P., Hagemann, T., Patel, A., . . . Suraweera, N. (2012). A distinct DNA methylation profile associated with microsatellite and chromosomal stable sporadic colorectal cancers. International Journal of Cancer, 130(5), 1082-1092. doi:10.1002/ijc.26104

Simon-Assmann, P., Kedinger, M., De Arcangelis, A., Rousseau, V., & Simo, P. (1995). Extracellular matrix components in intestinal development. Experientia, 51(9-10), 883-900. doi:10.1007/bf01921739

Simons, C. C. J. M., Hughes, L. A. E., Smits, K. M., Khalid-de Bakker, C. A., de Bruïne, A. P., Carvalho, B., . . . van Engeland, M. (2013). A novel classification of colorectal tumors based on microsatellite instability, the CpG island methylator phenotype and chromosomal instability: implications for prognosis. Annals of Oncology, 24(8), 2048-2056. doi:https://doi.org/10.1093/annonc/mdt076

Smith, G., Carey, F. A., Beattie, J., Wilkie, M. J. V., Lightfoot, T. J., Coxhead, J., . . . Wolf, C. R. (2002). Mutations in APC, Kirsten-ras, and p53—alternative genetic pathways to colorectal cancer. Proceedings of the National Academy of Sciences, 99(14), 9433. doi:10.1073/pnas.122612899

Smith, S. C., Oxford, G., Wu, Z., Nitz, M. D., Conaway, M., Frierson, H. F., . . . Theodorescu, D. (2006). The Metastasis-Associated Gene CD24 Is Regulated by Ral GTPase and Is a Mediator of Cell Proliferation and Survival in Human Cancer. Cancer Research, 66(4), 1917. doi:10.1158/0008-5472.CAN-05-3855

Snowsill, T., Coelho, H., Huxley, N., Jones-Hughes, T., Briscoe, S., Frayling, I. M., & Hyde, C. (2017). Molecular testing for Lynch syndrome in people with colorectal cancer: systematic reviews and economic evaluation. Health Technol Assess, 21(51), 1-238. doi:10.3310/hta21510

Sorich, M. J., Wiese, M. D., Rowland, A., Kichenadasse, G., McKinnon, R. A., & Karapetis, C. S. (2015). Extended RAS mutations and anti-EGFR monoclonal antibody survival benefit in metastatic colorectal cancer: a meta-analysis of randomized, controlled trials. Annals of Oncology, 26(1), 13-21. doi:https://doi.org/10.1093/annonc/mdu378

Sottoriva, A., Kang, H., Ma, Z., Graham, T. A., Salomon, M. P., Zhao, J., . . . Curtis, C. (2015). A Big Bang model of human colorectal tumor growth. Nature Genetics, 47(3), 209-216. doi:10.1038/ng.3214

Soussi, T., & Béroud, C. (2003). Significance of *TP53* mutations in human cancer: A critical analysis of mutations at CpG dinucleotides. Human Mutation, 21(3), 192-200. doi:10.1002/humu.10189

Spaggiari, G. M., Capobianco, A., Abdelrazik, H., Becchetti, F., Mingari, M. C., & Moretta, L. (2008). Mesenchymal stem cells inhibit natural killer-cell proliferation, cytotoxicity, and cytokine production: role of indoleamine 2,3-dioxygenase and prostaglandin E2. Blood, 111(3), 1327-1333. doi:10.1182/blood-2007-02-074997

Spranger, S., & Gajewski, T. F. (2018). Impact of oncogenic pathways on evasion of antitumour immune responses. Nature reviews. Cancer, 18(3), 139-147. doi:10.1038/nrc.2017.117

Stack, E. C., Wang, C., Roman, K. A., & Hoyt, C. C. (2014). Multiplexed immunohistochemistry, imaging, and quantitation: a review, with an assessment of Tyramide signal amplification, multispectral imaging and multiplex analysis. Methods, 70(1), 46-58. doi:10.1016/j.ymeth.2014.08.016

Stagg, J. (2008). Mesenchymal stem cells in cancer. Stem Cell Rev, 4(2), 119-124. doi:10.1007/s12015-008-9030-4

Stein, M. N., Bertino, J. R., Kaufman, H. L., Mayer, T., Moss, R., Silk, A., . . . Mehnert, J. M. (2017). First-in-Human Clinical Trial of Oral ONC201 in Patients with Refractory Solid Tumors. Clin Cancer Res, 23(15), 4163-4169. doi:10.1158/1078-0432.Ccr-16-2658

Steinbrunn, T., Stühmer, T., Sayehli, C., Chatterjee, M., Einsele, H., & Bargou, R. C. (2012). Combined targeting of MEK/MAPK and PI3K/Akt signalling in multiple myeloma. British Journal of Haematology, 159(4), 430-440. doi:10.1111/bjh.12039

Stewart, S., Wickramasinghe, D., Dorrance, A. E., & Robertson, A. E. (2011). Comparison of three microsatellite analysis methods for detecting genetic diversity in Phytophthora sojae (Stramenopila: Oomycete). Biotechnology Letters, 33(11), 2217. doi:10.1007/s10529-011-0682-9

Stoffel, E., Mukherjee, B., Raymond, V. M., Tayob, N., Kastrinos, F., Sparr, J., . . . Gruber, S. B. (2009). Calculation of risk of colorectal and endometrial cancer among patients with Lynch syndrome. Gastroenterology, 137(5), 1621-1627. doi:10.1053/j.gastro.2009.07.039

Su, J., Chen, X., Huang, Y., Li, W., Li, J., Cao, K., . . . Shi, Y. (2014). Phylogenetic distinction of iNOS and IDO function in mesenchymal stem cell-mediated immunosuppression in mammalian species. Cell Death & Differentiation, 21(3), 388-396. doi:10.1038/cdd.2013.149

Su, N., Peng, L., Xia, B., Zhao, Y., Xu, A., Wang, J., . . . Jiang, B. (2012). Lyn is involved in CD24-induced ERK1/2 activation in colorectal cancer. Molecular cancer, 11(1), 43. doi:10.1186/1476-4598-11-43

Sugita, J., Ohtani, H., Mizoi, T., Saito, K., Shiiba, K., Sasaki, I., . . . Nagura, H. (2002). Close association between Fas ligand (FasL; CD95L)-positive tumor-associated macrophages and apoptotic cancer cells along invasive margin of colorectal carcinoma: a proposal on tumor-host interactions. Japanese journal of cancer research : Gann, 93(3), 320-328. doi:10.1111/j.1349-7006.2002.tb02175.x

Sun, H.-L., Zhou, X., Xue, Y.-F., Wang, K., Shen, Y.-F., Mao, J.-J., . . . Miao, Z.-N. (2012). Increased frequency and clinical significance of myeloid-derived suppressor cells in human colorectal carcinoma. World journal of gastroenterology, 18(25), 3303-3309. doi:10.3748/wjg.v18.i25.3303

Suraweera, N., Duval, A., Reperant, M., Vaury, C., Furlan, D., Leroy, K., . . . Hamelin, R. (2002). Evaluation of tumor microsatellite instability using five quasimonomorphic mononucleotide repeats and pentaplex PCR. Gastroenterology, 123(6), 1804-1811. doi:10.1053/gast.2002.37070

Susanti, S., Fadhil, W., Ebili, H. O., Asiri, A., Nestarenkaite, A., Hadjimichael, E., . . . Ilyas, M. (2018). N_LyST: a simple and rapid screening test for Lynch syndrome. Journal of clinical pathology, 71(8), 713-720. doi:10.1136/jclinpath-2018-205013

Susanti, S., Fadhil, W., Murtaza, S., Hassall, J. C., Ebili, H. O., Oniscu, A., & Ilyas, M. (2018). Positive association of *PIK3CA* mutation with *KRAS* mutation but not *BRAF* mutation in colorectal cancer suggests co-selection is gene specific but not pathway specific. Journal of clinical pathology, jclinpath-2018-205483. doi:10.1136/jclinpath-2018-205483

Taieb, J., Le Malicot, K., Shi, Q., Penault-Llorca, F., Bouché, O., Tabernero, J., . . . Sinicrope, F. A. (2017). Prognostic Value of *BRAF* and *KRAS* Mutations in MSI and MSS Stage III Colon Cancer. J Natl Cancer Inst, 109(5). doi:10.1093/jnci/djw272

Taieb, J., Malicot, K. L., Penault-Llorca, F. M., Bouche, O., Shi, Q., Thibodeau, S. N., . . . Sinicrope, F. A. (2015). Prognostic value of *BRAF* V600E and *KRAS* exon 2 mutations in microsatellite stable (MSS), stage III colon cancers (CC) from patients (pts) treated with adjuvant FOLFOX+/- cetuximab: A pooled analysis of 3934 pts from the PETACC8 and N0147 trials. Journal of Clinical Oncology, 33(15_suppl), 3507-3507. doi:10.1200/jco.2015.33.15_suppl.3507

Tan, Y., Zhao, M., Xiang, B., Chang, C., & Lu, Q. (2016). CD24: from a Hematopoietic Differentiation Antigen to a Genetic Risk Factor for Multiple Autoimmune Diseases. Clinical Reviews in Allergy & Immunology, 50(1), 70-83. doi:10.1007/s12016-015-8470-2

Tanis, E., Julié, C., Emile, J. F., Mauer, M., Nordlinger, B., Aust, D., . . . Ruers, T. (2015). Prognostic impact of immune response in resectable colorectal liver metastases treated by surgery alone or surgery with perioperative FOLFOX in the randomised EORTC study 40983. Eur J Cancer, 51(17), 2708-2717. doi:10.1016/j.ejca.2015.08.014

Tariq, K., & Ghias, K. (2016). Colorectal cancer carcinogenesis: a review of mechanisms. Cancer biology & medicine, 13(1), 120-135. doi:10.28092/j.issn.2095-3941.2015.0103

Taube, J. M., Klein, A., Brahmer, J. R., Xu, H., Pan, X., Kim, J. H., . . . Anders, R. A. (2014). Association of PD-1, PD-1 Ligands, and Other Features of the Tumor Immune Microenvironment with Response to Anti–PD-1 Therapy. Clinical Cancer Research, 20(19), 5064. doi:10.1158/1078-0432.CCR-13-3271

Tauriello, D. V. F., & Batlle, E. (2016). Targeting the Microenvironment in Advanced Colorectal Cancer. Trends in Cancer, 2(9), 495-504. doi:https://doi.org/10.1016/j.trecan.2016.08.001

Taylor, C. F. (2009). Mutation scanning using high-resolution melting. Biochem Soc Trans, 37(Pt 2), 433-437. doi:10.1042/bst0370433

Testa, J. R., & Bellacosa, A. (2001). AKT plays a central role in tumorigenesis. Proc Natl Acad Sci U S A, 98(20), 10983-10985. doi:10.1073/pnas.211430998

Therkildsen, C., Bergmann, T. K., Henrichsen-Schnack, T., Ladelund, S., & Nilbert, M. (2014). The predictive value of *KRAS*, NRAS, *BRAF*, *PIK3CA* and PTEN for anti-EGFR treatment in metastatic colorectal cancer: A systematic review and meta-analysis. Acta Oncol, 53(7), 852-864. doi:10.3109/0284186x.2014.895036

Thiel, A., Heinonen, M., Kantonen, J., Gylling, A., Lahtinen, L., Korhonen, M., . . . Ristimäki, A. (2013). *BRAF* mutation in sporadic colorectal cancer and Lynch syndrome. Virchows Arch, 463(5), 613-621. doi:10.1007/s00428-013-1470-9

Thorsson, V., Gibbs, D. L., Brown, S. D., Wolf, D., Bortone, D. S., Ou Yang, T.-H., . . . Shmulevich, I. (2018). The Immune Landscape of Cancer. Immunity, 48(4), 812-830.e814. doi:https://doi.org/10.1016/j.immuni.2018.03.023

Tian, S., Simon, I., Moreno, V., Roepman, P., Tabernero, J., Snel, M., . . . Capella, G. (2013). A combined oncogenic pathway signature of *BRAF*, *KRAS* and PI3KCA mutation improves colorectal cancer classification and cetuximab treatment prediction. Gut, 62(4), 540-549. doi:10.1136/gutjnl-2012-302423

Tie, J., Gibbs, P., Lipton, L., Christie, M., Jorissen, R. N., Burgess, A. W., . . . Desai, J. (2011). Optimizing targeted therapeutic development: analysis of a colorectal cancer patient population with the *BRAF*(V600E) mutation. Int J Cancer, 128(9), 2075-2084. doi:10.1002/ijc.25555

Tilg, H., Adolph, T. E., Gerner, R. R., & Moschen, A. R. (2018). The Intestinal Microbiota in Colorectal Cancer. Cancer Cell, 33(6), 954-964. doi:https://doi.org/10.1016/j.ccell.2018.03.004

Tintelnot, J., & Stein, A. (2019). Immunotherapy in colorectal cancer: Available clinical evidence, challenges and novel approaches. World journal of gastroenterology, 25(29), 3920-3928. doi:10.3748/wjg.v25.i29.3920

Tlsty, T. D., & Hein, P. W. (2001). Know thy neighbor: stromal cells can contribute oncogenic signals. Curr Opin Genet Dev, 11(1), 54-59. doi:10.1016/s0959-437x(00)00156-8

Tolcher, A. W., Peng, W., & Calvo, E. (2018). Rational Approaches for Combination Therapy Strategies Targeting the MAP Kinase Pathway in Solid Tumors. Mol Cancer Ther, 17(1), 3-16. doi:10.1158/1535-7163.Mct-17-0349

Tommelein, J., Verset, L., Boterberg, T., Demetter, P., Bracke, M., & De Wever, O. (2015). Cancer-associated fibroblasts connect metastasis-promoting communication in colorectal cancer. Front Oncol, 5, 63. doi:10.3389/fonc.2015.00063

Toyota, M., Ahuja, N., Ohe-Toyota, M., Herman, J. G., Baylin, S. B., & Issa, J. P. (1999). CpG island methylator phenotype in colorectal cancer. Proc Natl Acad Sci U S A, 96(15), 8681-8686. doi:10.1073/pnas.96.15.8681

Trinh, A., Trumpi, K., De Sousa, E. M. F., Wang, X., de Jong, J. H., Fessler, E., . . . Vermeulen, L. (2017). Practical and Robust Identification of Molecular Subtypes in Colorectal Cancer by Immunohistochemistry. Clin Cancer Res, 23(2), 387-398. doi:10.1158/1078-0432.Ccr-16-0680

Tsujino, T., Seshimo, I., Yamamoto, H., Ngan, C. Y., Ezumi, K., Takemasa, I., . . . Monden, M. (2007). Stromal myofibroblasts predict disease recurrence for colorectal cancer. Clin Cancer Res, 13(7), 2082-2090. doi:10.1158/1078-0432.Ccr-06-2191

Tsurui, H., Nishimura, H., Hattori, S., Hirose, S., Okumura, K., & Shirai, T. (2000). Seven-color fluorescence imaging of tissue samples based on Fourier spectroscopy and singular value decomposition. J Histochem Cytochem, 48(5), 653-662. doi:10.1177/002215540004800509

Tumeh, P. C., Harview, C. L., Yearley, J. H., Shintaku, I. P., Taylor, E. J. M., Robert, L., . . . Ribas, A. (2014). PD-1 blockade induces responses by inhibiting adaptive immune resistance. Nature, 515(7528), 568-571. doi:10.1038/nature13954

Turley, S. J., Cremasco, V., & Astarita, J. L. (2015). Immunological hallmarks of stromal cells in the tumour microenvironment. Nature reviews. Immunology, 15(11), 669-682. doi:10.1038/nri3902

Umansky, V., Blattner, C., Gebhardt, C., & Utikal, J. (2016). The Role of Myeloid-Derived Suppressor Cells (MDSC) in Cancer Progression. Vaccines (Basel), 4(4). doi:10.3390/vaccines4040036

Umar, A., Boland, C. R., Terdiman, J. P., Syngal, S., de la Chapelle, A., Rüschoff, J., . . . Srivastava, S. (2004). Revised Bethesda Guidelines for hereditary nonpolyposis colorectal cancer (Lynch syndrome) and microsatellite instability. J Natl Cancer Inst, 96(4), 261-268. doi:10.1093/jnci/djh034

Vakiani, E. (2017). Molecular Testing of Colorectal Cancer in the Modern Era: What Are We Doing and Why? Surgical Pathology Clinics, 10(4), 1009-1020. doi:https://doi.org/10.1016/j.path.2017.07.013

Van Cutsem, E., Cervantes, A., Adam, R., Sobrero, A., Van Krieken, J. H., Aderka, D., . . . Arnold, D. (2016). ESMO consensus guidelines for the management of patients with metastatic colorectal cancer. Annals of Oncology, 27(8), 1386-1422. doi:10.1093/annonc/mdw235

Van Cutsem, E., Cervantes, A., Nordlinger, B., & Arnold, D. (2014). Metastatic colorectal cancer: ESMO Clinical Practice Guidelines for diagnosis, treatment and follow-up &#x2020. Annals of Oncology, 25, iii1-iii9. doi:10.1093/annonc/mdu260

Van Cutsem, E., Köhne, C. H., Láng, I., Folprecht, G., Nowacki, M. P., Cascinu, S., . . . Ciardiello, F. (2011). Cetuximab plus irinotecan, fluorouracil, and leucovorin as first-line treatment for metastatic colorectal cancer: updated analysis of overall survival according to tumor *KRAS* and *BRAF* mutation status. J Clin Oncol, 29(15), 2011-2019. doi:10.1200/jco.2010.33.5091

Van Cutsem, E., Peeters, M., Siena, S., Humblet, Y., Hendlisz, A., Neyns, B., . . . Amado, R. G. (2007). Open-label phase III trial of panitumumab plus best supportive care compared with best supportive care alone in patients with chemotherapy-refractory metastatic colorectal cancer. J Clin Oncol, 25(13), 1658-1664. doi:10.1200/jco.2006.08.1620

van Dijk, E., Biesma, H. D., Cordes, M., Smeets, D., Neerincx, M., Das, S., . . . Ylstra, B. (2018). Loss of Chromosome 18q11.2-q12.1 Is Predictive for Survival in Patients With Metastatic Colorectal Cancer Treated With Bevacizumab. J Clin Oncol, 36(20), 2052-2060. doi:10.1200/jco.2017.77.1782

Vaughn, C. P., Zobell, S. D., Furtado, L. V., Baker, C. L., & Samowitz, W. S. (2011). Frequency of *KRAS*, *BRAF*, and NRAS mutations in colorectal cancer. Genes Chromosomes Cancer, 50(5), 307-312. doi:10.1002/gcc.20854

Veigl, M. L., Kasturi, L., Olechnowicz, J., Ma, A. H., Lutterbaugh, J. D., Periyasamy, S., . . . Markowitz, S. D. (1998). Biallelic inactivation of hMLH1 by epigenetic gene silencing, a novel mechanism causing human MSI cancers. Proceedings of the National Academy of Sciences of the United States of America, 95(15), 8698-8702. doi:10.1073/pnas.95.15.8698

Velho, S., Moutinho, C., Cirnes, L., Albuquerque, C., Hamelin, R., Schmitt, F., . . . Seruca, R. (2008). *BRAF*, *KRAS* and *PIK3CA* mutations in colorectal serrated polyps and cancer: Primary or secondary genetic events in colorectal carcinogenesis? BMC cancer, 8(1), 255. doi:10.1186/1471-2407-8-255

Vilar, E., & Gruber, S. B. (2010). Microsatellite instability in colorectal cancer-the stable evidence. Nat Rev Clin Oncol, 7(3), 153-162. doi:10.1038/nrclinonc.2009.237

Vittal, A., Middinti, A., & Kasi Loknath Kumar, A. (2017). Are All Mutations the Same? A Rare Case Report of Coexisting Mutually Exclusive *KRAS* and *BRAF* Mutations in a Patient with Metastatic Colon Adenocarcinoma. Case reports in oncological medicine, 2017, 2321052-2321052. doi:10.1155/2017/2321052

Vittal, A., Sharma, D., Samanta, I., & Kasi, A. (2019). Rare case of triple mutant (*KRAS* + NRAS + *BRAF*) metastatic colon adenocarcinoma. BMJ Case Reports, 12(9), e221816. doi:10.1136/bcr-2017-221816

Vivanco, I., & Sawyers, C. L. (2002). The phosphatidylinositol 3-Kinase AKT pathway in human cancer. Nat Rev Cancer, 2(7), 489-501. doi:10.1038/nrc839

Vogel, D. Y., Glim, J. E., Stavenuiter, A. W., Breur, M., Heijnen, P., Amor, S., . . . Beelen, R. H. (2014). Human macrophage polarization in vitro: maturation and activation methods compared. Immunobiology, 219(9), 695-703. doi:10.1016/j.imbio.2014.05.002

Vogelstein, B., Fearon, E. R., Hamilton, S. R., Kern, S. E., Preisinger, A. C., Leppert, M., . . . Bos, J. L. (1988). Genetic alterations during colorectal-tumor development. The New England journal of medicine, 319(9), 525-532. doi:10.1056/nejm198809013190901

Waalkes, A., Smith, N., Penewit, K., Hempelmann, J., Konnick, E. Q., Hause, R. J., . . . Salipante, S. J. (2018). Accurate Pan-Cancer Molecular Diagnosis of Microsatellite Instability by Single-Molecule Molecular Inversion Probe Capture and High-Throughput Sequencing. Clinical Chemistry, 64(6), 950-958. doi:10.1373/clinchem.2017.285981

Wallace, D. I., & Guo, X. (2013). Properties of tumor spheroid growth exhibited by simple mathematical models. Front Oncol, 3, 51. doi:10.3389/fonc.2013.00051

Wan, P. T. C., Garnett, M. J., Roe, S. M., Lee, S., Niculescu-Duvaz, D., Good, V. M., . . . Marais, R. (2004). Mechanism of Activation of the RAF-ERK Signaling Pathway by Oncogenic Mutations of B-RAF. Cell, 116(6), 855-867. doi:https://doi.org/10.1016/S0092-8674(04)00215-6

Wang, G., Yang, Q., Li, M., Zhang, Y., Cai, Y., Liang, X., . . . Chen, Z. (2019). Quantitative proteomic profiling of tumor-associated vascular endothelial cells in colorectal cancer. Biology Open, 8(5), bio042838. doi:10.1242/bio.042838

Wang, H., Shao, Q., Sun, J., Ma, C., Gao, W., Wang, Q., . . . Qu, X. (2016). Interactions between colon cancer cells and tumor-infiltrated macrophages depending on cancer cell-derived colony stimulating factor 1. Oncoimmunology, 5(4), e1122157-e1122157. doi:10.1080/2162402X.2015.1122157

Wang, J. L., Guo, C. R., Su, W. Y., Chen, Y. X., Xu, J., & Fang, J. Y. (2018). CD24 Overexpression Related to Lymph Node Invasion and Poor Prognosis of Colorectal Cancer. Clin Lab, 64(4), 497-505. doi:10.7754/Clin.Lab.2017.171012

Wang, M. J., Ping, J., Li, Y., Adell, G., Arbman, G., Nodin, B., . . . Sun, X. F. (2015). The prognostic factors and multiple biomarkers in young patients with colorectal cancer. Sci Rep, 5, 10645. doi:10.1038/srep10645

Wang, R., Li, Y., Tsung, A., Huang, H., Du, Q., Yang, M., . . . Billiar, T. R. (2018). iNOS promotes CD24(+)CD133(+) liver cancer stem cell phenotype through a TACE/ADAM17-dependent Notch signaling

pathway. Proc Natl Acad Sci U S A, 115(43), E10127-e10136. doi:10.1073/pnas.1722100115

Wang, R., Wang, M.-J., & Ping, J. (2015). Clinicopathological Features and Survival Outcomes of Colorectal Cancer in Young Versus Elderly: A Population-Based Cohort Study of SEER 9 Registries Data (1988-2011). Medicine, 94(35), e1402-e1402. doi:10.1097/MD.0000000000001402

Wang, W., Kandimalla, R., Huang, H., Zhu, L., Li, Y., Gao, F., . . . Wang, X. (2018). Molecular subtyping of colorectal cancer: Recent progress, new challenges and emerging opportunities. Seminars in Cancer Biology. doi:https://doi.org/10.1016/j.semcancer.2018.05.002

Wang, W., Kandimalla, R., Huang, H., Zhu, L., Li, Y., Gao, F., . . . Wang, X. (2019). Molecular subtyping of colorectal cancer: Recent progress, new challenges and emerging opportunities. Semin Cancer Biol, 55, 37-52. doi:10.1016/j.semcancer.2018.05.002

Wang, X., Zhang, Y., Zhao, Y., Liang, Y., Xiang, C., Zhou, H., . . . Peng, L. (2016). CD24 promoted cancer cell angiogenesis via Hsp90-mediated STAT3/VEGF signaling pathway in colorectal cancer. Oncotarget, 7(34), 55663-55676. doi:10.18632/oncotarget.10971

Wang, Y., Chen, X., Cao, W., & Shi, Y. (2014). Plasticity of mesenchymal stem cells in immunomodulation: pathological and therapeutic implications. Nat Immunol, 15(11), 1009-1016. doi:10.1038/ni.3002

Wang, Y., Fan, H., Zhou, B., Ju, Z., Yu, L., Guo, L., . . . Lu, S. (2012). Fusion of human umbilical cord mesenchymal stem cells with esophageal carcinoma cells inhibits the tumorigenicity of esophageal carcinoma cells. Int J Oncol, 40(2), 370-377. doi:10.3892/ijo.2011.1232

Watanabe, T., Wu, T.-T., Catalano, P. J., Ueki, T., Satriano, R., Haller, D. G., . . . Hamilton, S. R. (2001). Molecular Predictors of Survival after Adjuvant Chemotherapy for Colon Cancer. New England Journal of Medicine, 344(16), 1196-1206. doi:10.1056/nejm200104193441603

Watson, A. J., Merritt, A. J., Jones, L. S., Askew, J. N., Anderson, E., Becciolini, A., . . . Hickman, J. A. (1996). Evidence of reciprocity of bcl-2 and p53 expression in human colorectal adenomas and carcinomas. British Journal of Cancer, 73(8), 889-895. doi:10.1038/bjc.1996.178

Webber, E. M., Kauffman, T. L., O'Connor, E., & Goddard, K. A. B. (2015). Systematic review of the predictive effect of MSI status in colorectal cancer patients undergoing 5FU-based chemotherapy. BMC cancer, 15, 156-156. doi:10.1186/s12885-015-1093-4

Wei, C., Yang, C., Wang, S., Shi, D., Zhang, C., Lin, X., . . . Xiong, B. (2019). Crosstalk between cancer cells and tumor associated macrophages is required for mesenchymal circulating tumor cell-mediated colorectal cancer metastasis. Molecular cancer, 18(1), 64. doi:10.1186/s12943-019-0976-4

Wei, C., Yang, C., Wang, S., Shi, D., Zhang, C., Lin, X., & Xiong, B. (2019). M2 macrophages confer resistance to 5-fluorouracil in colorectal cancer

through the activation of CCL22/PI3K/AKT signaling. OncoTargets and therapy, 12, 3051-3063. doi:10.2147/OTT.S198126

Weichert, W., Denkert, C., Burkhardt, M., Gansukh, T., Bellach, J., Altevogt, P., . . . Kristiansen, G. (2005). Cytoplasmic CD24 Expression in Colorectal Cancer Independently Correlates with Shortened Patient Survival. Clinical Cancer Research, 11(18), 6574. doi:10.1158/1078-0432.CCR-05-0606

Weisenberger, D. J., Siegmund, K. D., Campan, M., Young, J., Long, T. I., Faasse, M. A., . . . Laird, P. W. (2006). CpG island methylator phenotype underlies sporadic microsatellite instability and is tightly associated with *BRAF* mutation in colorectal cancer. Nat Genet, 38(7), 787-793. doi:10.1038/ng1834

Weiswald, L.-B., Bellet, D., & Dangles-Marie, V. (2015). Spherical cancer models in tumor biology. Neoplasia (New York, N.Y.), 17(1), 1-15. doi:10.1016/j.neo.2014.12.004

Wikberg, M. L., Edin, S., Lundberg, I. V., Van Guelpen, B., Dahlin, A. M., Rutegård, J., . . . Palmqvist, R. (2013). High intratumoral expression of fibroblast activation protein (FAP) in colon cancer is associated with poorer patient prognosis. Tumour Biol, 34(2), 1013-1020. doi:10.1007/s13277-012-0638-2

Williams, D. S., Mouradov, D., Jorissen, R. N., Newman, M. R., Amini, E., Nickless, D. K., . . . Sieber, O. M. (2019). Lymphocytic response to tumour and deficient DNA mismatch repair identify subtypes of stage II/III colorectal cancer associated with patient outcomes. Gut, 68(3), 465-474. doi:10.1136/gutjnl-2017-315664

Woodward, W. A., & Sulman, E. P. (2008). Cancer stem cells: markers or biomarkers? Cancer and Metastasis Reviews, 27(3), 459-470. doi:10.1007/s10555-008-9130-2

Worthley, D. L., Giraud, A. S., & Wang, T. C. (2010). The extracellular matrix in digestive cancer. Cancer microenvironment : official journal of the International Cancer Microenvironment Society, 3(1), 177-185. doi:10.1007/s12307-010-0053-4

Wright, M., Beaty, J. S., & Ternent, C. A. (2017). Molecular Markers for Colorectal Cancer. Surgical Clinics of North America, 97(3), 683-701. doi:https://doi.org/10.1016/j.suc.2017.01.014

www. seltarbase. Org. Accessed in May-December 2017

www. bioinformatics. Org. Accessed in May-December 2017

www.gene-quantification.de/ab-hrm-guide.pdf. Accessed in May 2017

Xanthopoulou, A., Ganopoulos, I., Koubouris, G., Tsaftaris, A., Sergendani, C., Kalivas, A., & Madesis, P. (2014). Microsatellite high-resolution melting (SSR-HRM) analysis for genotyping and molecular characterization of an Olea europaea germplasm collection. Plant Genetic Resources, 12(3), 273-277. doi:10.1017/S147926211400001X

Xiao, Y., & Freeman, G. J. (2015). The Microsatellite Instable Subset of Colorectal Cancer Is a Particularly Good Candidate for Checkpoint Blockade Immunotherapy. Cancer Discovery, 5(1), 16. doi:10.1158/2159-8290.CD-14-1397

Xie, Y.-H., Chen, Y.-X., & Fang, J.-Y. (2020). Comprehensive review of targeted therapy for colorectal cancer. Signal transduction and targeted therapy, 5(1), 22-22. doi:10.1038/s41392-020-0116-z

Xu, C., Zheng, L., Li, D., Chen, G., Gu, J., Chen, J., & Yao, Q. (2018). CXCR4 overexpression is correlated with poor prognosis in colorectal cancer. Life Sciences, 208, 333-340. doi:https://doi.org/10.1016/j.lfs.2018.04.050

Xu, F., Li, S., Zhang, J., Wang, L., Wu, X., Wang, J., . . . Lai, M. (2018). Cancer Stemness, Immune Cells, and Epithelial–Mesenchymal Transition Cooperatively Predict Prognosis in Colorectal Carcinoma. Clinical Colorectal Cancer, 17(3), e579-e592. doi:https://doi.org/10.1016/j.clcc.2018.05.007

Yahaya, M. A. F., Lila, M. A. M., Ismail, S., Zainol, M., & Afizan, N. A. R. N. M. (2019). Tumour-Associated Macrophages (TAMs) in Colon Cancer and How to Reeducate Them. Journal of immunology research, 2019, 2368249-2368249. doi:10.1155/2019/2368249

Yamanashi, T., Nakanishi, Y., Fujii, G., Akishima-Fukasawa, Y., Moriya, Y., Kanai, Y., . . . Hirohashi, S. (2009). Podoplanin Expression Identified in Stromal Fibroblasts as a Favorable Prognostic Marker in Patients with Colorectal Carcinoma. Oncology, 77(1), 53-62. doi:10.1159/000226112

Yamashita, S., Chun, Y. S., Kopetz, S. E., & Vauthey, J. N. (2018). Biomarkers in colorectal liver metastases. Br J Surg, 105(6), 618-627. doi:10.1002/bjs.10834

Yang, J., Liu, X., Bhalla, K., Kim, C. N., Ibrado, A. M., Cai, J., . . . Wang, X. (1997). Prevention of apoptosis by Bcl-2: release of cytochrome c from mitochondria blocked. Science, 275(5303), 1129-1132. doi:10.1126/science.275.5303.1129

Yang, Y., Wang, D., Jin, L., Wu, G., Bai, Z., Wang, J., . . . Zhang, Z. (2018). Prognostic value of the combination of microsatellite instability and *BRAF* mutation in colorectal cancer. Cancer management and research, 10, 3911-3929. doi:10.2147/CMAR.S169649

Yarden, Y., & Sliwkowski, M. X. (2001). Untangling the ErbB signalling network. Nature Reviews Molecular Cell Biology, 2(2), 127-137. doi:10.1038/35052073

Yokota, T., Ura, T., Shibata, N., Takahari, D., Shitara, K., Nomura, M., . . . Yatabe, Y. (2011). *BRAF* mutation is a powerful prognostic factor in advanced and recurrent colorectal cancer. Br J Cancer, 104(5), 856-862. doi:10.1038/bjc.2011.19

Yoon, H. H., Shi, Q., Heying, E. N., Muranyi, A., Bredno, J., Ough, F., . . . Sinicrope, F. A. (2019). Intertumoral Heterogeneity of CD3(+) and CD8(+) T-Cell Densities in the Microenvironment of DNA Mismatch-

Repair-Deficient Colon Cancers: Implications for Prognosis. Clinical cancer research : an official journal of the American Association for Cancer Research, 25(1), 125-133. doi:10.1158/1078-0432.CCR-18-1984

You, Y. N., Xing, Y., Feig, B. W., Chang, G. J., & Cormier, J. N. (2012). Young-Onset Colorectal Cancer: Is It Time to Pay Attention? Archives of Internal Medicine, 172(3), 287-289. doi:10.1001/archinternmed.2011.602

Young, M., & Reed, K. R. (2016). Organoids as a Model for Colorectal Cancer. Current colorectal cancer reports, 12(5), 281-287. doi:10.1007/s11888-016-0335-4

Yu, B., Zhang, X., & Li, X. (2014). Exosomes derived from mesenchymal stem cells. Int J Mol Sci, 15(3), 4142-4157. doi:10.3390/ijms15034142

Yuan, L., Chi, Y., Chen, W., Chen, X., Wei, P., Sheng, W., . . . Shi, D. (2015). Immunohistochemistry and microsatellite instability analysis in molecular subtyping of colorectal carcinoma based on mismatch repair competency. International journal of clinical and experimental medicine, 8(11), 20988-21000. Retrieved from https://pubmed.ncbi.nlm.nih.gov/26885030

https://www.ncbi.nlm.nih.gov/pmc/articles/PMC4723875/

Yuan, Z. X., Wang, X. Y., Qin, Q. Y., Chen, D. F., Zhong, Q. H., Wang, L., & Wang, J. P. (2013). The prognostic role of *BRAF* mutation in metastatic colorectal cancer receiving anti-EGFR monoclonal antibodies: a meta-analysis. PloS one, 8(6), e65995. doi:10.1371/journal.pone.0065995

Yuan, Z.-X., Wang, X.-Y., Qin, Q.-Y., Chen, D.-F., Zhong, Q.-H., Wang, L., & Wang, J.-P. (2013). The prognostic role of *BRAF* mutation in metastatic colorectal cancer receiving anti-EGFR monoclonal antibodies: a meta-analysis. PloS one, 8(6), e65995-e65995. doi:10.1371/journal.pone.0065995

Zhan, T., Rindtorff, N., & Boutros, M. (2017). Wnt signaling in cancer. Oncogene, 36(11), 1461-1473. doi:10.1038/onc.2016.304

Zhang, B., Wang, Z., Wu, L., Zhang, M., Li, W., Ding, J., . . . Zhao, K. (2013). Circulating and tumor-infiltrating myeloid-derived suppressor cells in patients with colorectal carcinoma. PloS one, 8(2), e57114. doi:10.1371/journal.pone.0057114

Zhang, B., Zhang, B., Chen, X., Bae, S., Singh, K., Washington, M. K., & Datta, P. K. (2014). Loss of Smad4 in colorectal cancer induces resistance to 5-fluorouracil through activating Akt pathway. British Journal of Cancer, 110(4), 946-957. doi:10.1038/bjc.2013.789

Zhang, J., Zheng, J., Yang, Y., Lu, J., Gao, J., Lu, T., . . . Liu, T. (2015). Molecular spectrum of *KRAS*, NRAS, *BRAF* and *PIK3CA* mutations in Chinese colorectal cancer patients: analysis of 1,110 cases. Scientific Reports, 5(1), 18678. doi:10.1038/srep18678

Zhang, L. (2008). Immunohistochemistry versus microsatellite instability testing for screening colorectal cancer patients at risk for hereditary

nonpolyposis colorectal cancer syndrome. Part II. The utility of microsatellite instability testing. The Journal of molecular diagnostics : JMD, 10(4), 301-307. doi:10.2353/jmoldx.2008.080062

Zhang, R., Qi, F., Zhao, F., Li, G., Shao, S., Zhang, X., . . . Feng, Y. (2019). Cancer-associated fibroblasts enhance tumor-associated macrophages enrichment and suppress NK cells function in colorectal cancer. Cell Death & Disease, 10(4), 273. doi:10.1038/s41419-019-1435-2

Zheng, K., Wan, H., Zhang, J., Shan, G., Chai, N., Li, D., . . . Zhang, C. (2020). A novel NGS-based microsatellite instability (MSI) status classifier with 9 loci for colorectal cancer patients. Journal of translational medicine, 18(1), 215. doi:10.1186/s12967-020-02373-1

Zhou, X. P., Hoang, J. M., Cottu, P., Thomas, G., & Hamelin, R. (1997). Allelic profiles of mononucleotide repeat microsatellites in control individuals and in colorectal tumors with and without replication errors. Oncogene, 15(14), 1713-1718. doi:10.1038/sj.onc.1201337

Zhu, L., Dong, C., Cao, Y., Fang, X., Zhong, C., Li, D., & Yuan, Y. (2016). Prognostic Role of *BRAF* Mutation in Stage II/III Colorectal Cancer Receiving Curative Resection and Adjuvant Chemotherapy: A Meta-Analysis Based on Randomized Clinical Trials. PloS one, 11(5), e0154795-e0154795. doi:10.1371/journal.pone.0154795

Zhu, L., Huang, Y., Fang, X., Liu, C., Deng, W., Zhong, C., . . . Yuan, Y. (2018). A Novel and Reliable Method to Detect Microsatellite Instability in Colorectal Cancer by Next-Generation Sequencing. The Journal of molecular diagnostics : JMD, 20(2), 225-231. doi:10.1016/j.jmoldx.2017.11.007

Zoetemelk, M., Rausch, M., Colin, D. J., Dormond, O., & Nowak-Sliwinska, P. (2019). Short-term 3D culture systems of various complexity for treatment optimization of colorectal carcinoma. Scientific Reports, 9(1), 7103. doi:10.1038/s41598-019-42836-0

Supplementary Materials

Table S.1. The epithelial density of tumour microenvironment cellular community in the Nottingham cohort of colorectal cancer

		Cellular community density on Epithelial (BerEP4 positive) (Mean ± SD)					
		Pan T-lymphocytes (CD3)	Cytotoxic T-lymphocytes (CD8)	B-lymphocytes (CD20)	Pan Macrophages (CD68)	M2-Macrophages (CD163)	NK cells (CD56)
MS/MSS	MSI (n=19)	0.0551±0.0252	0.0831±0.0299	0.0085±0.0034	0.0669±0.0503	0.0465±0.0138	0.0013±0.006
	MSS (n=24)	0.0186±0.037	0.0778±0.0207	0.0101±0.0027	0.0958±0.0529	0.0207±0.0026	0.0031±0.0011
Exact Sig. (2 sided)		0.807	0.525	0.212	0.366	0.379	0.091
BRAF	M (n=14)	0.0638±0.0315	0.1008±0.0376	0.0140±0.0049	0.0872±0.0681	0.04550.0162	0.0014±0.0008
	WT (n=29)	0.0208±0.0071	0.0702±0.0185	0.0072±0.0020	0.0810±0.0440	0.0256±0.0055	0.0027±0.0010
Exact Sig. (2 sided)		0.108	0.517	0.338	0.736	0.154	0.659
KRAS	M (n=15)	0.0222±0.0097	0.0908±0.0320	0.0050±0.0014	0.1415±0.0858	0.0229±0.0053	0.0036±0.0018
	WT (n=28)	0.0415±0.0169	0.0745±0.0207	0.0118±0.0031	0.0517±0.0324	0.0370±0.0095	0.0016±0.0005
Exact Sig. (2 sided)		0.372	0.980	0.308	0.491	0.541	0.524
PIK3CA	M (n=7)	0.0373±0.0193	0.1418±0.0421	0.0059±0.0025	0.1572±0.1352	0.0371±0.0163	0.0037±0.0019
	WT (n=36)	0.0343±0.0133	0.0682±0.0186	0.0101±0.0024	0.0686±0.0357	0.0311±0.072	0.0020±0.0008
Exact Sig. (2 sided)		0.664	0.067	0.760	0.176	0.860	0.263
TP53	M (n=20)	0.0504±0.0223	0.0977±0.0309	0.0111±0.0031	0.1620±0.0757	0.0338±0.0107	0.0039±0.014
	WT(n=23)	0.0211±0.0091	0.0649±0.0183	0.0079±0.0029	0.0144±0.0040	0.0306±0.0080	0.0009±0.0004
Exact Sig. (2 sided)		0.017*	0.233	0.151	0.049*	0.480	0.013*
Ploidy	Dip (n=26)	0.0454±0.0186	0.0824±0.0235	0.0082±0.0025	0.0903±0.0504	0.0408±0.0103	0.0024±0.0010
	Aneu (n=11)	0.0192±0.0055	0.1092±0.0368	0.0092±0.0043	0.0930±0.0822	0.0191±0.0030	0.0029±0.0012
Exact Sig. (2 sided)		0.832	0.366	0.682	0.935	0.460	0.501
MSS	CIN (n=11)	0.0192±0.0055	0.1092±0.0368	0.0092±0.0043	0.0930±0.0822	0.0193±0.0030	0.0029±0.0012
	MACS (n=7)	0.0189±0.0046	0.0803±0.0352	0.0074±0.0022	0.1537±0.1332	0.0254±0.0066	0.0054±0.0034
Exact Sig. (2 sided)		0.860	0.860	0.536	0.479	0.860	0.425

Mann–Whitney U test. Highlight in red: significant higher density on mutant (M). $p < 0.05$. MSI, microsatellite instability. MSS, microsatellite stable. WT, wildtype. Dip, diploid. Aneu, aneuploid. CIN, chromosomal instable. MACS, microsatellite and chromosomal stable

Table S.2. The non-epithelial/ stromal density of tumour microenvironment cellular community in the Nottingham cohort of colorectal cancer

		Cellular community density on non-epithelial/ stroma (BerEP4 negative) (Mean ± SD)					
		Pan T-lymphocytes (CD3)	Cytotoxic T-lymphocytes (CD8)	B-lymphocytes (CD20)	Pan Macrophages (CD68)	M2-Macrophages (CD163)	NK cells (CD56)
MS/MSS	MSI (n=19)	0.0471±0.0126	0.0211±0.0094	0.0300±0.0082	0.0293±0.0174	0.0369±0.0130	0.0087±0.0037
	MSS (n=24)	0.0211±0.0041	0.0108±0.0025	0.0189±0.0043	0.0304±0.0164	0.0176±0.0041	0.0106±0.040
Exact Sig. (2 sided)		0.240	0.826	0.642	0.732	0.195	0.392
BRAF	M (n=14)	0.0552±0.0138	0.0293±0.0123	0.0393±0.0103	0.0302±0.0230	0.0269±0.0087	0.0112±0.0049
	WT (n=29)	0.0217±0.0056	0.0086±0.0020	0.0164±0.0036	0.0298±0.0139	0.0257±0.0084	0.0091±0.0034
Exact Sig. (2 sided)		0.013*	0.074	0.062	0.551	0.154	0.917
KRAS	M (n=15)	0.0171±0.0035	0.0087±0.0028	0.0139±0.0035	0.0515±0.0300	0.0223±0.0064	0.0079±0.0041
	WT (n=28)	0.0409±0.0091	0.0192±0.0065	0.0292±0.0063	0.0184±0.0083	0.0281±0.0090	0.0108±0.0037
Exact Sig. (2 sided)		0.194	0.262	0.296	0.524	0.524	0.799
PIK3CA	M (n=7)	0.0236±0.0073	0.0128±0.0042	0.0207±0.0069	0.0571±0.0451	0.0333±0.0135	0.01490.0077
	WT (n=36)	0.0343±0.0073	0.0158±0.0052	0.0245±0.0051	0.0247±0.0113	0.0247±0.0070	0.0088±0.0030
Exact Sig. (2 sided)		1.000	0.410	0.885	0.339	0.356	0.067
TP53	M (n=20)	0.0286±0.095	0.0173±0.0088	0.0151±0.0036	0.0518±0.0242	0.0192±0.0055	0.0123±0.0047
	WT (n=23)	0.0361±0.084	0.0137±0.0033	0.0315±0.0073	0.0109±0.0047	0.0321±0.0106	0.0076±0.0032
Exact Sig. (2 sided)		0.644	0.846	0.342	0.125	0.436	0.088
Ploidy	Dip (n=26)	0.0400±0.0095	0.0367±0.0178	0.0265±0.0063	0.0367±0.0178	0.0314±0.0097	0.0134±0.0043
	Aneu (n=11)	0.0163±0.0042	0.0261±0.0193	0.0144±0.0050	0.0261±0.0193	0.0183±0.0072	0.0056±0.0022
Exact Sig. (2 sided)		0.160	0.658	0.523	0.961	0.270	1.000
MSS	CIN (n=11)	0.0163±0.0042	0.0093±0.0035	0.0144±0.0050	0.0261±0.0193	0.0183±0.0071	0.0056±0.0022
	MACS(n=7)	0.0207±0.0037	0.0126±0.0031	0.0169±0.0064	0.0568±0.0484	0.0166±0.0053	0.0259±0.0119
Exact Sig. (2 sided)		0.285	0.425	0.724	0.536	0.659	0.044*

Mann–Whitney U test. Highlight in red: significant higher density on mutant (M). Highlight in green: significant higher density on microsatellite and chromosomal stable (MACS). $p < 0.05$. MSI, microsatellite instability. MSS, microsatellite stable. WT, wildtype. Dip, diploid. Aneu, aneuploid. CIN, chromosomal instable.

Table S.3. The whole tissue section (WTS) density of tumour microenvironment cellular community in the Nottingham cohort of colorectal cancer

		Cellular community density on WTS (Mean±SD)					
		Pan T-lymphocytes (CD3)	Cytotoxic T-lymphocytes (CD8)	B-lymphocytes (CD20)	Pan Macrophages (CD68)	M2-Macrophages (CD163)	NK cells (CD56)
MS/MSS	MSI (n=19)	0.0555±0.0166	0.0477±0.0170	0.0269±0.0065	0.0488±0.0334	0.0437±0.0128	0.0079±0.0033
	MSS (n=24)	0.0230±0.0044	0.0344±0.0088	0.0188±0.0043	0.0557±0.0329	0.0120±0.0035	0.0091±0.0031
Exact Sig. (2 sided)		0.203	0.608	0.642	0.696	0.250	0.406
BRAF	M (n=14)	0.0656±0.0195	0.0607±0.0215	0.0351±0.0080	0.0566±0.0453	0.0357±0.0121	0.0102±0.0043
	WT (n=29	0.0237±0.0061	0.0304±0.0080	0.0162±0.036	0.0508±0.0273	0.0277±0.0072	0.0077±0.0026
Exact Sig. (2 sided)		0.007*	0.312	0.041*	0.678	0.178	0.917
KRAS	M (n=15)	0.0233±0.0057	0.0439±0.0155	0.0138±0.0036	0.1009±0.0613	0.0249±0.0059	0.0071±0.0029
	WT (n=28)	0.0449±0.0118	0.0383±0.0111	0.0270±0.0053	0.0268±0.0134	0.0332±0.0090	0.0093±0.0031
Exact Sig. (2 sided)		0.320	0.838	0.194	0.593	0.899	0.990
PIK3CA	M (n=7)	0.0356±0.0118	0.0673±0.0195	0.0198±0.0065	0.1062±0.0895	0.0394±0.0156	0.0129±0.0057
	WT (n=36)	0.0377±0.0093	0.0350±0.0098	0.0229±0.0043	0.0422±0.0221	0.0285±0.0068	0.0077±0.0025
Exact Sig. (2 sided)		0.664	0.053	0.936	0.198	0.277	0.062
TP53	M (n=20)	0.0399±0.0144	0.0496±0.0168	0.0162±0.0037	0.0980±0.485	0.0253±0.0075	0.0103±0.0036
	WT (n=23)	0.0351±0.0085	0.0322±0.0081	0.0278±0.0061	0.0132±0.0042	0.0346±0.096	0.0071±0.0028
Exact Sig. (2 sided)		0.808	0.394	0.480	0.108	0.903	0.111
Ploidy	Dip (n=26)	0.0466±0.0124	0.0451±0.0128	0.0237±0.0050	0.0665±0.0359	0.0375±0.0096	0.0113±0.0035
	Aneu (n=11)	0.0186±0.0047	0.0432±0.0169	0.0146±0.0054	0.0421±0.0334	0.0198±0.0058	0.0056±0.0020
Exact Sig. (2 sided)		0.150	0.731	0.384	0.961	0.300	0.935
MSS	CIN (n=11)	0.0186±0.0047	0.0432±0.0169	0.0146±0.0054	0.0421±0.0334	0.0198±0.0058	0.0056±0.0021
	MACS (n=7)	0.0224±0.0037	0.0379±0.0122	0.0053±0.0048	0.1146±0.1017	0.0208±0.0056	0.0207±0.0090
Exact Sig. (2 sided)		0.285	0.536	0.596	0.536	0.536	0.044*

Mann–Whitney U test. Highlight in red: significant higher density on MSI (microsatellite instability) or mutant (M). Highlight in green: significant higher density on microsatellite and chromosomal stable (MACS). $p < 0.05$. MSS, microsatellite stable. WT, wildtype. Dip, diploid. Aneu, aneuploid. CIN, chromosomal instable.

Table S.4. Statistical analysis on pairwise biomarker correlations in the Nottingham cohort of colorectal cancer based on microsatellite instability (MSI) status

	MSI Status		
Biomarker correlation	Epithelial (BerEP4 positive)	Non-epithelial/Stroma (BerEP4 negative)	Whole Tissue Section (WTS)
CD3-CD163	P= 0.4387; t=0.7816 df=43	P= 0.7261; t=0.3527 df=43	P= 0.8693; t=0.1656 df=43
CD3-CD20	P= 0.0418; t=2.099 df=43	P=0.6547; t=0.4504 df=43	P=0.2397; t=1.192 df=43
CD3-CD56	P= 0.6165; t=0.5046 df=41	P= 0.6437; t=0.466 df=41	P=0.3849; t=0.8782 df=41
CD3-CD68	P= 0.1213; t=1.58 df=43	P=0.4498; t=0.7627 df=43	P= 0.1958; t=1.314 df=43
CD3-CD8	P= 0.0731; t=1.837 df=43	P=0.1402; t=1.503 df=43	P= 0.1314; t=1.537 df=44
CD163-CD20	P=0.0205; t=2.405 df=43	P=0.0620; t=1.916 df=43	P=0.0216; t=2.385 df=43
CD163-CD56	P=0.0443; t=2.075 df=41	P= 0.5744; t=0.5661 df=41	P= 0.1622; t=1.423 df=41
CD163-CD68	P=0.0777; t=1.807 df=43	P= 0.4541; t=0.7554 df=43	P= 0.3363; t=0.9724 df=43
CD163-CD8	P=0.0919; t=1.724 df=43	P= 0.1563; t=1.443 df=43	P= 0.1151; t=1.608 df=43
CD20-CD56	P=0.6967; t=0.3925 df=41	P= 0.9933; t=0.008463 df=41	P=0.9632; t=0.04644 df=41
CD20-CD68	P= 0.0863; t=1.756 df=43	P=0.4485; t=0.7649 df=43	P=0.0671; t=1.879 df=43
CD20-CD8	P=0.1595; t=1.432 df=43	P=0.4391; t=0.781 df=43	P= 0.205; t=1.287 df=43
CD56-CD68	P=0.3721; t=0.9024 df=41	P= 0.7261; t=0.3527 df=41	P= 0.6741; t=0.4236 df=41
CD56-CD8	P=0.8953; t=0.1324 df=41	P= 0.9621; t=0.04781 df=41	P=0.5598; t=0.5879 df=41
CD68-CD8	P=0.0230; t=2.357 df=43	P= 0.3350; t=0.9747 df=44	P= 0.0467; t=2.048 df=43

Un-paired T-Test; highlight in red: significant higher correlation on MSI; highlight in green: Significant higher correlation on MSS; p< 0.05.

Table S.5. Statistical analysis on pairwise biomarker correlations in the Nottingham cohort of colorectal cancer based on *BRAF* mutation

***BRAF* Mutation**			
Biomarker correlation	Epithelial (BerEP4 positive)	Non-epithelial/Stroma (BerEP4 negative)	Whole Tissue Section (WTS)
CD3-CD163	P= 0.613; t=0.509, df=43	P=0.732; t=0.345, df=43	P= 0.367; t=0.911, df=43
CD3-CD20	P=0.116; t=1.605, df=43	p=0.070; t=1.860, df=43	P= 0.526; t=0.659, df=43
CD3-CD56	P= 0.200; t=1.301, df=41	P=0.925; t=0.094 df=41	P= 0.117; t=1.603, df=41
CD3-CD68	P=0.688; t= 0.405, df=43	P=0.358; t=0.930 df=43	P= 0.345; t=0.954, df=43
CD3-CD8	P=0.291; t= 1.069, df=43	P=0.851; t=0.189 df=43	P= 0.052; t=2.001, df=43
CD163-CD20	P= 0.168; t=1.404, df=43	P=0.196; t=1.313, df=43	P=0.973; t=0.033, df=43
CD163-CD56	P= 0.061; t=1.925, df=41	P=0.331; t=0.993 df=41	P= 0.259; t=1.145, df=41
CD163-CD68	P= 0.413; t=0.827, df=43	P=0.559; t=0.590 df=43	P=0.420; t=0.814, df=43
CD163-CD8	P= <0.0001; t=3.942, df=43	P= 0.524; t=0.642 df=43	P= 0.006; t=2.897, df=43
CD20-CD56	P= 0.129; t=1.548, df=41	P=0.494; t=0.689 df=41	P=0.069; t=1.867, df=41
CD20-CD68	P= 0.041; t=2.108, df=43	P=0.881; t=0.151 df=43	P=0.537; t=0.622, df=43
CD20-CD8	P=0.305; t= 1.038, df=43	P=0.173; t=1.386 df=43	P=0.897; t=0.130, df=43
CD56-CD68	P=0.046; t=2.057, df=41	P=0.865; t=0.171 df=41	P=0.205; t=1.288, df=41
CD56-CD8	P=0.065; t=1.893, df=41	P=0.867; t=0.169 df=41	P= 0.055; t=1.976, df=41
CD68-CD8	P=0.020; t=2.420, df=43	P=0.986; t=0.018 df=43	P=0.032; t=2.214, df=43

Un-paired T-Test. highlight in red: significant higher correlation on mutant. Highlight in green: significant higher correlation on wildtype. $p < 0.05$.

Table S.6. Statistical analysis on pairwise biomarker correlations in the Nottingham cohort of colorectal cancer based on *KRAS* mutation

***KRAS* Mutation**			
Biomarker correlation	Epithelial (BerEP4 positive)	Non-epithelial/Stroma (BerEP4 negative)	Whole Tissue Section (WTS)
CD3-CD163	P= 0.613; t=0.514 df=43	P=0.889; t=0.140 df=43	P= 0.880; t=0.152 df=43
CD3-CD20	P= 0.481; t= 0.711 df=43	P=0.398; t=0.854 df=43	P= 0.659; t=0.444 df=43
CD3-CD56	P=0.589; t=0.544 df=41	P=0.430; t=0.811 df=41	P= 0.521; t=0.647 df=41
CD3-CD68	P=0.153; t=1.454 df=43	P=0.526; t=0.639 df=43	P= 0.698; t=0.391 df=43
CD3-CD8	P=0.075; t= 1.825 df=43	P=0.774; t=0.289 df=43	P= 0.083; t=1.775 df=43
CD163-CD20	P=0.721; t=0.360 df=43	P=0.551; t=0.601 df=43	P=0.567; t=0.577 df=43
CD163-CD56	P= 0.180; t= 1.364 df=41	P=0.529; t=0.635 df=41	P=0.664; t=0.438 df=41
CD163-CD68	P= 0.567; t= 0.576 df=43	P=0.157; t=1.442 df=43	P=0.952; t=0.061 df=41
CD163-CD8	P=0.017; t=2.489 df=43	P=0.958; t=0.052 df=43	P=0.095; t=1.706 df=43
CD20-CD56	P=0.895; t=0.133 df=41	P= 0.556; t=0.593 df=41	P=0.246; t=1.178 df=41
CD20-CD68	P= 0.505; t= 0.672 df=43	P=0.880; t=0.152 df=43	P=0.305; t=1.038 df=43
CD20-CD8	P=0.572; t=0.638 df=43	P=0.335; t=0.976 df=43	P=0.518; t=0.652 df=43
CD56-CD68	P=0.301; t=1.047 df=41	P=0.977; t=0.029 df=41	P=0.413; t=0.828 df=41
CD56-CD8	P=0.789; t=0.269 df=41	P=0.849; t=0.192 df=41	P=0.935; t=0.082 df=41
CD68-CD8	P=0.002; t= 3.274 df=43	P=0.431; t=0.795 df=43	P= 0.397; t=0.856 df=43

Un-paired T-Test. Highlight in green: significant higher correlation on wildtype. Highlight in yellow: significant negative correlation on mutant. $p<0.05$.

Table S.7. Statistical analysis on pairwise biomarker correlations in the Nottingham cohort of colorectal cancer based on *PIK3CA* mutation

***PIK3CA* Mutation**			
Biomarker correlation	Epithelial (BerEP4 positive)	Non-epithelial/Stroma (BerEP4 negative)	Whole Tissue Section (WTS)
CD3-CD163	P=0.045; t=2.060 df=43	P=0.907; t=0.118, df=43	P=0.449; t=0.764 df=43
CD3-CD20	P= 0.548; t= 0.605 df=43	P=0.944; t=0.071 df=43	P=0.897; t=0.016 df=43
CD3-CD56	P=0.459; t=0.747 df=41	P=0.412; t=0.880 df=41	P=0.438; t=0.783 df=41
CD3-CD68	P=0.905; t=0.120 df=43	P=0.967; t=0.041 df=43	P=0.410; t=0.831 df=43
CD3-CD8	P= 0.239; t=1.194 df=43	P=0.561; t=0.586 df=43	P=0.395; t=0.860 df=43
CD163-CD20	P= 0.074; t= 1.828 df=43	P= 0.550; t=0.603 df=43	P=0.876; t=0.156 df=43
CD163-CD56	P=0.162; t= 1.426 df=41	P=0.308; t=1.111 df=41	P= 0.349; t=0.948 df=41
CD163-CD68	P= 0.406; t=0.840 df=43	P= 0.286; t=1.080 df=43	P= 0.172; t=1.387 df=43
CD163-CD8	P= 0.788; t=0.271 df=43	P=0.630; t=0.505 df=43	P=0.907; t=0.121 df=43
CD20-CD56	P=0.658; t= 0.446 df=41	P=0.783; t=0.277 df=41	P=0.730; t=0.347 df=41
CD20-CD68	P=0.346; t= 1.017 df=43	P=0.732; t=0.345 df=43	P=0.916; t=0.107, df=43
CD20-CD8	P= 0.556; t= 0.593 df=43	P= 0.998; t= 0.003 df=43	P=0.407; t=0.838 df=43
CD56-CD68	P=0.312; t= 1.023 df=41	P= 0.225; t= 1.348 df=41	P= 0.658; t=0.447 df=41
CD56-CD8	P=0.656; t=0.449 df=41	P= 0.413; t=0.875, df=41	P=0.991; t=0.012 df=41
CD68-CD8	P= 0.907; t= 0.118 df=43	P= 0.181; t=1.361 df=43	P= 0.126; t=1.559 df=43

Un-paired T-Test. Highlight in red: significant higher correlation on mutant. $p<0.05$.

Table S.8. Statistical analysis on pairwise biomarker correlations in the Nottingham cohort of colorectal cancer based on *TP53* mutation

	***TP53* Mutation**		
Biomarker correlation	Epithelial (BerEP4 positive)	Non-epithelial/Stroma (BerEP4 negative)	Whole Tissue Section (WTS)
CD3-CD163	P=0.025; t=2.317 df=43	P=0.732; t= 0.345 df=43	P=0.048; t=2.032 df=43
CD3-CD20	P= 0.891; t=0.138 df=43	P=0.070; t=0.160 df=43	P= 0.039; t=2.133 df=43
CD3-CD56	P=0.318; t=1.011 df=41	P=0.925; t=0.094 df=41	P=0.205; t=1.287 df=41
CD3-CD68	P=0.449; t=0.764 df=43	P=0.358; t=0.930 df=43	P=0.153; t=1.455 df=43
CD3-CD8	P= 0.306; t= 1.03 df=43	P=0.851; t=0.189 df=43	P= 0.811; t=0.241 df=43
CD163-CD20	P=0.893; t= 0.135 df=43	P=0.196; t=1.313 df=43	P=0.781; t=0.280 df=43
CD163-CD56	P=0.744; t=0.329, df=41	P=0.317; t=1.013 df=41	P=0.673; t=0.426 df=41
CD163-CD68	P= 0.279; t=1.097 df=43	P=0.559; t=0.590 df=43	P= 0.812; t=0.239 df=43
CD163-CD8	P=0.426; t= 0.804 df=43	P=0.524; t=0.642 df=43	P= 0.972; t=0.035 df=43
CD20-CD56	P=0.591; t=0.542 df=41	P=0.484; t=0.689 df=41	P=0.747; t=0.325 df=41
CD20-CD68	P=0.541; t=0.760, df=43	P=0.881; t=0.151 df=43	P= 0.156; t=1.444 df=43
CD20-CD8	P=0.766; t=0.300 df=43	P=0.173; t=1.386 df=43	P=0.388; t=0.872 df=43
CD56-CD68	P= 0.844; t= 0.198 df=41	P=0.865; t=0.171 df=41	P=0.988; t=0.015 df=41
CD56-CD8	P=0.937; t=0.079 df=41	P=0.867; t=0.169 df=41 P=	P= 0.678; t=0.418 df=41
CD68-CD8	P= 0.582; t= 0.554 df=43	P=0.986; t=0.1018 df=43	P= 0.787; t=0.272 df=43
CD68-Ki67	P=0.499; t= 0.682 df=43	P=0.109; t=1.636 df=43	P= 0.353; t=0.939 df=43

Un-paired T-Test. Highlight in red: significant higher correlation on mutant. Highlight in green: significant higher correlation on wildtype. $p<0.05$.

Table S.9. Statistical analysis on pairwise biomarker correlations in the Nottingham cohort of colorectal cancer based on ploidy status

	Ploidy		
Biomarker correlation	Epithelial (BerEP4 positive)	Non-epithelial/Stroma (BerEP4 negative)	Whole Tissue Section (WTS)
CD3-CD163	P=0.652; t=0.454 df=35	P=0.383; t=0.883 df=35	P=0.901; t= 0.125 df=35
CD3-CD20	P=0.051; t= 2.024 df=35	P=0.771; t= 0.293 df=35	P=0.186; t=1.348 df=35
CD3-CD56	P=0.345; t= 0.957 df=35	P=0.832; t= 0.214 df=35	P=0.369; t=0.911 df=35
CD3-CD68	P=0.661; t= 0.442 df=35	P=0.398; t= 0.855 df=35	P=0.822; t= 0.227 df=35
CD3-CD8	P=0.008; t= 2.812 df=35	P=0.322; t=1.005 df=35	P=0.026; t=2.323 df=35
CD163-CD20	P=0.535; t= 0.627 df=35	P=0.096; t=1.709 df= 35	P=0.488; t=0.700 df=35
CD163-CD56	P=0.029; t= 2.284 df=35	P=0.787; t=0.273 df=35	P=0.394; t= 0.864 df=35
CD163-CD68	P=0.088; t=1.754 df=35	P=0.449; t=0.765 df= 35	P=0.185; t= 1.351 df=35
CD163-CD8	P=0.020; t= 2.448 df=35	P=0.085; t=1.772 df=35	P=0.068; t= 1.882 df=35
CD20-CD56	P=0.437; t= 0.786 df= 35	P=0.930; t=0.089 df=35	P=0.731; t= 0.347 df=35
CD20-CD68	P=0.058; t= 1.964 df=35	P=0.490; t= 0.697 df=35	P=0.073; t= 1.845 df=35
CD20-CD8	P=0.552; t= 0.600 df=35	P=0.687; t=0.406 df=35	P=0.844; t= 0.199 df=35
CD56-CD68	P=0.159; t=1.438 df=35	P=0,541; t= 0.617 df=35	P=0.133; t=1.538 df=35
CD56-CD8	P=0.744; t= 0.329 df=35	P=0.105; t=1.663 df=35	P=0.551; t=0.603 df=35
CD68-CD8	P=0.090; t=1.746 df=35	P=0.728; t= 0.350 df=35	P=0.288; t=1.079 df=35

Un-paired T-Test. Highlight in red: significant higher correlation on diploid. Highlight in green: significant higher correlation on aneuploid. $p<0.05$.

Table S.10. Statistical analysis on pairwise biomarker correlations in the Nottingham cohort of microsatellite and chromosomal stable colorectal cancer

CIN vs MACS			
Biomarker correlation	Epithelial (BerEP4 positive)	Non-epithelial/Stroma (BerEP4 negative)	Whole Tissue Section (WTS)
CD3-CD163	P=0.720; t=0.364 df=16	P=0.929; t=0.091 df=16	P=0.954; t=0.059 df=16
CD3-CD20	P=0.256; t=1.178 df=16	P=0.510; t= 0.637 df=16	P=0.333; t=0.998 df=16
CD3-CD56	P=0.360; t=0.942 df=16	P=0.346; t=0.971 df=16	P=0.66; t=0.446 df=16
CD3-CD68	P=0.406; t= 0.853 df=16	P=0.432; t= 0.806 df=16	P=0.358; t= 0.946 df=16
CD3-CD8	P=0.114; t=1.673 df=16	P=0.929; t=0.090 df=16	P=0.307; t=1.056 df=16
CD163-CD20	P=0.480; t= 0.723 df=16	P=0.148; t= 1.519 df=16	P=0.551; t= 0.608 df=16
CD163-CD56	P=0.400; t= 0.864 df=16	P=0.783; t= 0.280 df=16	P=0.75; t= 0.318 df=16
CD163-CD68	P=0.651; t=0.461 df=16	P=0.57; t=0.568 df=16	P=0.511; t=0.673 df=16
CD163-CD8	P=0.113; t=1.678 df=16	P=0.272; t=1.138 df=16	P=0.388; t=0.887 df=16
CD20-CD56	P=0.925; t=0.095 df=16	P=0.835; t=0.211 df=16	P=0.948; t= 0.067 df=16
CD20-CD68	P=0.436; t=0.799 df=16	P=0.83; t=0.210 df=16	P=0.355; t=0.953 df=15
CD20-CD8	P=0.133; t=1.582 df=16	P=0.882; t=0.151 df=16	P=0.48; t= 0.722 df=16
CD56-CD68	P=0.289; t= 1.097 df=16	P=0.983; t=0.022 df=16	P=0.167; t=1.446 df=16
CD56-CD8	P=0.352; t= 0.959 df=16	P=0.188; t=1.374 df=16	P=0.884; t=0.148 df=16
CD68-CD8	P=0.673; t= 0.430 df=16	P=0.626; t=0.497 df=16	P=0.909; t= 0.117 df=16

Un-paired T-Test. CIN, chromosomal instable. MACS, microsatellite and chromosomal stable.

Table S.11. The whole tissue section (WTS) density of proliferating tumour microenvironment cellular community in the Nottingham cohort of colorectal cancer

		Proliferation (Ki67+) cellular community density on WTS (Mean±SD)					
		Pan T-lymphocytes (CD3)	Cytotoxic T-lymphocytes (CD8)	B-lymphocytes (CD20)	Pan Macrophages (CD68)	M2-Macrophages (CD163)	NK cells (CD56)
MSI/MSS	MSI (n=19)	0.0176±0.0094	0.0231±0.0102	0.0023±0.0009	0.0156±0.0119	0.0101±0.0048	0.0003±0.0001
	MSS (n=24)	0.0011±0.0003	0.0044±0.0013	0.0007±0.0001	0.0172±0.0135	0.0015±0.0005	0.0005±0.0002
Exact Sig. (2 sided)		0.080	0.478	0.573	0.668	0.019*	0.286
BRAF	M (n=14)	0.0189±0.0120	0.0275±0.0133	0.0031±0.0011	0.0193±0.0162	0.0095±0.0058	0.0003±0.0002
	WT (n=29	0.0033±0.0024	0.0055±0.0021	0.0006±0.0001	0.0152±0.0112	0.0033±0.0017	0.0004±0.0002
Exact Sig. (2 sided)		0.014*	0.108	0.040*	0.492	0.006*	0.937
KRAS	M (n=15)	0.0037±0.0029	0.0114±0.0069	0.0006±0.0002	0.0374±0.0253	0.0021±0.0007	0.0007±0.0004
	WT (n=28)	0.0109±0.0064	0.0134±0.0063	0.0019±0.0006	0.0054±0.0027	0.0070±0.0033	0.0002±0.00008
Exact Sig. (2 sided)		0.221	0.899	0.153	0.799	0.308	0.535
PIK3CA	M (n=7)	0.0081±0.0062	0.0250±0.0138	0.0011±0.0005	0.0342±0.0323	0.0046±0.0020	0.0007±0.0004
	WT (n=36)	0.0084±0.0050	0.0103±0.0049	0.0015±0.0005	0.0131±0.0091	0.0054±0.0026	0.0003±0.0002
Exact Sig. (2 sided)		0.356	0.038*	0.809	0.210	0.323	0.249
TP53	M (n=20)	0.0124±0.0086	0.0173±0.0093	0.0011±0.0003	0.0334±0.0191	0.0064±0.0041	0.0007±0.0003
	WT (n=23)	0.0049±0.0031	0.0086±0.0036	0.0017±0.0007	0.0019±0.0011	0.0043±0.0021	0.00006±0.00002
Exact Sig. (2 sided)		0.173	0.330	0.592	0.041*	0.422	0.003*
Ploidy	Dip (n=26)	0.0133±0.0070	0.0188±0.0076	0.0019±0.0007	0.0242±0.0147	0.0083±0.0035	0.0005±0.0002
	Aneu (n=11)	0.0007±0.0002	0.0045±0.0020	0.0005±0.0002	0.0066±0.0063	0.0007±0.0004	0.0003±0.0002
Exact Sig. (2 sided)		0.055	0.481	0.441	0.192	0.002*	0.731
MSS	CIN (n=11)	0.0007±0.0002	0.0045±0.0020	0.0005±0.0002	0.0066±0.0063	0.0007±0.0004	0.0003±0.0002
	MACS (n=7)	0.0016±0.0006	0.0069±0.0032	0.0009±0.0004	0.0475±0.0456	0.0032±0.0014	0.0011±0.0008
Exact Sig. (2 sided)		0.126	0.479	0.659	0.179	0.008*	0.285

Mann–Whitney U test. Highlight in red: significant higher density on microsatellite instable (MSI), mutant (M) or diploid (dip). Highlight in green: significant higher density microsatellite and chromosomal stable (MACS). $p < 0.05$. MSI, microsatellite instability. MSS, microsatellite stable. WT, wildtype. Aneu, aneuploid. CIN, chromosomal instable.

Table S.12. The epithelial density of proliferating tumour microenvironment cellular community in the Nottingham cohort of colorectal cancer

		Proliferating (Ki67+) cellular community density on Epithelial (BerEP4 positive) (Mean ± SD)					
		Pan T-lymphocytes (CD3)	Cytotoxic T-lymphocytes (CD8)	B-lymphocytes (CD20)	Pan Macrophages (CD68)	M2-Macrophages (CD163)	NK cells (CD56)
MSI/MSS	MSI (n=19)	0.0176±0.0094	0.0231±0.0102	0.0023±0.0009	0.0156±0.0120	0.0101±0.0048	0.0003±0.0001
	MSS (n=24)	0.0010±0.0003	0.0044±0.0014	0.0007±0.0002	0.0173±0.0135	0.0015±0.0005	0.0005±0.0002
Exact Sig. (2 sided)		0.080	0.478	0.573	0.668	0.019*	0.286
BRAF	M (n=14)	0.0189±0.0120	0.0275±0.0133	0.0031±0.0011	0.0193±0.0162	0.0095±0.0058	0.0003±0.0002
	WT (n=29)	0.0033±0.0024	0.0055±0.0021	0.0006±0.0001	0.0152±0.0112	0.0033±0.0017	0.0004±0.0002
Exact Sig. (2 sided)		0.014*	0.108	0.040*	0.492	0.006*	0.937
KRAS	M (n=15)	0.0037±0.0030	0.0114±0.0069	0.0006±0.0002	0.0374±0.0253	0.0021±0.0007	0.0007±0.0004
	WT (n=28)	0.0109±0.0064	0.0134±0.0063	0.0019±0.0006	0.0054±0.0027	0.0070±0.0033	0.0002±0.00008
Exact Sig. (2 sided)		0.221	0.899	0.153	0.799	0.308	0.535
PIK3CA	M (n=7)	0.0081±0.0062	0.0250±0.0138	0.0011±0.0005	0.0342±0.0323	0.0046±0.0020	0.0007±0.0004
	WT (n=36)	0.0084±0.0050	0.0103±0.0049	0.0015±0.0005	0.0131±0.0091	0.0054±0.0026	0.0003±0.0002
Exact Sig. (2 sided)		0.356	0.038*	0.809	0.210	0.323	0.249
TP53	M (n=20)	0.0124±0.0086	0.0173±0.0928	0.0011±0.0003	0.0334±0.0191	0.0064±0.0041	0.0007±0.0003
	WT(n=23)	0.0049±0.0031	0.0851±0.0036	0.0017±0.0007	0.0019±0.0011	0.0043±0.0021	0.00006±0.00002
Exact Sig. (2 sided)		0.173	0.330	0.592	0.041*	0.422	0.003*
Ploidy	Dip (n=26)	0.0133±0.0070	0.0018±0.0076	0.0019±0.0007	0.0242±0.0147	0.0083±0.0035	0.0005±0.0002
	Aneu (n=11)	0.0007±0.0002	0.0045±0.0020	0.0005±0.0002	0.0066±0.0063	0.0007±0.0004	0.0003±0.0002
Exact Sig. (2 sided)		0.055	0.481	0.441	0.192	0.002*	0.
MSS	CIN (n=11)	0.0007±0.0002	0.0045±0.0020	0.0005±0.0002	0.0066±0.0063	0.0007±0.0004	0.0003±0.0002
	MACS (n=7)	0.0016±0.0006	0.0069±0.0033	0.0009±0.0004	0.0475±0.0456	0.0032±0.0013	0.0011±0.0008
Exact Sig. (2 sided)		0.126	0.479	0.659	0.179	0.008*	0.285

Mann–Whitney U test. Highlight in red: significant higher density on microsatellite instable (MSI), mutant (M) or diploid (dip). Highlight in green: significant higher density microsatellite and chromosomal stable (MACS). $p < 0.05$. MSI, microsatellite instability. MSS, microsatellite stable. WT, wildtype. Aneu, aneuploid. CIN, chromosomal instable.

Table S.13. The non-epithelial/ stromal density of proliferating tumour microenvironment cellular community in the Nottingham cohort of colorectal cancer

		Proliferating (Ki67+) cellular community density on Non-Epithelial/ Stroma (BerEP4 negative) (Mean ± SD)					
		Pan T-lymphocytes (CD3)	Cytotoxic T-lymphocytes (CD8)	B-lymphocytes (CD20)	Pan Macrophages (CD68)	M2-Macrophages (CD163)	NK cells (CD56)
MSI/MSS	MSI (n=19)	0.0062±0.0031	0.0045±0.0028	0.0020±0.0011	0.0014±0.0006	0.0026±0.0014	0.00004±0.00002
	MSS (n=24)	0.0005±0.0001	0.0004±0.0001	0.0005±0.0001	0.0022±0.0016	0.0004±0.0002	0.00006±0.00002
Exact Sig. (2 sided)		0.040*	0.433	0.667	0.710	0.101	0.118
BRAF	M (n=14)	0.0069±0.0039	0.0051±0.0036	0.0027±0.0015	0.0012±0.0007	0.0023±0.0012	0.00003±0.00002
	WT (n=29	0.0011±0.0007	0.0008±0.0005	0.0004±0.0001	0.0022±0.0013	0.0009±0.0005	0.00005±0.00002
Exact Sig. (2 sided)		0.015*	0.055	0.148	0.752	0.040*	0.380
KRAS	M (n=15)	0.0004±0.0001	0.0004±0.0001	0.0005±0.0002	0.0029±0.0024	0.0003±0.0001	0.00004±0.00002
	WT (n=28)	0.0044±0.0021	0.0032±0.0018	0.0015±0.0007	0.0013±0.0005	0.0019±0.0009	0.00005±0.00002
Exact Sig. (2 sided)		0.146	0.371	0.065	0.979	0.211	0.538
PIK3CA	M (n=7)	0.0007±0.0002	0.0007±0.0003	0.0005±0.0003	0.0010±0.0006	0.0008±0.0005	0.00005±0.00002
	WT (n=36)	0.0035±0.0017	0.0025±0.0015	0.0013±0.0006	0.0020±0.0011	0.0015±0.0008	0.00005±0.00002
Exact Sig. (2 sided)		0.640	0.263	0.711	0.429	0.410	0.176
TP53	M (n=20)	0.0034±0.0027	0.0030±0.0025	0.0004±0.0001	0.0032±0.0019	0.0017±0.0012	0.00009±0.00003
	WT (n=23)	0.0026±0.0012	0.0015±0.0008	0.0018±0.0009	0.0006±0.0004	0.0011±0.0006	0.00009±0.00004
Exact Sig. (2 sided)		0.789	0.380	0.384	0.054	0.751	0.004*
Ploidy	Dip (n=26)	0.0047±0.0022	0.0034±0.0020	0.0017±0.0008	0.0026±0.0015	0.0022±0.0010	0.00007±0.00003
	Aneu (n=11)	0.0003±0.0001	0.0003±0.0001	0.0004±0.0001	0.0009±0.0008	0.0001±0.00004	0.00003±0.00001
Exact Sig. (2 sided)		0.021*	0.192	0.731	0.192	0.012	0.731
MSS	CIN (n=11)	0.0003±0.0001	0.0003±0.0001	0.0003±0.0001	0.0009±0.0008	0.0001±0.00004	0.00002±0.00001
	MACS(n=7)	0.0007±0.0002	0.0007±0.0003	0.0007±0.0004	0.0058±0.0053	0.0010±0.0005	0.0001±0.000080
Exact Sig. (2 sided)		0.151	0.179	0.860	0.126	0.044*	0.285

Mann–Whitney U test. Highlight in red: significant higher density on microsatellite instable (MSI), mutant (M) or diploid (dip). Highlight in green: significant higher density microsatellite and chromosomal stable (MACS). $p < 0.05$. MSI, microsatellite instability. MSS, microsatellite stable. WT, wildtype. Aneu, aneuploid. CIN, chromosomal instable.

Table S.14. The whole tissue section (WTS) density of BCL-2 expression within the tumour microenvironment cellular community in the Nottingham cohort of colorectal cancer

		BCL-2 expression within the cellular community on WTS (Mean±SD)					
		Pan T-lymphocytes (CD3)	Cytotoxic T-lymphocytes (CD8)	B-lymphocytes (CD20)	Pan Macrophages (CD68)	M2-Macrophages (CD163)	NK cells (CD56)
MSI/MSS	MSI (n=19)	0.0176±0.0094	0.0231±0.0102	0.0023±0.0009	0.0156±0.0120	0.0101±0.0048	0.0003±0.0001
	MSS (n=24)	0.0040±0.0013	0.0021±0.0007	0.0043±0.0015	0.0011±0.0010	0.0003±0.0001	0.00007±0.00003
Exact Sig. (2 sided)		0.095	0.008*	0.881	0.0003*	0.0003*	0.152
BRAF	M (n=14)	0.0207±0.0119	0.0283±0.0131	0.0044±0.0013	0.0191±0.0162	0.0094±0.0058	0.0003±0.0002
	WT (n=29	0.0049±0.0025	0.0032±0.0019	0.0029±0.0013	0.0019±0.0012	0.0023±0.0016	0.00009±0.00004
Exact Sig. (2 sided)		0.005*	0.001*	0.068	0.005*	0.000	0.039*
KRAS	M (n=15)	0.0045±0.0030	0.0075±0.0070	0.0014±0.0008	0.0154±0.0152	0.0010±0.0006	0.0002±0.0001
	WT (n=28)	0.0130±0.0064	0.0134±0.0063	0.0044±0.0014	0.0033±0.0015	0.0065±0.0033	0.0001±0.00005
Exact Sig. (2 sided)		0.029*	0.031*	0.045*	0.021*	0.005*	0.082
PIK3CA	M (n=7)	0.0091±0.0062	0.0196±0.0147	0.0026±0.0016	0.0329±0.0325	0.0030±0.0020	0.0005±0.0003
	WT (n=36)	0.0102±0.0050	0.0097±0.0049	0.0035±0.0011	0.0026±0.0012	0.0049±0.0026	0.0001±0.00004
Exact Sig. (2 sided)		0.962	0.936	0.885	0.855	0.834	0.277
TP53	M (n=20)	0.0144±0.0085	0.0159±0.0093	0.0032±0.0009	0.0143±0.0114	0.0050±0.0042	0.0003±0.0001
	WT (n=23)	0.0062±0.0032	0.0074±0.0035	0.0034±0.0016	0.0017±0.0010	0.0043±0.0021	0.00004±0.00002
Exact Sig. (2 sided)		0.233	0.461	0.187	0.910	0.553	0.056
Ploidy	Dip (n=26)	0.0134±0.0070	0.0173±0.0076	0.0021±0.0007	0.0114±0.0088	0.0074±0.0036	0.0002±0.0001
	Aneu (n=11)	0.0029±0.0010	0.0020±0.0010	0.0035±0.0014	0.0022±0.0022	0.0002±0.0001	0.0001±0.00006
Exact Sig. (2 sided)		0.658	0.270	0.544	0.141	0.031*	0.961
MSS	CIN (n=11)	0.0029±0.0010	0.0020±0.0010	0.0035±0.0014	0.0023±0.0022	0.0002±0.00009	0.0001±0.00006
	MACS (n=7)	0.0021±0.0015	0.0014±0.0010	0.0017±0.0012	0.000007±0.000007	0.0001±0.00008	0.00005±0.00003
Exact Sig. (2 sided)		0.328	0.375	0.285	0.179	0.285	0.479

Mann–Whitney U test. Highlight in red: significant higher density on microsatellite instable (MSI), mutant (M) or diploid (dip). Highlight in green: significant higher density on wildtype (WT). $p < 0.05$. MSI, microsatellite instability. MSS, microsatellite stable. Aneu, aneuploid. CIN, chromosomal instable. MACS, microsatellite and chromosomal stable.

Table S.15. The epithelial density of proliferating tumour microenvironment cellular community in the Nottingham cohort of colorectal cancer

		BCL-2 expression within the cellular community on Epithelial (BerEP4 positive) (Mean ± SD)					
		Pan T-lymphocytes (CD3)	Cytotoxic T-lymphocytes (CD8)	B-lymphocytes (CD20)	Pan Macrophages (CD68)	M2-Macrophages (CD163)	NK cells (CD56)
MSI/MSS	MSI (n=19)	0.0014±0.0004	0.0017±0.0007	0.0013±0.0006	0.0008±0.0006	0.0008±0.0003	0.00001±0.00001
	MSS (n=24)	0.0019±0.0006	0.0034±0.0016	0.0019±0.0007	0.0028±0.0027	0.0003±0.0001	0.0001±0.00006
Exact Sig. (2 sided)		0.424	0.682	0.572	0.572	0.336	0.959
BRAF	M (n=14)	0.0021±0.0006	0.0025±0.0009	0.0021±0.0008	0.0011±0.0008	0.0009±0.0003	0.00001±0.000001
	WT (n=29)	0.0014±0.0005	0.0027±0.0014	0.0015±0.0006	0.0023±0.0022	0.0004±0.0002	0.00008±0.000001
Exact Sig. (2 sided)		0.072	0.129	0.140	0.199	0.034*	0.466
KRAS	M (n=15)	0.0008±0.0005	0.0013±0.0010	0.0004±0.0002	0.0008±0.0007	0.0020±0.0001	0.00009±0.00008
	WT (n=28)	0.0021±0.0005	0.0034±0.0015	0.0024±0.0007	0.0025±0.0023	0.0007±0.0002	0.00005±0.00003
Exact Sig. (2 sided)		0.031*	0.040	0.077	0.262	0.024*	0.400
PIK3CA	M (n=7)	0.0020±0.0011	0.0043±0.0025	0.0009±0.0005	0.0018±0.0016	0.0007±0.0004	0.0002±0.0002
	WT (n=36)	0.0016±0.0004	0.0062±0.0015	0.0018±0.0006	0.0019±0.0018	0.0005±0.0002	0.00004±0.00002
Exact Sig. (2 sided)		0.711	1.000	0.711	0.323	0.987	0.687
TP53	M (n=20)	0.0024±0.0007	0.0044±0.0020	0.0020±0.0008	0.0040±0.0032	0.0006±0.0002	0.0003±0.0001
	WT(n=23)	0.0010±0.0003	0.0011±0.0006	0.0015±0.0006	0.0001±0.00004	0.0005±0.0002	0.00004±0.00002
Exact Sig. (2 sided)		0.142	0.103	0.516	0.144	0.312	0.042*
Ploidy	Dip (n=26)	0.0013±0.0003	0.0015±0.0005	0.0013±0.0005	0.0006±0.0004	0.0006±0.0002	0.00001±0.000006
	Aneu (n=11)	0.0025±0.0011	0.0063±0.0035	0.0024±0.0014	0.0059±0.0058	0.0005±0.0003	0.0002±0.001
Exact Sig. (2 sided)		0.935	0.781	0.731	0.523	0.935	0.316
MSS	CIN (n=11)	0.0025±0.0011	0.0063±0.0035	0.0024±0.0014	0.0059±0.0058	0.0005±0.0003	0
	MACS (n=7)	0.0011±0.0008	0.0008±0.0007	0.0010±0.0007	0.00001±0.000007	0.0001±0.00008	0
Exact Sig. (2 sided)		0.375	0.375	0.328	0.126	0.375	0.211

Mann–Whitney U test. Highlight in red: significant higher correlation on mutant (M). Highlight in green: significant higher density on wildtype (WT). $p < 0.05$. MSI, microsatellite instability. MSS, microsatellite stable. Dip, diploid. Aneu, aneuploid. CIN, chromosomal instable. MACS, microsatellite and chromosomal stable.

Table S.16. The non-epithelial/ stromal density of proliferating tumour microenvironment cellular community in the Nottingham cohort of colorectal cancer

		BCL-2 expression within the cellular community on Non-Epithelial/ Stroma (BerEP4 negative) (Mean ± SD)					
		Pan T-lymphocytes (CD3)	Cytotoxic T-lymphocytes (CD8)	B-lymphocytes (CD20)	Pan Macrophages (CD68)	M2-Macrophages (CD163)	NK cells (CD56)
MSI/MSS	MSI (n=19)	0.0080±0.0023	0.0017±0.0006	0.0096±0.0028	0.0006±0.0004	0.0008±0.0004	0.0001±0.00004
	MSS (n=24)	0.0042±0.0015	0.0015±0.0006	0.0043±0.0015	0.0006±0.0005	0.0002±0.00009	0.00005±0.00001
Exact Sig. (2 sided)		0.063	0.154	0.047*	0.288	0.115	0.288
BRAF	M (n=14)	0.0100±0.0025	0.0036±0.0011	0.0115±0.0032	0.0008±0.0005	0.0011±0.0005	0.0002±0.00005
	WT (n=29	0.0038±0.0014	0.0007±0.0002	0.0044±0.0015	0.0005±0.0004	0.0002±0.0001	0.00004±0.00001
Exact Sig. (2 sided)		0.015*	0.003*	0.013*	0.062	0.006*	0.009*
KRAS	M (n=15)	0.0019±0.0009	0.0018±0.00009	0.0021±0.0010	0.0005±0.0005	0.00006±0.00003	0.00003±0.00001
	WT (n=28)	0.0080±0.0019	0.0024±0.0006	0.0091±0.0022	0.0006±0.0004	0.0007±0.0003	0.0001±0.00003
Exact Sig. (2 sided)		0.019*	0.007*	0.025*	0.071	0.009*	0.027
PIK3CA	M (n=7)	0.0043±0.0025	0.0014± 0.0012	0.0047±0.0028	0.0012±0.0011	0.0011±0.0010	0.0002±0.0001
	WT (n=36)	0.0062±0.0015	0.0016±0.0005	0.0071±0.0018	0.0005±0.0004	0.0004±0.0001	0.00006±0.00002
Exact Sig. (2 sided)		0.488	0.711	0.529	0.784	0.962	0.374
TP53	M (n=20)	0.0036±0.0012	0.0017±0.0007	0.0034±0.0009	0.0011±0.0007	0.0003±0.0001	0.00007±0.00002
	WT (n=23)	0.0078±0.0021	0.0015±0.0005	0.0095±0.0026	0.0001±0.00005	0.0006±0.0003	0.00008±0.00003
Exact Sig. (2 sided)		0.553	0.823	0.505	0.406	0.950	0.486
Ploidy	Dip (n=26)	0.0065±0.0018	0.0017±0.0006	0.0075±0.0021	0.0004±0.0003	0.0006±0.0003	0.00009±0.00003
	Aneu (n=11)	0.0027±0.0011	0.0006±0.0003	0.0035±0.0014	0.0012±0.0011	0.0001±0.00003	0.00007±0.00004
Exact Sig. (2 sided)		0.460	0.384	0.523	0.806	0.682	0.961
MSS	CIN (n=11)	0.0027±0.0011	0.0006±0.0003	0.0035±0.0014	0.0012±0.0011	0.0001±0.00003	0.00007±0.00004
	MACS(n=7)	0.0025±0.0020	0.0016±0.0014	0.0019±0.0015	0.000007±0.000007	0.00009±0.00008	0.00006±0.00004
Exact Sig. (2 sided)		0.375	0.596	0.285	0.425	0.285	0.596

Mann–Whitney U test. Highlight in red: significant higher correlation on microsatellite instable (MSI) or mutant (M). Highlight in green: significant higher density on wildtype (WT). p< 0.05. MSS, microsatellite stable. Dip, diploid. Aneu, aneuploid. CIN, chromosomal instable. MACS, microsatellite and chromosomal stable.

MATLAB Code for *fm*-IHC (faux multiplex immunohistochemistry) analysis

Density of cellular biomarkers

```
%whole
recap_whole = zeros(12,1);
recap_whole_final = zeros(12,27);
for n = [1 2 3 5 6 7 9 10 11 13 16 17 18 19 20 23 24 25 26] %number 12 and 27 were removed
because only one marker with values, the rest was only NaN
filename = sprintf('superpixelIntensities_MSI#%d.csv',n);
data = xlsread(filename);
    for i = [3,5,7,8,9,10,11,12]
    marker_x = sum(data(:,i) > 75); %markers excluding BerEP4
    marker_y = sum(~isnan(data(:,6))); %marker BerEP4
    density = marker_x/marker_y;
    recap_whole(i,1) = density;
    end
recap_whole_final(:,n) = recap_whole;
end

%positive
recap_pos = zeros(12,1);
recap_pos_final = zeros(12,27);
for n = [1 2 3 5 6 7 9 10 11 13 16 17 18 19 20 23 24 25 26] %number 12 and 27 were removed
because only one marker with values, the rest was only NaN
filename = sprintf('superpixelIntensities_MSI#%d.csv',n);
data = xlsread(filename);
    for i = [3,5,7,8,9,10,11,12]
    marker_x = sum(data(:,i) > 75 & data(:,6) > 75); %markers excluding BerEP4
    marker_y = sum(data(:,6) > 75); %marker BerEP4
    density = marker_x/marker_y;
    recap_pos(i,1) = density;
    end
recap_pos_final(:,n) = recap_pos;
end

%negative
recap_neg = zeros(12,1);
recap_neg_final = zeros(12,27);
for n = [1 2 3 5 6 7 9 10 11 13 16 17 18 19 20 23 24 25 26] %number 12 and 27 were removed
because only one marker with values, the rest was only NaN
filename = sprintf('superpixelIntensities_MSI#%d.csv',n);
data = xlsread(filename);
    for i = [3,5,7,8,9,10,11,12]
    marker_x = sum(data(:,i) > 75 & data(:,6) < 75); %markers excluding BerEP4
    marker_y = sum(data(:,6) < 75); %marker BerEP4
    density = marker_x/marker_y;
    recap_neg(i,1) = density;
    end
recap_neg_final(:,n) = recap_neg;
end
%MSS

%whole
```

```
recap_whole = zeros(12,1);
recap_whole_final = zeros(12,28);
for n = [1 2 3 4 5 7 9 10 11 12 13 14 15 16 17 18 19 20 21 22 23 24 25 26 27 28] %number 8
was removed
filename = sprintf('superpixelIntensities_MSS#%d.csv',n);
data = xlsread(filename);
    for i = [3,5,7,8,9,10,11,12]
    marker_x = sum(data(:,6) > 75); %markers excluding BerEP4
    marker_y = sum(~isnan(data(:,6))); %marker BerEP4
    density = marker_x/marker_y;
    recap_whole(i,1) = density;
    end
recap_whole_final(:,n) = recap_whole;
end

%positive
recap_pos = zeros(12,1);
recap_pos_final = zeros(12,28);
for n = [1 2 3 4 5 7 9 10 11 12 13 14 15 16 17 18 19 20 21 22 23 24 25 26 27 28] %number 8
was removed
filename = sprintf('superpixelIntensities_MSS#%d.csv',n);
data = xlsread(filename);
    for i = [3,5,7,8,9,10,11,12]
    marker_x = sum(data(:,i) > 75 & data(:,6) > 75); %markers excluding BerEP4
    marker_y = sum(data(:,6) > 75); %marker BerEP4
    density = marker_x/marker_y;
    recap_pos(i,1) = density;
    end
recap_pos_final(:,n) = recap_pos;
end

%negative
recap_neg = zeros(12,1);
recap_neg_final = zeros(12,28);
for n = [1 2 3 4 5 7 9 10 11 12 13 14 15 16 17 18 19 20 21 22 23 24 25 26 27 28] %number 8
was removed
filename = sprintf('superpixelIntensities_MSS#%d.csv',n);
data = xlsread(filename);
    for i = [3,5,7,8,9,10,11,12]
    marker_x = sum(data(:,i) > 75 & data(:,6) < 75); %markers excluding BerEP4
    marker_y = sum(data(:,6) < 75); %marker BerEP4
    density = marker_x/marker_y;
    recap_neg(i,1) = density;
    end
recap_neg_final(:,n) = recap_neg;
end
```

Published with MATLAB® R2020a

Density of functional (KI67+ and BCL2+) cellular community

```
%whole tissue CD with Ki
recap_whole = zeros(12,1);
```

```
recap_whole_final = zeros(12,27);
for n = [1 2 3 5 6 7 9 10 11 13 16 17 18 19 20 23 24 25 26] %number 12 and 27 were removed
because only one marker with values, the rest was only NaN
filename = sprintf('superpixelIntensities_MSI#%d.csv',n);
data = xlsread(filename);
    for i = [3,7,8,9,10,11]
    marker_x = sum(data(:,i) > 75 & data(:,12) > 75); %markers excluding BerEP4, AE13, BCL2
    marker_y = sum(~isnan(data(:,6))); %marker BerEP4
    density = marker_x/marker_y;
    recap_whole(i,1) = density;
    end
recap_whole_final(:,n) = recap_whole;
end

%positive CD with Ki
recap_pos = zeros(12,1);
recap_pos_final = zeros(12,27);
for n = [1 2 3 5 6 7 9 10 11 13 16 17 18 19 20 23 24 25 26] %number 12 and 27 were removed
because only one marker with values, the rest was only NaN
filename = sprintf('superpixelIntensities_MSI#%d.csv',n);
data = xlsread(filename);
    for i = [3,7,8,9,10,11]
    marker_x = sum(data(:,i) > 75 & data (:,12) > 75 & data(:,6) > 75); %markers excluding
BerEP4, AE13, BCL2
    marker_y = sum(data(:,6) > 75); %marker BerEP4
    density = marker_x/marker_y;
    recap_pos(i,1) = density;
    end
recap_pos_final(:,n) = recap_pos;
end

%negative Cd with Ki
recap_neg = zeros(12,1);
recap_neg_final = zeros(12,27);
for n = [1 2 3 5 6 7 9 10 11 13 16 17 18 19 20 23 24 25 26] %number 12 and 27 were removed
because only one marker with values, the rest was only NaN
filename = sprintf('superpixelIntensities_MSI#%d.csv',n);
data = xlsread(filename);
    for i = [3,7,8,9,10,11]
    marker_x = sum(data(:,i) > 75 & data(:,12) > 75 & data(:,6) < 75); %markers excluding
BerEP4, AE13, BCL2
    marker_y = sum(data(:,6) < 75); %marker BerEP4
    density = marker_x/marker_y;
    recap_neg(i,1) = density;
    end
recap_neg_final(:,n) = recap_neg;
end
```

```
%MSS

%whole tissue CD with Ki
recap_whole = zeros(12,1);
recap_whole_final = zeros(12,28);
for n = [1 2 3 4 5 7 9 10 11 12 13 14 15 16 17 18 19 20 21 22 23 24 25 26 27 28] %number 8
was removed
filename = sprintf('superpixelIntensities_MSS#%d.csv',n);
data = xlsread(filename);
    for i = [3,7,8,9,10,11]
```

```
    marker_x = sum(data(:,i) > 75 & data(:,12) > 75); %markers excluding BerEP4, AE13, BCL2
    marker_y = sum(~isnan(data(:,6))); %marker BerEP4
    density = marker_x/marker_y;
    recap_whole(i,1) = density;
    end
recap_whole_final(:,n) = recap_whole;
end

%positive CD with Ki
recap_pos = zeros(12,1);
recap_pos_final = zeros(12,28);
for n = [1 2 3 4 5 7 9 10 11 12 13 14 15 16 17 18 19 20 21 22 23 24 25 26 27 28] %number 8
was removed
filename = sprintf('superpixelIntensities_MSS#%d.csv',n);
data = xlsread(filename);
    for i = [3,7,8,9,10,11]
    marker_x = sum(data(:,i) > 75 & data (:,12) > 75 & data(:,6) > 75); %markers excluding
BerEP4, AE13, BCL2
    marker_y = sum(data(:,6) > 75); %marker BerEP4
    density = marker_x/marker_y;
    recap_pos(i,1) = density;
    end
recap_pos_final(:,n) = recap_pos;
end

%negative CD with Ki
recap_neg = zeros(12,1);
recap_neg_final = zeros(12,28);
for n = [1 2 3 4 5 7 9 10 11 12 13 14 15 16 17 18 19 20 21 22 23 24 25 26 27 28] %number 8
was removed
filename = sprintf('superpixelIntensities_MSS#%d.csv',n);
data = xlsread(filename);
    for i = [3,5,7,8,9,10,11,12]
    marker_x = sum(data(:,i) > 75 & data(:,12) > 75 & data(:,6) < 75); %markers excluding
BerEP4, AE13, BCL2
    marker_y = sum(data(:,6) < 75); %marker BerEP4
    density = marker_x/marker_y;
    recap_neg(i,1) = density;
    end
recap_neg_final(:,n) = recap_neg;
end
```

Published with MATLAB® R2020a

```
%MSI

%whole tissue CD with BCL
recap_whole = zeros(12,1);
recap_whole_final = zeros(12,27);
for n = [1 2 3 5 6 7 9 10 11 13 16 17 18 19 20 23 24 25 26] %number 12 and 27 were removed
because only one marker with values, the rest was only NaN
filename = sprintf('superpixelIntensities_MSI#%d.csv',n);
data = xlsread(filename);
    for i = [3,7,8,9,10,11]
    marker_x = sum(data(:,i) > 75 & data(:,5) > 75); %markers excluding BerEP4, AE13, Ki67
    marker_y = sum(~isnan(data(:,6))); %marker BerEP4
    density = marker_x/marker_y;
```

```
    recap_whole(i,1) = density;
    end
recap_whole_final(:,n) = recap_whole;
end

%positive CD with BCL
recap_pos = zeros(12,1);
recap_pos_final = zeros(12,27);
for n = [1 2 3 5 6 7 9 10 11 13 16 17 18 19 20 23 24 25 26] %number 12 and 27 were removed
because only one marker with values, the rest was only NaN
filename = sprintf('superpixelIntensities_MSI#%d.csv',n);
data = xlsread(filename);
    for i = [3,7,8,9,10,11]
    marker_x = sum(data(:,i) > 75 & data (:,5) > 75 & data(:,6) > 75); %markers excluding
BerEP4, AE13, Ki67
    marker_y = sum(data(:,6) > 75); %marker BerEP4
    density = marker_x/marker_y;
    recap_pos(i,1) = density;
    end
recap_pos_final(:,n) = recap_pos;
end

%negative Cd with BCL
recap_neg = zeros(12,1);
recap_neg_final = zeros(12,27);
for n = [1 2 3 5 6 7 9 10 11 13 16 17 18 19 20 23 24 25 26] %number 12 and 27 were removed
because only one marker with values, the rest was only NaN
filename = sprintf('superpixelIntensities_MSI#%d.csv',n);
data = xlsread(filename);
    for i = [3,7,8,9,10,11]
    marker_x = sum(data(:,i) > 75 & data(:,5) > 75 & data(:,6) < 75); %markers excluding
BerEP4, AE13, Ki67
    marker_y = sum(data(:,6) < 75); %marker BerEP4
    density = marker_x/marker_y;
    recap_neg(i,1) = density;
    end
recap_neg_final(:,n) = recap_neg;
end
```

```
%MSS

%whole tissue CD with BCL
recap_whole = zeros(12,1);
recap_whole_final = zeros(12,28);
for n = [1 2 3 4 5 7 9 10 11 12 13 14 15 16 17 18 19 20 21 22 23 24 25 26 27 28] %number 8
was removed
filename = sprintf('superpixelIntensities_MSS#%d.csv',n);
data = xlsread(filename);
    for i = [3,7,8,9,10,11]
    marker_x = sum(data(:,i) > 75 & data(:,5) > 75); %markers excluding BerEP4, AE13, Ki67
    marker_y = sum(~isnan(data(:,6))); %marker BerEP4
    density = marker_x/marker_y;
    recap_whole(i,1) = density;
    end
recap_whole_final(:,n) = recap_whole;
end
```

```
%positive CD with BCL
recap_pos = zeros(12,1);
recap_pos_final = zeros(12,28);
for n = [1 2 3 4 5 7 9 10 11 12 13 14 15 16 17 18 19 20 21 22 23 24 25 26 27 28] %number 8
was removed
filename = sprintf('superpixelIntensities_MSS#%d.csv',n);
data = xlsread(filename);
    for i = [3,7,8,9,10,11]
    marker_x = sum(data(:,i) > 75 & data (:,5) > 75 & data(:,6) > 75); %markers excluding
BerEP4, AE13, Ki67
    marker_y = sum(data(:,6) > 75); %marker BerEP4
    density = marker_x/marker_y;
    recap_pos(i,1) = density;
    end
recap_pos_final(:,n) = recap_pos;
end

%negative CD with BCL
recap_neg = zeros(12,1);
recap_neg_final = zeros(12,28);
for n = [1 2 3 4 5 7 9 10 11 12 13 14 15 16 17 18 19 20 21 22 23 24 25 26 27 28] %number 8
was removed
filename = sprintf('superpixelIntensities_MSS#%d.csv',n);
data = xlsread(filename);
    for i = [3,5,7,8,9,10,11,12]
    marker_x = sum(data(:,i) > 75 & data(:,5) > 75 & data(:,6) < 75); %markers excluding
BerEP4, AE13, Ki67
    marker_y = sum(data(:,6) < 75); %marker BerEP4
    density = marker_x/marker_y;
    recap_neg(i,1) = density;
    end
recap_neg_final(:,n) = recap_neg;
end
```

Published with MATLAB® R2020a

Correlation of cellular biomarkers

```
%MSI

%table and marker identification
recap1 = zeros(45,1);
recapfinal = zeros(45,30);
marker = combntns(1:10,2);
numfiles  = [1 2 3 5 6 7 9 10 11 13 16 17 18 19 20 23 24 25 26]; %number 12 and 27 were
removed because only one marker with values, the rest was only NaN

%correlation
for n = [1 2 3 5 6 7 9 10 11 13 16 17 18 19 20 23 24 25 26]
    filename = sprintf('superpixelIntensities_MSI#%d.csv',n); %load file
    data = xlsread(filename);
    data(:,[1 2]) = []; %delete 1st and 2nd columns
    for i = 1:45
        correlation = corrcoef(data, 'Rows', 'pairwise'); %correlation coefficient
        coef = correlation(marker(i,1),marker(i,2)); %recap
        recap1(i,1) = coef; %recap per sample
    end
```

```
    recapfinal(:,n) = recap1; %recap all samples
end
```

```
%MSS

%table and marker identification
recap1MSS = zeros(45,1);
recapfinalMSS = zeros(45,30);
markerMSS = combntns(1:10,2);
numfilesMSS  = [1 2 3 4 5 7 9 10 11 12 13 14 15 16 17 18 19 20 21 22 23 24 25 26 27 28];
%number 8 was removed

%correlation
for n = [1 2 3 4 5 7 9 10 11 12 13 14 15 16 17 18 19 20 21 22 23 24 25 26 27 28]
    filename = sprintf('superpixelIntensities_MSS#%d.csv',n); %load file
    dataMSS = xlsread(filename);
    dataMSS(:,[1 2]) = []; %delete 1st and 2nd columns
    for i = 1:45
        correlationMSS = corrcoef(dataMSS, 'Rows', 'pairwise'); %correlation coefficient
        coefMSS = correlationMSS(marker(i,1),marker(i,2)); %recap
        recap1MSS(i,1) = coefMSS; %recap per sample
    end
    recapfinalMSS(:,n) = recap1MSS; %recap all samples
end
```

```
%correlation for markers accross samples MSI

%load data (#12 and #27 excluded)
for n = [1 2 3 5 6 7 9 10 11 13 16 17 18 19 20 23 24 25 26]
    str = ['C:\Users\ezxrap\Documents\Santi\Alains registration MSI
MSS\MSI\superpixelIntensities_MSI#',num2str(n),'.csv'];
    data{n} = xlsread(str);
end

%concenate matrices (maaf bagian ini gak bisa bikin loop-nya, manual aja yak)
datarecap = vertcat(data{1,1},...
                    data{1,2},...
                    data{1,3},...
                    data{1,5},...
                    data{1,6},...
                    data{1,7},...
                    data{1,9},...
                    data{1,10},...
                    data{1,11},...
                    data{1,13},...
                    data{1,16},...
                    data{1,17},...
                    data{1,18},...
                    data{1,19},...
                    data{1,20},...
                    data{1,23},...
                    data{1,24},...
                    data{1,25},...
                    data{1,26});

%delete 1st and 2nd columns
datarecap(:,[1 2]) = [];

%table and marker identification
```

```
recap1 = zeros(45,1);
marker = combntns(1:10,2);

%correlation
for i = 1:45
    correlation = corrcoef(datarecap, 'Rows', 'pairwise'); %correlation coefficient
    coef = correlation(marker(i,1),marker(i,2)); %recap
    recap1(i,1) = coef; %recap per sample
end
```

```
%correlation for markers accross samples MSS

%load data (#8 excluded)
for n = [1 2 3 4 5 7 9 10 11 12 13 14 15 16 17 18 19 20 21 22 23 24 25 26 27 28]
    str = ['C:\Users\ezxrap\Documents\Santi\Alains registration MSI
MSS\superpixelIntensities_MSS#',num2str(n),'.csv'];
    data{n} = xlsread(str);
end

%concenate matrices (maaf bagian ini gak bisa bikin loop-nya, manual aja yak)
datarecap = vertcat(data{1,1},...
                    data{1,2},...
                    data{1,3},...
                    data{1,4},...
                    data{1,5},...
                    data{1,7},...
                    data{1,9},...
                    data{1,10},...
                    data{1,11},...
                    data{1,12},...
                    data{1,13},...
                    data{1,14},...
                    data{1,15},...
                    data{1,16},...
                    data{1,17},...
                    data{1,18},...
                    data{1,19},...
                    data{1,20},...
                    data{1,21},...
                    data{1,22},...
                    data{1,23},...
                    data{1,24},...
                    data{1,25},...
                    data{1,26},...
                    data{1,27},...
                    data{1,28});

%delete 1st and 2nd columns
datarecap(:,[1 2]) = [];

%table and marker identification
recap1 = zeros(45,1);
marker = combntns(1:10,2);

%correlation
for i = 1:45
    correlation = corrcoef(datarecap, 'Rows', 'pairwise'); %correlation coefficient
    coef = correlation(marker(i,1),marker(i,2)); %recap
```

```
    recap1(i,1) = coef; %recap per sample
end
```

```
%%BerEP negative MSI

%table and marker identification
recap1 = zeros(45,1);
recapfinal = zeros(45,30);
z_recapfinal = zeros(45,30);
marker = combntns(1:10,2);
numfiles  = [1 2 3 5 6 7 9 10 11 13 16 17 18 19 20 23 24 25 26]; %number 12 and 27 were
removed because only one marker with values, the rest was only NaN

%correlation
for n = [1 2 3 5 6 7 9 10 11 13 16 17 18 19 20 23 24 25 26]
    filename = sprintf('superpixelIntensities_MSI#%d.csv',n); %load file
    data = xlsread(filename);
    data(:,[1 2]) = []; %delete 1st and 2nd columns
    berEP_negative = data(:,4) > 76.5; %logical index to later remove datapoint greater than
76.5
    data(berEP_negative,:) = [];
    for i = 1:45
        correlation = corrcoef(data, 'Rows', 'pairwise'); %correlation coefficient
        coef = correlation(marker(i,1),marker(i,2)); %recap
        recap1(i,1) = coef; %recap per sample
    end
    recapfinal(:,n) = recap1; %recap all samples
    z_recapfinal(:,n) = atanh(recap1); %recap zscore all sample
end
```

```
%%BerEP positive MSI

%table and marker identification
recap1 = zeros(45,1);
recapfinal = zeros(45,30);
z_recapfinal = zeros(45,30);
marker = combntns(1:10,2);
numfiles  = [1 2 3 5 6 7 9 10 11 13 16 17 18 19 20 23 24 25 26]; %number 12 and 27 were
removed because only one marker with values, the rest was only NaN

%correlation
for n = [1 2 3 5 6 7 9 10 11 13 16 17 18 19 20 23 24 25 26]
    filename = sprintf('superpixelIntensities_MSI#%d.csv',n); %load file
    data = xlsread(filename);
    data(:,[1 2]) = []; %delete 1st and 2nd columns
    berEP_positive = data(:,4) <= 76.5; %logical index to later remove datapoint equal to 0
    data(berEP_positive,:) = [];
    for i = 1:45
        correlation = corrcoef(data, 'Rows', 'pairwise'); %correlation coefficient
        coef = correlation(marker(i,1),marker(i,2)); %recap
        recap1(i,1) = coef; %recap per sample
    end
    recapfinal(:,n) = recap1; %recap all samples
    z_recapfinal(:,n) = atanh(recap1); %recap zscore all sample
end
```

```
%BerEP negative MSS

%table and marker identification
recap1MSS = zeros(45,1);
```

```
recapfinalMSS = zeros(45,30);
z_recapfinalMSS = zeros(45,30);
markerMSS = combntns(1:10,2);
numfilesMSS  = [1 2 3 4 5 7 9 10 11 12 13 14 15 16 17 18 19 20 21 22 23 24 25 26 27 28];

%correlation
for n = [1 2 3 4 5 7 9 10 11 12 13 14 15 16 17 18 19 20 21 22 23 24 25 26 27 28]
    filename = sprintf('superpixelIntensities_MSS#%d.csv',n); %load file
    dataMSS = xlsread(filename);
    dataMSS(:,[1 2]) = []; %delete 1st and 2nd columns
    berEP_negative = dataMSS(:,4) > 76.5; %logical index to later remove datapoint greater
than 0
    dataMSS(berEP_negative,:) = [];
    for i = 1:45
        correlationMSS = corrcoef(dataMSS, 'Rows', 'pairwise'); %correlation coefficient
        coefMSS = correlationMSS(markerMSS(i,1),markerMSS(i,2)); %recap
        recap1MSS(i,1) = coefMSS; %recap per sample
    end
    recapfinalMSS(:,n) = recap1MSS; %recap all samples
    z_recapfinalMSS(:,n) = atanh(recap1MSS); %recap zscore all sample
end
```

```
%BerEP positive MSS

%table and marker identification
recap1MSS = zeros(45,1);
recapfinalMSS = zeros(45,30);
z_recapfinalMSS = zeros(45,30);
markerMSS = combntns(1:10,2);
numfilesMSS  = [1 2 3 4 5 7 9 10 11 12 13 14 15 16 17 18 19 20 21 22 23 24 25 26 27 28];

%correlation
for n = [1 2 3 4 5 7 9 10 11 12 13 14 15 16 17 18 19 20 21 22 23 24 25 26 27 28]
    filename = sprintf('superpixelIntensities_MSS#%d.csv',n); %load file
    dataMSS = xlsread(filename);
    dataMSS(:,[1 2]) = []; %delete 1st and 2nd columns
    berEP_positive = dataMSS(:,4) <= 76.5; %logical index to later remove datapoint equal to
0
    dataMSS(berEP_positive,:) = [];
    for i = 1:45
        correlationMSS = corrcoef(dataMSS, 'Rows', 'pairwise'); %correlation coefficient
        coefMSS = correlationMSS(markerMSS(i,1),markerMSS(i,2)); %recap
        recap1MSS(i,1) = coefMSS; %recap per sample
    end
    recapfinalMSS(:,n) = recap1MSS; %recap all samples
    z_recapfinalMSS(:,n) = atanh(recap1MSS); %recap zscore all sample
end
```

```
%correlation for markers accross samples MSI BerEP negative

%load data (#12 and #27 excluded)
for n = [1 2 3 5 6 7 9 10 11 13 16 17 18 19 20 23 24 25 26]
    str = ['C:\Users\ezxrap\Documents\Santi\Alains registration MSI
MSS\MSI\superpixelIntensities_MSI#',num2str(n),'.csv'];
    data{n} = xlsread(str);
end

%concenate matrices (maaf bagian ini gak bisa bikin loop-nya, manual aja yak)
datarecap = vertcat(data{1,1},...
```

```
                    data{1,2},...
                    data{1,3},...
                    data{1,5},...
                    data{1,6},...
                    data{1,7},...
                    data{1,9},...
                    data{1,10},...
                    data{1,11},...
                    data{1,13},...
                    data{1,16},...
                    data{1,17},...
                    data{1,18},...
                    data{1,19},...
                    data{1,20},...
                    data{1,23},...
                    data{1,24},...
                    data{1,25},...
                    data{1,26});

datarecap(:,[1 2]) = []; %delete 1st and 2nd columns
berEP_negative = datarecap(:,4) > 0; %logical index to later remove datapoint greater than 0
datarecap(berEP_negative,:) = [];

%table and marker identification
recap1 = zeros(45,1);
marker = combntns(1:10,2);

%correlation
for i = 1:45
    correlation = corrcoef(datarecap, 'Rows', 'pairwise'); %correlation coefficient
    coef = correlation(marker(i,1),marker(i,2)); %recap
    recap1(i,1) = coef; %recap per sample
end
```

```
%correlation for markers accross samples MSI BerEP positive

%load data (#12 and #27 excluded)
for n = [1 2 3 5 6 7 9 10 11 13 16 17 18 19 20 23 24 25 26]
    str = ['C:\Users\ezxrap\Documents\Santi\Alains registration MSI
MSS\MSI\superpixelIntensities_MSI#',num2str(n),'.csv'];
    data{n} = xlsread(str);
end

%concenate matrices (maaf bagian ini gak bisa bikin loop-nya, manual aja yak)
datarecap = vertcat(data{1,1},...
                    data{1,2},...
                    data{1,3},...
                    data{1,5},...
                    data{1,6},...
                    data{1,7},...
                    data{1,9},...
                    data{1,10},...
                    data{1,11},...
                    data{1,13},...
                    data{1,16},...
                    data{1,17},...
                    data{1,18},...
                    data{1,19},...
```

```
                    data{1,20},...
                    data{1,23},...
                    data{1,24},...
                    data{1,25},...
                    data{1,26});

datarecap(:,[1 2]) = []; %delete 1st and 2nd columns
berEP_positive = datarecap(:,4) == 0; %logical index to later remove datapoint equal to 0
datarecap(berEP_positive,:) = [];

%table and marker identification
recap1 = zeros(45,1);
marker = combntns(1:10,2);

%correlation
for i = 1:45
    correlation = corrcoef(datarecap, 'Rows', 'pairwise'); %correlation coefficient
    coef = correlation(marker(i,1),marker(i,2)); %recap
    recap1(i,1) = coef; %recap per sample
end
```

```
%correlation for markers accross samples MSS BerEP negative

%load data (#8 excluded)
for n = [1 2 3 4 5 7 9 10 11 12 13 14 15 16 17 18 19 20 21 22 23 24 25 26 27 28]
    str = ['C:\Users\ezxrap\Documents\Santi\Alains registration MSI
MSS\MSS\superpixelIntensities_MSS#',num2str(n),'.csv'];
    data{n} = xlsread(str);
end

%concenate matrices (maaf bagian ini gak bisa bikin loop-nya, manual aja yak)
datarecap = vertcat(data{1,1},...
                    data{1,2},...
                    data{1,3},...
                    data{1,4},...
                    data{1,5},...
                    data{1,7},...
                    data{1,9},...
                    data{1,10},...
                    data{1,11},...
                    data{1,12},...
                    data{1,13},...
                    data{1,14},...
                    data{1,15},...
                    data{1,16},...
                    data{1,17},...
                    data{1,18},...
                    data{1,19},...
                    data{1,20},...
                    data{1,21},...
                    data{1,22},...
                    data{1,23},...
                    data{1,24},...
                    data{1,25},...
                    data{1,26},...
                    data{1,27},...
                    data{1,28});
```

```
datarecap(:,[1 2]) = []; %delete 1st and 2nd columns
berEP_negative = datarecap(:,4) > 0; %logical index to later remove datapoint greater than 0
datarecap(berEP_negative,:) = [];

%table and marker identification
recap1 = zeros(45,1);
marker = combntns(1:10,2);

%correlation
for i = 1:45
    correlation = corrcoef(datarecap, 'Rows', 'pairwise'); %correlation coefficient
    coef = correlation(marker(i,1),marker(i,2)); %recap
    recap1(i,1) = coef; %recap per sample
end
```

```
%correlation for markers accross samples MSS BerEP positive

%load data (#8 excluded)
for n = [1 2 3 4 5 7 9 10 11 12 13 14 15 16 17 18 19 20 21 22 23 24 25 26 27 28]
    str = ['C:\Users\ezxrap\Documents\Santi\Alains registration MSI
MSS\MSS\superpixelIntensities_MSS#',num2str(n),'.csv'];
    data{n} = xlsread(str);
end

%concenate matrices (maaf bagian ini gak bisa bikin loop-nya, manual aja yak)
datarecap = vertcat(data{1,1},...
                    data{1,2},...
                    data{1,3},...
                    data{1,4},...
                    data{1,5},...
                    data{1,7},...
                    data{1,9},...
                    data{1,10},...
                    data{1,11},...
                    data{1,12},...
                    data{1,13},...
                    data{1,14},...
                    data{1,15},...
                    data{1,16},...
                    data{1,17},...
                    data{1,18},...
                    data{1,19},...
                    data{1,20},...
                    data{1,21},...
                    data{1,22},...
                    data{1,23},...
                    data{1,24},...
                    data{1,25},...
                    data{1,26},...
                    data{1,27},...
                    data{1,28});

datarecap(:,[1 2]) = []; %delete 1st and 2nd columns
berEP_positive = datarecap(:,4) == 0; %logical index to later remove datapoint greater than 0
datarecap(berEP_positive,:) = [];

%table and marker identification
recap1 = zeros(45,1);
```

```
marker = combntns(1:10,2);

%correlation
for i = 1:45
    correlation = corrcoef(datarecap, 'Rows', 'pairwise'); %correlation coefficient
    coef = correlation(marker(i,1),marker(i,2)); %recap
    recap1(i,1) = coef; %recap per sample
end
```

Published with MATLAB® R2020a

Cell line authentication certificate



School of Medicine
Division of Cancer and Stem Cell
Teresa Pereira Raposo
D Floor, West Block QMC
Nottingham, NG7 2UH
UK

06.02.2017

Certificate

Order
By order of Teresa Pereira Raposo (School of Medicine) we were requested to perform a cell line authentication test. Following samples were examined:

Our sample number	Client sample name	
CL170130_006	SW480	
CL170130_007	DLD1	
CL170130_008	SW620 (A)	A - OLD, SW620 Cten KO
CL170130_009	HCT116	
CL170130_010	RKO	
CL170130_011	SW620 (B)	B - SW620 WT

Method:
Genetic characteristics were determined by PCR-single-locus-technology. 21 independent PCR-systems Amelogenin, D3S1358, D1S1656, D6S1043, D13S317, Penta E, D16S539, D18S51, D2S1338, CSF1PO, Penta D, TH01, vWA, D21S11, D7S820, D5S818, TPOX, D8S1179, D12S391, D19S433 and FGA were investigated (Promega, PowerPlex 21 PCR Kit).
In parallel, positive and negative controls were carried out yielding correct results.

Eurofins Medigenomix Forensik GmbH
Anzinger Str. 7a
D-85560 Ebersberg

Tel: + 49 (0) 8092 8289 260
Fax: + 49 (0) 8092 8289 190
www.eurofins.de/forensik-de
forensik@eurofins.com

Geschäftsführer
Dr. Peter Persigehl
Dr. Brigitte Obermaier
Dr. Bruno Poddevin

HRB 20 12 60
Amtsgericht München

Ust-Id Nr. DE 285161076
Steuernummer 114/116/00159

eurofins | Genomics eurofins | Forensik

DAkkS ISO 17025:2005 accredited

Results:

DNA-System	DNA-criteria SW480 CL170130_006	DNA-criteria DLD1 CL170130_007	DNA-criteria SW620 (A) CL170130_008	DNA-criteria HCT116 CL170130_009	DNA-criteria RKO CL170130_010
AM	X, X	X, Y	X, X	X, X	X, X
D3S1358	15, 15	17, 17	16, 16	12, 16, 17, 18, 19	12, 16, 17, 18, 19
D1S1656	13, 14	17.3, 19.3	13, 14	12, 13, 14, 15	12, 13, 14, 16.3
D6S1043	11, 12	11, 13	11, 12	12, 13, 14	12, 13, 14.1, 20
D13S317	12, 12	8, 11	12, 12	10, 12, 13	8, 10, 11, 12
Penta E	10, 10	7, 14	10, 10	13, 14	10, 13, 14
D16S539	13, 13	12, 13	9, 13	11, 12, 13, 14	11, 12, 13
D18S51	13, 13	11, 17	13, 13	16, 17, 18	11, 12, 16, 17
D2S1338	17, 24	17, 25	17, 24	16, 16	16, 16
CSF1PO	13, 14	11, 12	13, 14	7, 10	7, 8, 10
Penta D	9, 15	9, 14	9, 15	9, 13	9, 10, 13
TH01	8, 8	7, 9.3	8, 8	8, 9	8, 9, 10
vWA	16, 16	18, 19	16, 16	17, 22, 23	17, 21, 22, 23
D21S11	30, 30.2	29, 32.2	30, 30.2	29, 30	29, 30
D7S820	8, 8	10, 12	8, 9	11, 12	11, 12
D5S818	13, 13	13, 13	13, 13	10, 11	10, 11
TPOX	11, 11	8, 11	11, 11	8, 8	8, 8
D8S1179	13, 13	15, 15	13, 13	12, 13, 14	9, 12, 13, 14
D12S391	17, 17	19, 22	17, 17	17, 18, 20, 21, 22	15, 17, 18, 20, 21, 22
D19S433	13, 13	14, 16	13, 13	12, 13	12, 13, 14, 18.2
FGA	24, 24	22, 22	24, 24	18, 19, 21, 22, 23	18, 19, 22, 23

DNA-System	DNA-criteria SW620 (B) CL170130_011
AM	X, X
D3S1358	16, 16
D1S1656	13, 14
D6S1043	11, 12
D13S317	12, 12
Penta E	10, 10
D16S539	9, 13
D18S51	13, 13
D2S1338	17, 24
CSF1PO	13, 14
Penta D	9, 15
TH01	8, 8
vWA	16, 16
D21S11	30, 30.2
D7S820	8, 9
D5S818	13, 13
TPOX	11, 11
D8S1179	13, 13
D12S391	17, 17
D19S433	13, 13
FGA	24, 24

Eurofins Medigenomix Forensik GmbH
Anzingerstr. 7a
D-85560 Ebersberg

Tel. + 49 (0) 8092 8289 260
Fax. + 49 (0) 8092 8289 190
www.eurofins.de/forensik-de
forensik@eurofins.com

Geschäftsführer
Dr. Peter Persigehl
Dr. Brigitte Obermaier
Dr. Bruno Poddevin

HRB 20 12 60
Amtsgericht München

Ust-Id Nr. DE 285161076
Steuernummer 114/116/60159

eurofins | Genomics eurofins | Forensik

DAkkS ISO 17025:2005 accredited

Summary:
The following cell lines could be detected in the online database of the DSMZ (http://www.dsmz.de/de/service/services-human-and-animal-cell-lines/online-str-analysis.html):

Our sample number	Client sample name	DSMZ name
CL170130_006	SW480	SW-480
CL170130_007	DLD1	DLD-1
CL170130_008	SW620 (A)	SW620 [SW-620]
CL170130_009	HCT116	HCT-116
CL170130_010	RKO	RKO can be present in the mixture but the main component is HCT-116
CL170130_011	SW620 (B)	SW620 [SW-620]

Dr. Burkhard Rolf
Director Forensic Services

Dr. Michaela Bosch
Project Manager DNA-Forensics

Eurofins Medigenomix Forensik GmbH carries out all analyses with greatest care and on the basis of state of the art scientific knowledge. All results solely refer to the analysed samples. Our expert's reports must not be duplicated in extracts without consent of Eurofins Medigenomix Forensik GmbH.
Cell_line-certificate_eng_V03_141211

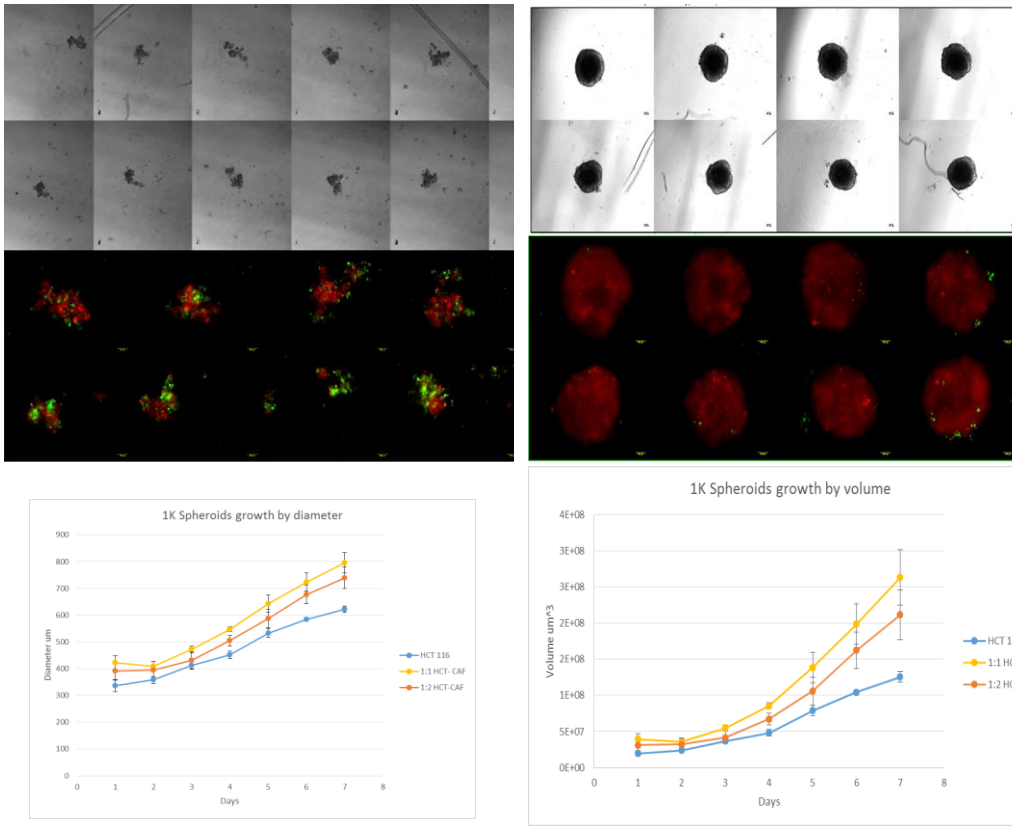


Figure S.7.1. The Growth of three-dimensional (3D) co-culture spheroid of colorectal cancer (CRC) cell line, HCT116, and cancer-associated fibroblast (CAF). Live-cell brightfield and fluorescence imaging of three-dimensional (3D) multicellular co-culture spheroid of colorectal cancer (CRC) cell line, HCT116, with cancer-associated fibroblast (CAF) (above panel). The brightfield images were taken at 4x magnification and the fluorescence images were taken at 10x magnification using a widefield inverted microscope (Nikon TiE). HCT116 was co-culture with CAF at 1:1 ratio at total number of 1000 cells/ well on a 96-well black ultralow attachment plate (Corning, Cat: CLS4515). The HCT116 and CAF were transduced with tomato (red) and GFP (green), respectively. The brightfield images of the spheroid were used to calculate the mean spheroid radius by assuming an approximation to the area of the circle and from there inferred the volume of the spheroid, as an approximation to the volume of a sphere (below panel).